A Horizon Sensing Vertically Oriented Radiometer Antenna Study

By Chester L. Smith and Hugh P. Taylor

March 1969

Prepared under Contract No. NAS 12-2001 by
EWEN KNIGHT CORPORATION
East Natick, Massachusetts 01760

Electronics Research Center
National Aeronautics and Space Administration
Cambridge, Massachusetts 02139

NASA CR-

A HORIZON SENSING VERTICALLY ORIENTED RADIOMETER ANTENNA STUDY

By Chester L. Smith and Hugh P. Taylor

March 1969

Prepared under Contract No. NAS 12-2001 by
EWEN KNIGHT CORPORATION
East Natick, Massachusetts 01760

Electronics Research Center
NATIONAL AERONAUTICS AND SPACE ADMINISTRATION
Cambridge, Massachusetts 02139

Janis Vilcans
Technical Monitor
NAS 12-2001
Electronics Research Center
575 Technology Square
Cambridge, Massachusetts 02139

FOREWORD

This study and investigation was initiated under Contract No. NAS 12-2001 for the purpose of determining the feasibility and design of a precise and reliable earth vertical tracking antenna.

Ewen Knight personnel who participated in the study were:

H. P. Taylor, Director Advanced Electronic Information Systems

C. L. Smith, Senior Research Engineer

A. W. Gruhn, Microwave Engineer

TABLE OF CONTENTS PAGE #

LIST OF FIGURES

LIST OF TABLES

ABSTRACT

A satellite system antenna design suitable for observing the 5 mm emission from the oxygen of the earth's atmosphere in order to obtain a vertical sense is presented. An approach capable of reducing the uncertainity in the vertical error to less than 1 arc minute (3 sigma) is discussed. A trade-off analysis between performance and system complexity is included. It is shown that a significant simplification in complexity can be realized if the accuracy goal is increased to 2-3 arc minutes (1 sigma) of error.

The antenna performance requirements are discussed with reference to the performance requirements imposed on the other major subsystems of the earth vertical sensor, particularly the radiometric receiver and the measurement coordinate system.

1.0 SUMMARY

Various antenna configurations were considered in the design study. Each was assigned to one of three general classifications:

Mechanically scanned

Electromechanically scanned

Completely electronic

As a result of this investigation, it was concluded that mechanically scanned antennas offer greatest promise for near-future system applications. A decision theoretic array is considered to be a strong potential contender for this system application; however, the present status of theoretical, as well as experimental work on antennas of this type, eliminates their consideration as a near-future practical solution.

The following table cross-references the Statement of Work with the subjects discussed in the Final Report.

TABLE 1-1

CROSS-REFERENCE TO CONTRACT STATEMENT OF WORK

Statement of Work		Report
Item 1 - Parametric Study		
a)	Error Budget to Achieve 1 arc Minute Accuracy	Appendix B
	Radiometer Types	Appendix F
	Amplitude Monopulse	Appendix C
b)	Wideband vs Narrow Band Receivers	Appendix G
	Effect of Varying Antenna Beamwidths	Appendix B, E
c)	Antenna System Design, Antenna Scanning Methods	Section 3.0, 3.1, 3.2, 3.3
	Beamwidth, Sidelobe and Backlobe Requirements	Section 4.2, Appendix E
	Affects of Atmospheric Temperature Variations with Season and Latitude	Appendix D
	Flight Orbit Changes	Appendix A, G
	Space Environment	Appendix H
	Comparison of Various Antenna Scanning Techniques	Section 5.0, 5.1, 5.2, 5.3

Item 2 - Antenna Design Phase

a)	Trade-off of Design Parameters	Section 4.1
b)	Engineering Design	Section 4.2, 4.3, 4.4

Item 3 - Computational and Evaluation Phase

a)	Performance Computations for the Antenna	Section 4.1, 4.2, Appendix E
b)	Performance Computations for the Horizon Sensor	Section 4.2 Appendix A, B, C, D, E
c)	Power Requirements	Section 2.2
d)	Antenna Size and Weight Estimate	Section 2.2
e)	Polarization	Section 2.1
f)	R.F. Receiver Requirements	Appendix F
g)	Relative Deformation of the Antenna Main Beam Caused by Beam Steering and its Effect on the Accuracy of the Horizon Sensor	Appendix B*
h)	Complete Set of Drawings	Figures 4.1, 4.4, 4.11, 4.12, 4.13, 4.14, 4.15

*An error of 10^{-3} of the beam angle has been allowed for all variations in the aperture distribution including those caused by beam steering.

1.1 Introduction

The prime objective of this study and investigation was the design of a millimeter wave receiving antenna to be used as an integral part of a radiometer system. The function of the total sensor system, consisting of the antenna and radiometric receiver, is to determine the attitude of an orbiting spacecraft by detecting the thermal centroid of molecular atmospheric oxygen emission at a wavelength of 5 mm. The total system accuracy goal for local vertical determination was established as one arc minute (3 sigma). The performance characteristics of the system were predicated on the restraints imposed by an elliptical orbit with a 100 nautical mile perigee and a 1,000 nautical mile apogee.

Those portions of the investigation concerned with various aspects of the total system for this specific application are treated separately in the Addenda to this report. Table 1-1 cross references the report and addenda to the contract statement of work. The performance requirements imposed on the antenna derived from these various system considerations are summarized in Section 2. The main body of the report is devoted to the development of a practical antenna design approach to meet these requirements.

2.0 ANTENNA PERFORMANCE REQUIREMENTS

The objective is to provide an antenna system which will, in conjunction with appropriate electronic circuitry, locate the centroid of a spherical source to within 1 arc minute (3 sigma). The source may be considered as a sphere subtending an angle which varies from 102° to 156° in an average period of 103 minutes with a maximum change in the subtended angle rate of $1/2^{\circ}$ per minute. It is further assumed that the received signal is describable as a uniform power distribution over the entire sphere.

The performance specifications for an antenna system meeting these requirements are:

2.1 Electrical

. . . Four symmetrical antenna beams projected in paired orthogonal coordinates about the line drawn from the point of observation to the center of the sphere.

. . . The main beam angle of each of the four elements is restricted to:

6° maximum in the horizontal plane (plane tangent to the surface of the sphere)

2° maximum in the vertical plane (plane perpendicular to the surface of the sphere)

. . . Main beam efficiency for each element shall be 90% minimum, and in particular 99% of the total received power when the antenna element is positioned in the nominal operating direction shall be contained within an angle subtended by 10° about the boresight of the main beam of each individual element.

. . . The first sidelobe level shall be not greater than:

-24 db in the vertical plane

-17 db in the horizontal plane

. . . The frequency of operation shall be 60.8 GHz with a minimum of 3 GHz instantaneous bandwidth centered at the operating frequency.

. . . . Each antenna element shall be linearly polarized, and each must have the same polarization. The polarization may be either horizontal or vertical.

. . . The voltage standing wave ratio shall be a maximum of 1.05:1 with a maximum variation during scan of 1%.

. . . The insertion loss between the input antenna terminal and the sensor receiver shall not exceed 0.5 db

2.2 Mechanical

. . . Each of the paired sets of antenna beams in either coordinate must be coupled to two waveguide input flanges rigidly attached to a common structural member.

. . . The beam positioning mechanism must be capable of pointing each beam to the same angle relative to the central axis of the antenna system in the local framework of reference to an accuracy of 5 arc seconds rms.

. . . The size of the antenna package shall not exceed 7 3/16 x 7 3/16 x 8 3/8 inches in its folded position.

. . . The weight of the antenna package shall not exceed 32 ounces, not including receiver and electronics.

. . . The primary mechanism used for positioning of the antenna elements shall occupy a volume no greater than 11 cubic inches and weigh no more than 8 ounces, not including the linkages and encoders used in attaching to the individual antenna elements.

. . . The antenna element attachment mechanism includes the waveguide coupling device, the axle, the fine position control element, and the differential angle error sensor. This device shall be maintained at a minimum size and weight consistent with the accuracy specifications.

. . . The power requirements of the beam positioning control subsystem shall not exceed 7 watts, not including the gimbal system; if any, used to interface the antenna with the vehicle.

. . . A volume of 36 cubic inches, with approximate dimensions of 4" x 3" x 3" is allowed for the receiver's input R.F. circuitry.

3.0 SURVEY OF ANTENNA SCANNING TECHNIQUES

A general review of available antennas and means of scanning them to meet the specifications is presented. The various antenna types are divided into three major groups. A number of antenna configurations were investigated under each group designation. An example from each group is selected to illustrate the general limitations of the group.

The true electronically steerable phased array is not considered in detail primarily because phased arrays are best suited to applications where high speed acquisition, or multiple target capability (or both) is required. The acquisition times of interest here are in the order of seconds to minutes, and the source is assumed to be isolated in space. The advantages usually associated with a steerable phased array are consequently not applicable. Within the group of fully electronic systems the decision theoretic array appears to warrant further study not only as an attitude sensor, but also as a data gathering and sorting device.

A list of the scanning systems considered is shown in Table 3-1 along with the main features of each. The antennas are classified on the basis of the method used to position or scan the beam. There are three categories defined as follows:

3.1 Mechanical Scan-System

Antennas which require mechanical positioning of a feed or an aperture in order to control the pointing direction of the main lobe of the secondary pattern. Designs 1-5 Table 3-1 fall into this group.

3.2 Electro-Mechanical

Antennas in which the position of the beam in the secondary pattern is varied by mechanically controlling a device which electronically reforms the beam. Phased arrays in which a mechanical device is used to vary the phase controlling elements are an example of the type scanning mechanism envolved. Designs 6-11 of Table 3-1 are also representative of this group, although designs 10 and 11 also tend, in some ways, to be more representative of a true electronic scan system.

TABLE 3-1

SUMMARY

SCAN SYSTEM	ANTENNA TYPE	BEAM FORM	POLARITY	PKG SIZE	DWG NR.	GEOM.	NOTES
1	FOUR PARABOLIC $6\frac{1}{2}$" DIA ANTENNA	PENCIL 2°x2°	ANY	13" DIA X 10" HEIGHT	SK400238	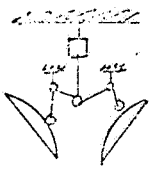	1) FOUR SEPARATE APERTURE OPERATE IN PAIRS OR AS A QUAD. 2) ELECTRICAL 1 TO 3 ROTARY JOINTS PER UNIT OR FLEX. 3) IN HOLE SYSTEM GIMBALED.
2	FLYSWATTER FOUR $6\frac{1}{2}$" DIA PARABOLAS LOOKING AT FLAT-PLATE DEFLECTOR	PENCIL BEAM 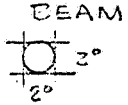 2°x2°	OPEN	$15\frac{1}{2}$" HIGH X 17" DIA	SK400238	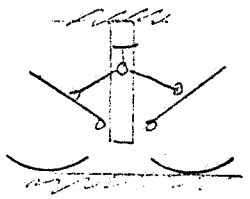	1) FOUR SEPARATE APERTURES OPERATES IN PAIRS OR AS QUAD. 2.) NO ROTARY JOINTS OR FLEX GUIDE REQ'D 3) WHOLE SYSTEM GIMBALED 4) SPILL OVER F.B. SEE'S THE SPACECRAFT.
3	FOLDED HORN FOLED PARABOLA. CORNUCOPIA	PENCIL BEAM ASYMMETRIC SIDE LOBES DUE TO COMA.	OPEN	20" DIA X 7" HIGH	SK400280	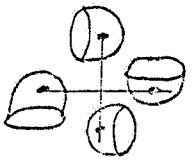	1) FOUR SEPARATE APERTURE PAIRED OR QUAD. 2) NO ROTARY JOINTS OR FLEX 3) WHOLE SYSTEM GIMBALED. 4) LOW BACK LOBES DUE TO VERY LOW SPILLOVER TO THE REAR.
4	FOUR FLARED HORNS FED BY ONE OR MORE LINE SOURCES	"BEAVER-TAIL" 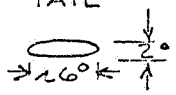	OPEN BUT HOR FAVORED BY FORM OF THE LINE SOURCE	6" DIA X 8" HIGH	SK400279 E 500218	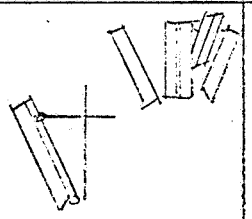	1) FOUR SEPARATE APERTURES PAIRED OR IN QUAD. 2) FLEX OR ROTARY JOINT REQ'D FOR EACH UNIT. 3) WHOLE SYSTEM GIMBALED. 4) FORWARD LOOK FAVORS LOW AFT SPILLOVER 5) VERY COMPACT.
POLARIZATION 5 SYSTEM	TWO DUAL POLARIZED HORNS (OR PARABOLA) & POLARIZATION SEPARTING GRATING	PENCIL	OPP, LOOKING BEAMS ORTHOGONALLY POLARIZED	12" HIGH X 24" WIDE X 24" LONG	SK400284	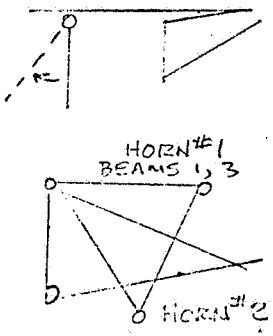	1) TWO APERTURE PAIRED BEAMS 2) NO FLEX GUIDE OR ROTARY JOINTS 3) SYSTEM GIMBAL REQ'D. 4) SPILL OVER & BACK LOBES DEPENDING ON SOURCES. 5) SIDE LOBES "SEE" STRUCTURE 6) TWO MOVING VANES ACCOMPLISH NECESSARY SCAN. 7) STRICT OPTICAL SYMMETRY ON OPPOSITE FACING BEAMS

TABLE 3-1
SUMMARY

SCAN SYSTEM	ANTENNA TYPE	BEAM FORM	POLARITY	PKG SIZE	DWG NR.	GEOM.	NOTES
LENSES 6	LUNEBURG LENS	PENCIL	OPEN IF TWO SOURCES USE POLARITY OF PAIRED BEAMS IS ORTHOGONAL	6" DIA X 7" HIGH (INCLUDES HDWR)		 6" DIA SPHERE	1) LUNEBERG LENS IS LOSSY (EFF SELDOM OVER 5-6 db DOWN) 2) POLARIZATION SEPARATION SCREENS MAY BE BUILT INTO LENS TO REDUCE NUMBER OF SOURCE HORNS AND CONTROL ASYMMETRY. 3) POOR SIDE LOBE AND BACKLOBE PERFORMANCE.
ELECTRO-MECH PHASE CONTROL 7	FLARED HORN & LINE SOURCE DIELECTRIC VANE	BEAVER TAIL	OPEN HORIZONTAL FAVORED	SMALL		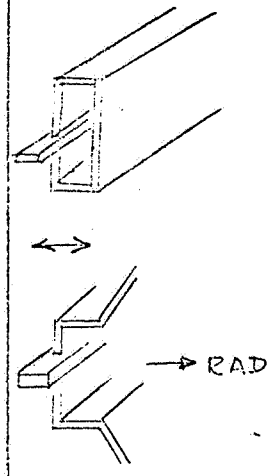	1) DIELECTRIC VANE MOVED INTO W/G SLOWS THE WAVE INSIDE OF GUIDE 2) BEAM SCANS TOWARD BROADSIDE FOR INCREASING DEPTH
8	METAL VANE					SAME AS ABOVE EXCEPT METAL VANE USED	1) METAL VANE DRIVEN INTO GUIDE INCREASES PHASE VELOSITY 2) BEAM SCANNED TOWARD END FIRE WITH INCREASING DEPTH
9	TOOTHED SLOTTED LINE					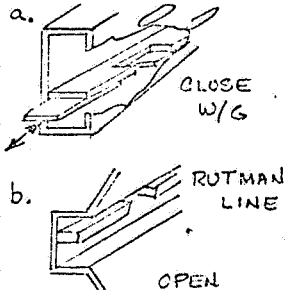	1) SLIDING VANE VARIES NOTCH WIDTH OF PHASE CONTROL STRUCTURE. 2) THE STRUCTURE GOES FROM FAST WAVE TO SLOW WAVE WITH MOTION OF VANE 3) ACTUAL BEHAVIOR DEPENDS ON DETAIL DESIGN.

TABLE 3-1
SUMMARY

SCAN SYSTEM	ANTENNA TYPE	BEAM FORM	POLARITY	PKG SIZE	DWG NR.	GEOM.	NOTES
10	MAGNETIC PERMEABILITY & PHASE CONTROL	BEAVER TAIL	OPEN (HORIZONTAL)	SMALL		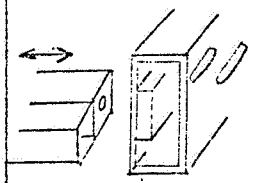	1) MAGNETIC FIELD POSITIVE NEAR FERRITE MATERIAL BY ELECTRO-MECHANICAL SYSTEM
11	SPECIFIC PERMITTIVITY PHASE CONTROL	BEAVER TAIL	OPEN (HORIZONTAL)	SMALL		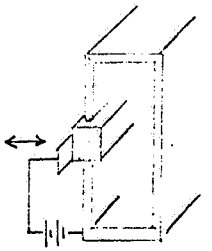	1) VOLTAGE STRESS OR BARIUM STRONTIUM TITANATE (OR SIMULAR MAT'L) VANE EFFECTIVE VALUE of ϵ. 2) POTENTIAL IN FIXED AND THE FIELD STRESS (V/ METER) CONTROLED ELECT MECHANICALLY

3.3 Electronic Scan

"Electronic" included frequency, permittivity, and switched line scanning. The beam is positioned through electrical control of the beam forming parameters of the radiators. In general, no mechanical motion is associated with a truly electronic system.

Data processing antennas are a special class of electronic scan. They do not exhibit a "beam", as such, but utilize broad beam elements and various kinds of circuitry to "process" the element outputs to extract the data sought. Adaptive systems require either a carrier or an *a priori* phase scheme in order to synthesize a response appropriate to the signal being received. Power Envelope coherence may substitute for signal phase coherence in radiometry applications.

4.0 RECOMMENDED SYSTEM

The antenna system selected as most appropriate for this application incorporates four small rectangular apertures. Figure 4-1 is a photograph of a full scale articulated model of this system using mockups of actual "off-the-shelf" electronic hardware.

4.1 Antenna Performance Characteristics

Antenna characteristics commonly used in evaluating an antenna design are:

a) Directivity

b) Gain

c) Aperture Efficiency

d) Antenna Efficiency

e) Beam Efficiency

These performance characteristics are seperately discussed for the purpose of clarifying their significance with respect to the specific design selected.

Directivity

Directivity or pattern gain is defined as the ratio of the maximum radiation intensity to the average radiation intensity.

$$D = \frac{4\pi}{W} = \frac{4\pi f(\theta,\phi)_{MAX}}{\int\int f(\theta,\phi) \sin\theta \, d\theta \, d\phi}$$

Where θ_3, ϕ_3 is used to designate the half-power beamwidth in radians then:

$$D \approx \frac{4\pi}{\theta_3 \phi_3}$$

Gain

Directivity takes no notice of the actual input power, only that in the radiation field. Gain compares the maximum radiation intensity to maximum radiation intensity of a lossless, matched reference antenna with the same power input. The reference antenna can be any type. The most common are the (1) half-wave dipole, (2) infinitessimal dipole, (3) the monopole and (4) the convenient, (but fictitious), isotropic radiator.

Gain is related to directivity by:

$$G = \eta D$$

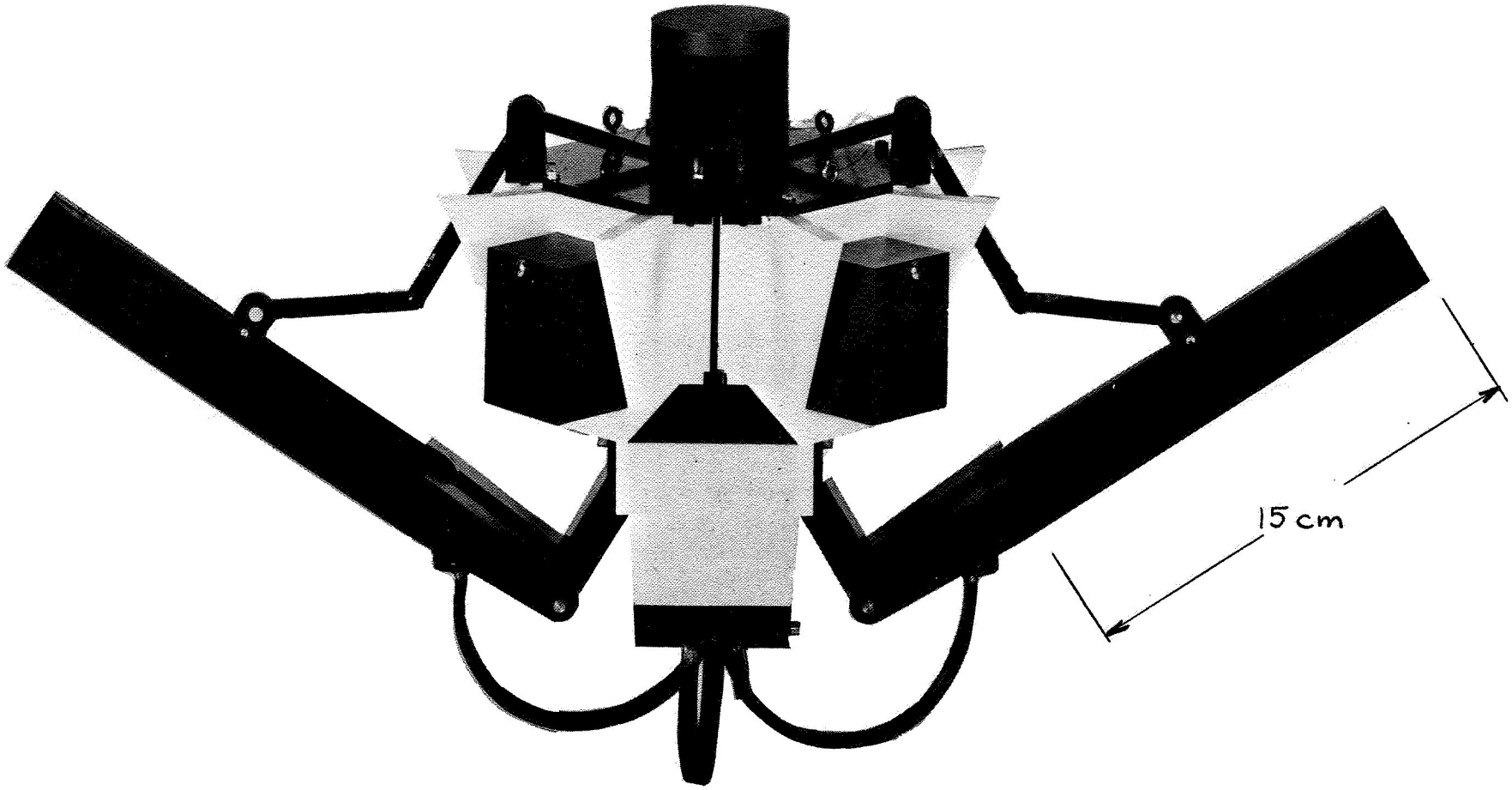

FIGURE 4-1

FORM MODEL SATELLITE HORIZON SENSOR

η is an efficiency number between 0 and 1, and includes the mismatch and heat losses in the antenna.

Aperture Efficiency

The aperture efficiency of an antenna is the ratio of the integral of the aperture illumination power distribution to the integral of a uniformly illuminated aperture of the same size and shape. Expressed mathematically:

$$\eta = \frac{\int_0^a \int_0^{2\pi} F(r, \phi)\, r\, dr\, d\phi}{\int_0^a \int_0^{2\pi} r\, dr\, d\phi}$$

where:

r, ϕ = the aperture radial and angle coordinates respectively.

a = the aperture radius.

Analogous expressions can be written for regtangular and other apertures. Typical values of η for the usual tapers of circular apertures are .50 to .65 (depending on the form of the taper and the edge illumination used). The effect of taper on the aperture distribution is illustrated in Figure 4-2.

Antenna Efficiency

By antenna efficiency is meant the ratio of the total power radiated in the collimated field to the total power delivered to the antenna terminals. This definition considers as loss all spill-over, blockage, scattering, heat (resistance), and mismatch return. This definition is often applied to communication satellite ground station antennas.

Beam Efficiency

In the case where an antenna has a single well defined major lobe, a figure-of-merit called "beam efficiency" is useful. It is not a true efficiency, and resembles directivity in that only elements of the collimated pattern enter into its definition.

Beam efficiency, η , is the ratio of the power within the contour of the first null (the main lobe to its nulls) to the power in the complete pattern.

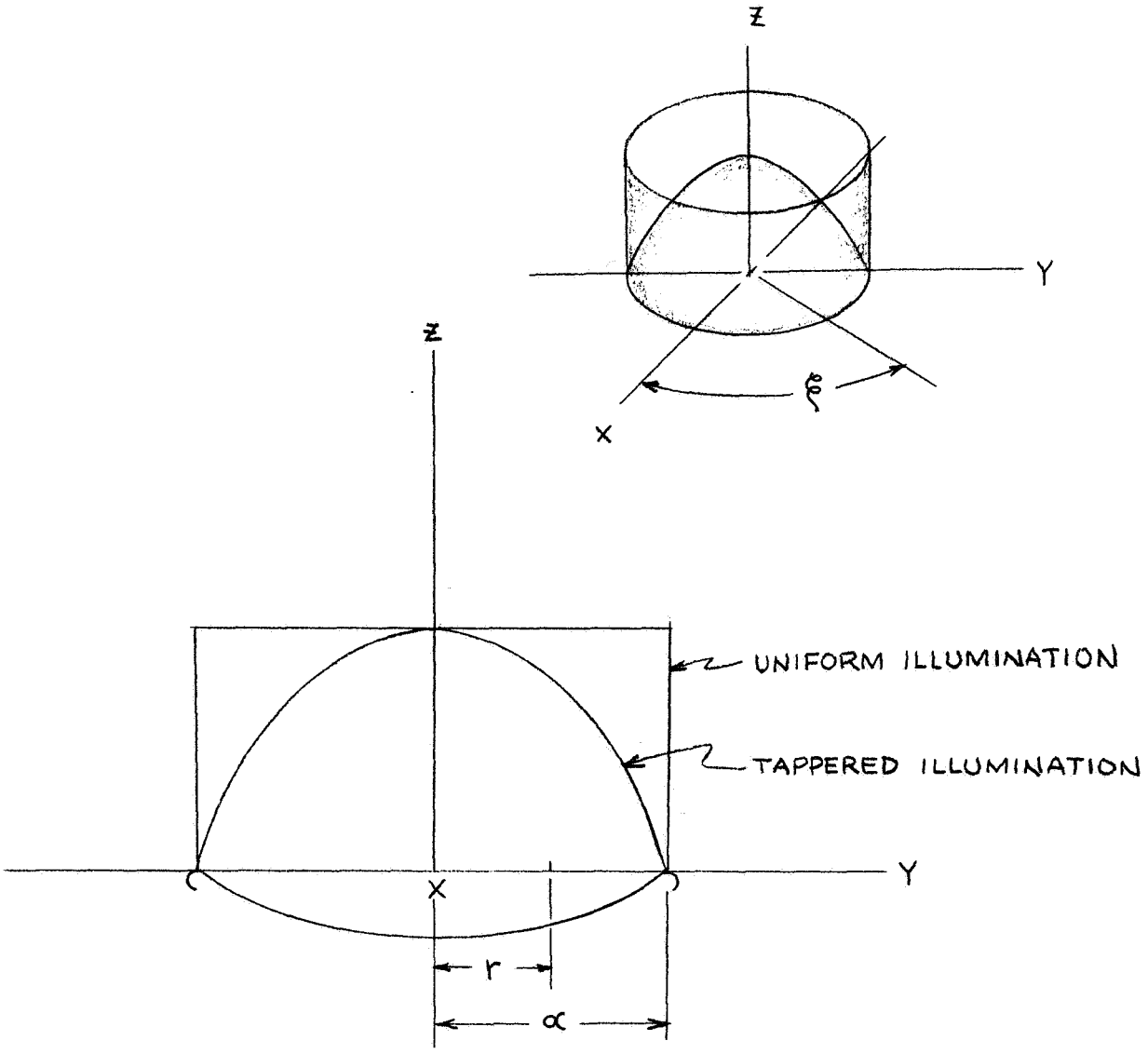

FIGURE 4-2

EFFECT OF TAPER ON APERATURE EFFICIENCY

In polar coordinates, Figure 4-3:

$$\eta_B = \frac{\int_0^{2\pi}\int_0^{\varphi_n} |E(\varphi,\varphi)|^2 \sin\varphi \, d\varphi \, d\varphi}{\int_0^{2\pi}\int_0^{\pi} |E(\varphi,\varphi)| \sin\varphi \, d\varphi \, d\varphi}$$

where the pattern is symmetrical about the Z axis.

$$\eta_B = \frac{\int_0^{\varphi_n} |E(\varphi)|^2 \sin\varphi \, d\varphi}{\int_0^{2\pi} |E(\varphi)|^2 \sin\varphi \, d\varphi}$$

Redefinition of Beam Efficiency for Rim Sensing Applications

The usual sense of beam efficiency in an antenna relates to the ratio of power in the main beam to its first nulls to the total power in the entire collimated pattern. However, here the value of a given antenna figure-of-merit is basically in its ability to evaluate the proposed designs in terms of the mission requirements, and not so much in comparing A to B, and B to C etc. The concept of beam efficiency given may not be as meaningful as one that compares power in the main lobe, its side lobes and the vertical side lobes along the rim to the total. This would compare that part of the pattern that "sees" the rim of the source to the total pattern including that portion which looks towards the source. Because of the low temperature of space, the upward looking lobes can be neglected.

Analytically:

$$\eta = \frac{\int_{-\frac{\pi}{2}}^{+\frac{\pi}{2}}\int_{-\varphi_n}^{+\frac{\pi}{2}} |E(\theta,\varphi)|^2 \, d\theta \, d\varphi}{\int_{-\frac{\pi}{2}}^{\frac{\pi}{2}}\int_{-\pi/2}^{\pi/2} |E(\theta)|^2 d\theta \, |E(\varphi)|^2 d\varphi}$$

$-\varphi_n$ = lower side of main lobe (first downward null)

where $E(\theta, \varphi)$ is a separable function (rectangular apertures)

$$\eta = \frac{\int_{-\frac{\pi}{2}}^{\frac{\pi}{2}} |E(\theta)|^2 d\theta \cdot \int_{-\theta_n}^{\pi/2} |E(\Phi)|^2 d\alpha}{\int_{-\frac{\pi}{2}}^{\frac{\pi}{2}} |E(\theta)|^2 d\theta \cdot \int_{-\pi/2}^{\pi/2} |E(\varphi)|^2 d\varphi} = \frac{\int_{-\varphi_n}^{\pi/2} |E(\alpha)|^2 d\varphi}{\int_{-\pi/2}^{-\pi/2} |E(\varphi)|^2 d\varphi}$$

The azimuth pattern disappears, and using finite differences:

$$\eta = \frac{\sum_{-\alpha_n}^{90^\circ} |E(\varphi)|^2 \Delta\varphi}{\sum_{-90^\circ}^{+90^\circ} |E(\varphi)|^2 \Delta\varphi}$$

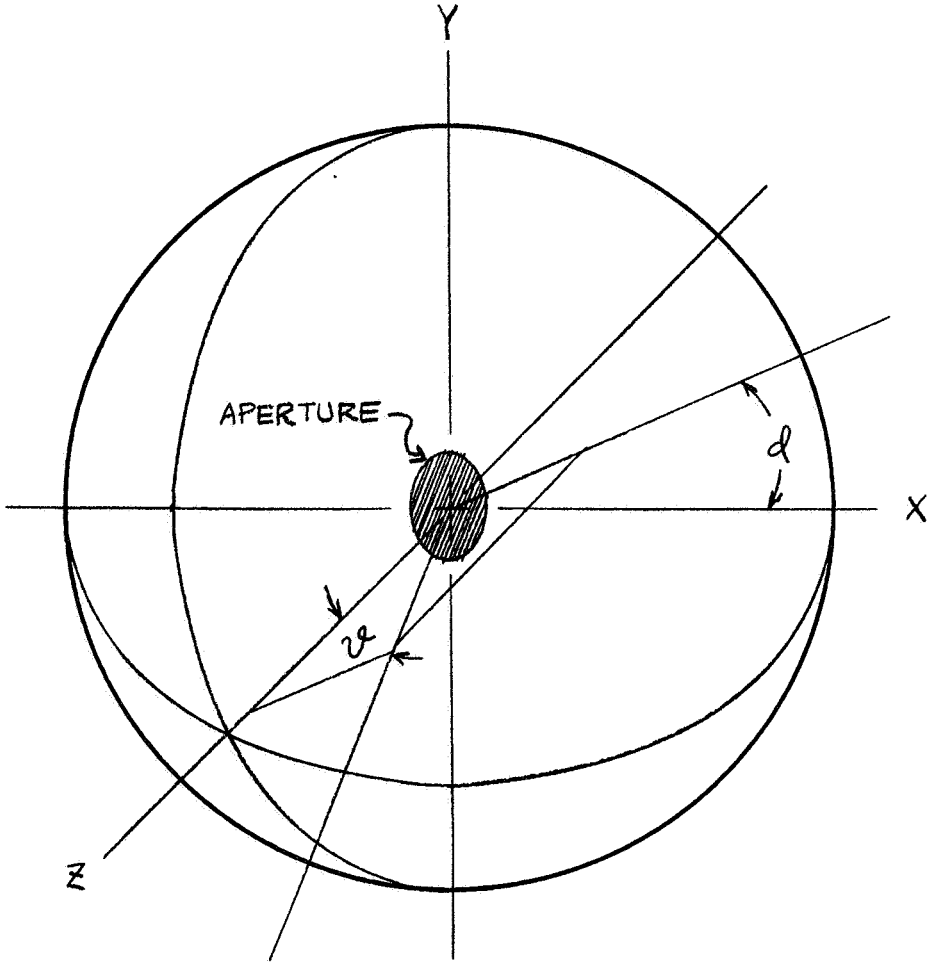

FIGURE 4-3

POLAR COORDINATE SYSTEM

Case 1 - Cosine Distribution:

$$E(\varphi) = \int_{-1}^{-1} \left|\cos\left(\frac{\pi\xi}{2}\right)\right| e^{j\nu\xi}\, d\xi$$

Case II - Cosine squared Distribution:

$$E_{(\varphi)} = \int_{-1}^{-1} \left|\cos^2\left(\frac{\pi\xi}{2}\right)\right| e^{j\nu\xi}\, d\xi$$

in both

$$\nu = \frac{\beta\ell}{2} \sin\varphi$$

Case I integrates to :

$$E(\varphi) = 2\,\frac{\pi/2\cos(\nu)}{(j\nu)^2 + (\pi/2)^2}$$

which normalized and V replaced:

$$E_{(\varphi)} = \frac{\pi^2 \cos\left(\frac{\beta\ell}{2}\sin\varphi\right)}{4\left(\frac{\pi}{2}\right)^2 - \left(\frac{\beta\ell}{2}\sin\varphi\right)^2}$$

$$\eta = \frac{\sum_{\varphi_n}^{90^\circ} \frac{\cos^2\left(\frac{\beta\ell}{2}\sin\varphi\right)}{\left[\frac{\pi}{2}^2 - \left(\frac{\beta\ell}{2}\sin\varphi\right)^2\right]^2}\Delta\varphi}{\sum_{\varphi_0}^{+90} \frac{\cos^2\frac{\beta\ell}{2}\sin\varphi}{\left[\left(\frac{\pi}{2}\right)^2 - \left(\frac{\beta\ell}{2}\sin\varphi\right)^2\right]^2}\Delta d}$$

The second case (cosine squared):

$$E_{(\varphi)} = \frac{\pi^2}{\pi^2 - \nu^2} \cdot \frac{\sin\nu}{\nu}$$

and:

$$\eta = \frac{\sum_{\varphi_n}^{90} \left[\frac{\sin\left(\frac{\beta\ell}{2}\sin\varphi\right)}{\pi^2\left(\frac{\beta\ell}{2}\sin\varphi\right)}\right]^2 \Delta d}{\sum_{-90}^{+90} \left[\frac{\sin\left(\frac{\beta\ell}{2}\sin\varphi\right)}{\pi^2 - \left(\frac{\beta\ell\sin\varphi}{2}\right)^2}\right] \Delta d}$$

The beam efficiency of an antenna with three parallel lines fed according to 1-2-1 power ratio with both cosine squared distributions was calculated using the conventional definition. These efficiencies were 89.2 and 90.1 respectively.

A simple argument leads to the conclusion that either of these configurations would be highly efficient as a rim cutting sensor.

Consider the cosine case; the first and second vertical sidelobes are - 23 and -30 db respectively, the first satellite lobes are -42 and -40 respectively. The highest level found off-axis elsewhere i -41 db. The others can be expected to be no greater than the next lower lobe -36 db combined, or -33 db including the third side lobe. The upper lobes contribute very little to the noise temperature since they are directed toward space.

The efficiency under these rules would be:

$$\eta = \frac{1 - \sum}{1 + \sum} \times 100 \text{ percent}$$

$\sum$ is the sum of all of the significant sidelobes below the main beam. Table 4-1 is a summary of the cosine and cosine squared cases based on the sidelobe level method just outlined.

4.2 Antenna Patterns

The original scheme used a sectoral horn with a small amount of orthogonal plane flare at the aperture. In order to conserve space, and reduce weight, a line source has been substituted for the sectoral horn resulting in the aperture shown in Figure 4-4 . The patterns are calculated by the separation method. Two versions each of vertical and horizontal illimunations were treated in the analysis.

Vertical	Horizontal
cosine	uniform
cosine squared	three element binary (1-2-1)

There are a variety of slot-type elementary radiators that could be used, but two are particularly suited - (1) the half-wave longitudinal slot, cut in the broad face of the waveguide, and (2) the angled slot cut in the narrow face. Since there is less mutual coupling with the essentially end-to-end longitudinal slots, it was chosen for the demonstration analysis. The use of longitudinal slots results in horizontal polarization.

The sort of pattern this antenna produces is shown in Figure 4-5 in contour form oriented with the broad dimension along the line of tangency to the source.

TABLE 4-1

EFFECTIVE BEAM EFFICIENCY

LOBE	COSINE		COSINE SQUARED	
	DB	ABS	DB	ABS
Main Lobe	0	1.00	0	1.00
First Sidelobe	-23	.005	-31.5	.000706
2nd S.L.	-30	.001	-41.5	.000071
3rd & higher S.L.	-33	.0005	-45.5	.000028
1st Satellite Lobe	-42	.00006	-46.5	.000022
2nd Satellite Lobe	-40	.0001	-48.5	.000014
$\sum$		.00666		.000841
η		98.68%		99.98%

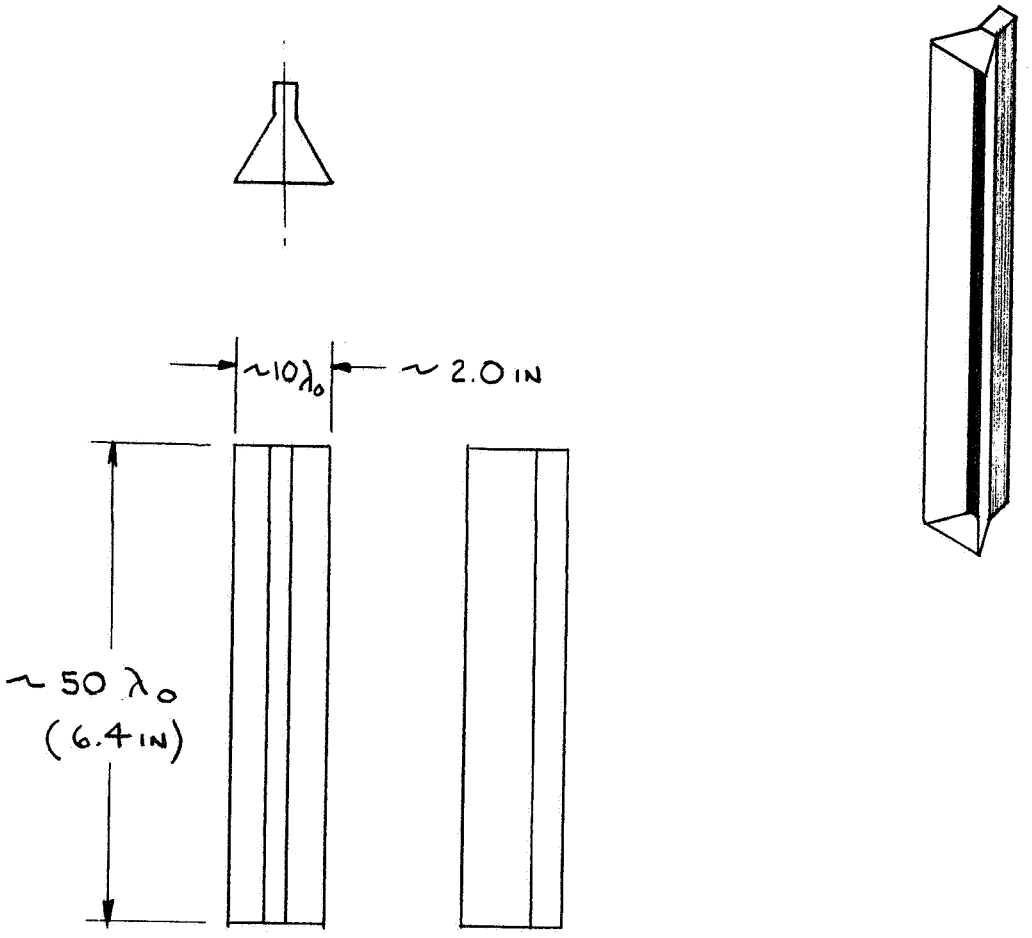

FIGURE 4-4
LINE SOURCE AND FLARED HORN
RECTANGULAR APERTURE ANTENNA

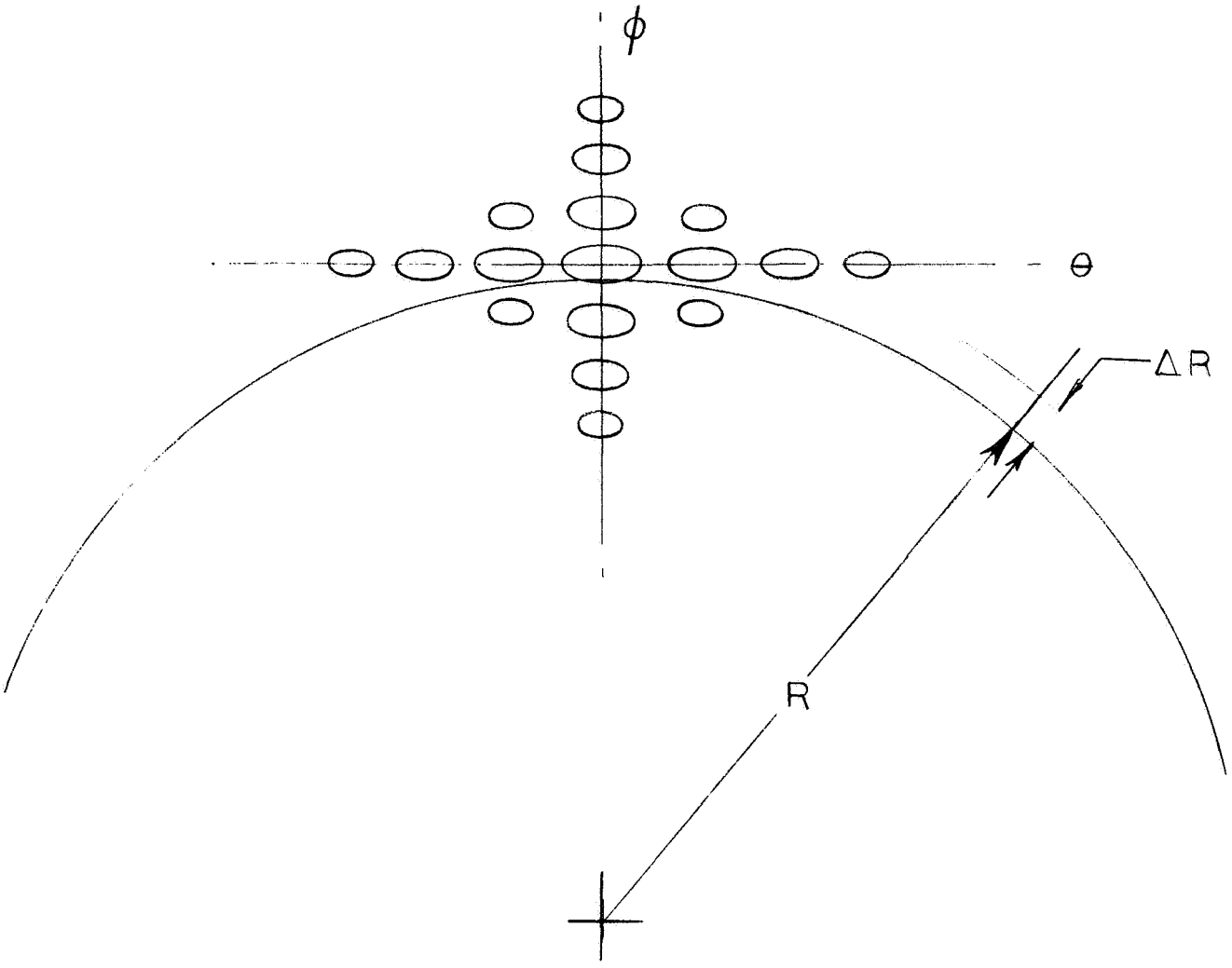

FIGURE 4-5
CONTOUR PATTERN PROJECTED ON
THE LIMB OF THE SPHERICAL SOURCE

The general form of the pattern equation[26] is:

$$E_{(u,v)} = \int_{a_1}^{a_2} \int_{b_1}^{b_2} F(\xi,\eta)\, e^{ju\xi}\, e^{jv\eta}\, e^{-j\Phi(\xi)}\, e^{j\Phi(\eta)}\, d\xi\, d\eta$$

where u, v the spacial coordinates of the pattern.

$a_1, a_2; b_1, b_2$ are the aperture limits.

ξ, η the aperture coordinates.

$\Phi(\xi)$, $\Phi(\eta)$ are phase distributions

and,

$$u = \beta \ell_\xi \sin\left(\frac{\pi}{2}\xi\right)$$

$$v = \beta \ell_\eta \sin\left(\frac{\pi}{2}\eta\right)$$

$F(\xi,\eta)$ is the aperture distribution.

The equation can be very much simplified if certain conditions hold. In the coordinates of Figure 4-6 (u,v) are identified with (θ, ϕ) and (ξ, η) with (x, y). $(a_2\ a_1)$ and (b_2, b_1) correspond to $(+\frac{\ell_x}{2}, -\frac{\ell_x}{2})$ and $(+\frac{\ell_y}{2}, -\frac{\ell_y}{2})$. For rectangular apertures and certain others the distribution F can be separated into the product of two distributions on orthogonal coordinates; that is, they are independent. The specific form is:

$$E(\theta,\phi) = \frac{\ell_x}{2} \cdot \frac{\ell_y}{2} \int_{-1}^{+1} \int_{-1}^{+1} F_{(x)}\, F_{(y)}\, e^{j(ux - \Phi_{(x)})}\, e^{j(vy - \Phi_{(y)})}\, dy\, dx$$

This further separates into:

$$E(\theta,\phi) = E(\theta) \cdot E(\phi) = \left[\frac{\ell_y}{2} \int_{-1}^{1} F(y)\, e^{jvy - j\Phi(y)}\, dy\right] \cdot \left[\frac{\ell_x}{2} \int_{-1}^{1} F_{(x)}\, e^{jux - j\Phi(y)}\, dx\right]$$

The pattern can now be computed by specifying $F_{(x)}, \Phi_{(x)}, F_{(y)}, \Phi(y)$ for each integral and taking the product of the result separately arrived at. The cases where $F(y) = 1$ and $F(x) = \text{cosine}\left(\frac{\pi}{2} x\right)$ and $\Phi_{(x)} = \Phi_{(y)} = 0$ were calculated.

The first integral is:

$$E_{(\phi)} = \frac{\ell_y}{2} \int_{-1}^{1} F_{(y)}\, e^{jvy}\, dy = \frac{\ell_y}{2} \left(\frac{e^{jvy}}{jv}\right) \Bigg|_{-1}^{1}$$

$$= \ell_y \left[\frac{e^{+jv} - e^{-jv}}{2jv}\right] = \ell_y \frac{\sin v}{v}$$

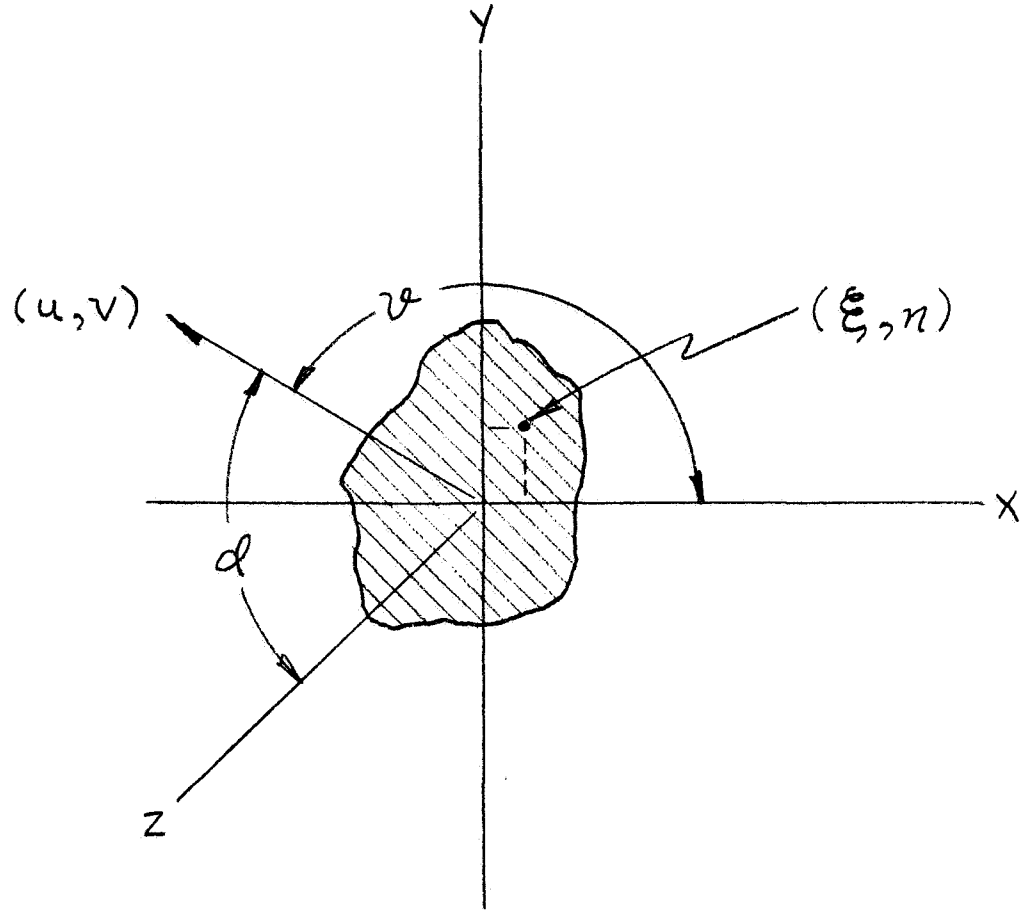

FIGURE 4-6

RELATIONS AMONG X, Y & Z; α, ν; μ, ν AND ξ, η FOR A GENERALIZED APERTURE

The second integral is:

$$E(\alpha) = \frac{\ell_x}{2} \int_{-1}^{1} \cos\left(\frac{\pi x}{2}\right) e^{jux}\, dx$$

$$= \frac{\ell_x}{2} \left[\frac{e^{jux}\, ju\cos\left(\frac{\pi}{2}x\right) + \frac{\pi}{2}\sin\left(\frac{\pi}{2}x\right)}{\frac{\pi^2}{4} - u^2} \right]_{-1}^{+1}$$

$$= \frac{\ell_x}{2} \cdot \frac{\pi}{2} \cdot \left[\frac{e^{ju} + e^{-ju}}{\frac{\pi^2}{4} - u^2} \right] = \frac{\pi}{2} \cdot \frac{\ell_x}{\frac{\pi^2}{8} - u^2} \cos u$$

$$E(\theta, \alpha) = E(\theta) \cdot E(\alpha) = \ell_y \frac{\sin v}{v} \cdot \frac{\pi \ell_y \cos u}{2\left(\frac{\pi^2}{4} - u^2\right)}$$

$$u = \beta \frac{\ell_x}{2} \sin\alpha$$

To normalize to the peak of the pattern the values of θ & α were set to (0, 0) and $\frac{E(\theta, \alpha)}{E(\theta, 0)}$ evaluated.

$$E(0,0) = \frac{\ell_y \ell_x}{\frac{\pi^2}{4}} \cdot \frac{\pi}{2} = \frac{\pi \ell_x \ell_y}{2}$$

$$\frac{E(\theta\alpha)}{E(0,0)} = \frac{4}{\pi^2} \cdot \frac{\sin v}{v} \cdot \frac{\cos u}{\left(\frac{\pi^2}{4} - u^2\right)}$$

Patterns for the cosine and cosine squared vertical distribution were calculated. Figure 4-7 is a plot of the first 10° of the cosine case, and Figure 4-8 is the same region for the cosine squared distribution. Complete pattern data from zero to ninety degrees are given on the Tables A1 and A2, in Appendix A-A.

The azimuth plane pattern for the uniform was not plotted since it is $\frac{\sin x}{x}$, and tables and graphs have been published many times (Reference 17 and 23, for example). Figure 4-9 is a plot of the case where three parallel lines are fed according to a 1-2-1 power ratio. The sources radiate into a constrained region which modified the patterns. The 3 db beamwidth was set to 6° by adjusting the flared horn width to 4.437 cm (1 3/4 inches). The calculated data for the pattern is contained in Appendix A-A.

The off-axis patterns for a rectangular aperture can be obtained by multiplying the principle plane patterns together.

Figure 4-10 is a contour plot of the cosine and uniform illumination case down to -30 db. The horizontal sidelobes have secondary vertical sidelobes of their own, but only the first (-13.2 db) azimuth lobe has a satellite lobe over - 40 db. (-36.3 db). The data

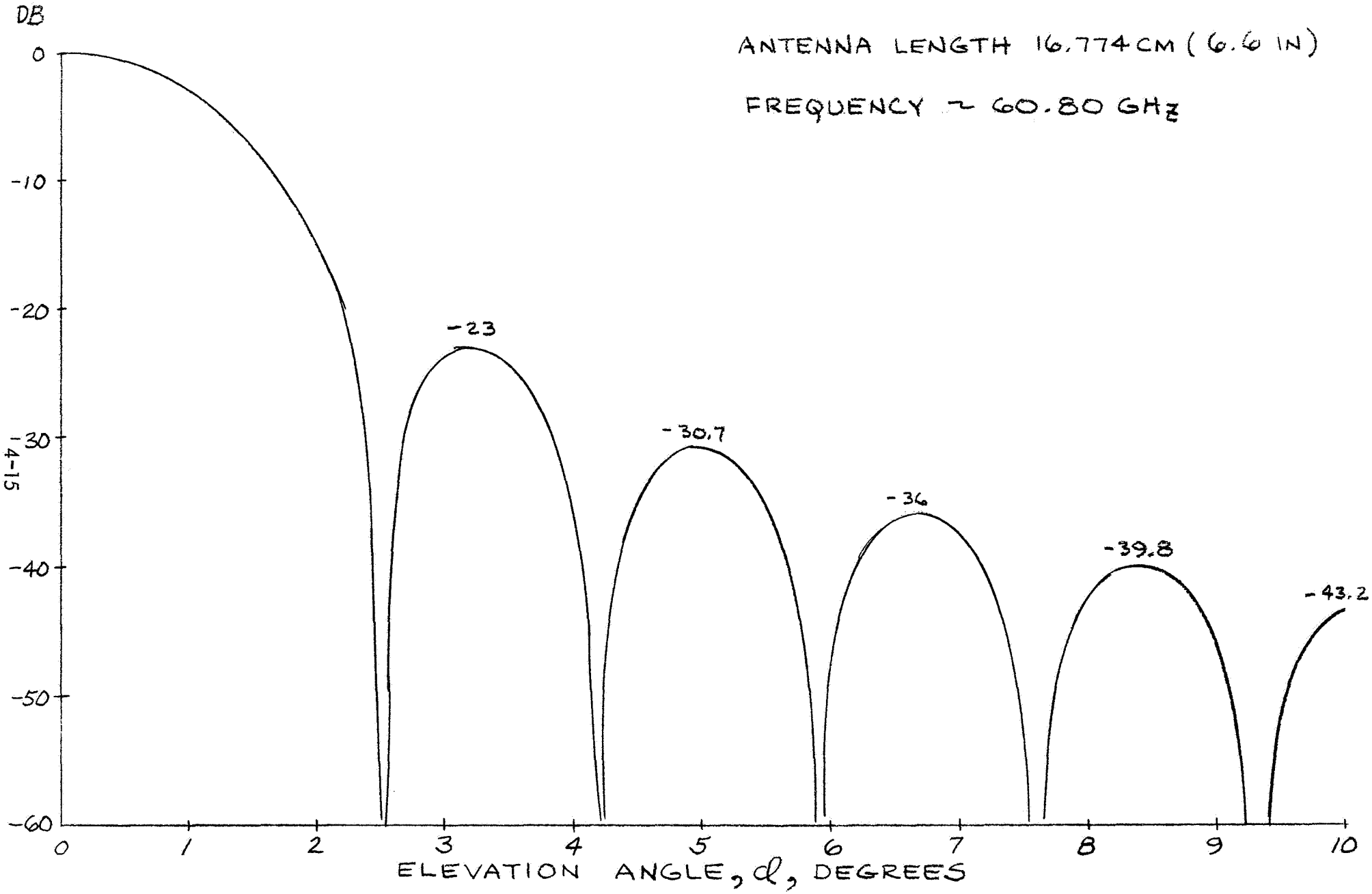

FIGURE 4-7

ELEVATION PLANE PATTERN COSINE ILLUMINATION

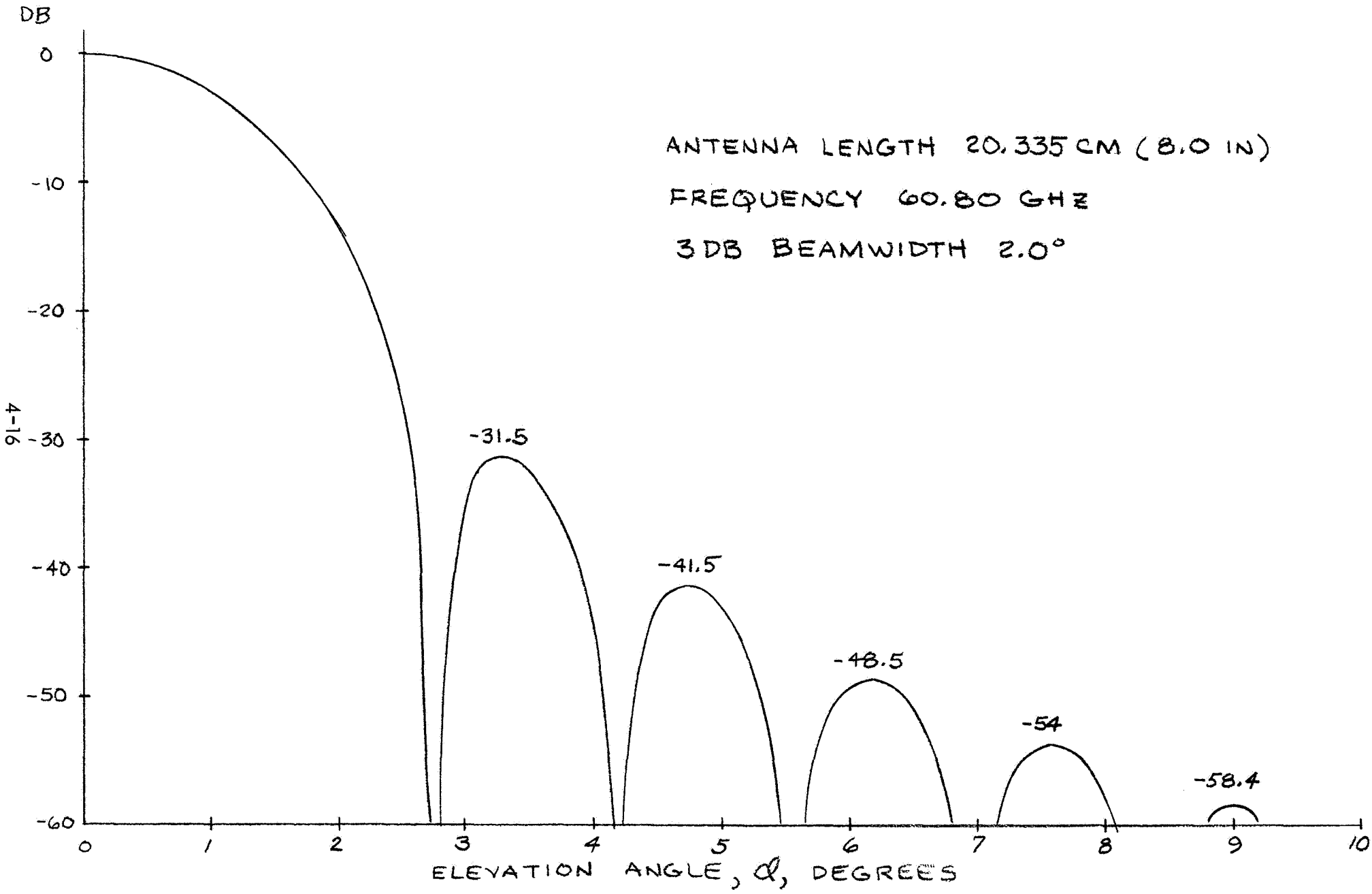

FIGURE 4-8

ELEVATION PLANE PATTERN COSINE SQUARE ILLUMINATION

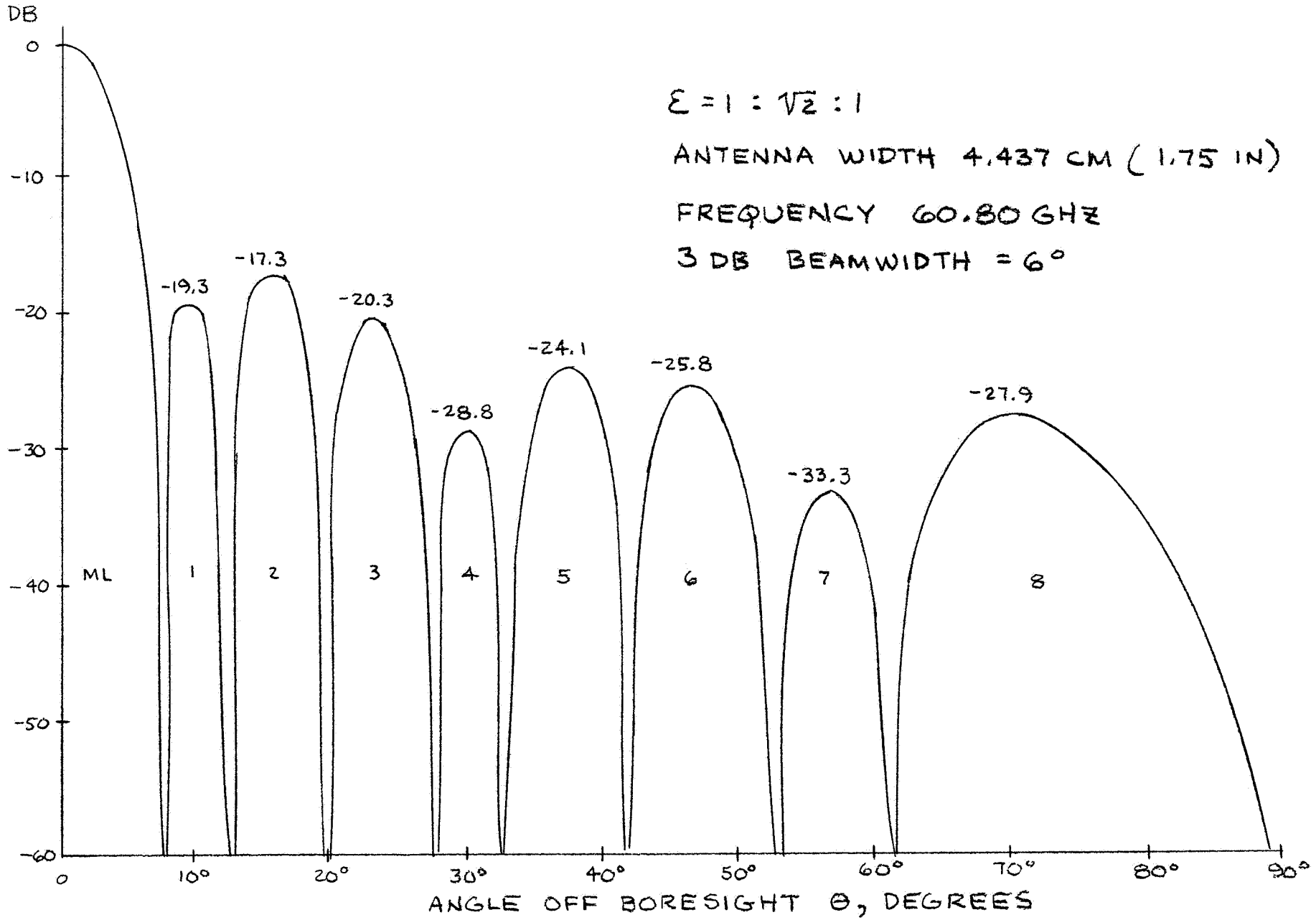

FIGURE 4-9
AZIMUTH PLANE PATTERNS FLARED HORN
EXCITED BY THREE LINE SOURCES FED.

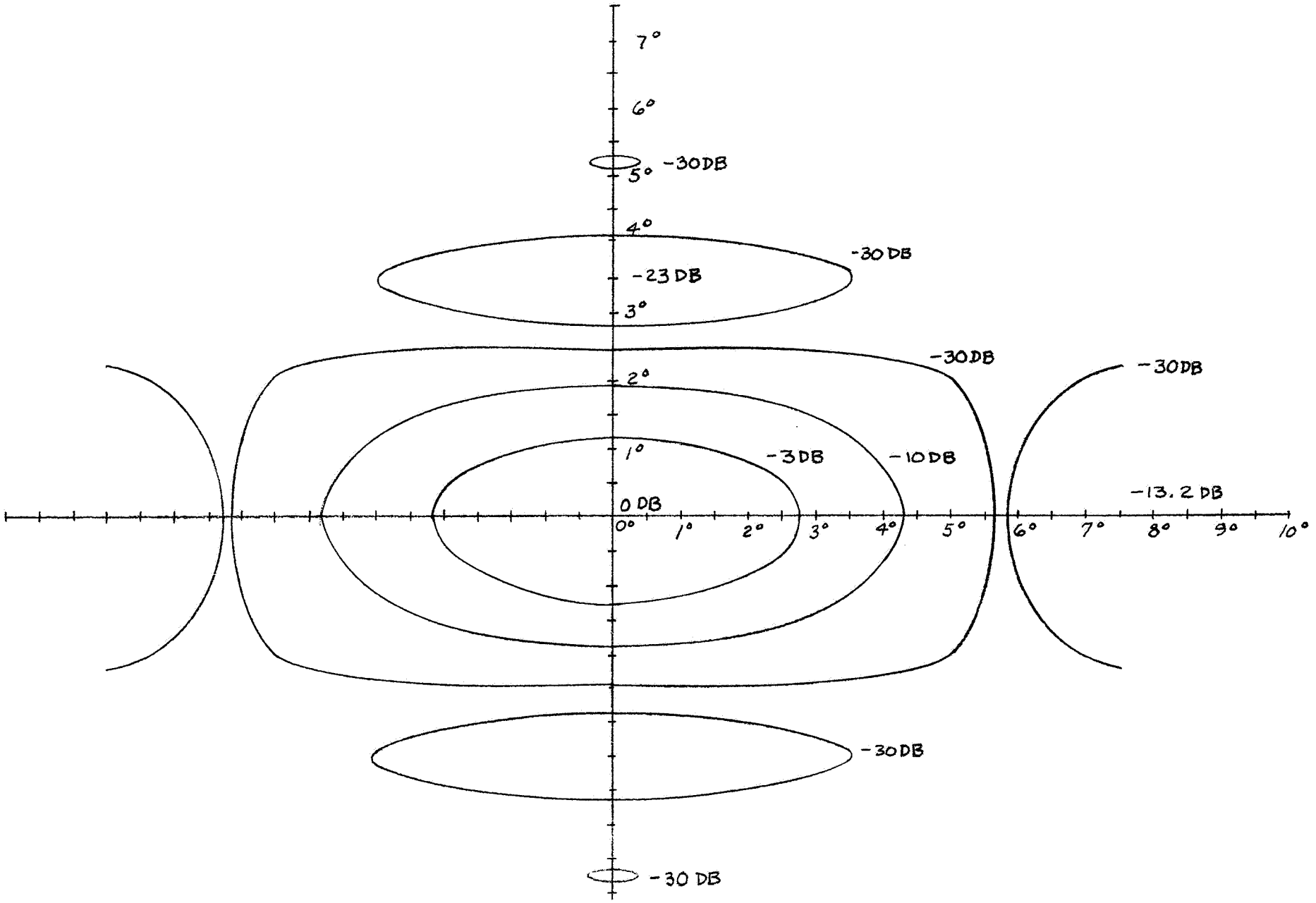

FIG 4-10 POWER PATTERN CONTOURS VERT. DISTRIBUTION COSINE HOR. DISTRIBUTION UNIFORM F=60.80

for the plot of Figure 4-10 was taken from Table A-A-4, Appendix A-A. The calculations of Table A-A-4 were done fairly early in the study, and while representative of the field of a rectangular aperture antenna, are not quite in agreement with the data of the final configuration.

4.3 Element Offset in a Line Source Array

The wave in a traveling wave line source is usually introduced at one end, and each element in turn extracts energy from the field according to some rule such that a prescribed illumination is achieved. The illumination function is usually one of the cosine series (cosine or cosine squared). As each element in the line extracts its assigned portion the power is attenuated along the line and coupling of the succeeding elements must be increased accordingly.

If there are N elements distributed uniformly along the length of a waveguide L units long, the element to element spacing is:

$$S = \frac{L}{N-1}$$

The intensity of the field at each point is dictated by the taper - usually one of the cosine forms. For the simple cosine function:

$$E_1 = \frac{|\sin n\xi|}{\sum_{n=1}^{N} |\sin n\xi|}$$

$$\xi = \frac{\pi S}{L} = \frac{\pi}{N-1}$$

The intensity of the field across the waveguide varies with the width as:

$$\cos\left(\frac{\pi X}{W}\right)$$

W = width of the interior of the guide.

X = distance from the center line.

The susceptance of a longitudinal slot, however, varies from zero at the center to unity at the edge. The product has a maximum somewhere between the center and the edge, and:

$$E = G\left(\frac{X}{W}\right)\cos\left(\frac{\pi X}{W}\right)$$

The transverse fields of the TE m,n modes are:

$$TE_X = H_X = \frac{m\pi e^{-r_{m,n} z}}{k^2_{m,n}\, a} \sin\left(\frac{m\pi x}{a}\right)\cos\left(\frac{n\pi y}{b}\right)$$

If the guide is amplified:

$$k_{m,n} = 1$$

$$\gamma_{m,n} z = \beta_{m,n} z$$

Since only the transverse field is of interest here; the dominant mode ($TE_{1,0}$) is considered. The normalized field is:

$$E = SIN\left(\frac{\pi x}{a}\right) \cdot \cos SIN\left(\frac{\pi x}{a}\right)$$

For purposes of positioning slots it is convenient to take the origin at the center-line of the guide.

$$E = \cos\left(\pi \frac{x}{a}\right)$$

The range of x is $0 < x < \frac{a}{2}$

The conductance g is given for a resonant slot by:

$$g = 2.09 \frac{\lambda g}{\lambda o} \cos^2\left(\frac{\pi \lambda_o}{2 \lambda g}\right) \cdot SIN^2\left(\frac{\pi x}{a}\right)$$

The voltage at the slot is then:

$$E_s = E \text{ guide} \cdot g$$

$$E_s = \cos\left(\frac{\pi x}{a}\right) \cdot SIN^2\left(\frac{\pi x}{a}\right)$$

$$A_{-a} \text{ constant} = 2.09 \cdot \frac{\lambda g}{\lambda_o} \frac{a}{b} \cos^2\left(\frac{\pi \lambda_o}{2 \lambda g}\right)$$

Figure 4-11 is a plot of E_S vs distance $\frac{x}{a}$ from the center line of the guide for WR-15 guide at 60.80 GHz.

Since g= 0, $\frac{x}{a} = 0$, and $E_g = 0, \left(\frac{x}{a}\right) = .5$, by Rolle's Theorem, there exists a maximum, (or a minimum).

$$\frac{d E_s}{d\left(\frac{x}{a}\right)} = \frac{d}{d \frac{x}{a}} \left[A \cos\left(\frac{\pi x}{a}\right) \cdot SIN^2\left(\frac{\pi x}{a}\right)\right]$$

$$\frac{d E_s}{d\left(\frac{x}{a}\right)} = A\pi\left(-SIN^3\left(\frac{\pi x}{a}\right) + 2\cos^2\left(\pi \frac{x}{a}\right) \cdot SIN\left(\frac{\pi x}{a}\right)\right)$$

$$2\cos^2\left(\pi \frac{x}{a}\right) - SIN^2\left(\frac{\pi x}{a}\right) = 0$$

For the case given this occurs when $\frac{x}{a} = .301633$.

There is a maximum offset beyond which there is less coupling, and in some long arrays or very flat taper cases this limit is reached rather quickly. Once the limit is reached,

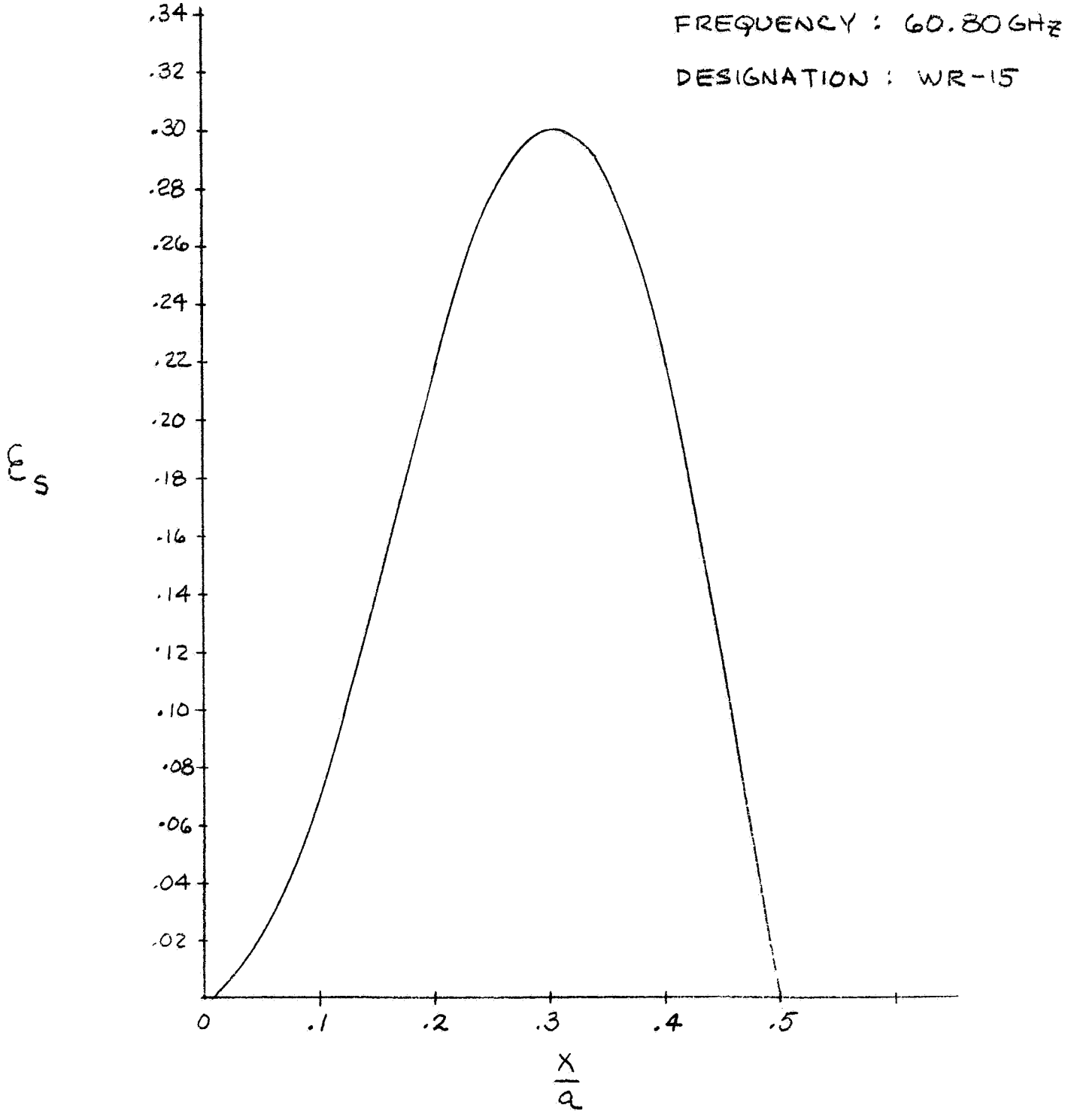

FIGURE 4-11

SLOT VOLTAGE VS DISTANCE OF SLOT FROM W/G CENTERLINE FOR RESONANT LONGITUDINAL SLOT

the illumination departs from the prescribed taper, and decays exponentially at a rapid rate. Such an array is self-truncated.

The detail design of the radiator for the cosine tapered case is shown in Figure 4-12. The E-plane (azimuth) distribution is binomial (1-2-1), and can be fed by a simple corporate structure. In the H-plane (elevation) distribution the first slot is less than a hundred thousandth of an inch off the center line, while the last six are at the maximum deviation. The distribution calls for 71 slots, but only about 66 contribute to the pattern. A long array such as this can be made by electrophotographic milling. A somewhat simple method of fabrication would be to break-up the array into three or four subarrays fed in parallel.

Figure 4-13 is the corresponding design data for the cosine squared taper line source antenna. Although the taper beamwidths requirement (Cos^2, 2°, at 3 db) calls for 85 slots, only about 63 are functional. An antenna of this sort would not be made in a single piece, but rather in segments individually designed. Each segment would require a secondary feed system of their own.

4.4 Mechanical Configuration

The mechanical configuration of the sensor package that yields the lowest weight and smallest size, yet meets the specifications is shown in Figure 4-14.

The form is generally that of an inverted truncated octagonal pyramid with the four antennas arranged 90° around the faces from one another.

4.4.1 RF Coupling

The coupling of energy from the movable antenna to the receiver requires some sort of articulated line capable of transmitting 60 GHz waves. Three forms were investigated in terms of insertion loss, VSWR, WOW (differential VSWR), and generalized ranking as to cost. These were (1) commercially available rotary joints, (2) oversize guide, and (3) a special surface wave coupling device.

Rotary Joints

Rotary joints are described in the catalogs of several companies. Typical values for $TE_{0,1}$ mode rotary joint was insertion loss .3 db and VSWR of 1.1:1. Rotary joints should be regarded as a well-known, but high cost solution to the flexible line problem.

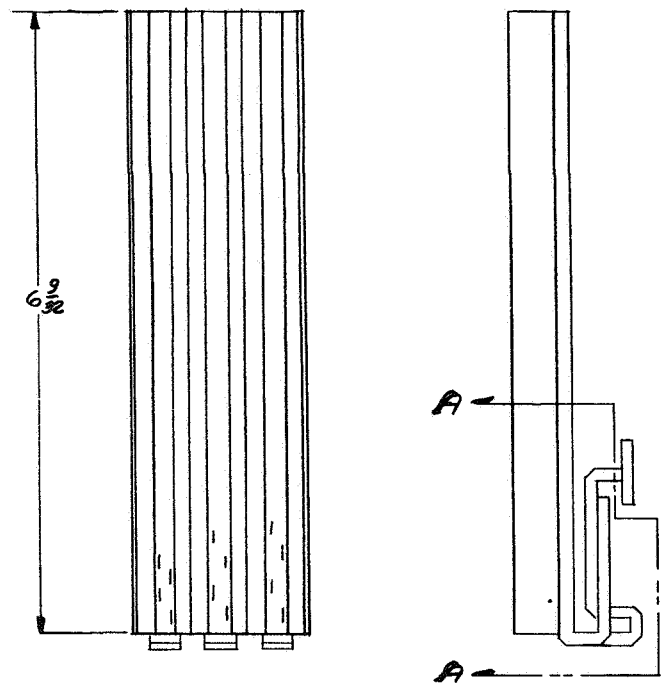

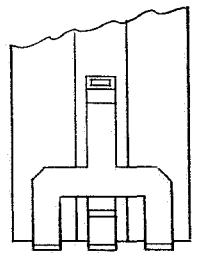

VIEW A-A
POWER DIVIDER NETWORK

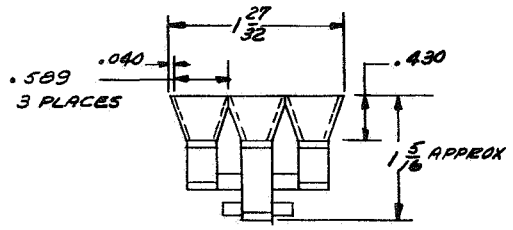

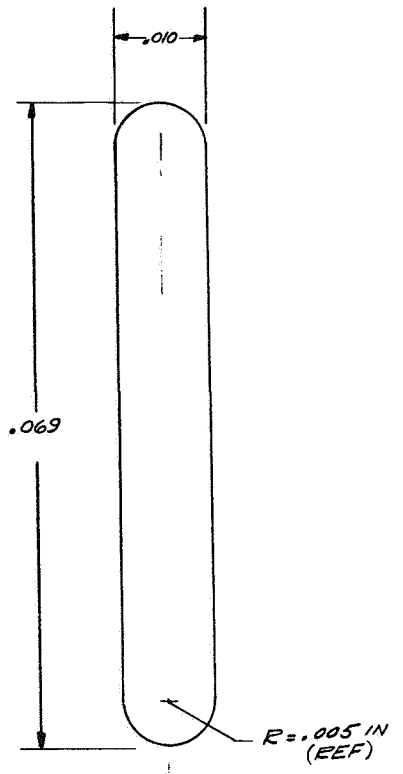

SLOT DETAIL

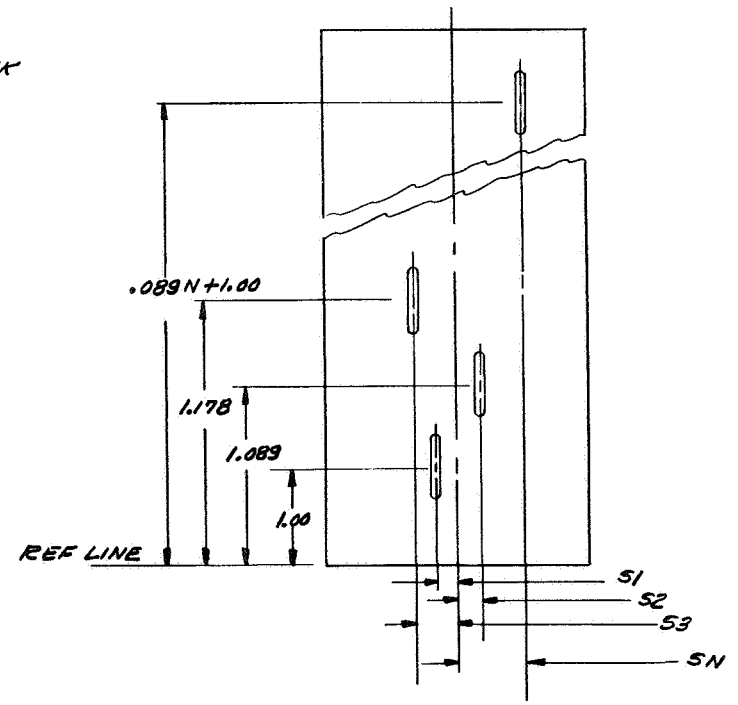

OFFSET & SPACING DETAIL

NOTE:
FOR OFFSETS OF ALL SLOTS
SEE "TABLE OF OFFSETS"

WAVEGUIDE ARRAY OF RESONANT LONGITUDINAL SLOTS
TABLE OF OFFSETS

NUMBER OF SLOTS = 71 LONGITUDINAL SPACING = .1287 IN.

ILLUM FUNCTION--COSINE FREQ = 60.80 GHz

NOTE: * INDICATES MAXIMUM DEVIATION FROM CENTERLINE

SLOT NUMBER	OFFSET IN INCHES
1	0.00000
2	.00222
3	.00237
4	.00296
5	.00333
6	.00370
7	.00407
8	.00444
9	.00474
10	.00518
11	.00533
12	.00562
13	.00592
14	.00614
15	.00636
16	.00666
17	.00688
18	.00710
19	.00740
20	.00755
21	.00777
22	.00814
23	.00829
24	.00851
25	.00873
26	.00895
27	.00918
28	.00940
29	.00962
30	.00992
31	.01014
32	.01036
33	.01066
34	.01088
35	.01117
36	.01140
37	.01169
38	.01199
39	.01228
40	.01258
41	.01288
42	.01325
43	.01354
44	.01391
45	.01428
46	.01473
47	.01510
48	.01554
49	.01598
50	.01650
51	.01702
52	.01761
53	.01828
54	.01894
55	.01968
56	.02057
57	.02153
58	.02257
59	.02383
60	.02531
61	.02716
62	.02945
63	.03263
64	.03781
65	.04464*
66	.04464*
67	.04464*
68	.04464*
69	.04464*
70	.04464*
71	.04464*

FIGURE 4-12

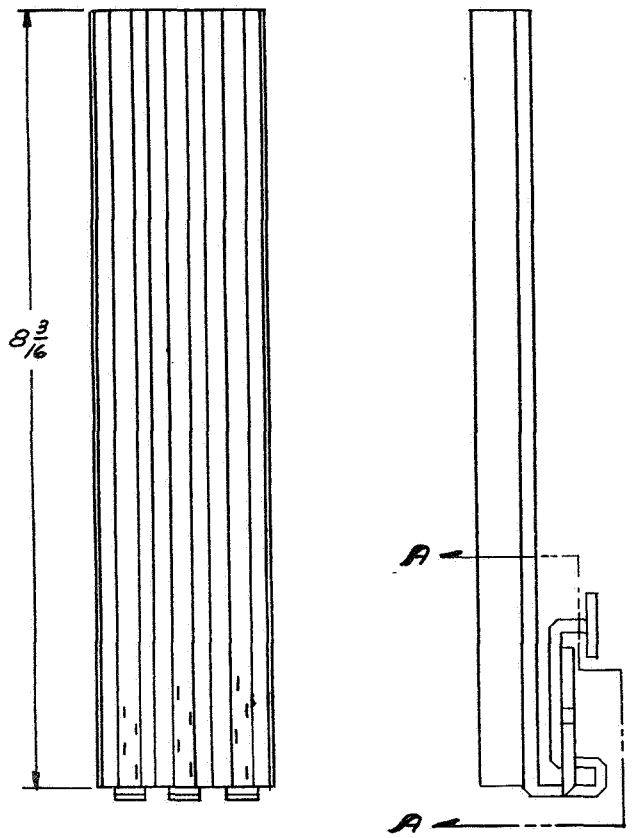

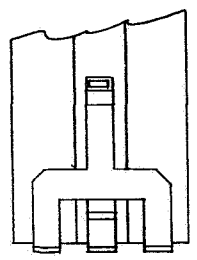

POWER DIVIDER NETWORK

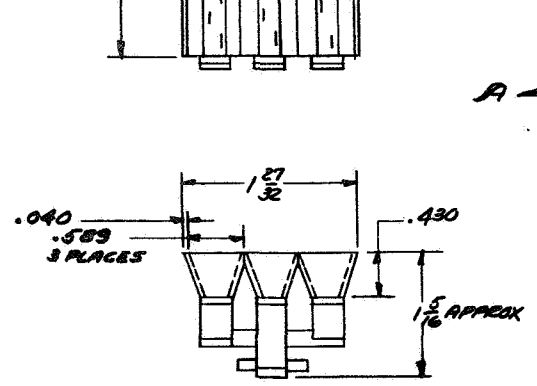

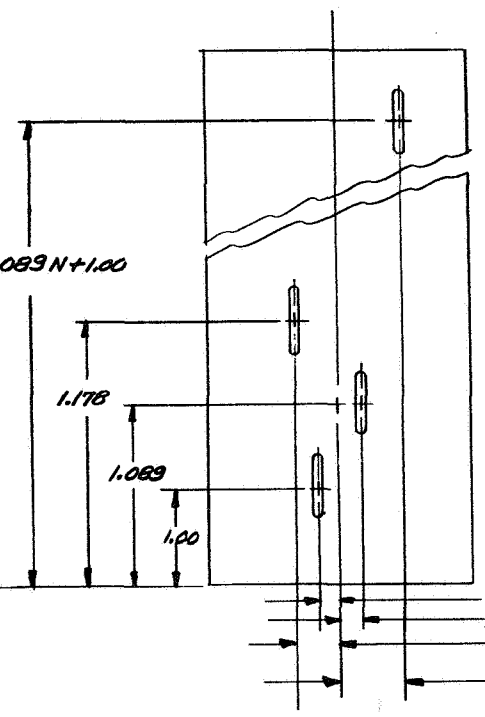

OFFSET & SPACING DETAIL

NOTE: FOR OFFSETS OF ALL SLOTS SEE "TABLE OF OFFSETS"

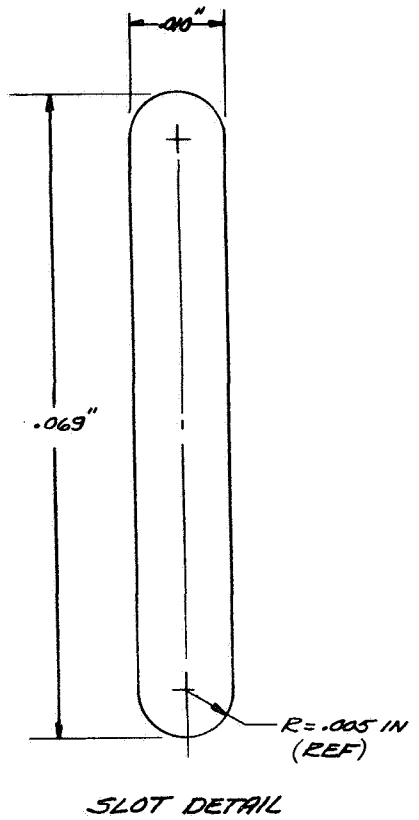

SLOT DETAIL

WAVEGUIDE ARRAY OF RESONANT LONGITUDINAL SLOTS
TABLE OF OFFSETS

NUMBER OF SLOTS = 85 LONGITUDINAL SPACING = .1287 IN.

ILLUM FUNCTION--COSINE SQUARED FREQ. = 60.80 GHz

NOTE: • INDICATES MAXIMUM DEVIATION FROM CENTERLINE

SLOT NUMBER	OFFSET IN INCHES
1	0.00000
2	0.00000
3	0.00000
4	0.00000
5	0.00000
6	.00074
7	.00148
8	.00222
9	.00222
10	.00244
11	.00296
12	.00311
13	.00370
14	.00370
15	.00400
16	.00444
17	.00459
18	.00488
19	.00518
20	.00548
21	.00592
22	.00599
23	.00629
24	.00666
25	.00681
26	.00710
27	.00740
28	.00762
29	.00792
30	.00821
31	.00844
32	.00873
33	.00903
34	.00925
35	.00962
36	.00984
37	.01006
38	.01036
39	.01066
40	.01095
41	.01125
42	.01154
43	.01184
44	.01214
45	.01243
46	.01280
47	.01310
48	.01339
49	.01376
50	.01413
51	.01450
52	.01487
53	.01524
54	.01569
55	.01606
56	.01650
57	.01702
58	.01746
59	.01798
60	.01859
61	.01909
62	.01968
63	.02035
64	.02109
65	.02183
66	.02264
67	.02361
68	.02464
69	.02583
70	.02716
71	.02879
72	.03071
73	.03315
74	.03663
75	.04464*
76	.04464*
77	.04464*
78	.04464*
79	.04464*
80	.04464*
81	.04464*
82	.04464*
83	.04464*
84	.04464*
85	.04464*

FIGURE 4-13

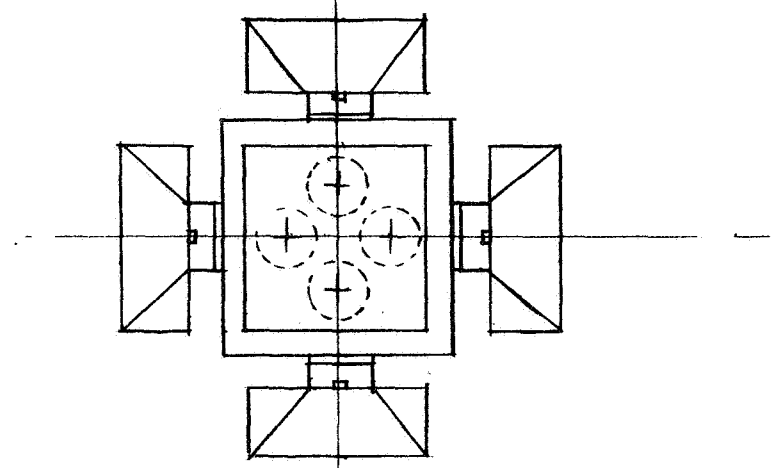

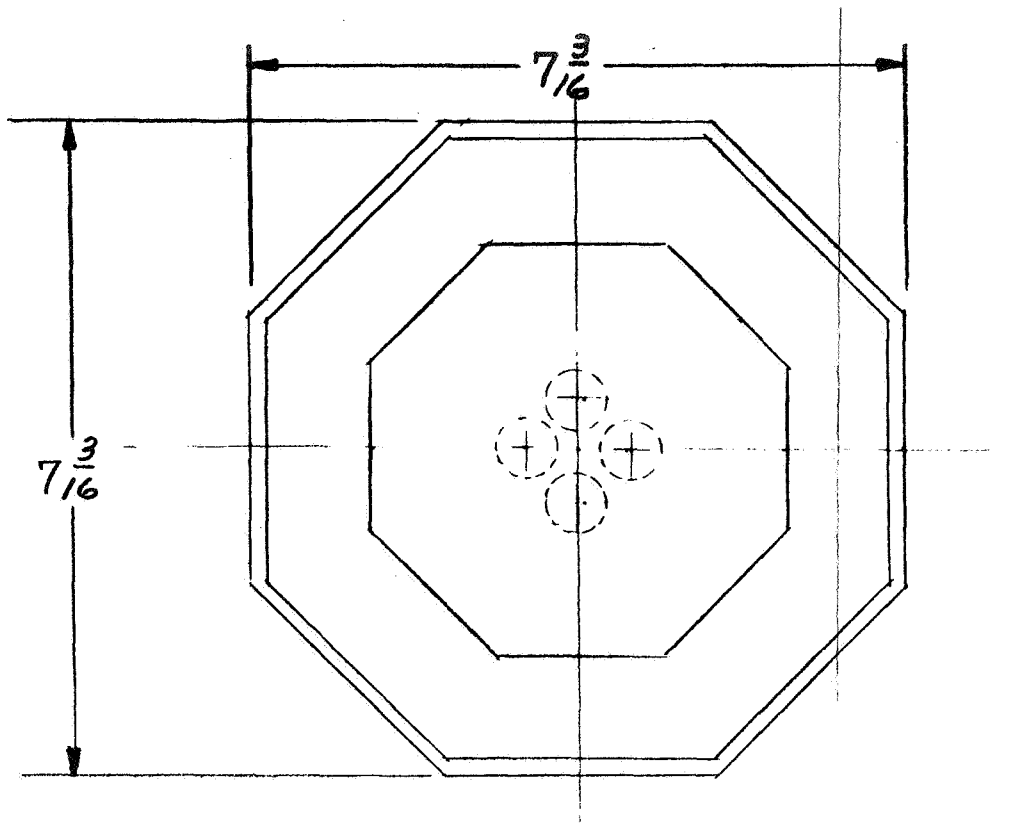

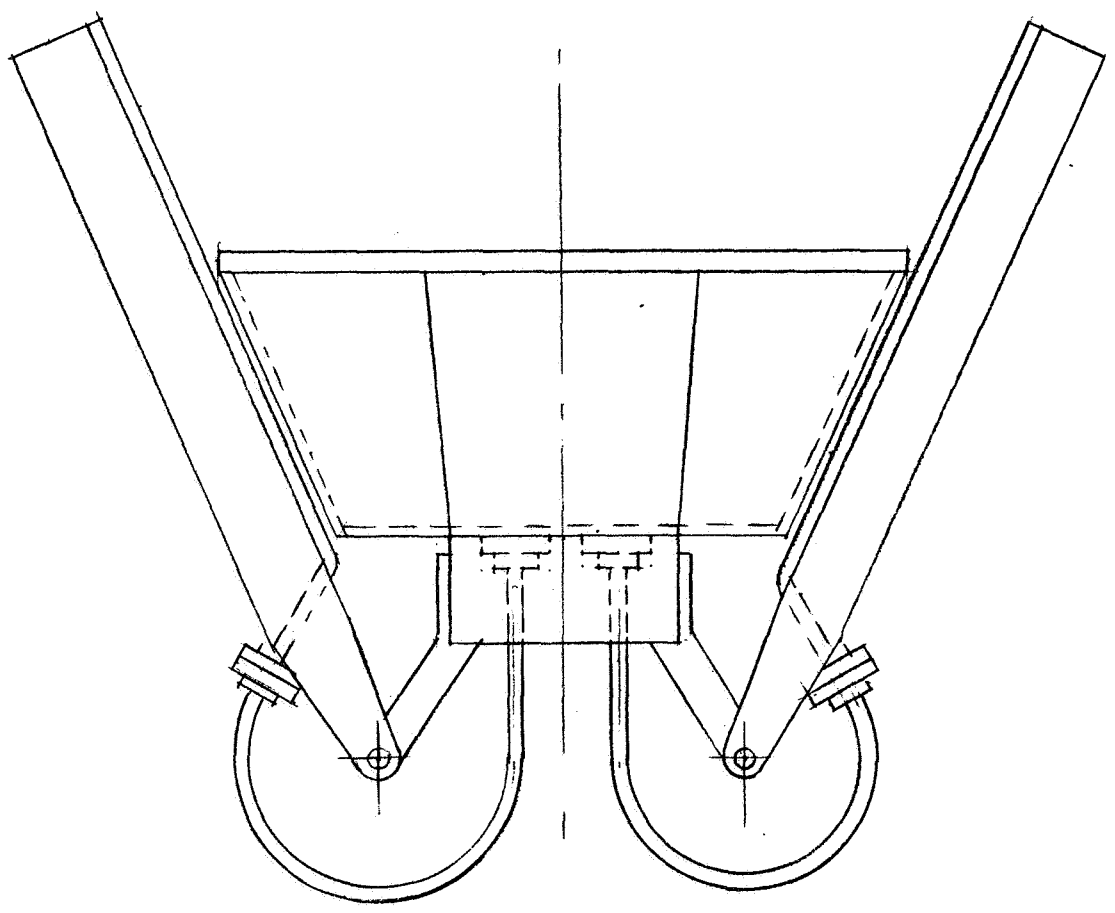

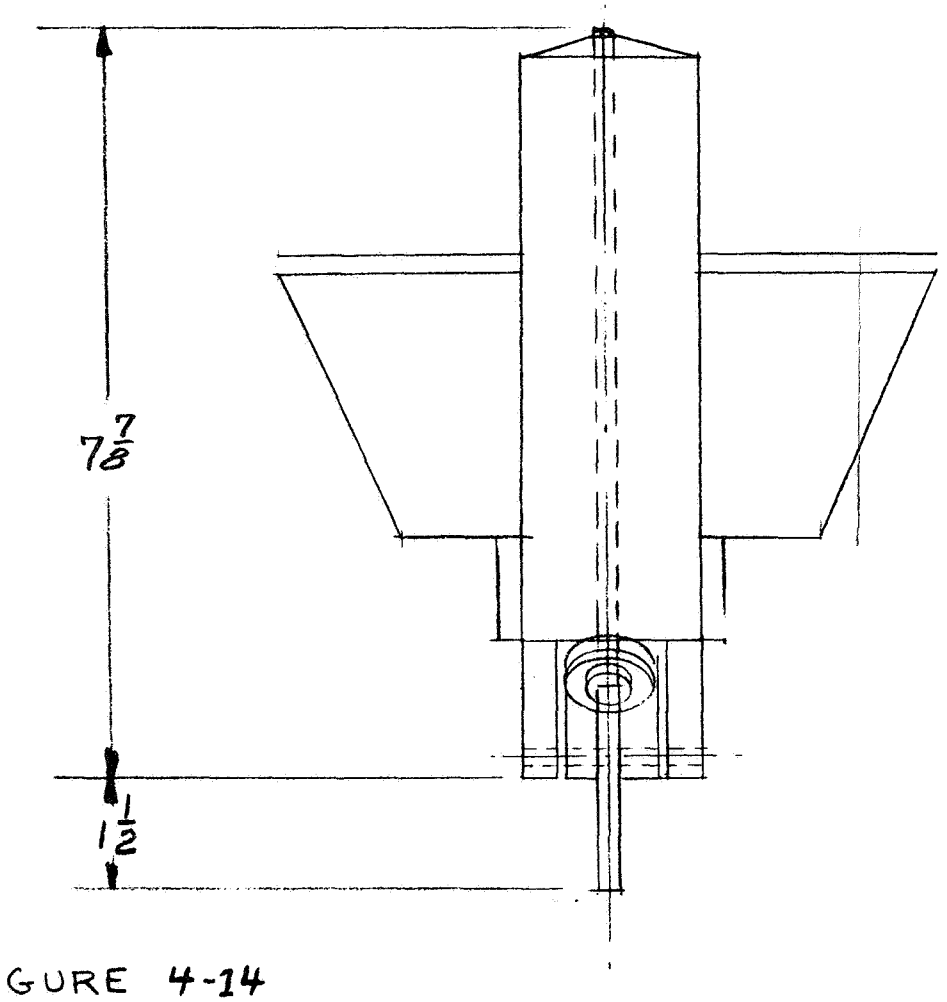

FIGURE 4-14

MECHANICAL CONFIGURATION OF HORIZON SENSOR

EWEN KNIGHT CORPORATION
EAST NATICK, MASS.

Over-sized Guide

Although 60 GHz flexible guide has been manufactured experimentally in the past (information source - Bell Laboratories, Whippany N.J.), it is not now available, and no manufacturer seems interested in producing it.

Measurements were performed using over-sized flexible guide in the line. The results were successful in that useful low loss sub-bands were found in the 50-65 GHz band.

The oversize flexible guide (35 GHz) showed strong resonances throughout the band, evidently due to mode conversion from the periodicity of the line. The line was not completely catalogued as to pass and stop bands, but our tests indicated that such a line could be used by carefully selecting the operating frequency. This is the lowest cost solution.

Norton-Sommerfeld Wave Device

This device is basically a short length of rectangular cross-section teflon, on which a surface wave has been launched. It was found that the guide line could be twisted along its axis through 360° in either direction from rest, with a negligible WOW. Since the total scan is only 27° the device appears to be the most satisfactory solution to the line problem. The experimental model was six inches long, an inch in diameter, and weighed 2 1/2 ounces (70.9 grams). In cost it would rank between the oversize flexible guide and the rotary joint, but closer to the flexible guide than the rotary joint. In appearance it resembles a coaxial line rotary joint, but it is incapable of continous rotation.

4.4.2 Positioning System

The squint angle adjusting mechanism (Figure 4-15) consists of a DC motor driving a lead screw on the centerline of the antenna structure. The lead screw moves a nut with preloaded recirculating balls up and down. The nut provides coarse angular positioning of all four antenna axles by means of connecting rods and cranks on each axle. All pivots in the mechanism use preloaded ball bearings to eliminate backlash.

Each antenna axle is mounted on preloaded ball bearings. The antenna is attached at each end of the axle by means of a flexural pivot. One end of the axle has a brushless moving coil torque motor with its stator in the antenna hub and its rotor on the

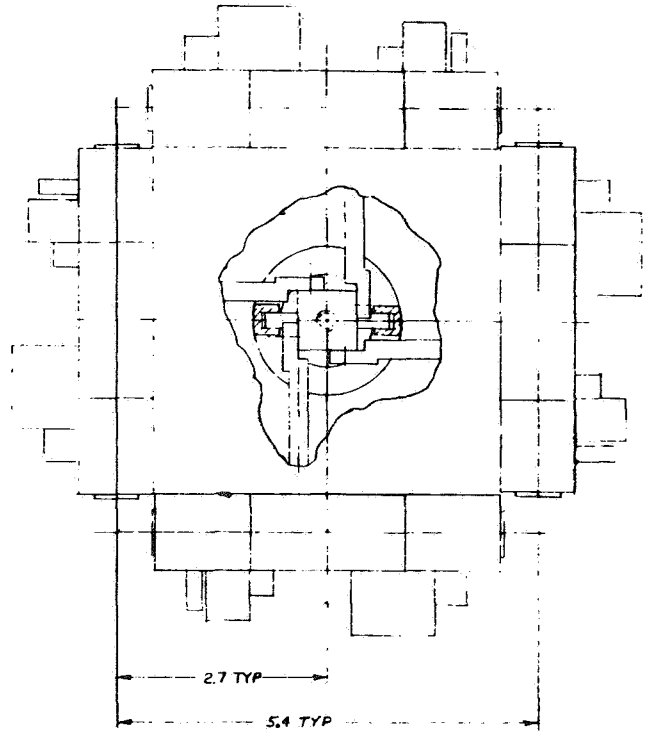

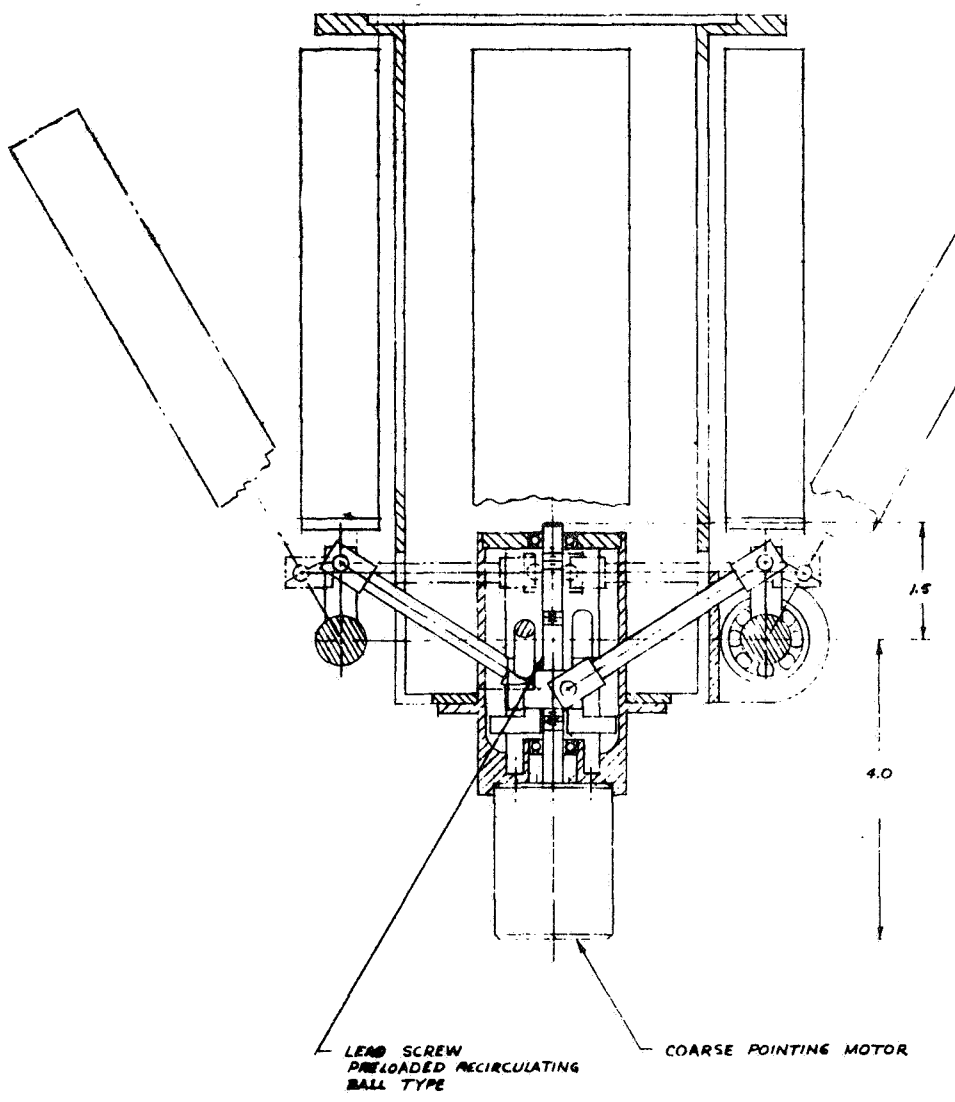

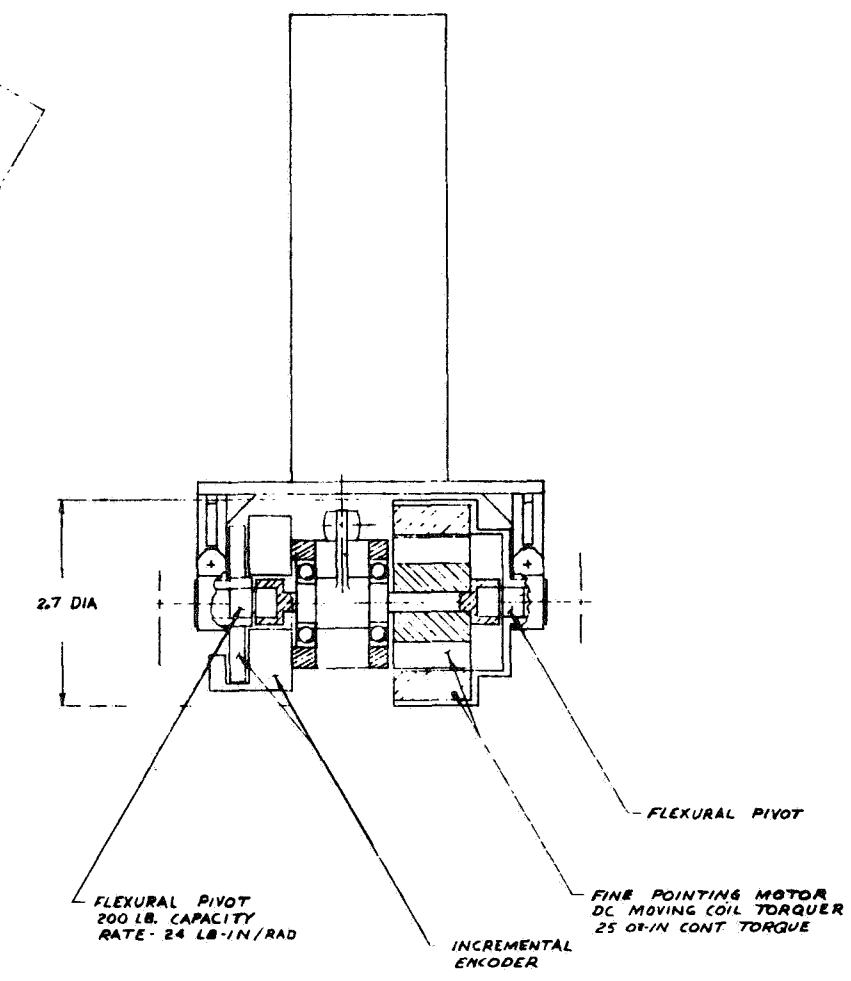

FIGURE 4-15

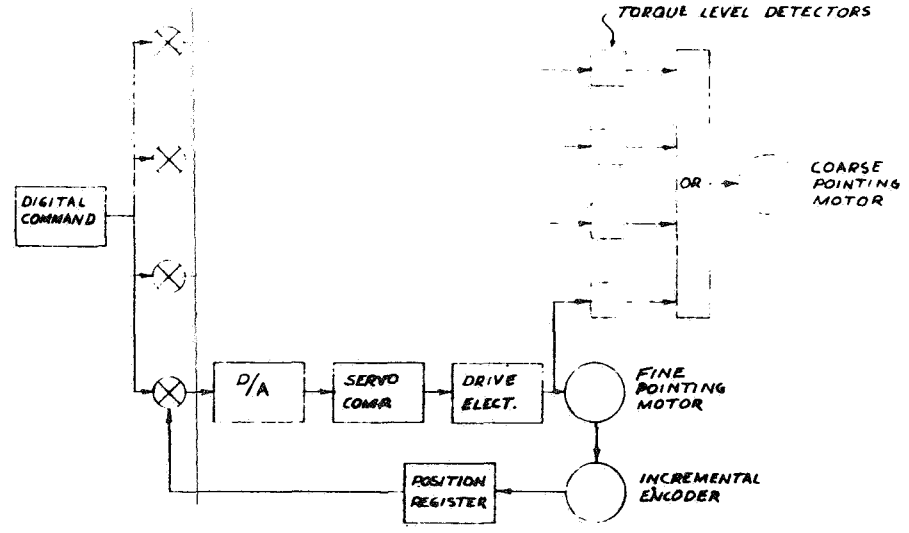

SERVO BLOCK DIAGRAM

RELIABILITY		BALL BROTHERS RESEARCH CORPORATION	
MATL & PROC		BOULDER	COLORADO
GROUP ENG		PROPOSAL LAYOUT	
DESIGNER	R.C. Hooper 7/30/64	ANTENNA DRIVE MECHANISM	
CHECKED			
PREP BY	S.L. HOOBER 7/28/64	SIZE E	CODE IDENT NO 13993
BALL PROJ		SCALE FULL	SHEET 1 of 1

axle. This motor is used to trim the angular position of the antenna with respect to the axle and thus provide fine pointing. On the other end of the axle an optical encoder determines the angular position of the antenna relative to the antenna housing. The fine pointing motors drive the antennas to the reference position which is arbitrarily defined as the position of one of the elements. The positioning accuracy achieved is as precise as the encoders used.

5.0 COMPETITIVE SYSTEMS

5.1 Mechanically Scanned Systems

Mechanically scanned antennas in this discussion are those antenna systems in which the aperture is mechanically controlled to point the main lobe in some specific direction. Most of the schemes described or suggested below require flexible lines or rotary joints although some do not. A resolver is required to provide data on the angle of look about the center line of the set.

For any immediate applications mechanically scanned systems offer the most in terms of simplicity, reliability, compactness, and ease of design and fabrication. Because of its compactness and also its promise of extreme accuracy (to one arc second rms) the system described in 5.1.4 was selected as the most appropriate for the application. Detailed analysis of pattern, beam efficiency, weight, etc. is presented in the preceeding section.

5.1.1 Mechanical Scan of Parabolic Antennas

A simple system capable of scanning through 27° from 51° to 78° is shown in Figure 5-1. Four parabolic antennas of the desired gain (approximately 37 db) are mounted in pairs on two sets of servo controlled linkages. A double ended screw with right and left hand threads on opposite ends is driven to carry a threaded sleeve back and forth.

5.1.2 A Scan System Based On The Flat Plate ("Fly-Swatter") Reflector

A Flat plate reflector scan system is shown in Figure 5-2. The four source antennas (shown as parabolas), are mounted rigidly on a cruciform frame and look into a set of flat plate reflectors. In this way, all waveguide and wiring is contained on a rigid structure. A servo positioned linkage is used to traverse the flat plates through $13\text{-}1/2^{\circ}$ by means of a single threaded screw.

Although the structure is bulky, it can be made both light and rigid by the generous use throughout of aluminum honeycomb construction as indicated in the cut away of the flat plate.

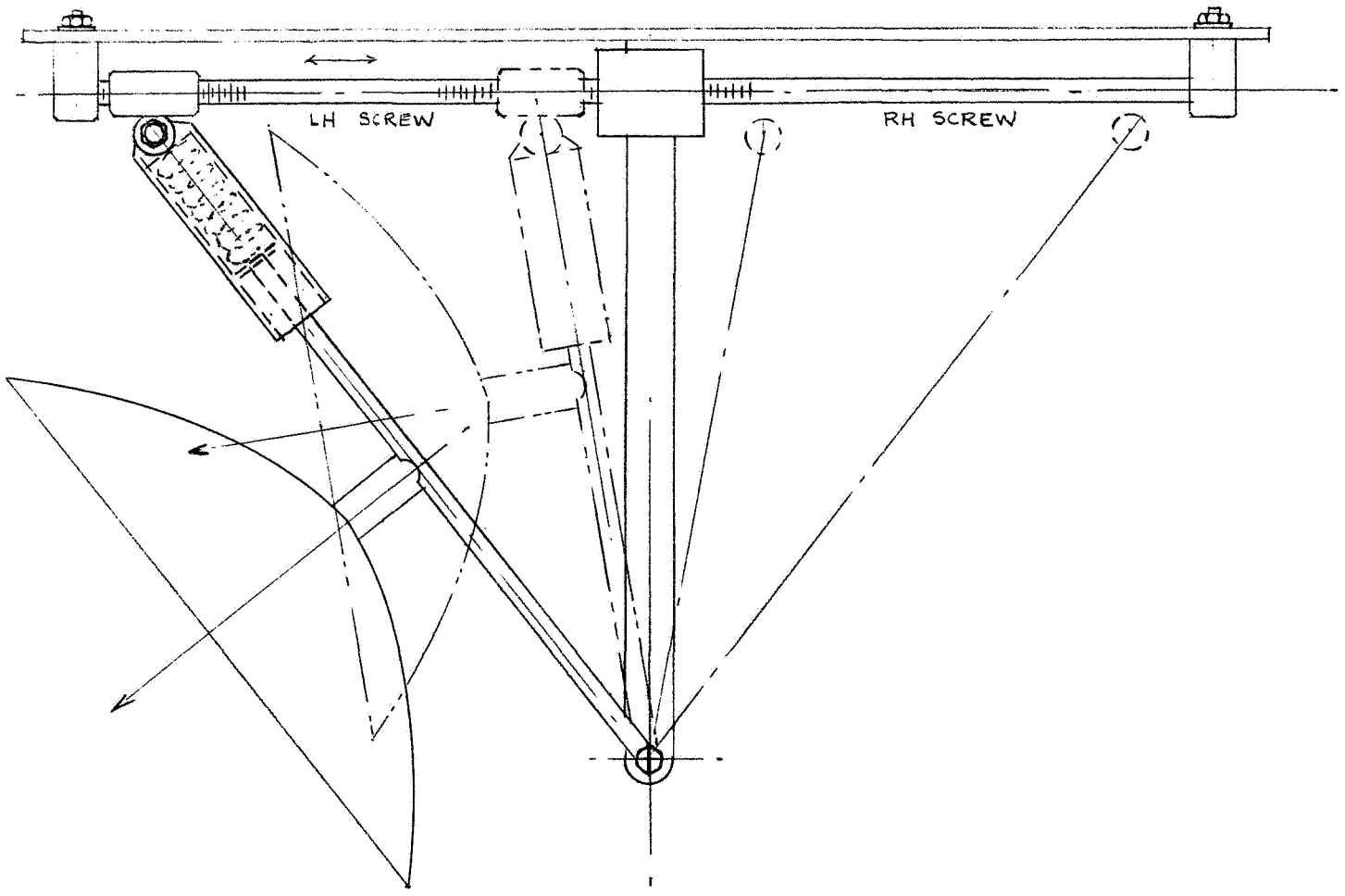

FOUR APERTURE MECHANICALLY SCANNED
ANTENNA SYSTEM

FIGURE 5-1

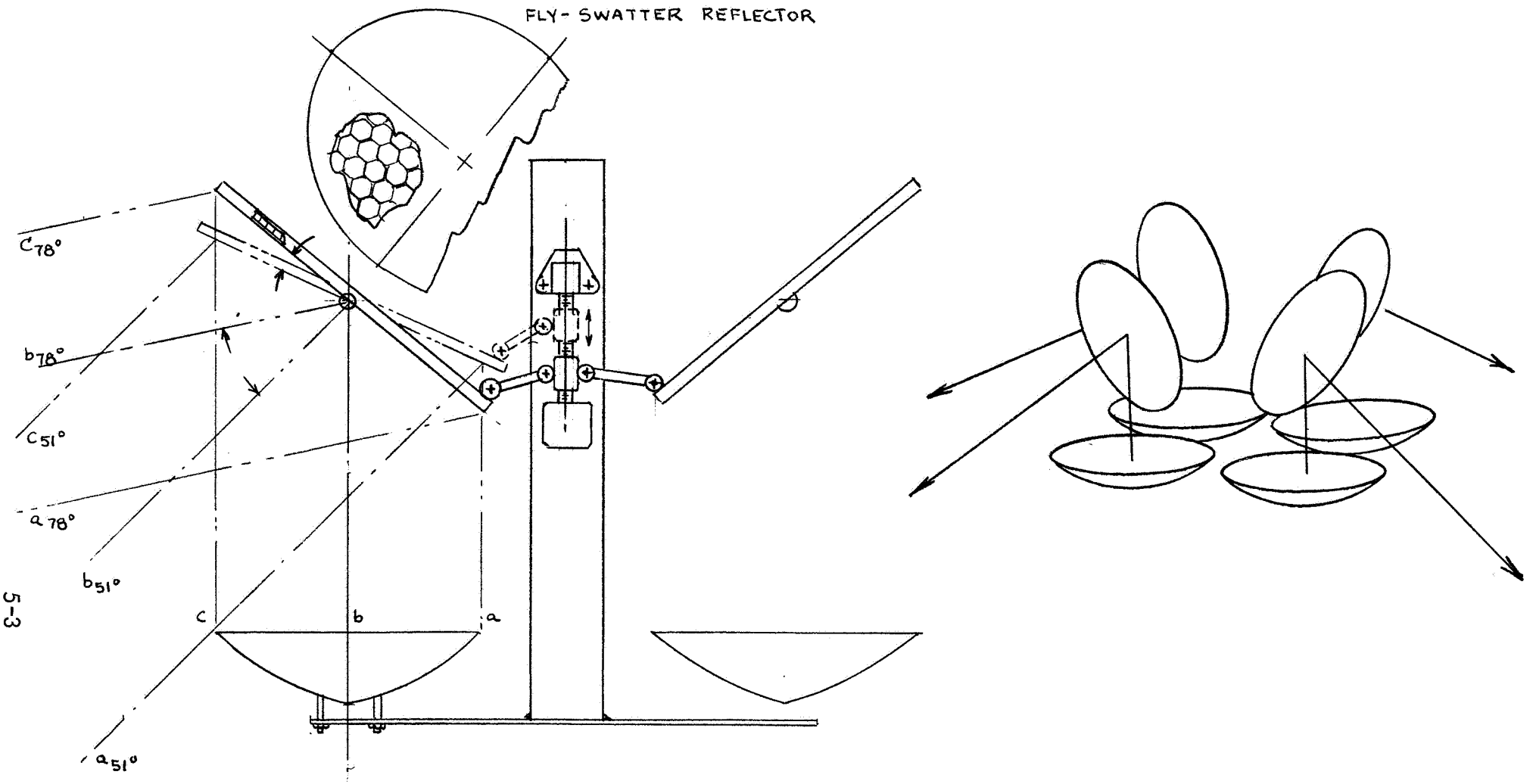

FLY-SWATTER SCAN SYSTEM

FIGURE 5-2

The patterns are those of the sources.

5.1.3 Offset Folded Parabola

The well-known cornucopia antenna is basically an off-axis paraboloid in which the problem of spill-over has been circumvented by enclosing the volume from the feed horn to the paraboloidal surface in a horn-like shroud. The desirable features of the cornucopia can be retained and much of the bulkiness eliminated by inserting a flat reflecting plate to fold the optical train back on itself. Figure 5-3 illustrates such a compact folded parabolic antenna. The spherical phase front from the horn returns to the paraboloid, is collimated and is radiated through the circular aperture.

The four beams required for the millimeter wave sensor would require four folded parabolic horns arranged somewhat as shown in Figure 5-4 . The feed horn receivers and all other circuitry is rigidly mounted to the cruciform frame and only the paraboloidal and flat plate structure is rotated to accomplish the scan.

All off-set parabolic antennas suffer from coma unless compensating measures are taken. This is a cubic phase error in the secondary illumination function and shows up in the pattern as asymmetric sidelobes. The lack of aperture symmetry also contributes to a rather pronounced cross-polarized pattern. Neither of these pattern features is likely to be a serious restraint in the application investigated.

5.1.4 Flared Horn or Line Source System

A fairly compact four source system is shown in Figure 5-5. The package shown in Figure 5-5 would be realizable with solid state components. If these are not readily available, a form using off-the-shelf hardware is shown in Figure 5-6. The sources used are derived from a line source in which the c/v ratio produces a tilt of 12° from the normal. When the radiators are in the vertical position, the beam is scanned to 78°. By tilting them through 27°, the beams are steered to 51°.

The antenna shown is about 10λ across by 50λ long and produces a

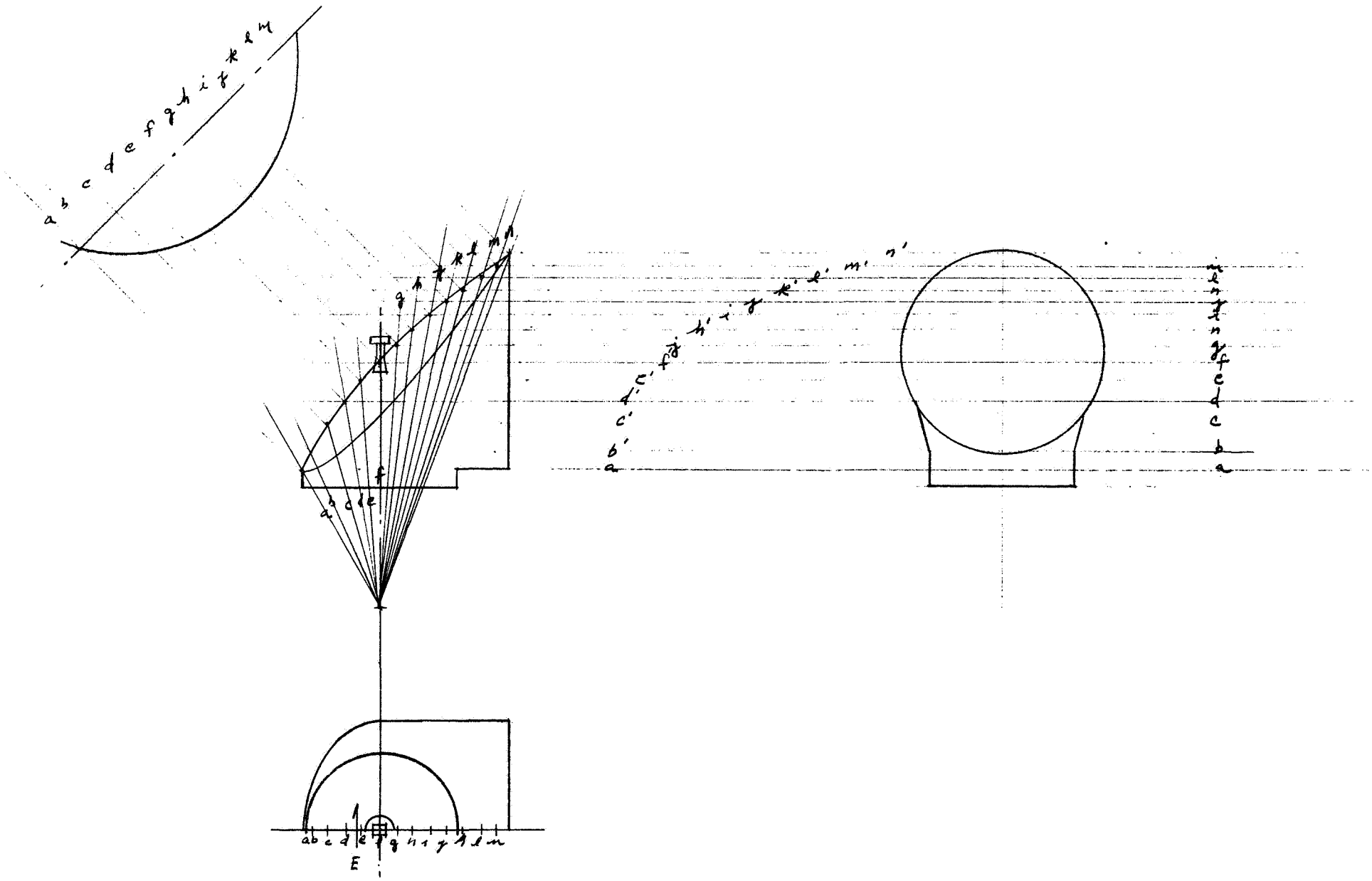

OFF SET FOLDED PARABOLIC

ANTENNA

FIGURE 5-3

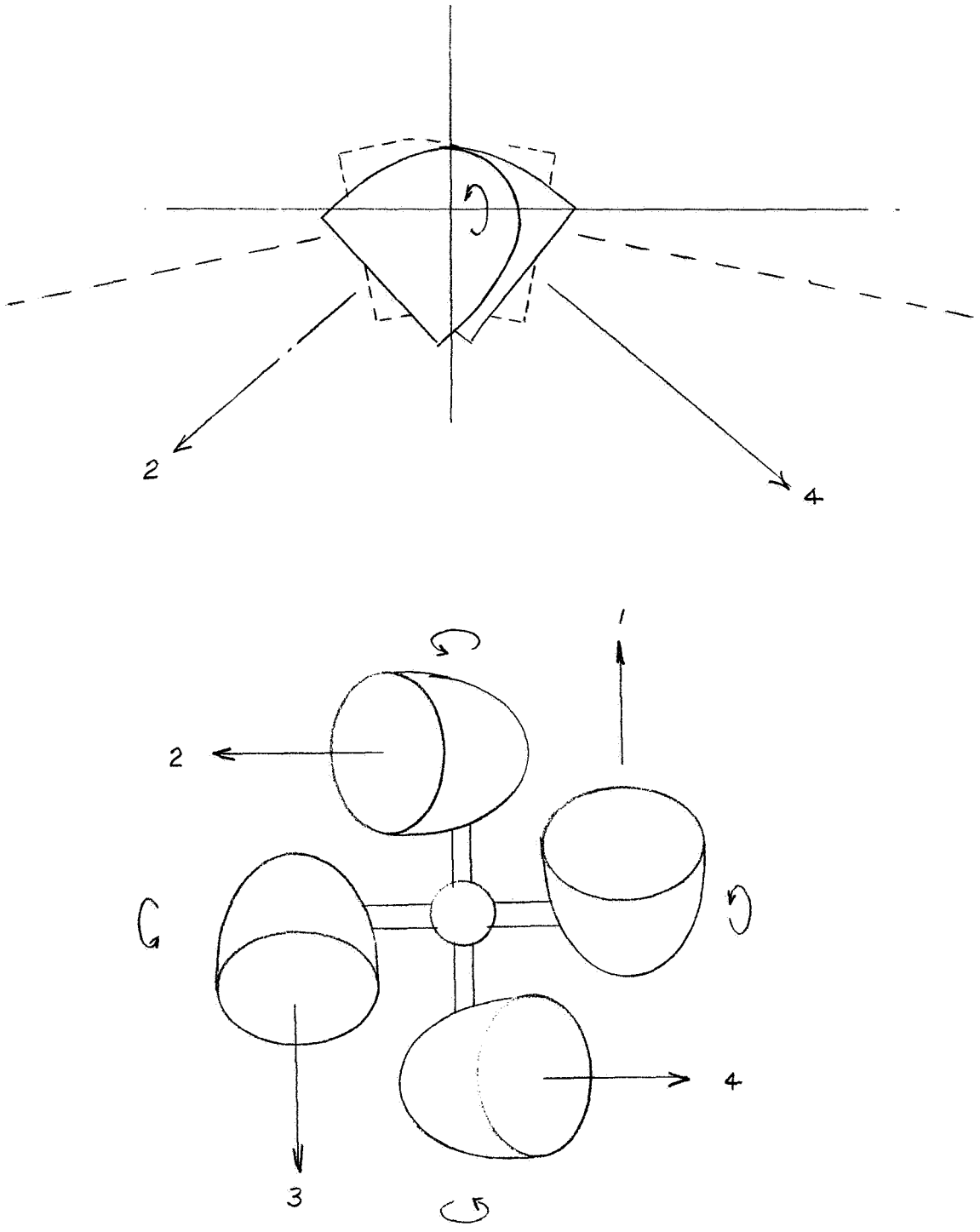

SCAN OF FOLDED PARABOLA

FIGURE 5-4

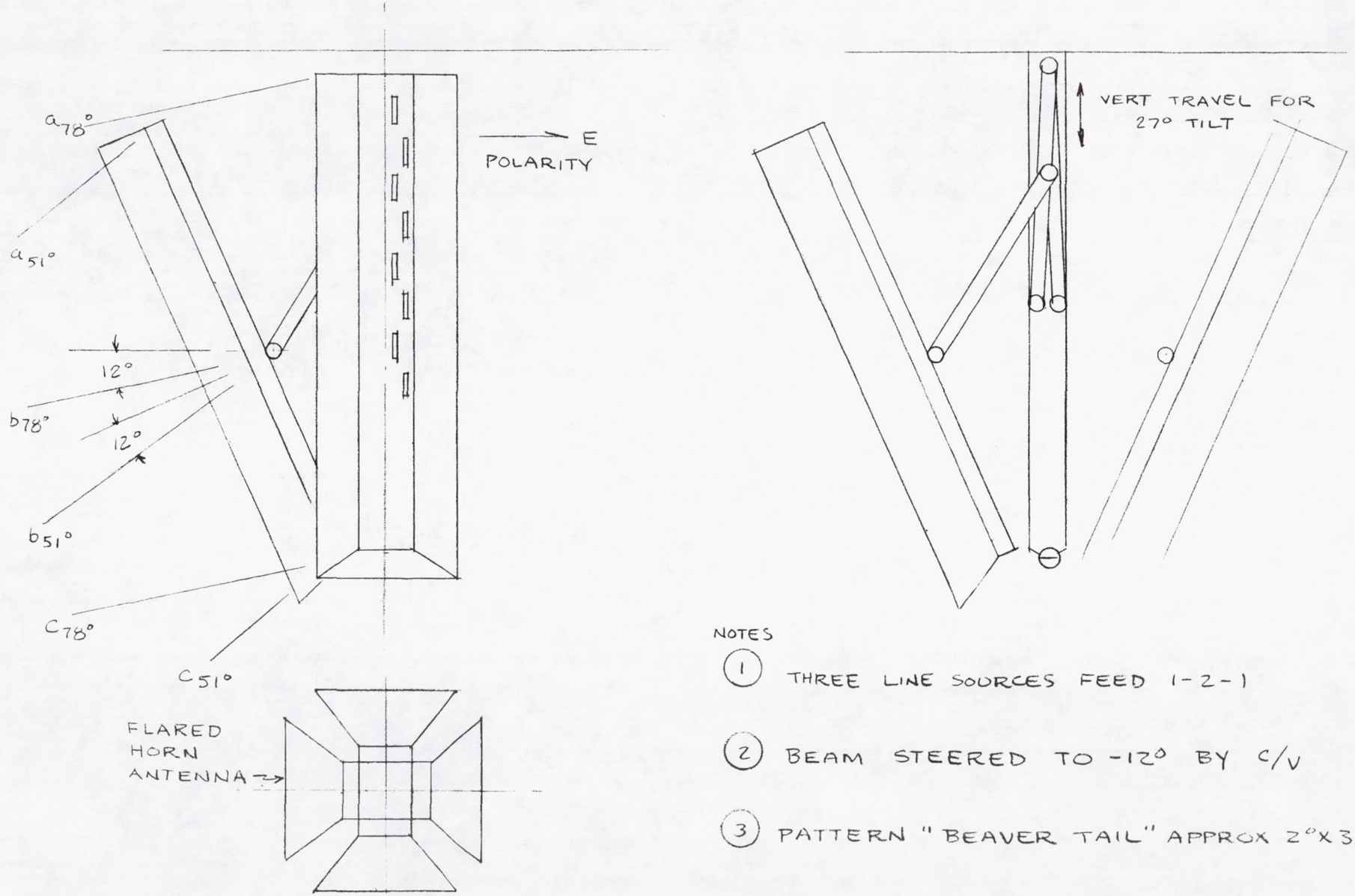

NOTES

(1) THREE LINE SOURCES FEED 1-2-1

(2) BEAM STEERED TO -12° BY C/V

(3) PATTERN "BEAVER TAIL" APPROX 2°X3°

FOUR FACED LINE SOURCE ANTENNA SYSTEM

FIGURE 5-5

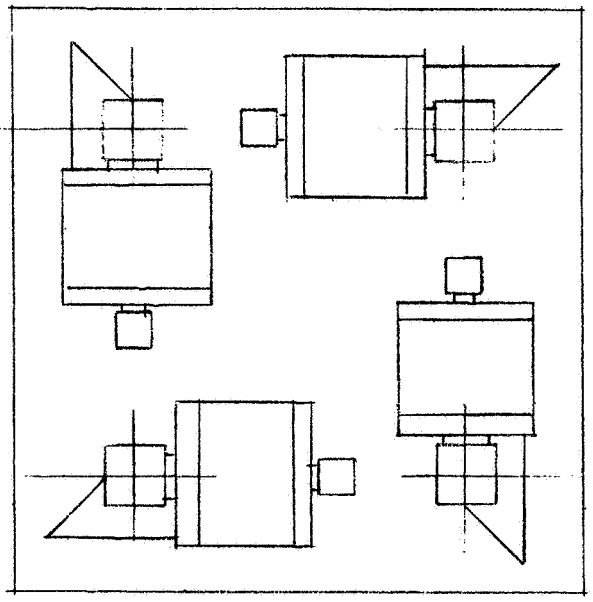

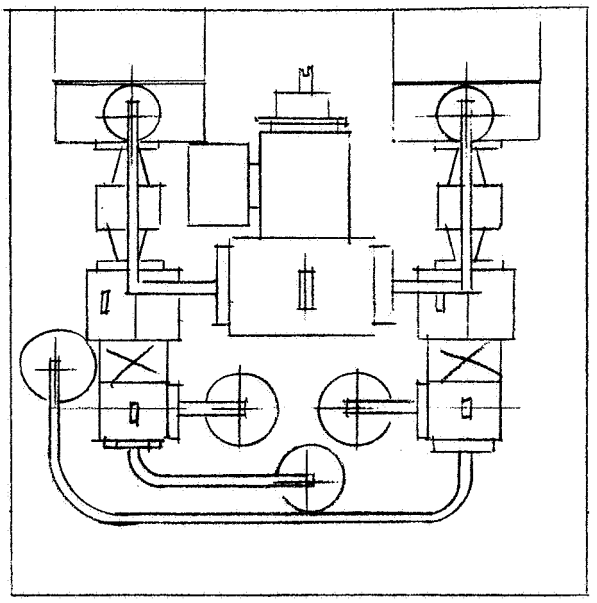

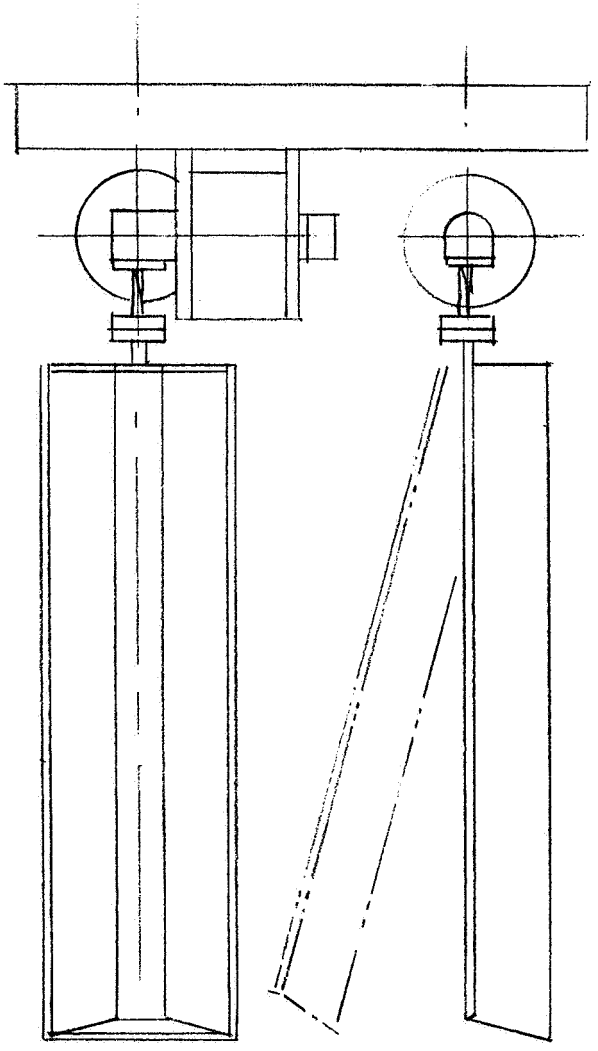

LINE SOURCE SYSTEM USING "OFF-THE-SHELF" HARDWARE
FIGURE 5-6

"beaver tail" pattern with the narrow direction in the vertical plane[22]. A cosine taper along the line source will produce a 3 db beamwidth of 2°. The azimuth plane pattern has been calculated for uniform illumination to producing 3 db beamwidth is 6° the sidelobe levels remain high (e.g. above - 40 db) to nearly 90°.[23] The first sidelobe of the vertical pattern is -23 db and the decay is rapid. The effect is that of an almost symmetrical (3 db level) main beam with slowly decaying horizontal sidelobes and a rapidly decaying vertical sidelobe system.

By using three line sources fed by an in-phase, binary amplitude (1-2-1) corporate structure the sidelobe levels in the horizontal case can be improved. The 3 db beamwidth opens up to a little over 3°, and the first sidelobe level drops from -13 db to -19, but the second sidelobe increased from -18 to -17 db. All others remained below -20 db.

Two variations of this antenna have been investigated briefly using a computer program with every indication that considerable improvement in pattern can be achieved.

The simplicity and compact size, 2-3/4 x 2-3/4 x 6-1/2 inches, (7 x 7 x 16-1/2 cm) make this antenna attractive for the millimeter wave sensor system investigated.

5.1.5 Dual Polarized System Using A Moving Polarization Separating Grating

A simple system which enforces strict symmetry in beam pair formation is shown in Figure 5-7. The source is a dual polarized horn (or parabola) mounted to project its main beam downward at 12° (78° scan) from a reference platform. It illuminates a polarization separating screen. The screen is moveable through an arc of 27°.

The electrical effect is shown in the detail A-A. A grid of fine, closely spaced parallel wires illuminated by radiation polarized parallel to the wires is almost totally reflecting. The leakage of parallel polarized energy through the grating is of the order of -40 db if the spacing is much less than a half wavelength while energy polarized

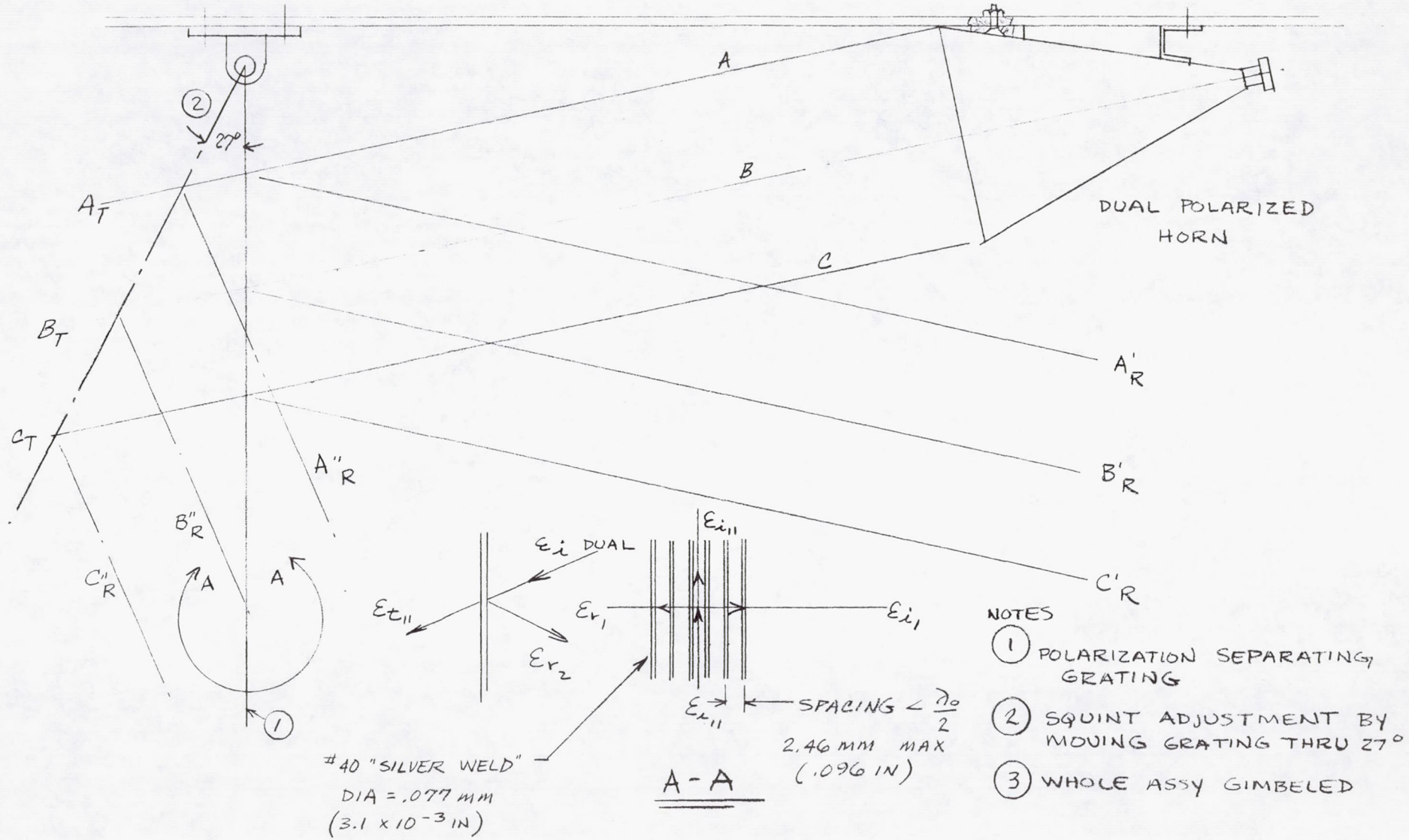

DUAL POLARIZED HORN
(OR PARABOLA) SYSTEM

FIGURE 5-7

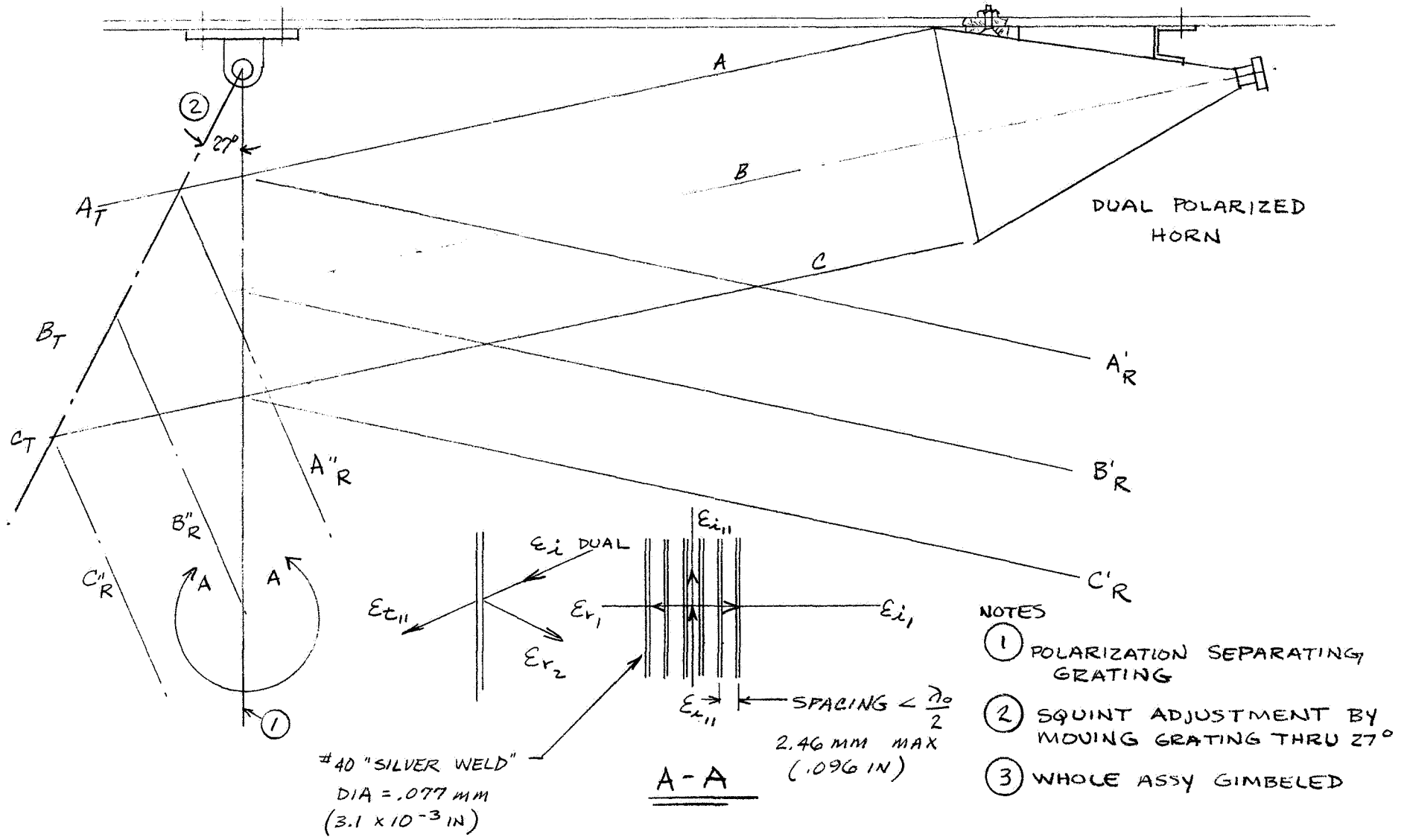

DUAL POLARIZED HORN
(OR PARABOLA) SYSTEM

FIGURE 5-7

perpendicular to the grid passes through with very little loss. When the spacing is chosen to lie between $\frac{\lambda_o}{2}$ and $\frac{\lambda_o}{4}$ (a 2:1 bandwidth for a fixed spacing) the one way transmission loss is very close to the aperture blockage. At the highest frequency in the band to which this study is directed is about 61 GHz, hense, grating would have to be spaced less than 2.46 mm for example, 2.3 mm. The loss due to blockage would be about .12 db or an increase in the effective noise temperature of about 7° to 8°. The advantages are: (1) the use of an available dual polarized source and(2) the rigid angular beam symmetry enforced by the optical properties of the grating.

5.1.6 Phased Array and Polarization Separating Grating

The polarization separating grating can be used with a line source array. Two independent orthogonally polarized arrays are interlaced to form a dual polarized source. The length of the array (150 wavelengths - 30 inches) is a result of the fall-off of gain as the beam is steered toward the endfire case.

A broadside 2° beamwidth requires an antenna approximately 6.2 inches long (31.6 wavelengths) at 60 GHz. The oblique length depends on the secant of the scan angle (78°). The increase in length is nearly five times. The effective aperture varies dramatically in scanning from 78° to 51° with consequent variation in beamwidth; and gain (from 37 to 47.4 db). This has a strong effect on overall system gain and stability.

Polarization grating, Figure 5-8, allows the insertion of signal from one end only, the use of interlaced arrays at the expense of the addition of a rather large and probably delicate structure. Ferrite delay structures are suggested to control the c/v ratio to obtain scanning action. There does not appear to be a simple way of introducing the material into the waveguides over a length of 30 inches. The slot radiators shown enforce the orthogonalit conditions, but require a closed structure. The great length of the arrays also makes the tolerances on the slots extremely tight in order to hold the low coupling coefficients (average α = .0067). Open faced lines are possible using $TM_{0,1}$ and $TE_{1,0}$ modes to produce orthogonal polarization, but would not provide an easy means for controlling the coupling coefficients. The illumination would be a simple exponentially decaying function which

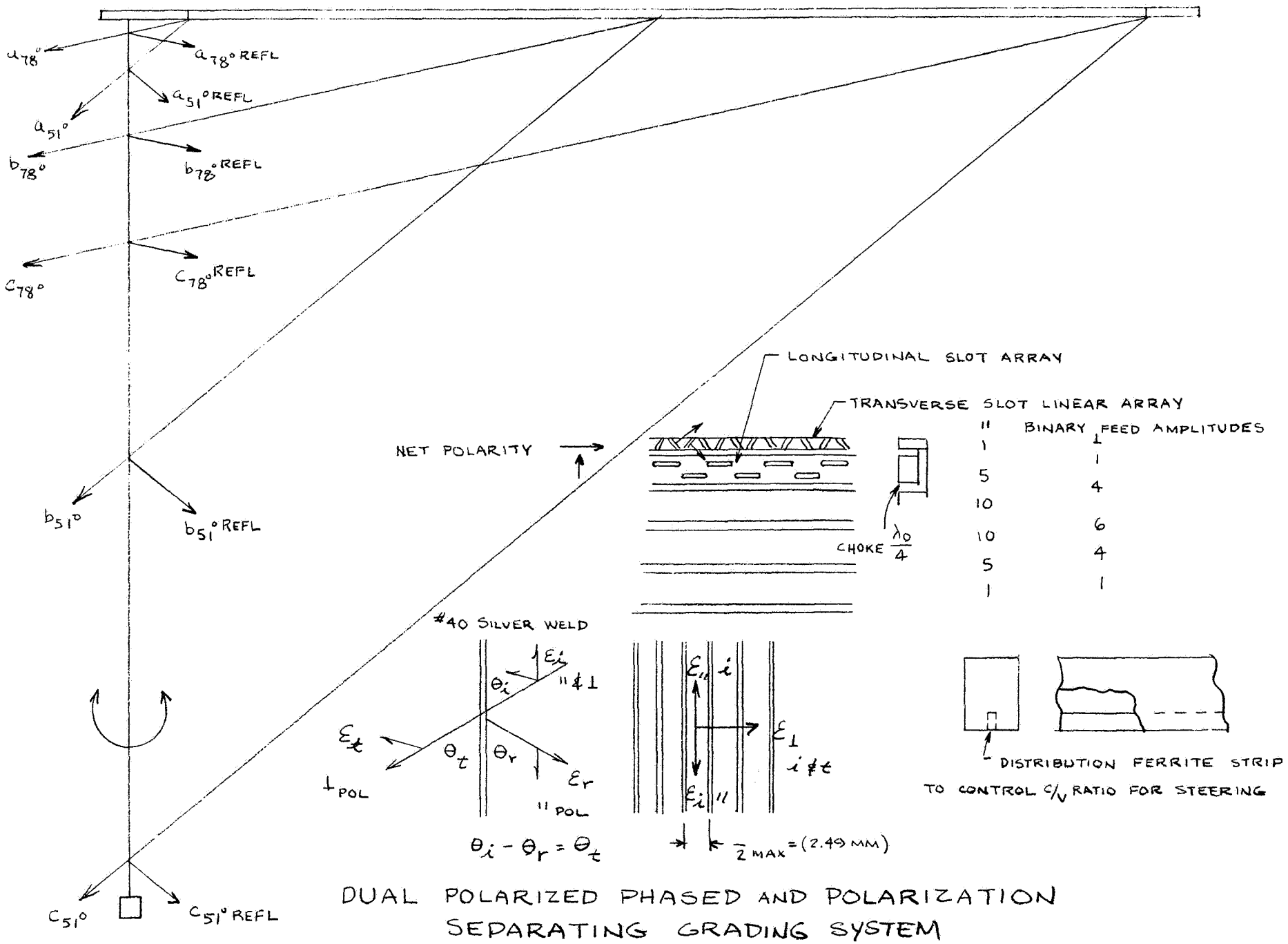

DUAL POLARIZED PHASED AND POLARIZATION SEPARATING GRADING SYSTEM

FIGURE 5-8

yields neither good sidelobe control nor optimum aperture efficiency. (The effect would be that of truncation long before an effective length was reached).

This form of the sensor antenna should be considered in detail only if there are no other simpler ways of accomplishing the desired performance.

5.1.7 Forward Firing Line Source Array

If a symmetrical waveguide line source is fed from both ends, a pair of symmetrical beams will be formed. These are independent of one another as no cross coupling in space occurs. An array design based on this idea is shown in Figure 5-9.

The array is flush mounted and scan is controlled by modifying the c/v ratio by ferrite or other decay structures. The effective aperture varies with scan over about 5:1 with consequent changes in the input impedance and effective gain.

The c/v ratio can range (theoretically) over all positive values from 0 to ∞. That is, the wave inside the array structure can be either slow or fast and the direction of the external wave front controlled by operating on this parameter. There are two values of c/v corresponding fast or slow wave forms of the fields.

The longitudinal illumination function of a source of this type is the product of a cosine and an exponential function so that an aperture efficiency of 25% or so is about all that can be obtained. Losses must be added to this figure.

A "beaver tail" pattern can be produced from an array of this kind by using only enough lines to fill a width of about 2 inches. The horizontal pattern would remain fixed, but the vertical beamwidth would vary from approximately 2.0° at 78° to around $.42^\circ$ at 51° scan.

Four beams could be produced by two arrays set at right angles to one another in the form of a "T". As in the other systems, a single antenna could be turned through 90° to sense the other horizons.

5.2 Electromechanically Scanned Antennas

By electromechanical scanning is meant a system in which the effective radiating aperture of the antenna remains fixed, but the direction of the main lobe of the power pattern

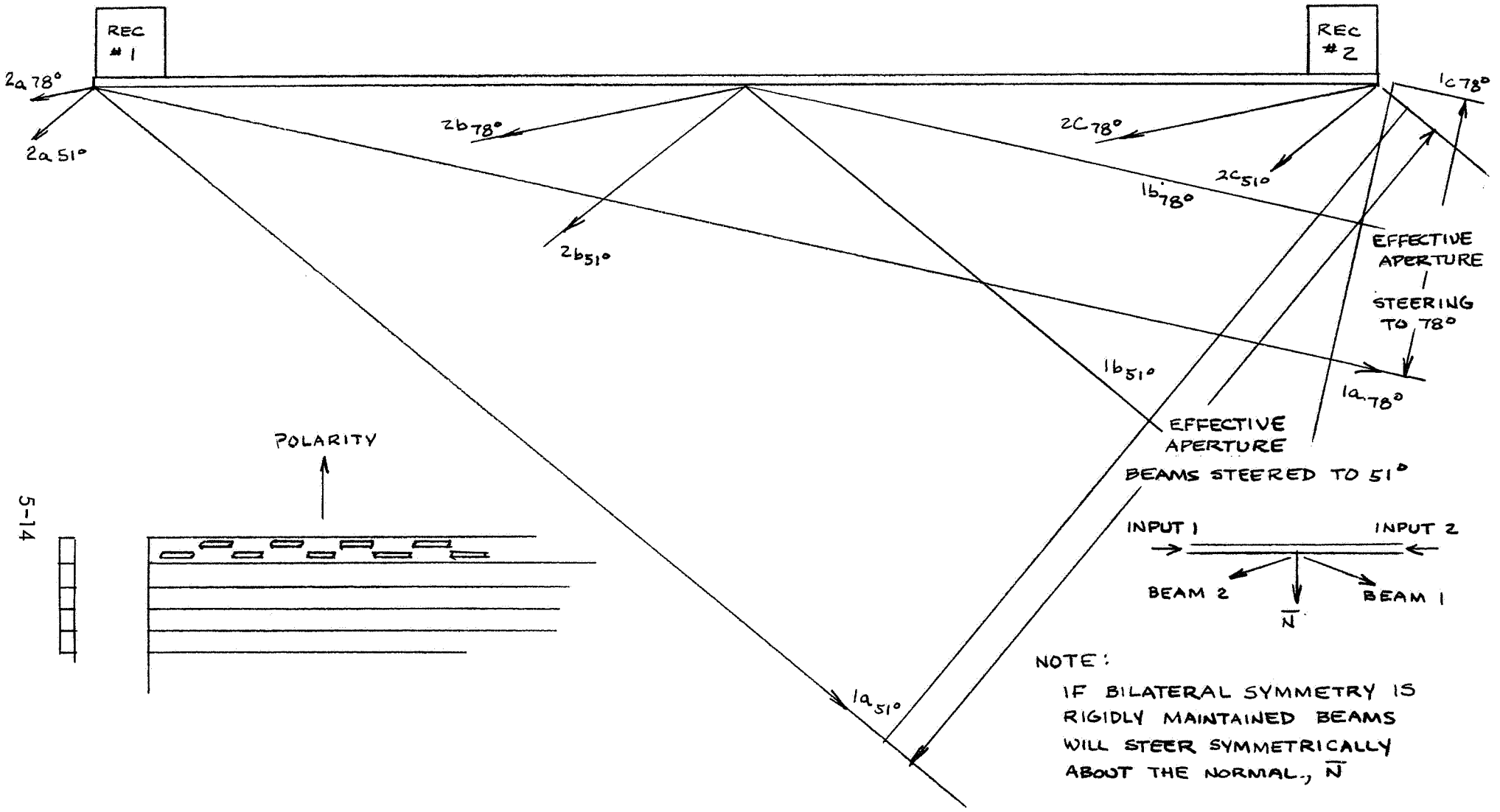

FORWARD FIRING LINE SOURCE ARRAY
SYSTEM FEED FROM BOTH ENDS

FIGURE 5-9

is directed through a mechanical positioning device. The category is a broad one and many antenna systems in use loosely called phased arrays are in actuality electromechanically controlled. Large scale systems of this sort have been built with every indication of satisfactory operation. Hybrids that control one plane electronically and the other electromechanically are also in use (e.g. AN/MPQ-32). A partial listing is:

1) Goniometer controlled Wullenwebber arrays (e.g., AN/FLR-9)
2) Optically fed arrays
3) Geodes.ic lens fed arrays
4) Line sources with mechanical phase velocity control (variable ratio Rotman line antennas)
5) Luneberg lens (and relatives) with movable source

These will not all be discussed in detail. The Luneberg lens group was investigated in more depth than the others, and is more or less typical of an electromechanically scanned antenna.

5.2.1 Line Source - Electrically Steered Arrays

The launch angle of a set of sources deriving power from a traveling wave on a line is controlled by the ratio of the phase velocity of the wave on the line to that of free space. The ways in which the v/c ratio can be modified electronically are:

1) Varying the frequency of operation, or
   the insertion of a strip of material in the line.
2) Varying the permeability, μ, by varying a magnetic field, or,
3) Varying the specific permittivity, ϵ, by a changing electrical stress.

Depending upon the specific device used to control the v/c ratio this type of antenna falls in both the electro-mechanical and electronic scan system categories.

Frequency Scan

The use of varying frequency as a means of scanning is incompatible with mission requirements.

Magnetic Permeability

There is no theoretical restraint on the use of a ferrite delay line, however,

the ferrite materials available for use at frequencies above 10 GHz tend to be either switched or ferroresonant types.

The simpler ferrites, whose permeability can be varied smoothly tend to have high magnetic loss tangents at frequencies much over 10 GHz.[9] The problem areas are:

1) Materials- There are ferrite materials for similar applications at lower frequencies, but at 60 GHz would require some development or perhaps an advance in the state of the art. No doubt this is possible, but materials research tends heavily to experimental recycling, a time consuming and often costly process.

2) Circuit Design - Ferrite devices in this part of the spectrum utilize the ferrite material to control a very localized microwave phenomenon. The "all-or-nothing" quality of these applications lend themselves to relatively simple control circuitry, e.g., the bias is "on" or "off" on a ferrite switch and not somewhere between. The smooth steering required to position a beam from a traveling wave antenna would require a much more sophisticated magnetic bias control than now used for latching, isolation and similar applications of ferrite circuit elements.

Again there is no apparent reason at this time to preclude such control circuitry but considerable development seems indicated to obtain smooth operation. It is hard to visualize producing a variable antenna beam control system along these lines in a year or less, except on a crash program.

5.2.2 The Luneberg Lens and Related Devices

The very compact simple antenna system is one based on the Luneberg Lens[10]. For an approximately $2^{\circ} \times 2^{\circ}$ principle lobe the diameter of the lens would be about 6 1/4 inches. A simple Luneberg Lens is shown in Figure 5-10.

The Luneberg lens is one of a family of spherical lenses that have the property of collimating a spherical wave introduced into the lens anywhere on its surface.[11,12,13]

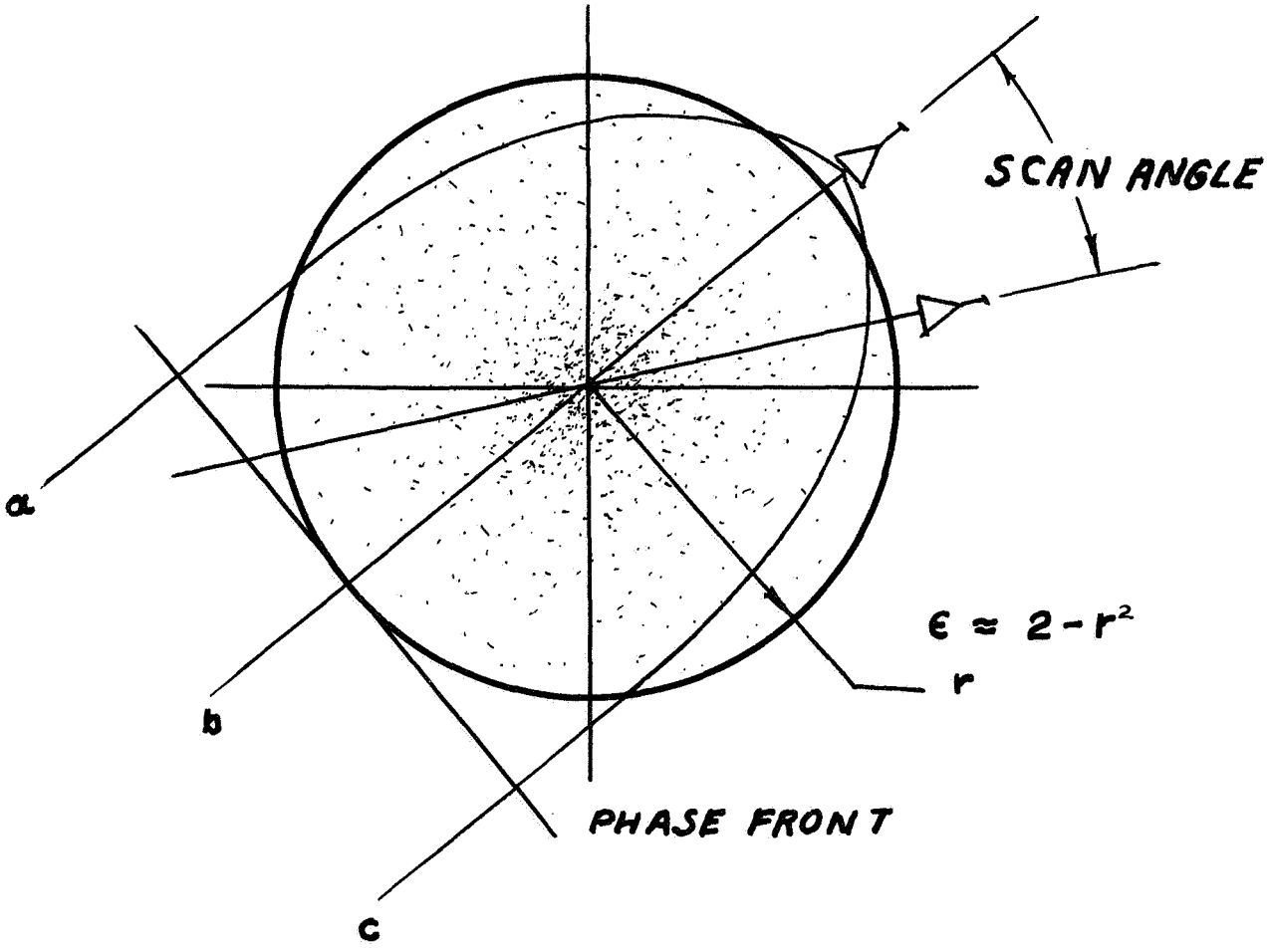

LUNEBERG LENS
FIGURE 5-10

In the Luneberg lens a small horn or source is moved about the surface of the lens according to the scanning motion required. The index of refraction of the lens varies from point to point such that all the rays from the source encounter the same phase delay and emerge as a nearly flat phase front directly opposite the source. In other forms of the spherical lens the dielectric constant variations are distributed so that the collimated beam emerges in a direction other than directly opposite the feed or else produces a particular phase front. For example, the constant -K and Eaton-Lippmann lenses are retrodirective without the use of metallic reflectors.[14]

The use of the class of spherically symmetric lens antennas can be illustrated with the Luneberg Lens as an example. In a simple Luneberg Lens four feeds would be required to develop the four horizon seeking beams. By quartering the lens and inserting a pair of polarization separating screens four beams can be generated from two horns (see Figure 5-11).

The horns must be dual polarized and the lens material isotropic. A further constraint is that the horns move in the plane determined by the lines of the grid and a normal to it. When the E-field is parallel to the wire grid the field undergoes nearly total reflection. The cross-polarized field is transmitted with a scattering loss essentially proportional to the blockage. When the spacing, d, of the grids begins to approach (Figure 5-12),

$$d = \frac{\lambda_o}{\sqrt{\epsilon}}$$

the parallel portion begins to be transmitted and the polarization separating property weakens.

At 60 GHz d max = $\frac{\lambda_o}{2\sqrt{2}}$ at the center of the lens or 1.77 mm (.0696 inches). If the d is arbitrarily set to .050 inches (1.27 mm) and the grid made of AWG#40 "Silver-Weld"* (dia - .0031 inches(.079 mm). The condition that $d < 1.77$ mm would be met and the blockage would cause a transmission blockage loss of .28 db. This energy will appear in the secondary field as a grating pattern dependent on the spacing, the primary illumination function and the angle of incidence.

The Aperture Distribution

The geometry of the Luneberg Lens and its equivalent circular aperture are shown in Figure 5-13.

* Trade name of Copperweld Steel Company, Glassport, Pa.

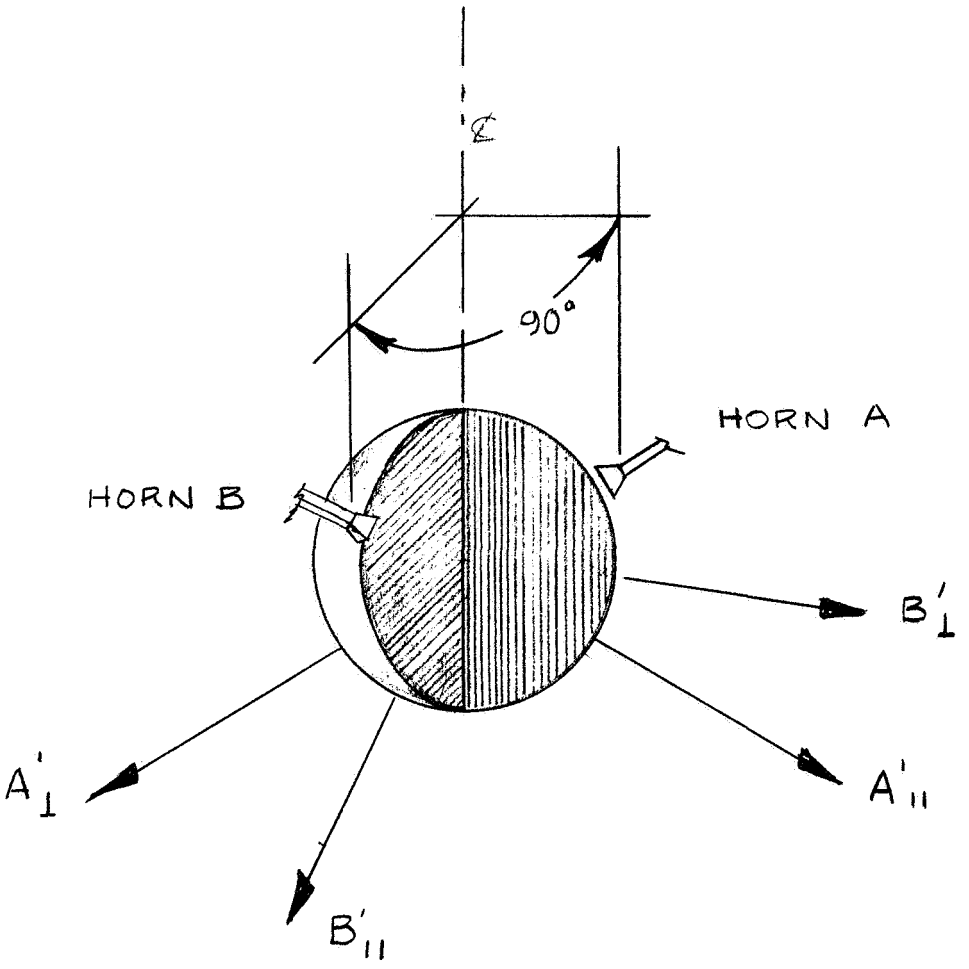

FOUR BEAM LUNEBERG LENS USING TWO DUAL POLARIZED FEED HORNS AND POLARIZATION SEPARATING WIRE GRATINGS

FIGURE 5-11

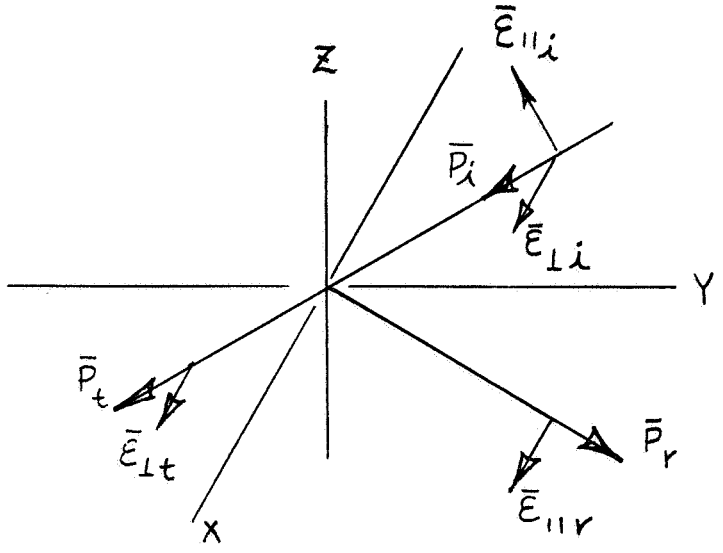

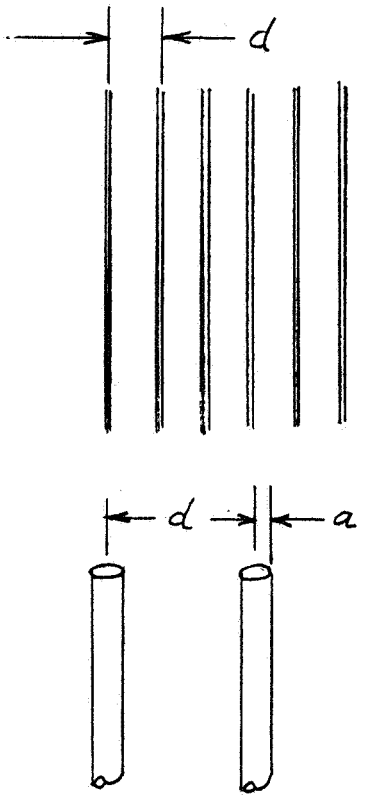

GRID DETAIL

POLARIZATION SEPARATION
COORDINATE SYSTEM

FIGURE 5-12

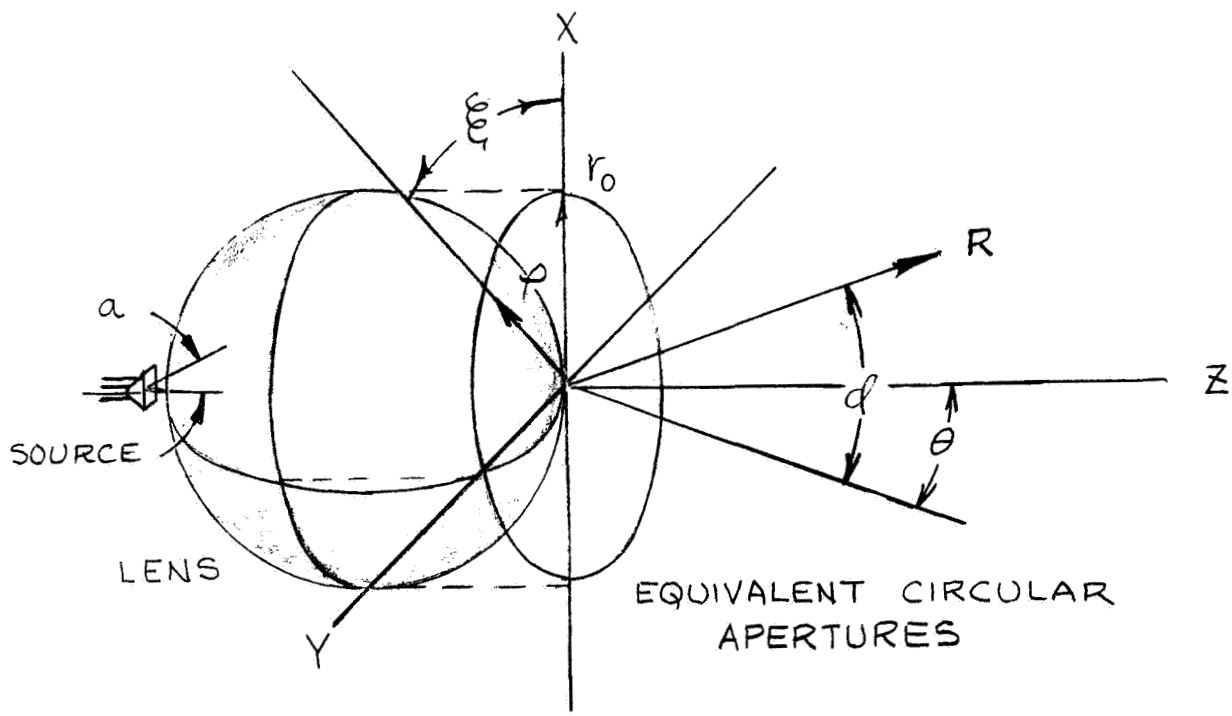

LUNEBERG LENS ANTENNA

FIGURE 5-13

The aperture illumination function is dependent on three properties of the system:

(1) The path loss along each ray through the lens.

(2) The actual path or "lay" of the ray in the lens.

(3) The source illumination function.

That the path loss varies with the path position is clear from a consideration of the traces.

The center or crown ray must traverse the densest parts of the lens, while the outer ray travels a much longer track through material approaching free space in density. The loss is proportional to the loss tangent and the density. The resulting circular aperture illumination is cusped with an almost 2 db depression in the center.

Luneberg Lenses have a tendency to "crowd the rim" so that energy in the source field at the higher angles (e.g., 50° up) show up near the edge of the circular aperture.

The third distortion is a result of a compromise with the dual polarization requirement and is not a necessary constraint on the four source form. In selecting a source the designer must choose among favoring the E plane, H-plane or compromising both of them. For illustrative purposes the E-plane has been favored in the numerical data below.

The path loss along a ray is:

$$L = |E_o| \, e^{-\pi \tan\delta \cdot \ell}$$

where:

$$\tan\delta = \frac{\sigma}{\epsilon\omega} = \frac{\epsilon''}{\epsilon'}$$

$$\ell = \frac{2r_o}{\lambda_o}\left(\frac{\pi}{2} + \cos\alpha\right)$$

The rays emerge from the far side of the lens crowded toward the outer rim by:

$$P = r_o \, \text{SIN}\,\alpha$$

The source illumination and function were obtained from Kraus[17] for the case where $\bar{E}$ at 90° was set to zero. The $\bar{H}$-plane source pattern was determined using the

aperture dimension of the $\bar{E}$-plane since dual polarization was postulated. $\bar{E}$ & $\bar{H}$ plane curves vs. angle α is shown in Figure 5-14.

Figure 5-15 shows equivalent circular aperture distribution for the $\bar{E}$ and $\bar{H}$ plane modified by losses. The case where $F(\alpha) = 1$ is shown for comparison the average ohmic (or heat) loss is 1.90 db over the face of the antenna.

The Secondary Pattern

The pattern[18] is obtained from the Fourier transform of the aperture distribution.

$$G(\theta,\phi) = \int_0^{2\pi}\int_0^{r_o} [F(\alpha)\cdot\rho] \left[e^{-(\pi\tan\alpha)\left(\frac{\pi}{2}+\cos\alpha\right)\frac{2r_o}{\lambda_o}}\right] \cdot \left[e^{j\beta\rho\sin\theta\cdot\cos(\phi-\phi')}\right] \rho\, d\rho\, d\phi'$$

where

$$\rho = r_o \sin\alpha$$

$$\beta = \frac{2\pi}{\lambda_o}$$

and

$$F(\alpha) = F(\xi,\rho) = F_H(\alpha)\sin^2\xi + F_E(\alpha)\cos^2\xi$$

also $\alpha = \text{arc}\sin\left(\frac{\rho}{r_o}\right)$

The constant terms can be taken outside of the integral:

$$G(\theta,\phi) = e^{-\frac{\beta\pi\tan\delta}{2}} \int_0^{2\pi}\int_0^{r_o} F(\alpha)\rho^2 e^{-\beta\left[r_o\cos+j\rho(\sin\theta)\cdot\cos(\phi-\phi')\right]} d\rho\, d\phi'$$

This equation can be evaluated by numerical integration, but since the average loss through the Luneberg Lens made of even high quality teflon is 1.9 db, the Luneberg Lens is too lossy to be considered a leading candidate for the sensor antenna although it is capable of a very compact package. However, to obtain an idea of the general shape of the secondary patterns and sidelobe levels Gaussian distributions with edge illuminations nearly the same as those calculated were derived from Lechtreck's[19,20] papers. The principle plane patterns using the Gaussian approximations are shown in Figure 5-16 .

Scanning the Luneberg Lens

Scanning systems using Luneberg Lenses are either switched fixed feed, or moving horn.

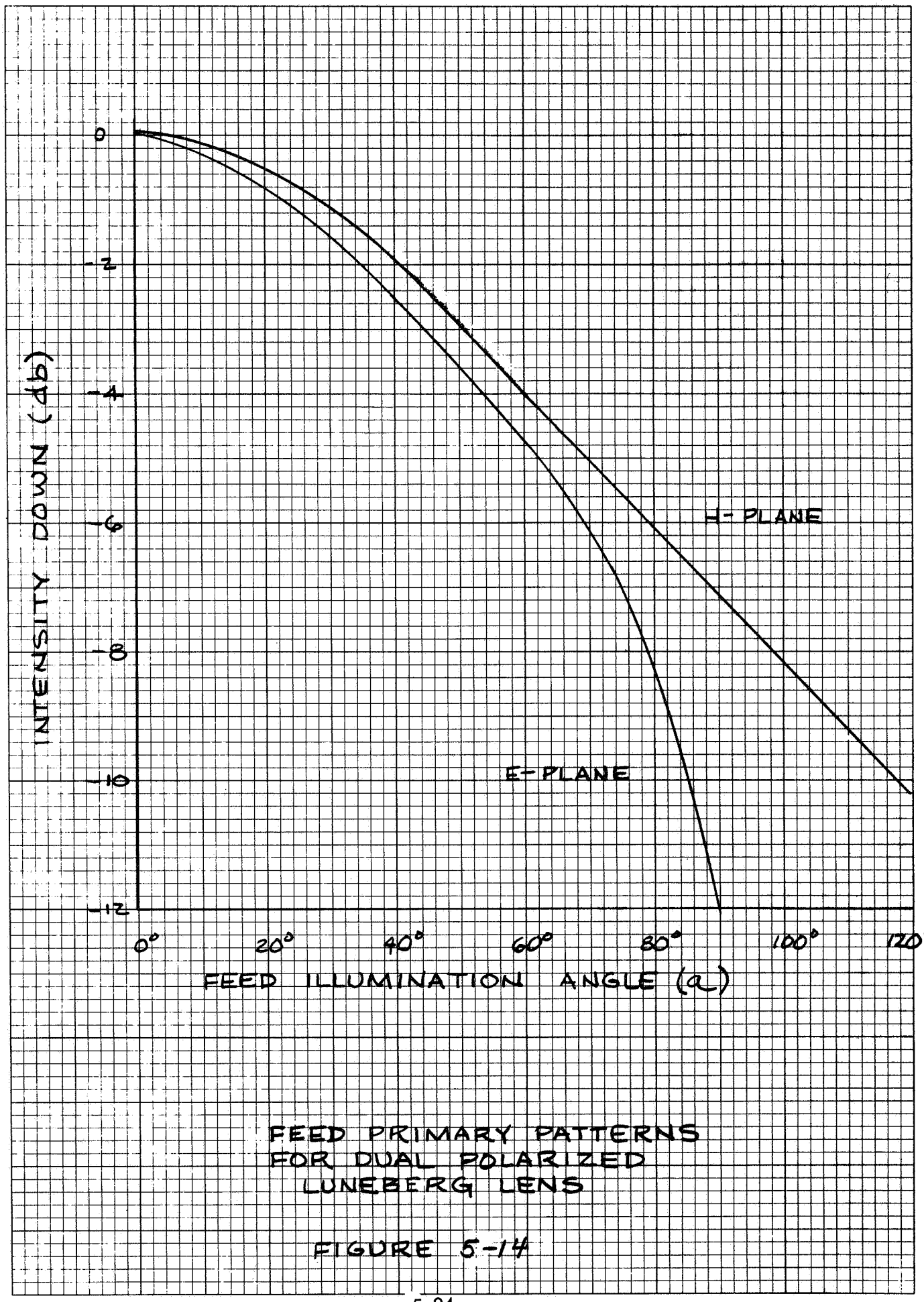

FEED PRIMARY PATTERNS
FOR DUAL POLARIZED
LUNEBERG LENS

FIGURE 5-14

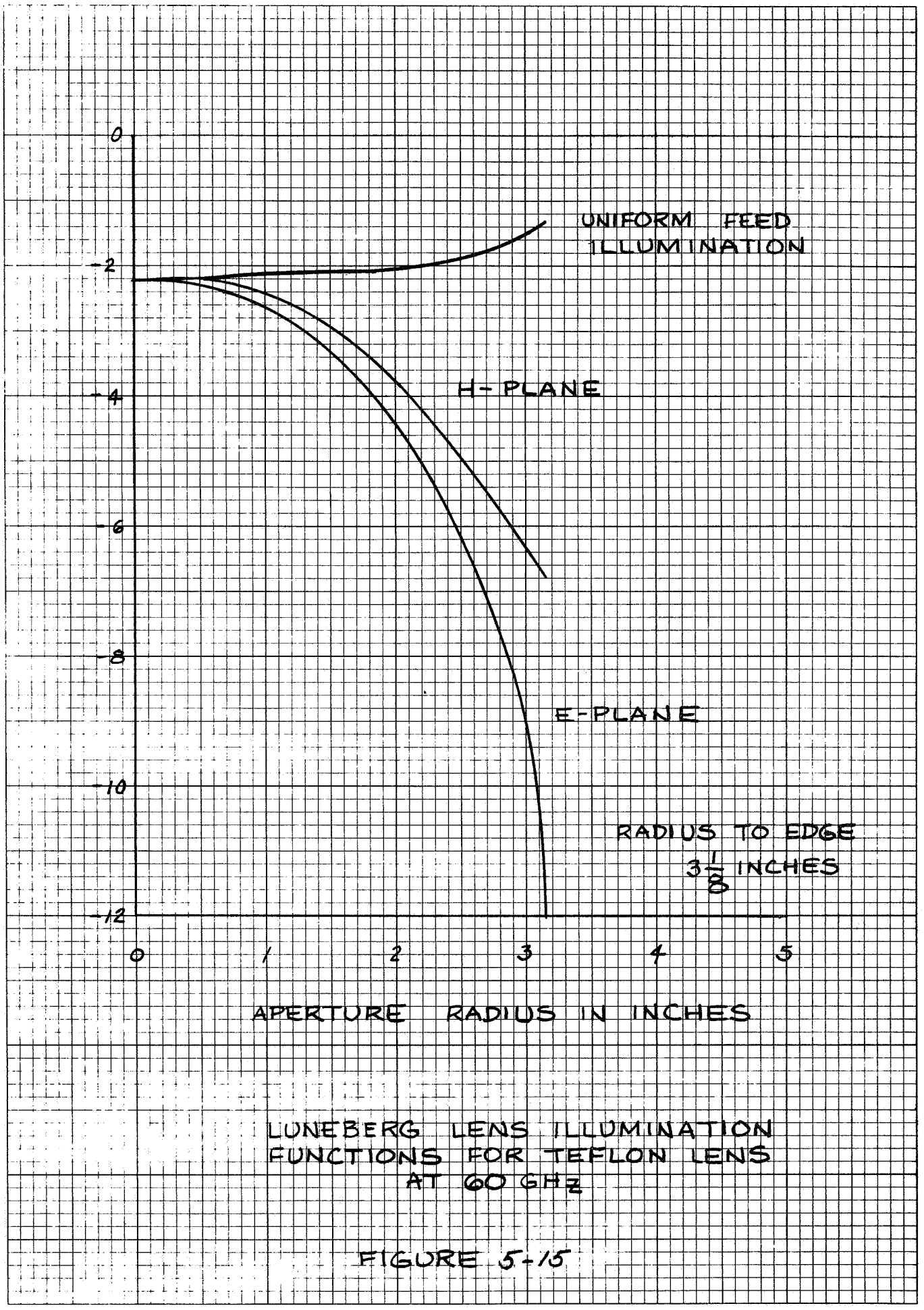

LUNEBERG LENS ILLUMINATION FUNCTIONS FOR TEFLON LENS AT 60 GHz

FIGURE 5-15

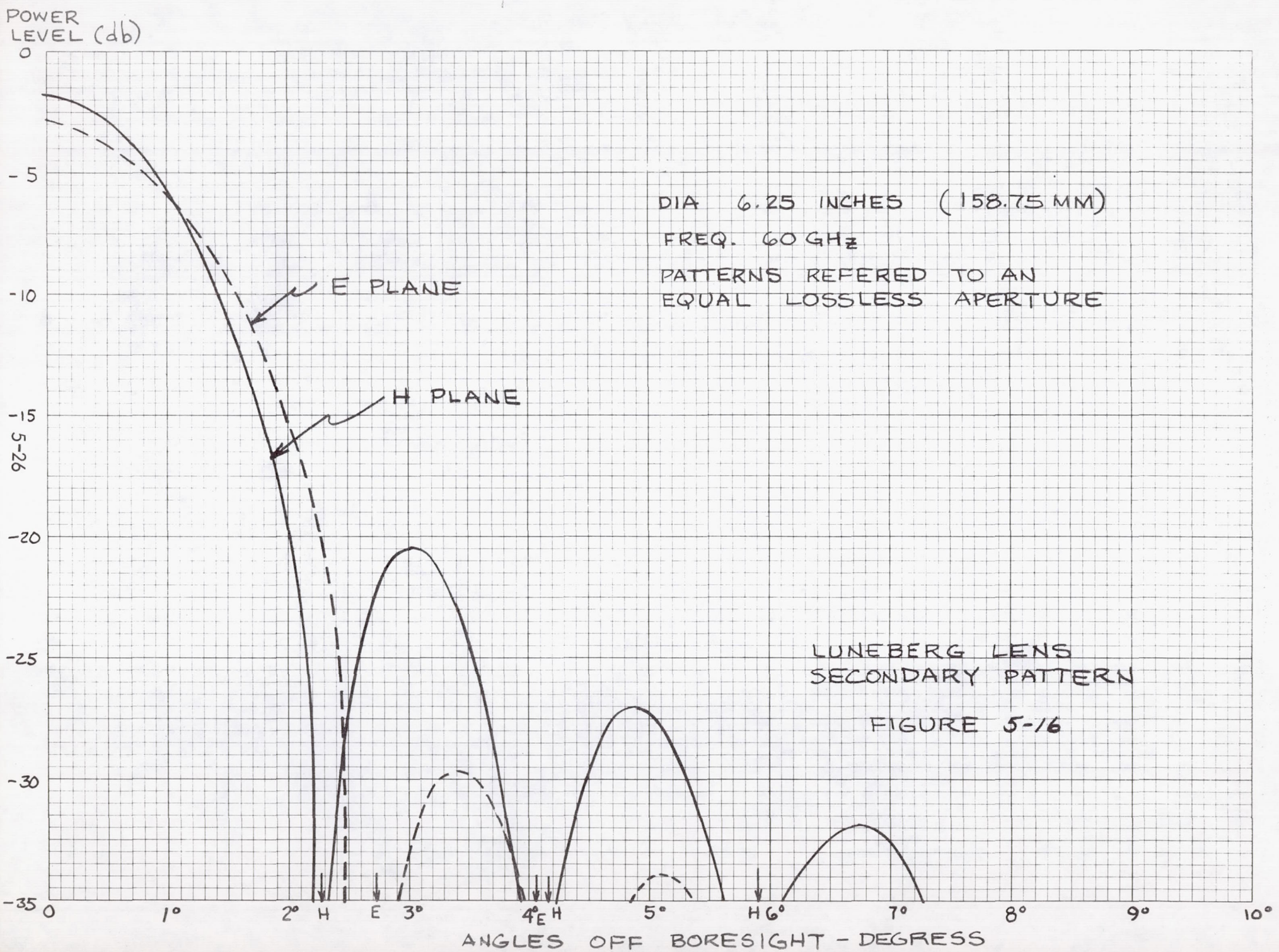

1) Non-Mechanical (Beam Switching)

The beam switching form, illustrated in Figure 5-17 , requires a separate feed for each fixed position of the beam. The length of the arc of scan is $r \cdot \theta$ The radius is $3\frac{1}{8}$" and θ is 27° (.47 radians).

$$L = \frac{3.125'' \cdot \pi \cdot 27^{\circ} = 1.47}{180^{\circ}}$$

By thinning the waveguide slightly, a feed system containing 10 horns could be installed along the arc. The center-to-center beam separation would be 2.7° which would place the adjacent beam cross-over points a little beyond the 3 db levels and at some satellite altitudes the 3 db would appear as an added loss. The crossover level can be brought up by decreasing the size of the lens and widening the beams, but fewer beams can be accommodated this way. The other method requires moving the feed to defocus the lens.

Although solid state switches could be used and would permit a non-mechanical scan system, the other disadvantages seem to outweigh the value obtained.

2) Mechanically Scanned

The basic motion of a mechanically driven feed horn is in Figure 5-18 . The feed scan track must be constrained to a circular arc about the center of the lens. The actual linkage can get complicated as suggested in the sketch (Figure 5-19).

While rotary joints are shown, flexible line, if carefully laid in, could be used. The positioner is shown moving a vertically moving rider on a screw to accommodate either the two or four horn versions of the systems.

Some height can be saved by laying the positioner mechanism horizontally, but at the expense of duplication for the other feeds.

The guide slot, linkages and drive mechanism may also be placed horizontally, but at the expense of duplication for the other feeds.

The guide slot, linkages and drive mechanism must be above a certain level determined by the clearance requirements for the beam at its highest angular position (78°). If this constraint is observed to the only aperture blockage is due to the feed itself, and to its waveguide.

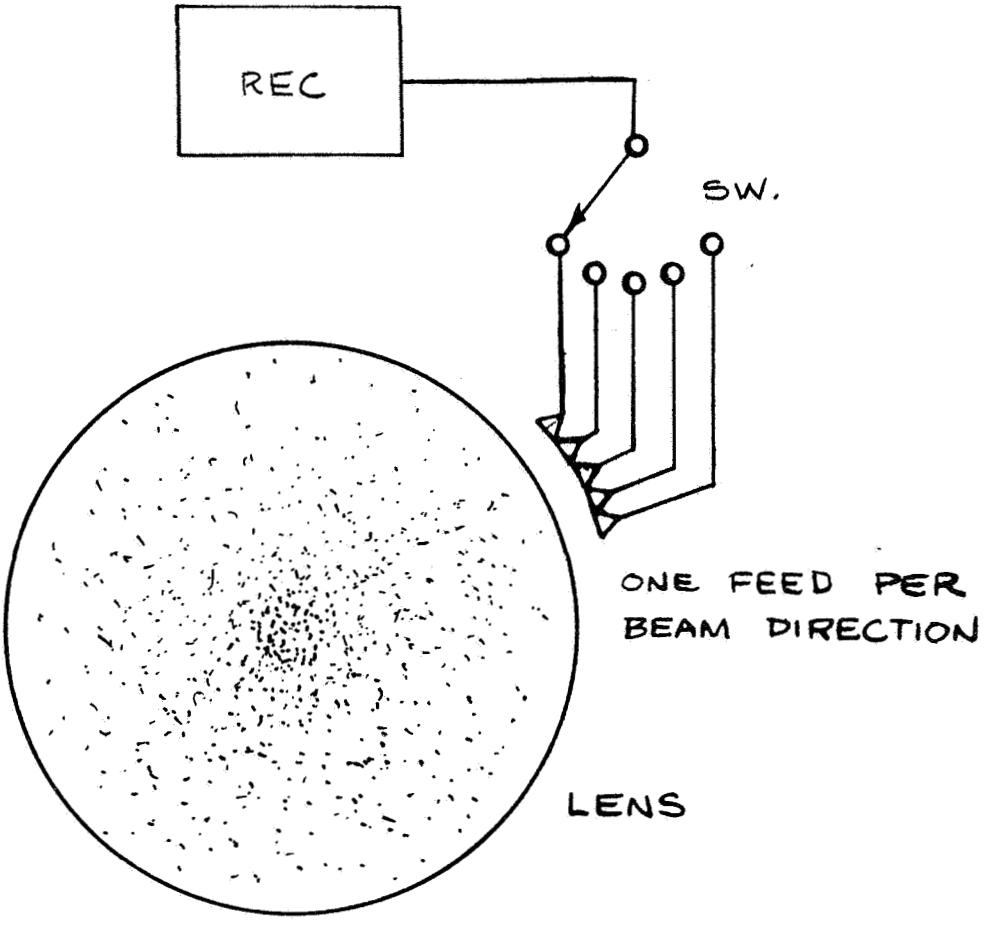

SWITCHED BEAM SCANNING OF
A LUNEBERG LENS ANTENNA

FIGURE 5-17

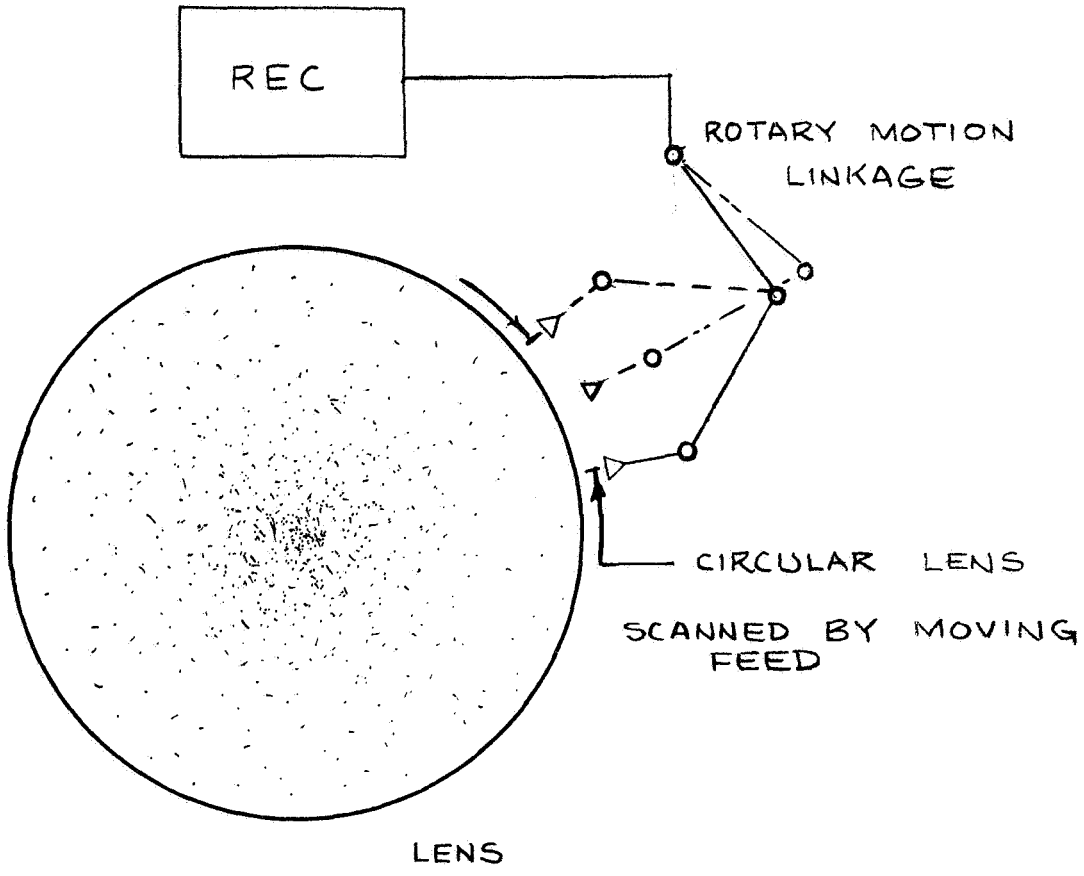

MECHANICALLY SCANNED LUNEBERG ANTENNA SYSTEM

FIGURE 5-18

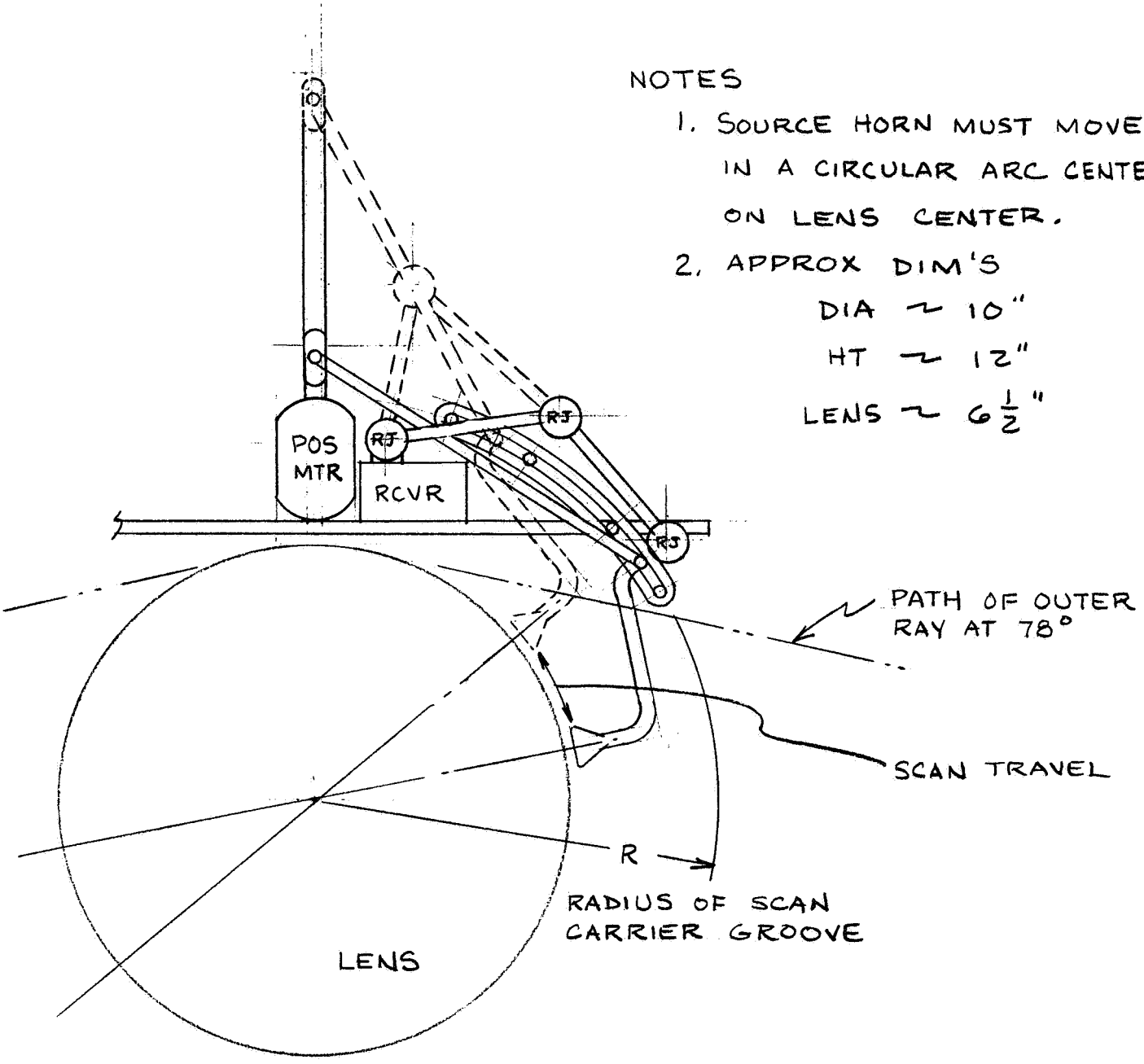

LUNEBERG LENS SCAN MECHANISM USING ROTARY JOINT

FIGURE 5-19

Summary

The Luneberg Lens has the advantages of small size and a minimum of bulk in moving parts as a mechanically scanned antenna. It can be used with four sources and a simple spherical lens with good pattern control.

The efficiency is poor (-5 to -6 db) and although the sidelobe level can be held reasonably low, there is not the degree of control over these pattern features that a simple parabolic aperture antenna affords. Weight estimates are not available for lenses designed specifically for millimeter use, but 6 inch lenses of polyfoam weigh about 1/2 lb (275.6 gr.).

5.3 Electronic Scan Antennas

Electronically controlled antenna systems are those in which the pattern is formed and aligned entirely by the use of electronic devices. The control devices employed may be switches of the diode or ferrite varieties, or variable delay lines of one form or another.

Frequency scan is a form of variable delay in which the frequency dependence of the line phase velocity is exploited for control purposes. For a number of reasons discussed at length in other reports, this form of scan is not suitable for radiometric purposes.

Included under the general topic of electronically controlled systems are those which involve computer-like data processing systems. There are three basic forms (1) with simple threshold controlled redundant system (2) the adaptive forms, and (3) the quite sophisticated "decision theoretic" forms. As usual, when categories are setup some hybrid cases turn up. The "redundant designs" while relying on a deceision device, may be constructed of subsystems of any of the three categories, "electronic", "electromechanical", or "mechanical".

The appeal in the electronically scanned moving beam antennas is due mainly to their lack of moving parts. This eliminates the need for space qualified lubricated surfaces, rotary joints, or flexible lines, and actuator mechanisms.

5.3.1 Method of Control

In phased arrays the phase (and frequently, the amplitude as well) of each element is varied according to some rule to produce a collimated beam (s) in space. Devices for doing this are switches, variable lines, and lenses.

Switching

The switches may be diodes or ferrites. Diode switches must be designed with care to (1)keep bias current requirements down and, (2) to reduce diode noise. The ferrites can be either the bias or the latching types.

The latching ferrite switch offers the possibility of eliminating the holding bias requirement. A magnetic pulse on the ferrite is used to flip it from one state to the other, and the associated circuitry determines the effect on the system. Problems have centered around reducing the latching energy pulse and in switching times. For example, in a large scale radar, the switching rate is often high enough so that even when the latching ferrites draw no power when resting, in either closed or open states, the power requirements are still as high or higher than an equivalent diode scheme. Where the scan rate is slow, a latching ferrite scanner control system would require very little power.

The state-of-the-art is not yet equal to producing latching ferrite switches for use directly at 60 GHz, however, phased arrays permit the handling of logic operations at any convenient frequency and conversion by either heterodyne or multiplicative frequency translation to the operating frequency. The control circuitry does however, tend to be bulky even in stripline, and the added loss and power requirements of the frequency translation chain must be included.

Ideally the switch has precisely two states; open and shorted. In practice diode and ferrite switches are neither completely open nor quite shorted. There are always residual reactance and resistence effects that reduce efficiency and produce detuning. These effects increase with frequency, and become severe in the millimeter spectrum.

Phase Delay

Switches are incorporated into the lines only to control the element phase delay. The techniques for directly producing the phase delay are:

1) Real time delay by introducing and removing line segments.

2) Frequency scan.

3) Phase split and recombination devices.

Real time delay systems depend upon the propagation time of a TEM mode wave along a transmission line. The line has a physically variable length section either directly changed, or indirectly by substitutionary switching, which produces the time delay, and ineffect, a time phase change at the element. Ideally, control networks of this class are not frequency sensitive. There is some incidental frequency dispersion due to residual reactance effects at switch points, branch points, and terminations. The state-of-the-art is well developed in stripline form for arrays up through L-Band (1500 MHz), and somewhat extrapolated to (10-12 GHz). Phase control using real time switching would have to be done at perhaps 6 GHz and translated.

Frequency Scan

Phase differences in a fixed line distribution network can be realized by using a frequency dispersive line or mode (e.g., $TE_{m,n}$). Frequency scan is not suitable for radiometry because of the very steady frequency required for the long integration times (e.g., seconds).

Phase Splitting

Phase split and recombination devices separate the wave on the line into two parts. One wave train is passed through a phase active element, and the other through either a passive line, or phase conjugate element. For example, if the one line has $+90^{\circ}$ shift, and the other -90°, with respect to the original wave, by combining the outputs in an amplitude summer, the output phase can be varied over 180°. Again devices for doing this are available up through X-Band, but would require development for 60 GHz. Again frequency translation as suggested above could be employed.

5.3.2 Types

Two general system types are considered:

(1) Phased Arrays at 60 GHz

Phased Arrays have been under intensive investigation in recent years

and a number of large scale radars incorporating this method of beam control have been built. In the older form of phased array, the energy from a signal source was routed through a power divider network then through the phase control elements to the radiator. When it was realized that the logic of the array could be separated from the power or signal paths, and extremely high powers and/or low noise operation on a large scale were viewed as possible. Radars, such as HAPDAR and MAR, perform control functions at low power and use linear amplifiers at the elements. The separate, but associated, receiving arrays equip each element with a low noise amplifier.

If the losses at L and S-Bands are sufficiently high that separation of signal level and steering control are necessary, the situation is orders of magnitude worse at millimeter wavelengths. Since phase is preserved in a heterodyne mixer, it is possible to perform steering at a low frequency, and to convert to the required signal frequency. Frequency multiplication (or division) also preserves phase information as a linear multiple. Both methods have been used.

The heterodyne array is the heart of the so-called "Adaptive" systems, and the linear multiplier technique was used in the MERA radar. If a millimeter wavelength phased array were required for this application, the latter method would probably have to be used, because of the frequency constraint problem previously discussed.

The actual distribution network would be designed in stripline at some convenient frequency in the centimeter wave spectrum (for example, 6 GHz). Each element in the array would require a separate radiator, low noise amplifier, frequency divider and phase shifter. Tapering would have to be introduced at the amplifiers, or through attenuators in the line between the divider and the Mixer (Figure 5-20). The number of elements in a phased array is approximately $N = \frac{10^4}{\theta_3 \cdot \varphi_3}$ where θ_3 , φ_3 are the 3 db beamwidths in degrees of the principle plane (no side lobes over -10 db). The number of active elements required for a $2^\circ \times 2^\circ$ is approximately 2500. To generate four pencil beams an equivalent of 10,000 elements would be required. If a cylindrical or spherical

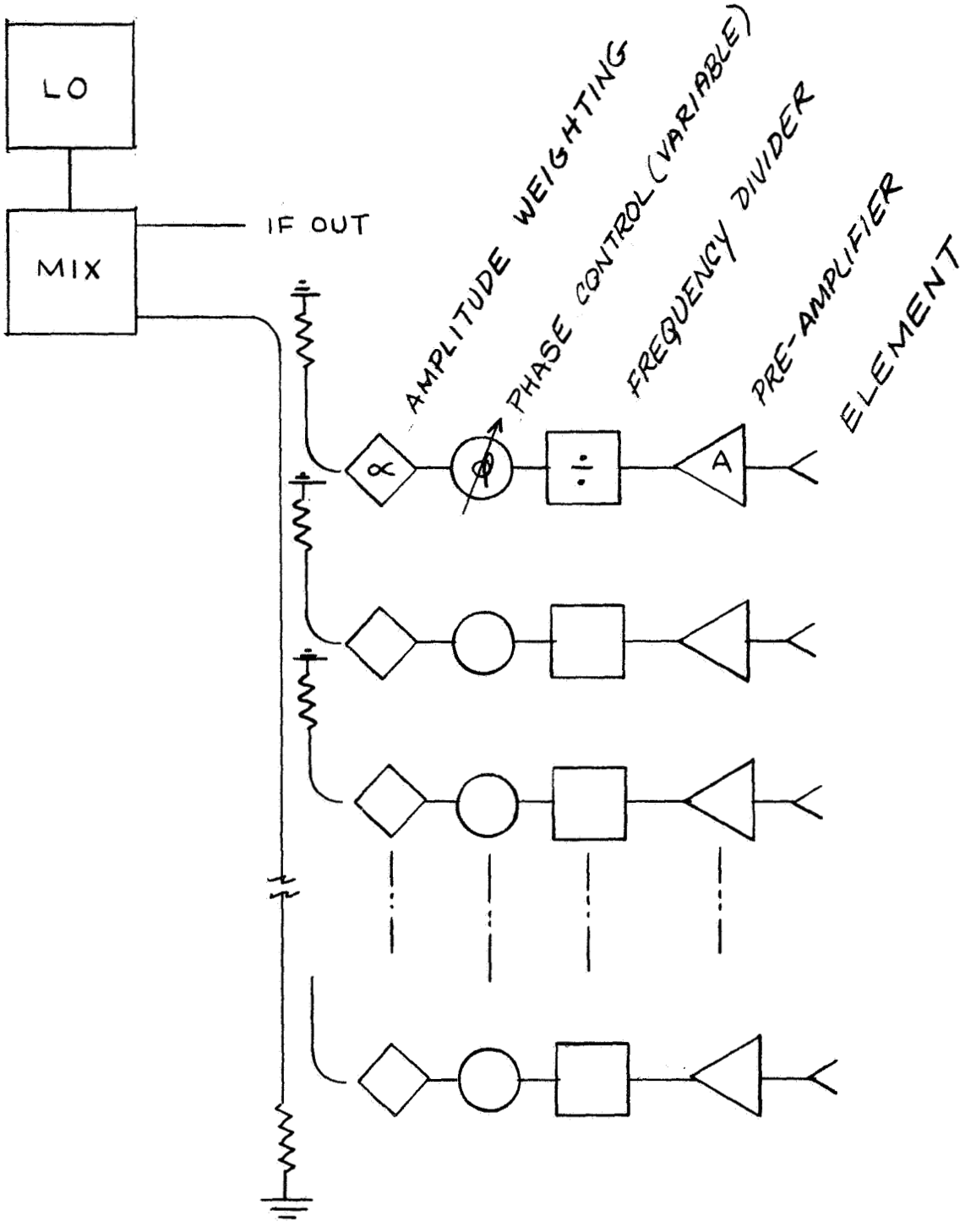

LINE FEED PHASED ARRAY

FIGURE 5-20

form of the array is used even more elements would be required to compensate for the loss of aperture due to oblique angles. The "beaver-tail" pattern would take fewer elements ($\sim$ per aperture 833).

In order to prevent grating lobes appearing in real space, the element spacing would have to be held to a half wavelength or less. The aperture required by 2° x 6° beam is 50λ x 10λ. This is compatible with a set of parallel lines of radiators, 100 elements long by 20 wide. Thinning to eight lines (800 elements) would introduce a grating lobe series in real space along the horizontal plane - (little improvement over the simple line source and flared horn).

Arrays of this sort seem to be a complicated way to achieve the advantages, if any, of electronic steering. Only one form of amplitude and phase control has been used for illustration purposes, and no discussion of the detail system for steering has been presented. The various forms of phase control, real time; diode switching, ferrite latching, variable parameter etc., have been all used with success at lower frequencies, and while these techniques may possibly be extended to 60 GHz, their use at 60 GHz is best circumvented by the heterodyning technique previously suggested, none of these appear feasible in a one year schedule. However, as ultimate systems, any or all of the possible schemes may prove feasible as better integrated circuitry becomes available.

(2) Redundant, Adaptive, and Decision Theoretic Systems

Undoubtedly the ultimate sensor will belong to that class of non-linear and adaptive antenna groups in which the computation of output is as much a part of the functioning of the antenna as the collection of the signal energy itself. Classical distinctions of pattern, gain, and other tests of "goodness" become virtually meaningless, or must be extensively redefined, and the effectiveness of the total system in terms of its prescribed performance emerges as the best test of worth.

If constraints on vehicle motion are not to be imposed, then systems which can perform under arbitrary or unspecified attitudes must be sought. There are three methods of meeting a situation of this sort.

1) Redundant System - Enough independent, but essentially complete

sensing systems are installed to cover all possible attitude states.

2) Adaptive Arrays - An array which sums and in some way uses this datum to provide relative control of each elementary output to maximize the sum, or over all output. The rates at which variation must be applied to each element also provides the data from which vehicle attitude and other information may be obtained.

3) Decision Theoretic Arrays - The decision - theoretic systems require an a priori model of the anticipated input signal in the system, and operates by making comparison computations against this model.

Redundancy

If the antenna is allowed to tumble or spin, and the horizons are to be viewed at all times, then more than one vertical sense system is required. If each sensor system can be gimballed through 140° (± 70°)spherical coverage can be obtained with four systems in a tetrahedral configuration, (see Figure 5-21).

With more data on the size and shape of the vehicle, the sensor locations and the nature of the vehicle motion, the number of units needed could be better estimated.

Some sort of a priori means of selecting the output of the sensor viewing the source from among the others must be provided. If each system is fully gimballed then only one or two would be able to place four beams on the horizons. If two systems succeed, then either will suffice to measure the vertical. The nature of the receiver outputs as each antenna system crosses the source, provides the criteria by which the value of the outputs is assessed.

The integration time of the receivers would need to be correlated to the satellite motion at least in a rudimentary manner. If the integration time were too long for the motion then no system would respond in time to provide a sense of vertical. Some form of gating and time segment integration could overcome this difficulty, but again some modest a priori knowledge of the spin environment seems indicated. A summary

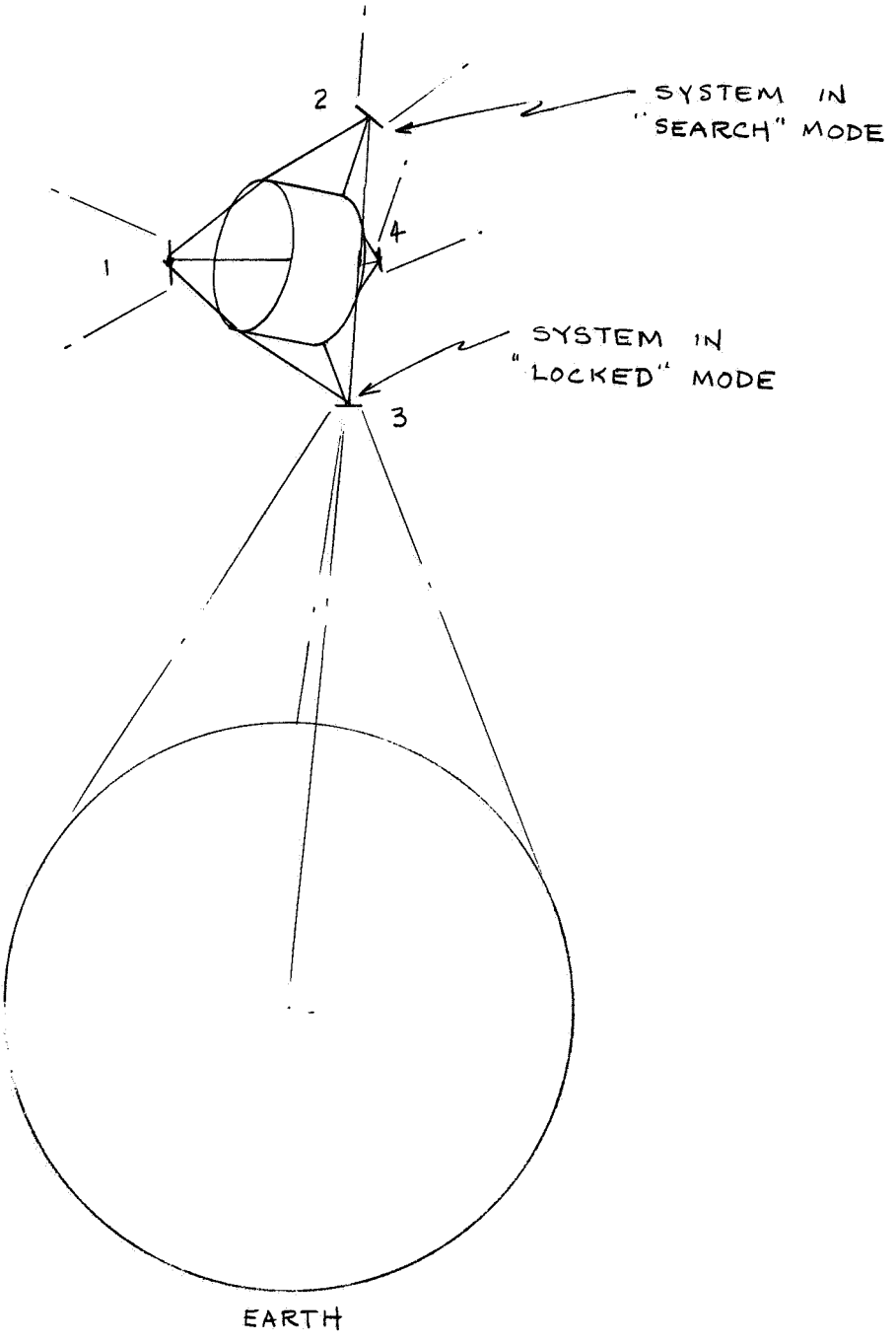

FIGURE 5-21

TETRAHEDRAL INSTALLATION ON AN ARBITRARILY TUMBLING VEHICLE

of these possibilities is provided in Table 5-1.

Electronically adaptive arrays seem to have descended from the Van Atta[1] retrodirective array. According to Skolnik and King[2], the idea of self-focusing is due to W.F. Morrow. A number of papers on the subject were published in 1964, in a special issue of the IEEE Transactions on Antennas and Propagation (AP-12 Vol., 2 March 1964) from which most of this material is taken.

The basic idea can be illustrated from the retrodirective Van Atta array shown in simplified form in Figure 5-22. The array elements are inter-connected by equal lengths of line so that $A_{i,j} \longrightarrow A_{-i,-j}$. The center element A_o is used for reference. It is shown connected to a shorted length of line $\beta \frac{\ell}{2}$ radians long, where

$$\beta = \frac{2\pi}{\lambda_o}$$

The phase shift from the input to return output is:

$$\mathcal{E}_{oin} = \mathcal{E}_o e^{(-\alpha + j\beta)\frac{\ell}{2}}$$

The other elements are inter-connected according to $A_k \rightarrow A_{-k}$ by a length of line ℓ units long.

A wave in at A_k:

$$_i A_K = \mathcal{E}_o e^{j\beta k \sin\theta}$$

Would arrive at A_{-k}:

$$_o A_{-K} = \mathcal{E}_o e^{-\alpha\ell} e^{j\beta(k\sin\theta + \ell\sqrt{\mu\epsilon}}$$

A wave entering at A_{-k} and traveling to A_k is similarly:

$$_o A_k = \mathcal{E}_o e^{-\alpha\ell} e^{j\beta(-k\sin\theta + \ell\sqrt{\mu\epsilon}}$$

Except for attenuation $(e^{-\alpha\ell})$ and a constant phase term $\beta\ell\sqrt{\mu\epsilon}$ the emerging wave is the phase conjugate everywhere of the incomming wave.

The waves traveling in opposite directions are phase conjugates of one another. Phase conjugacy is the criterion for a phase front of a transmitted wave

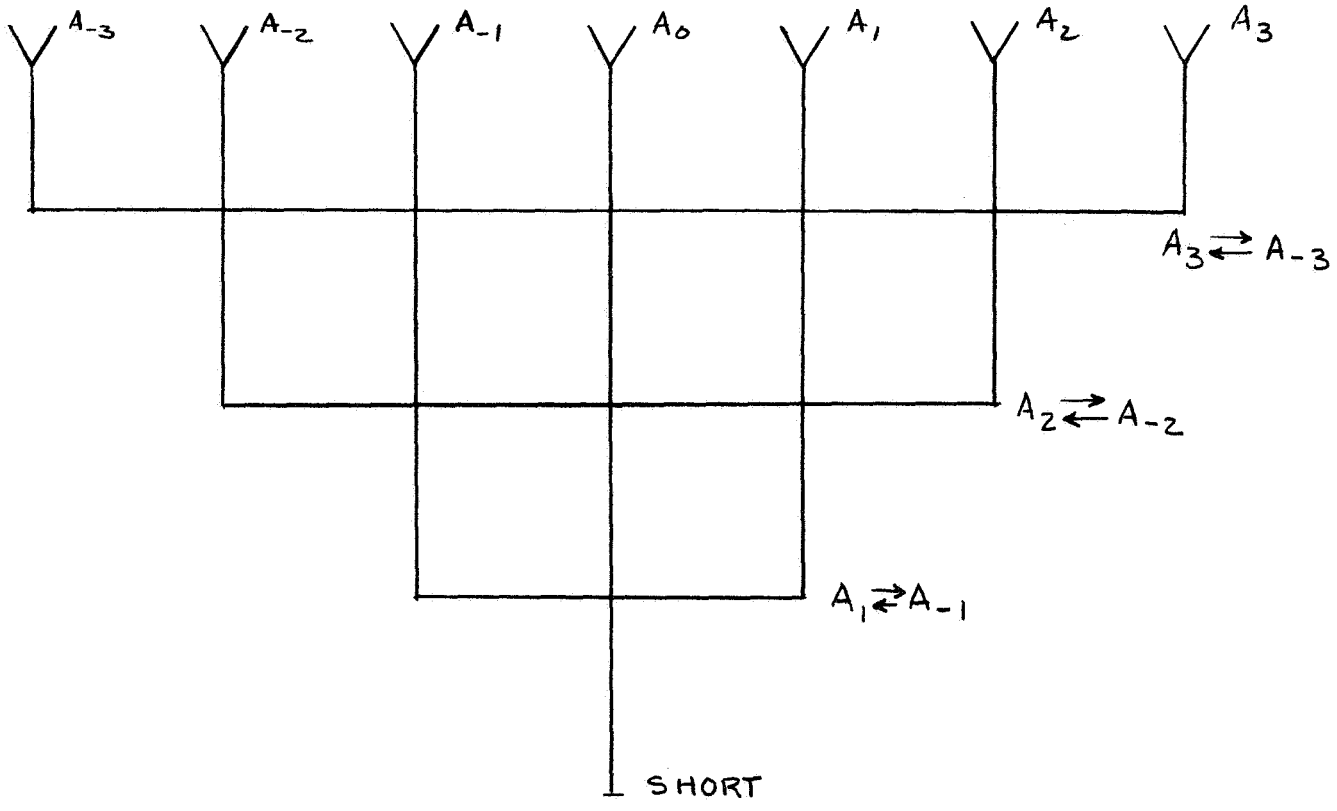

FIGURE 5-22
A SIMPLIFIED SINGLE LINE RETRODIRECTIVE ARRAY OF THE VAN ATTA TYPE

TABLE 5-1

REDUNDANT MOVING SATELLITE INSTALLATIONS

O_2 VERTICAL SENSING

Satellite Motion	Vertical Sense System
Spin stabilized	Single unit "de spun"
Tumbling (small satellite)	Four units at apeces of a tetrahedron
Tumbling or maneuvering large satellite	1) Four units plus enough more to cover all blind directions. 2) Time modulated integration system reduction of number of units.
Adjusted motion	1) Controlled from one or more units. 2) A priori data available for selection of degree of redundancy.

returning in the direction of θ. The introduction of an additional delay term line to line will steer the retro beam in another direction, and also modulated retrodirected output can be obtained by introducing a bilateral power amplifier at the center of each line.[3]

The adaptive feature can be brought into a tracking system similar to that indicated schematically in Figure 5-23 . The outputs of the two antennas are:

$$\mathcal{E}_{a_1} = \mathcal{E}_o \, e^{(j\beta \frac{s}{2} \sin\theta - j\varphi_1)}$$

$$\mathcal{E}_{a_{-1}} = \mathcal{E}_o \, e^{(-j\beta \frac{s}{2} \sin\theta + j\varphi_2)}$$

Servo controlled phase shift units φ_{-1}, φ_1, are controlled by a null tracker connected to the difference output receiver, Δ , such that: $\varphi_{-1} = \varphi_1 = \beta \frac{s}{2} \sin\theta$

The equations of the sum and difference outputs are:

$$\begin{cases} \mathcal{E}_\Sigma = 2\mathcal{E}_o \\ \mathcal{E}_\Sigma = 0 \end{cases}$$

Schrader[4] and others have shown that the adaptivity feature, shown semi-mechanically for illustrative purposes, can be implemented electronically by taking advantage of the phase conjugate properties of opposite side bands in a mixer.

An Adaptive Radiometer

Phase coherence, as such, does not exist in a thermal source, however, power envelope phase does exist, and can be used to add adaptivity to a system. Consider an arbitrary set of horns A_1 to A_n, placed at opportunity on a vehicle of some shape, as shown (two dimensionally) in Figure 5-24 . Each horn has a pattern sufficiently broad to provide some overlap with its neighbors. A receiver at each horn detects the noise power envelope, the output of which is similar to that shown in Figure 5-25.

The data processing of the receiver outputs would provide one of two results. (1) Steering commands to place a particular reference angle (space craft coordinates) on the vertical, or (2) a measure of the rate of change of the vertical in the space craft coordinates.

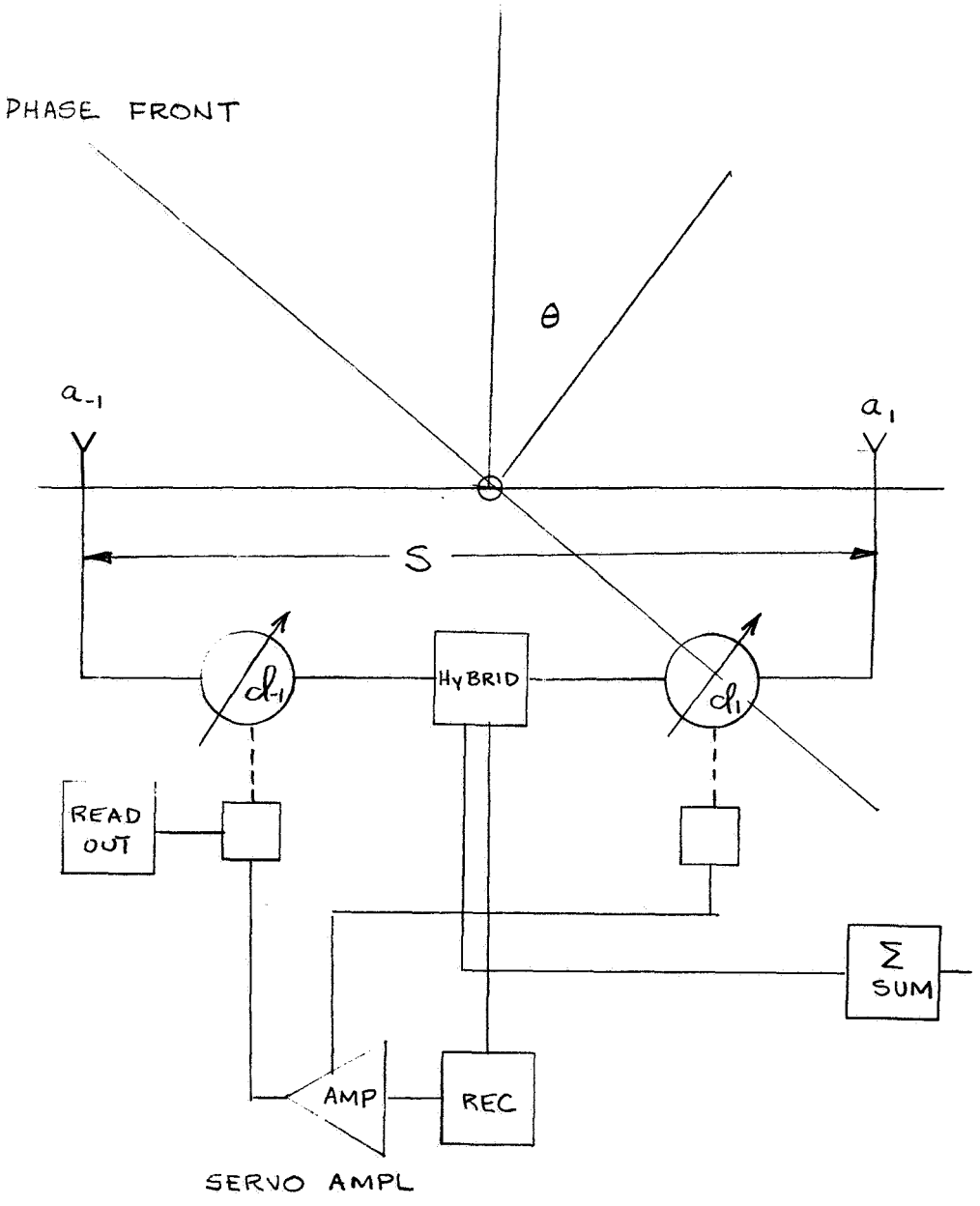

FIGURE 5-23

SIMPLE TWO ELEMENT "ADAPTIVE" SYSTEM WITH PHASE TRACKING READ-OUT

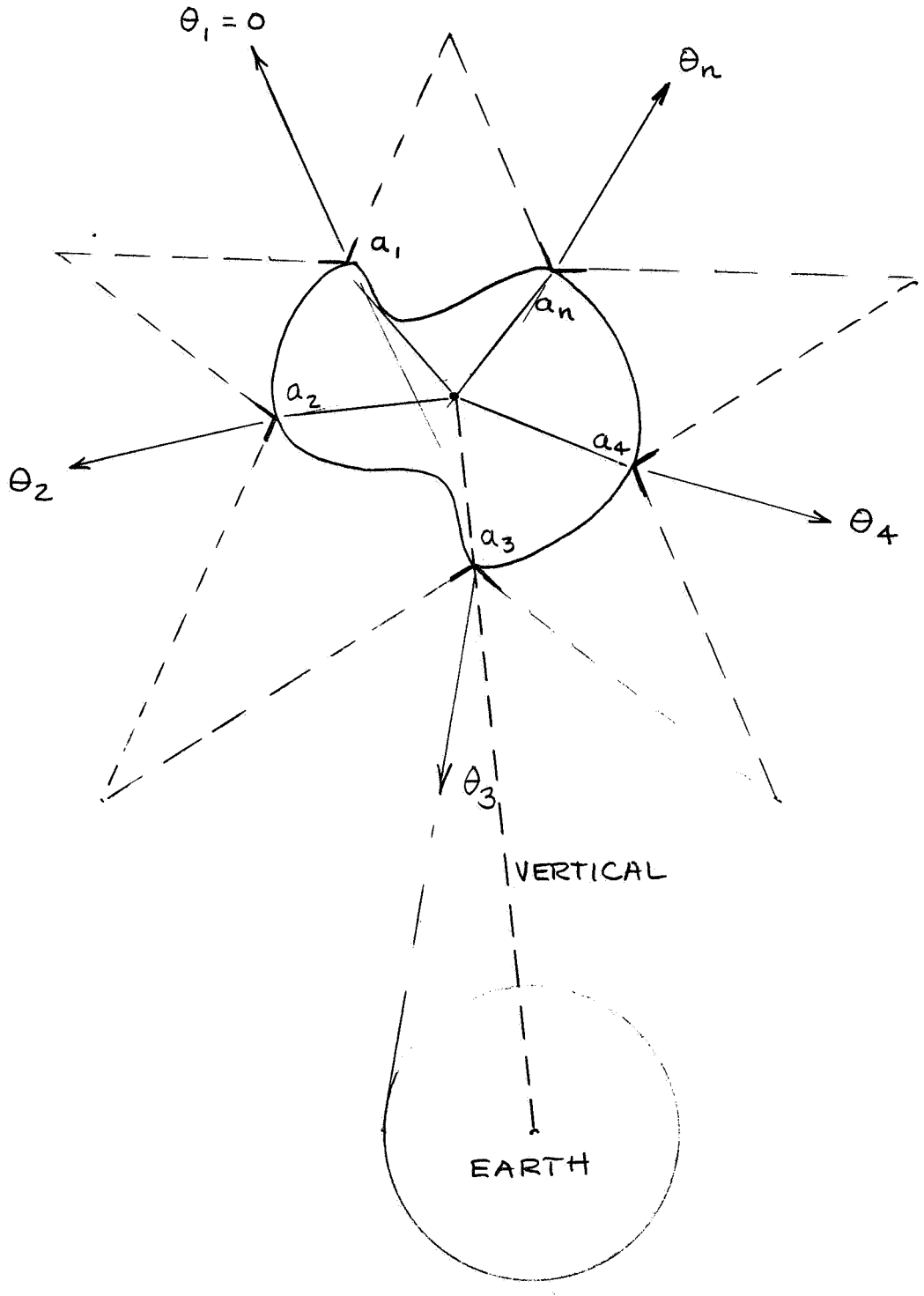

FIGURE 5-24
ACTIVE ADAPTIVE RADIOMETRIC
VERTICAL SENSING SYSTEM

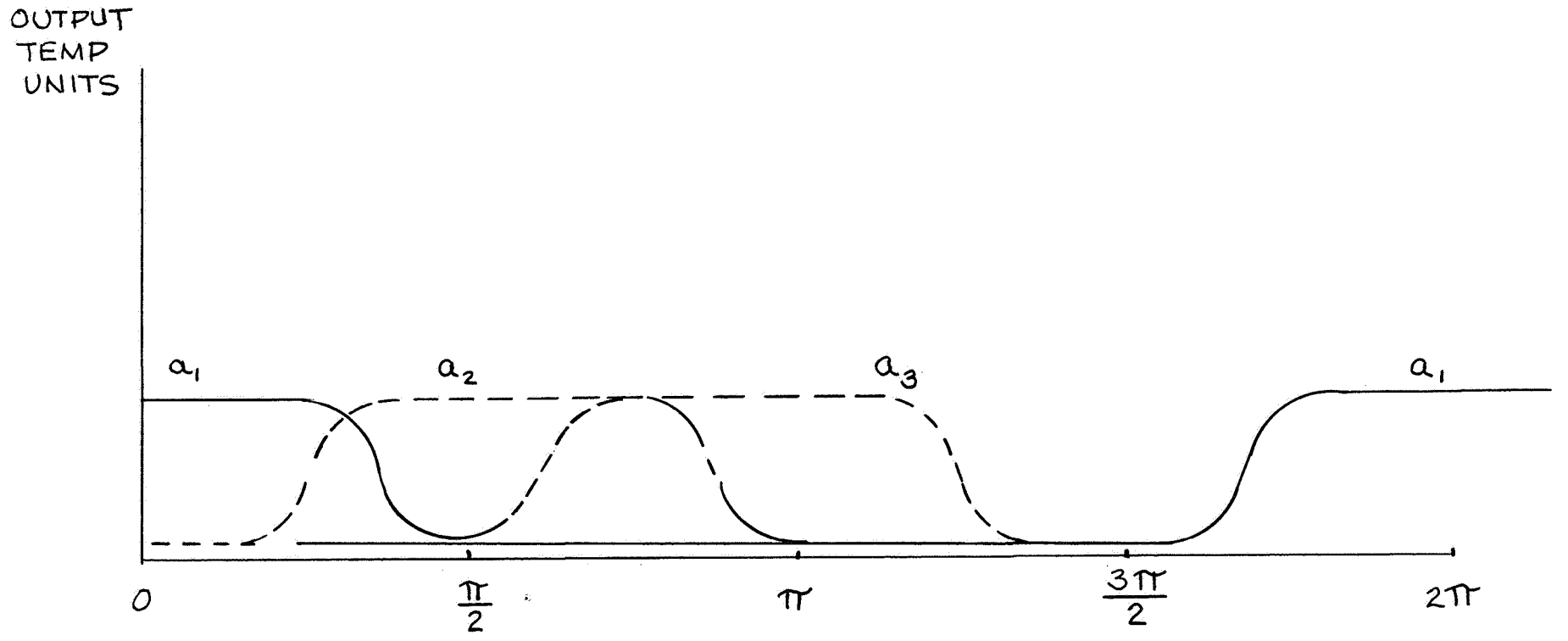

FIGURE 5-25

ANTENNA ELEMENT OUTPUTS
REFERRED TO AN ARBITRARY ANGLE
SYSTEM CENTERED ON ELEMENT a

By comparing A_1 with A_2, A_2 with A_3, and so on the pair centered most closely on the planetary mask would be found. By sliding, in a time sense, the crossing points of the first one edge, and then the other power patterns could be brought into coincidence. This provides the adaptive feature needed to compensate for the divorce of constraint on the array configuration. The amplitudes are shown clipped and the lower threshold given an arbitrarily low level to provide a simple computer absolute levels to determine when an elementary antenna is, or is not,crossing the rim.

The advantages of a system devised along these general lines are:

1) Small elements are used.
2) Array elements are located at "opportunity" in sufficient number to provide spherical coverage.
3) No severe constraint on spacecraft attitude or motion .
4) All data processing performed at low audio rates in a simple computer.

The draw-backs, however, are:

1) Each element has its own receiver and integrator.
2) An on-board data processor is required.
3) Although the initial selection of the element sites is arbitrary, once chosen their location with respect to the satellite coordinate system must be measured closely.

The requirement that each element have its own radiometric receiver is not too serious, if integrated circuitry is available by the time a system such as this is projected. Once a suitable I.C. receiver has been developed it can be duplicated in large numbers.

The third problem is a matter of knowing precisely the size and shape of the vehicle and the location of the elements on it. This data would be developed as a matter of course in the preparation of installation drawing station numbers.

Decision - Theoretic Antenna Process

The Decision Theoretic Concept

Decision Theoretic antenna systems have been receiving attention recently for radar application, primarily because of the promise such systems hold for very high resolution and for target detection in extremely cluttered or noisy fields. A decision theoretic system seeks to solve the equation:

$$P_{(m/r)} = \frac{P_{(r/m)} \cdot P_{(m)}}{P_{(r)}}$$

where

P(m/r) = probability that the true signal form is m given that the received signal is r.

p(r/m) = probability of receiving r given m.

p (r) = a priori probability of receiving r.

p (m) = a priori probability that m is the true signal form.

also

r = m+n

n = receiver noise

Note that the actual signal is unknown; only a probability that it is "m" is available as a datum.

In the extended discussions of these systems by Ksienski[5], Young[6], and Howard[8] the point is repeatedly made that the effectiveness of decision - theoretic detection is greatly improved by a good a priori model of the target configuration. When little (or nothing) is known about the target, a generalized or inclusive a priori model is assumed, upon which the system proceeds. For example, a radar looking for an unknown number, but less than some maximum number, m of discrete targets in unknown directions may use the a priori model of m + 1 targets equally likely everywhere within a volume of space. The decision theoretic array and its associated computer would sift the input data and assign probabilities (or "risk" numbers) approaching unity to some n targets ($n<m$) located at a set of points $(\rho_i, \varphi_i, \theta_i)$, and $p \rightarrow 0$ to the others.

A system intended to view the oxygen mantle of the earth, for example, has an enormous advantage over the radar case, in that one and only one target is known to exist in the field. Furthermore, a great deal more is known about the source, its size, shape and thermal distribution than the radar designer can hope for in his targets. All of this data is of considerable value in constructing an accurate a priori model against which the data processing computer must compare the sensor input information.

The ambiguities which the data processor must resolve, involve the location (ρ, φ, θ) of the sub-satellite point in a spherical coordinate system centered on the satellite itself.

Decision theoretic systems operate by comparing element by element of each segment of the array with an anticipated output derived by assuming certain things about the region being investigated. The true signal cannot be known, but only an actual measured signal. The problem is whether or not the measured input has an acceptable probability, having been generated by the source about which information is sought. Figure 5-26 illustrates the concept for two, more or less Gaussian forms.

One curve, $F_a(T)$, constructed from the outputs of the array is expected to be measured if a source with certain features is postulated. The sampling of the total array,

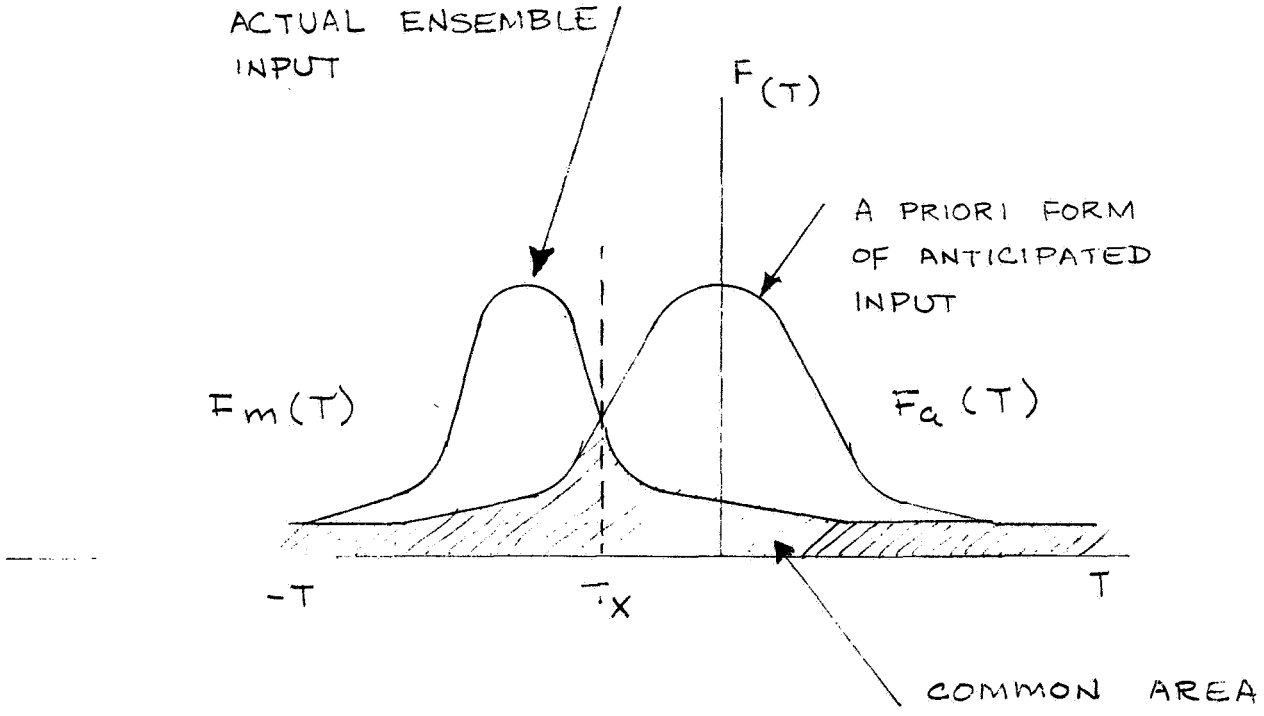

FIGURE 5-26

A POSSIBLE DATA PROCESSING FORMAT

however, develops another curve, $F_m(T)$. T is some function variable dependent on (ρ, φ, θ) of the spacecraft.

The error is due to the lack of congruency of the two curves, and various figures of merit, or error outputs can be derived from it. Assuming that the two functions have a common range $[-T, T]$, the product function, f will have a value ranging from 0 to 1.

$$f = \frac{\int_{-T}^{T} [F_a(T)] \cdot [F_m(T)] \, dT}{\int_{-T}^{T} [F_a(T)]^2 \, dT}$$

If the a priori model is an exact fit to the measured data, then the output would be unity, but in general the number would be less. If the system could modify the working version of the a priori model by a scheme of updating, then it would be adaptive.

Neither Ksienski nor Young consider the possibility of making their systems adaptive. Such a system, however, would provide considerable new data on the Thermal mantle. If an a priori model derived from a mathematical concept were used to obtain the first measurements of vertical, and satellite altitude, it could continue to do so as long as desired, but if however, after these parameters are established the new measured distribution is substituted for the original a priori model and all points of variance noted, two results would be obtained: (1) the navigational parameters can be refined, and (2) the variances used to correct the thermal model of the source.

An adaptive decision theoretic system of this sort would be more useful for orbiting missions to other planets where an atmospheric thermal mantle can only be guessed at the time of launch.

Operational System Concept

Suppose that a number, k , of low gain antennas have been deployed over the spacecraft, such that each segment of a sphere enclosing it will be viewed by at least i elements. The beam centers of each element are known with a precision, p.

The receivers in each element are set to respond in an all or nothing manner. That is, if the source is in view of an element, then the output of its receiver will be 1, if not then a squelch threshold would hold its output to 0. If a set of antenna elements S(a) have outputs of 1 and the set S'(a) 0, then the earth would be directly opposite the centroid of S to a precision, $1-p^a$, where a is the number of antennas in the set. The limiting elements in the set S, set a measure of the arc of the source from which the altitude can be obtained, subject to the error in the threshold response of the peripheral elements.

As an element begins to view the rim of the source, the noise power will build up. The transition zone from squelched to saturation will take some finite time, and consequently some error will occur. There is a risk that an error may creep in if the a priori distribution assumes that a 1 should exist, but, in fact, a zero is indicated. The probability of an error will be reduced by having a better a priori model, and by a larger sample (e.g. more elements). The second approach is limited by the practicalities of introducing more elements. The former can be implemented by correcting the computer's model by adaptivity. That is, after the first data processing cycle has been completed, the initial a priori model is replaced by the measurements, after each cycle the thermal mantle model is updated to the most recent measured distribution.

The "on board" computer would obtain its input by sampling all of the elementary receivers, and perform a centroid computation of all of those showing an output of unity. The direction cosines of this vector constitute the output information of the sub-satellite point. The second step would be to compare the locations of the set of all elements having near neighbors with zero output. This set is the "ring" of antennas that can barely "see" the source, and provides a measure of the angular extent of the source.

A simple two dimensional model is shown in Figure 5-27. Antennas a_1, a_2 and a_6-a_{11} do not see the earth above the 3 db levels in their patterns. Their outputs are consequently set to zero. Antennas a_3 and a_5 are the extreme members of the set that "see" the source and to a first approximation the angle of the sub-satellite point is 1/2

OUTPUT TABLE

ANT	OUT
a_1	0
a_2	1
a_3	1
a_4	1
a_5	1
a_6	0
a_7	0
a_8	0
a_9	0
a_{10}	0
a_{11}	0

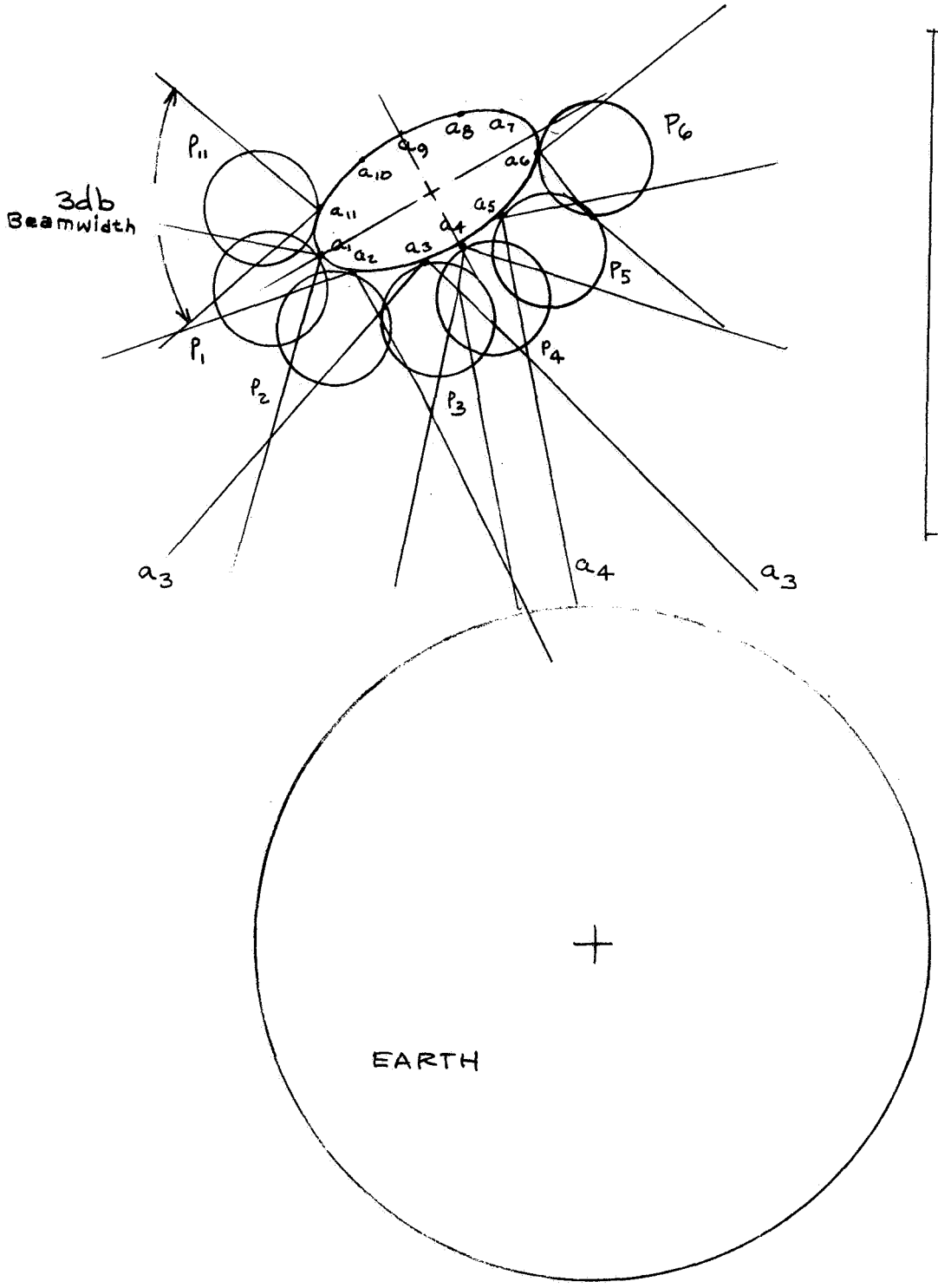

FIGURE 5-27
A SIMPLIFIED TWO-DIMENSIONAL DECISION - THEORETIC ARRAY

$(\emptyset a_3 + \emptyset a_5)$. Including all the elements in the set serves to refine the accuracy. Adding more elements to the set will improve the accuracy, and the precision up to a point set by the requirements and by environmental effects beyond the control of the space craft designers.

Advantages and Disadvantages

The advantages of a system of this sort are:

1) Arbitrary location of elements.
2) Electrical independence of all antenna elements.
3) Spherical coverage without restriction on satellite motion.
4) If the total number of elements is large, the system can "fail gracefully." That is, the loss of an element in an ensemble would have little effect on the probability that the measurement being made was the true one.
5) It can be made "adaptive" to provide scientific data on the thermal mantle.

Against these advantages must be set the following considerations:

1) A fairly extensive system design program would be required to reduce the concept to working hardware.
2) A special purpose compter would be required, preferably on board. For a near-earth mission, telemetry to a ground based computer could provide necessary output. For distances where the signal time becomes large (to the outer planets) on-board data processing is indicated.
3) Each element must be equipped with a complete receiver. With the state-of-the-art in integrated circuitry progressing as it is, this is not seen as a serious problem.

Summary

The non-linear data processing class of systems can be adapted to the

purposes of spacecraft orientation, and to scientific measurements. These systems would require fairly extensive development, with the exception of the redundant forms of current "off-the-shelf" hardware. Considerable freedom in array arrangement appears possible in the adaptive and decision - theoretic systems, and this may be quite valuable in working around interface problems. A self-correcting decision - theoretic system can provide nearly continuous "updating" of the mantle model. It could also be used to obtain data about other planets by correction of an arbitrary a priori model, as well as providing data for guidance.

Because of the freedom in form and to the probable scientific instrument functioning of an adaptive decision-theoretic system, it is recommended that a continuing study of these systems be carried on. The objectives would be:

1) Continue to follow closely the radar research in this area.
2) Review all available work on decision - theoretic radars.
3) Seek ways of adapting such systems to radiometry.
4) Conduct a review of the state of this art in:
    a) Integrated circuit receiver systems.
    b) I.C. computer technology.
5) Do a trade-off of the various ways of processing the data, and determine the most useful form in terms of (1) complexity, (2) cost, and (3) availability in terms of a projected time period of eight years (e.g., in time for the "Grand Tour.")

REFERENCES:

1. Van Atta, L.C., "Electromagnetic Reflector", U.S. Pat. 2,908,002, October 6, 1959.
2. Skolnick, M.I., and D.D. King, "Self-Phasing Array Antennas", IEEE Trans. AP-12 V2, March 1964, p. 142 ff.
3. Andre, S.N., and D.J. Leonard, "An Active Retrodirective Array for Satellite Communications", IEEE AP-12, p. 181 ff.
4. Schrader, J.H., "A Phase-Lock Receiver for the Arraying of Independently Directed Antennas", IEEE Trans. AP-12, Vol. 2, March 1964, p. 155 ff.
5. Ksienski, A.A., "Very High Resolution Techniques", Hughes Aircraft Co. Rept. P65-97, Contract DA36(039) - SC 90772.
6. Ksienski, A, A,- "Signal Processing Antenna Systems", Antenna and Scattering Theory: Recent Advances",The Ohio State University 1966, Vol. 1, p. 44.
7. Young, G.O., and J.E. Howard, "Comparison of Multidimensional Decision-Theoretic Antenna Processing System and Conventional Systems", Hughes Aircraft, May 1968 for AFCRL, AFCRL-68-0366.
8. Young, G.O., "Antenna Processing for Surface Target Detection", 1968 G-AP, Int'l. Symposium, September 9-11, 1968, Boston, pp 31-32.
9. See Bulletin 29, "Microwave Ferrites for Rotators, Isolators, Duplexers" - The Indiana General Co., Keasby, New Jersey 08832.
10. R.K. Luneberg, Mathematical Theory of Optics, Brown University Press, 1944.
11. J.E. Eaton, "An Extension of the Luneberg-Type Lenses", NRL Rpt. 4110, February, 1953.
12. B. A. Lippmann, "An Elementary Discussion of the Luneberg Lenses", TRG Technical Report #1 on AF 9 (604)-1015, 1954.
13. G. D. M. Peeler and D.H. Archer, "A Two-Dimensional Microwave Luneberg Lense", NRL Report 4115, March 1953.

For a general discussion of Luneberg, Eaton, Eaton-Lippmann, Peeler-Archer lenses etc., see:

14. R. C. Rudduck & C.H. Walter, "Surface Wave and Geodesie Lenses Antennas"., The Ohio State University, "Antenna and Scattering Theory, Recent Advances, Volume II, 1966.

15. K. H. Breeden & A. P. Shepherd, "Millimeter and Sub-Millimeter Wave Dielectric Materials", Microwave Journal. Volume 10, No. 12 - pp 59-62, November 1967.

16. K. S. Kelleher, "Scanning Antennas", Chapter 15, Antenna Engineering Handbook H. Jasik ed. p 15-21ff

17. J. D. Kraus, Antennas, McGraw-Hill, 1950 - pp 344 and 380.

18. S. Silver, Microwave Antenna Theory and Design. McGraw Hill 1949, p 192 ff Volume 12, Rad. Lab Series).

19. L. Lechtreck, "Radiation Charts for Paraboloidal Antennas", Electronics, September 12, 1958 - pp 104.

20. L. Lechtreck, "Radiation from Gaussian Sources", (Abstract from unpublished doctoral dissertation - Washington University, St. Louis 1961).

21. Constant K and Luneberg Lenses are available from:

    Emerson and Cumming
    Canton, Massachusetts

    and

    Armstrong Cork,
    Defense Products Division
    Pittsburgh, Pennsylvania

22. Cheston, T.C., "Array Antennas", The John Hopkins University, Silver Spring, Maryland. TG - 956, March 1968. (AD 668 137), pp 2-4.

23. Walter, C.H., Traveling Wave Antennas, McGraw - Hill, 1965, P. 405.

24. Silver, S., Microwave Antenna Theory and Design, McGraw - Hill 1949, p. 180 ff (Vol. 26, Rad Lab Series)

REFERENCES

25. Dicke, R.H., "The Measurement of Thermal Radiation at Microwave Frequencies", Rev. SCI. Instr., Volume 17, July 1946, pp. 268-275.

26. Drake, F.D., Ewen, H.I., "A Broadband Microwave Source Comparison Radiometer for Advanced Research in Radio Astromony", IRE Proc., Volume 46, No. 1, 1958 PP. 53-60.

27. Taylor, H.P., "The Radiometer Equation", Microwave Journal, May 1967, pp. 39-42.

28. Taylor, H.P., Zulch, D.I., "Radiometric Monopulse Receiver Systems", Patent Application.

29. Ryerson, et al, "RADC Reliability Notebook," Vol. II, RADC-TR-67-108.

30. Hess, W.N., "The Radiation Belt and Magnetosphere, "Blaisdell Publishing Company, Waltham, Mass., 1968.

31. Hodgeman and Lange, "Handbook of Chemistry and Physics," Chemical Rubber Publishing Company, Cleveland, Ohio, 1927.

32. Shklowsky, "Cosmic Radio Waves," Eq. (1-5).

APPENDIX A

SYSTEM DESCRIPTION

1.0 INTRODUCTION

A millimeter wave oxygen sensing radiometer system is examined for the capability of determining the local vertical from a spacecraft.

The complete system (Figure A-1) consists of an antenna, a radiometric receiver, and a servo control subsystem. The output is a display of the earth vertical direction in local spacecraft coordinates.

The antenna subsystem consists of the antenna aperture, the feed, and the squint angle servo. The squint angle is defined as the angle between the tracking line and the beam line-of-sight. When properly set the line-of-sight intercepts the rim of the oxygen mantle. The angle is dependent upon the vehicle's altitude. This dependence is given for $\eta = 1$, by the expression:

$$\sin \theta_o = \frac{R + h_M}{R + h_S}$$

θ_o = The angle between the local vertical and the line to the oxygen mantle rim;

R = The Earth's radius;

h_M = The effective tangential height of the oxygen mantle;

h_S = The spacecraft altitude;

η = The index of refraction.

A gimbal system is used to interface the antenna with the vehicle. The vertical tracking problem is now a two-dimensional one that is accomplished by the determination of the tilt angle between the spacecraft normal and the local coordinates in the orthogonal coordinate frame associated with the antenna. If a spinning satellite is assumed a sampled data control system is required.

The receiver develops both the squint angle error and the gimbal axis error signals. The gimbal axis error signals are obtained via a lobe comparison processing method and the squint angle error is obtained by introducing a radial sweep modulation by rocking the antenna boresight line.

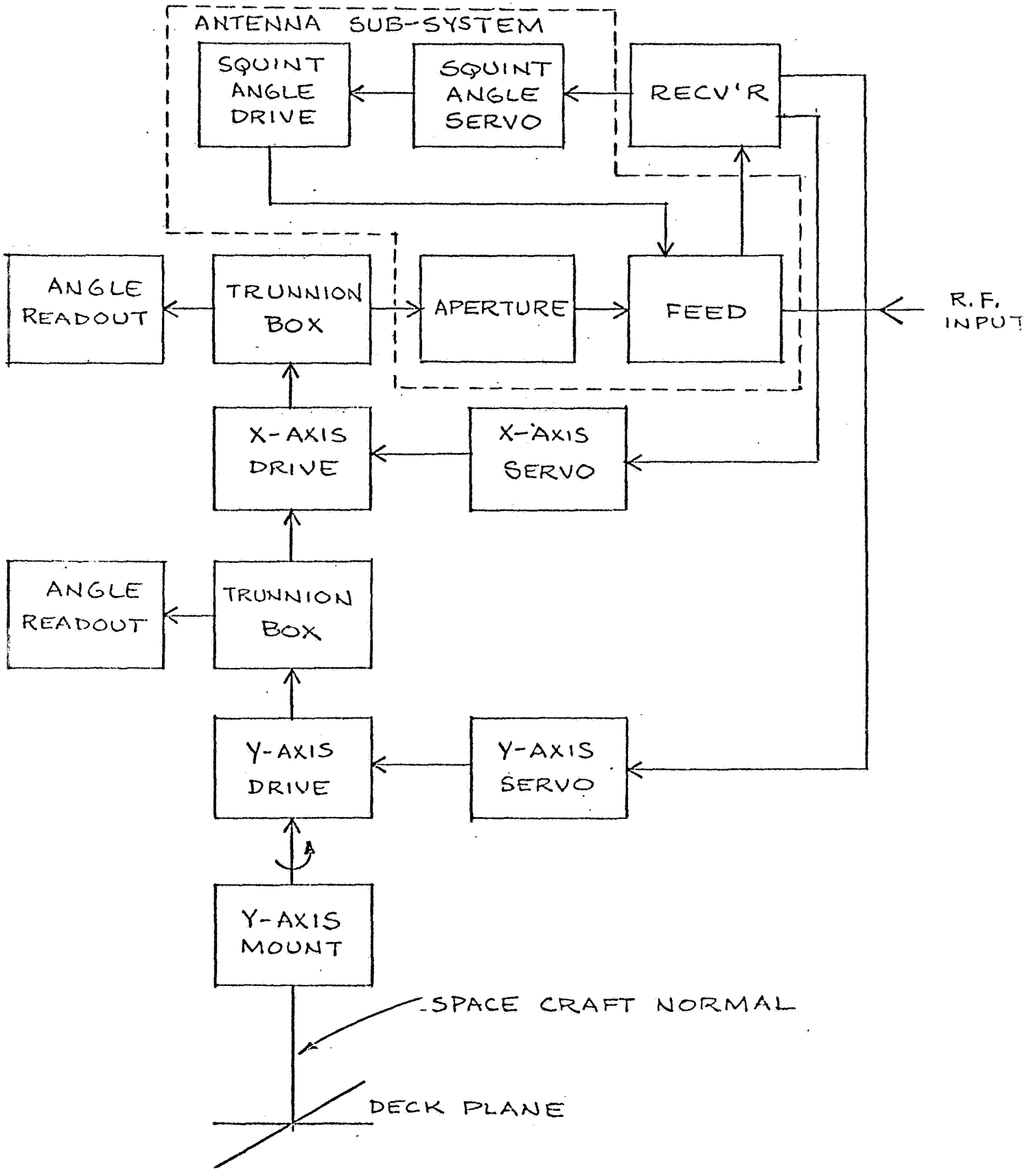

FIGURE A-1

SYSTEM FUNCTIONAL BLOCK DIAGRAM

An appropriate detection scheme is used to detect the modulation on the received signal.

Coordinate System Description

The local coordinates are conventionally given in the rectangular coordinate system defined by the local vertical, and two other axes perpendicular to this line; one of which corresponds to the downtrack direction of the vehicle's orbit.

The tracking line coordinate frame is analogous to the local coordinate frame, but is fixed to the antenna rather than the orbit geometry. The radiometric sensor brings the tracking line into coincidence with the local vertical.

A complicating factor is introduced because the angle between the line-of-sight to the oxygen mantle rim and the antenna tracking line measured in the vertical plane is a function of spacecraft altitude. This requires the introduction of an internal feedback loop within the antenna subsystem to adjust the squint angle measured between the center of the antenna beam and the tracking line.

The tracking line orientation is,of course, referenced to the vehicle's coordinates. The vehicle's coordinate frame is an orthogonal set with axes in the deck plane; one of which defines forward, and a third normal to the deck plane. The vehicle's orientation relative to the local coordinate frame of reference is constantly changing; hence, vehicular angular rates and acceleration cause disturbance torques to be applied to the tracking line. The magnitude of these torques and the rates at which they change define the servo system requirements and the limitations on the radiometer integration time.

The tracking line orientation measured with respect to the vehicle coordinate system results in the desired output information and is available directly from the gimbal readouts.

SYSTEM OPERATION

The operation of the instrument is explained by the following sequence of

operations.

The horizon tracker is activated and a search mode is initiated to obtain a coarse determination of the earth center of illumination, which then provides a starting point for limb acquisition by the squint angle servo. Limb acquisition is achieved by applying a radial sweep motion with a superimposed rocking modulation on the squint angle axis. The rocking modulation signal is phase detected to generate a radial tracking signal as the radiometer beam line-of-sight approaches the planet rim. (See Figure A-2) Upon detection of the modulation signal, the sweep motion stops, and the tracking loop takes over control of the squint angle adjusting mechanism. This completes the limb acquisition mode and automatically initiates the tracking mode.

In the tracking mode, short-term angular perturbations and drift of the earth across the aperature field-of-view are nulled by extracting error signals from orthogonal axis processing channels and applying them to their appropriate control mechanism.

The orientation of the vehicle, with respect to the local coordinate frame, is obtained by measurement of the angular correction required to obtain a null with the servo controlled gimbal system.

LOCAL VERTICAL

Tracking Methods

There are two principle methods by which a microwave radiometer may be utilized for sensing the local vertical of a spacecraft. These methods are rim tracking and thermal centroid tracking.

Rim Tracking

A rim tracking mode utilizes some form of scanning antenna system. The geometry is illustrated in Figure A-3. Scanning the antenna across the rim of the oxygen mantle results in a repetitive waveform with a period equal to the reciprocal of the scanning frequency. The duty cycle is a function of the squint angle. If the squint angle is properly adjusted for the orbital altitude, the duty cycle will be 50 percent.

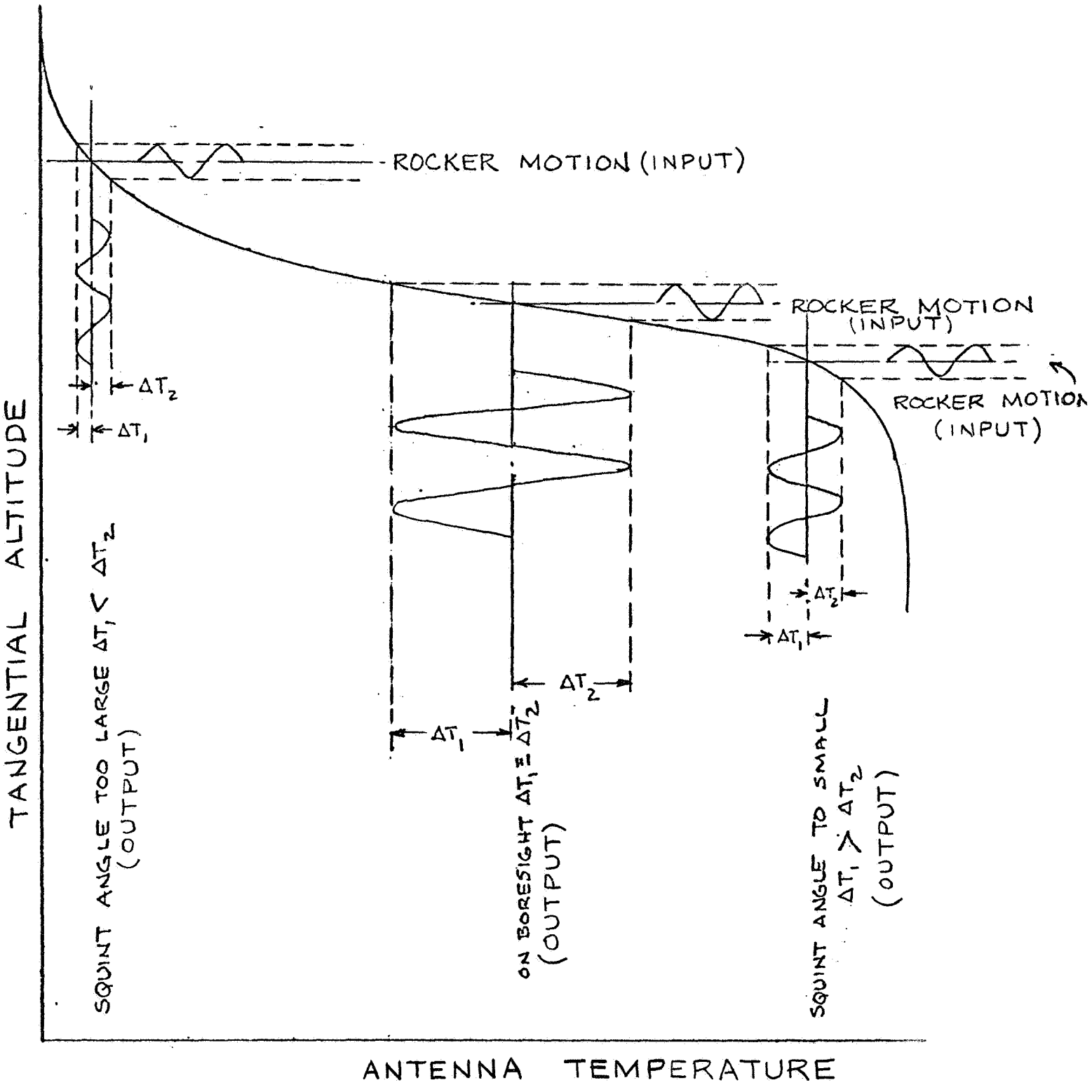

FIGURE A-2

DERIVATION OF SQUINT ANGLE ERROR FROM MANTLE TEMPERATURE

DISTRIBUTION AS SENSED BY THE ANTENNA

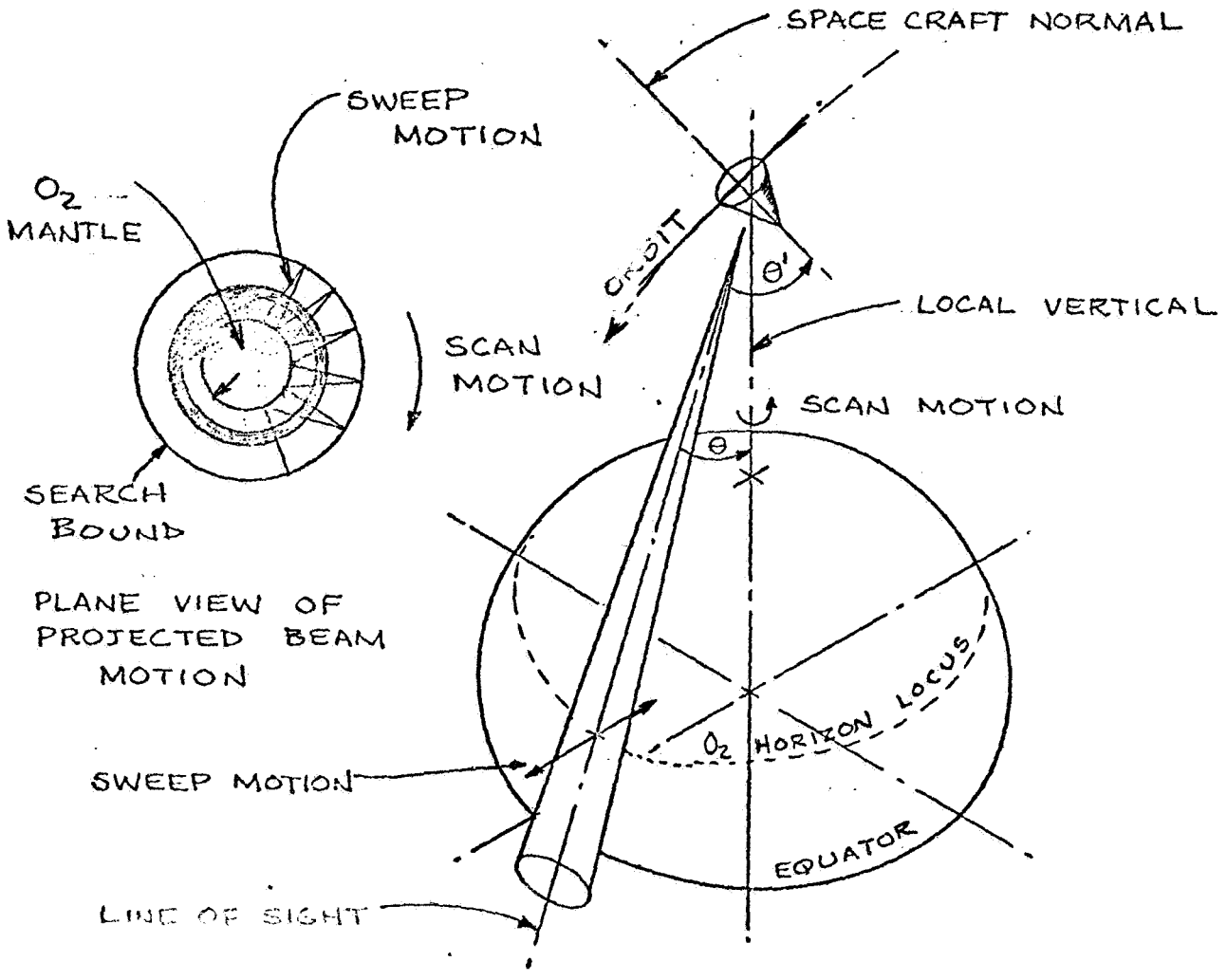

FIGURE A-3

RIM TRACKING HORIZON

SENSOR GEOMETRY

If the squint angle is either too small or too large for the orbital altitude, the waveform will experience a duty cycle change.

The method by which the control signals are obtained may be visualized by noting that as the antenna beam is swept on and off the rim, while scanning around the rim, a signal at the sweep frequency will be obtained at the sensor output. A phase comparison of this signal with the reference drive signal results in a DC output signal proportional to the magnitude of the squint angle error. The sign (plus or minus) indicates the direction of the error.

In a similar manner, a signal at the scan frequency is obtained at the receiver output. Phase comparison of the detected scan frequency signal with the reference drive signal provides error signals proportional to the magnitude and sense of the error between the tracking line and the local vertical in orthogonal coordinates.

Thermal Centroid Tracking

A thermal centroid tracking system may use either sequential or simultaneous antenna lobing techniques. The geometry for systems of this type is illustrated in Figure A-4. Vertical tracking is accomplished by adjusting the directions of paired antenna beams such that their respective boresight axes intercept the rim of the oxygen mantle. When the oxygen emission sensed by one antenna lobe is compared with that received by the second lobe in the same plane, a zero difference output is obtained when the plane of the tracking line (defined by the plane bisecting the beam pair) intersects the center of the earth. As the tracking line departs from the local vertical, an error signal is generated in the coordinate that the error appears, and the tracking line is then made to follow the local vertical using the output error voltage as a forcing function.

Introduction of a slight "rocking motion" about either or both axes of the antenna coordinate frame allows sensing of the squint angle error in a manner suitable for driving a servo mechanism. This mechanism automatically adjusts the beam line-of-sight to the point on the mantle rim for which the maximum change in antenna temperature occurs at the rocking rate.

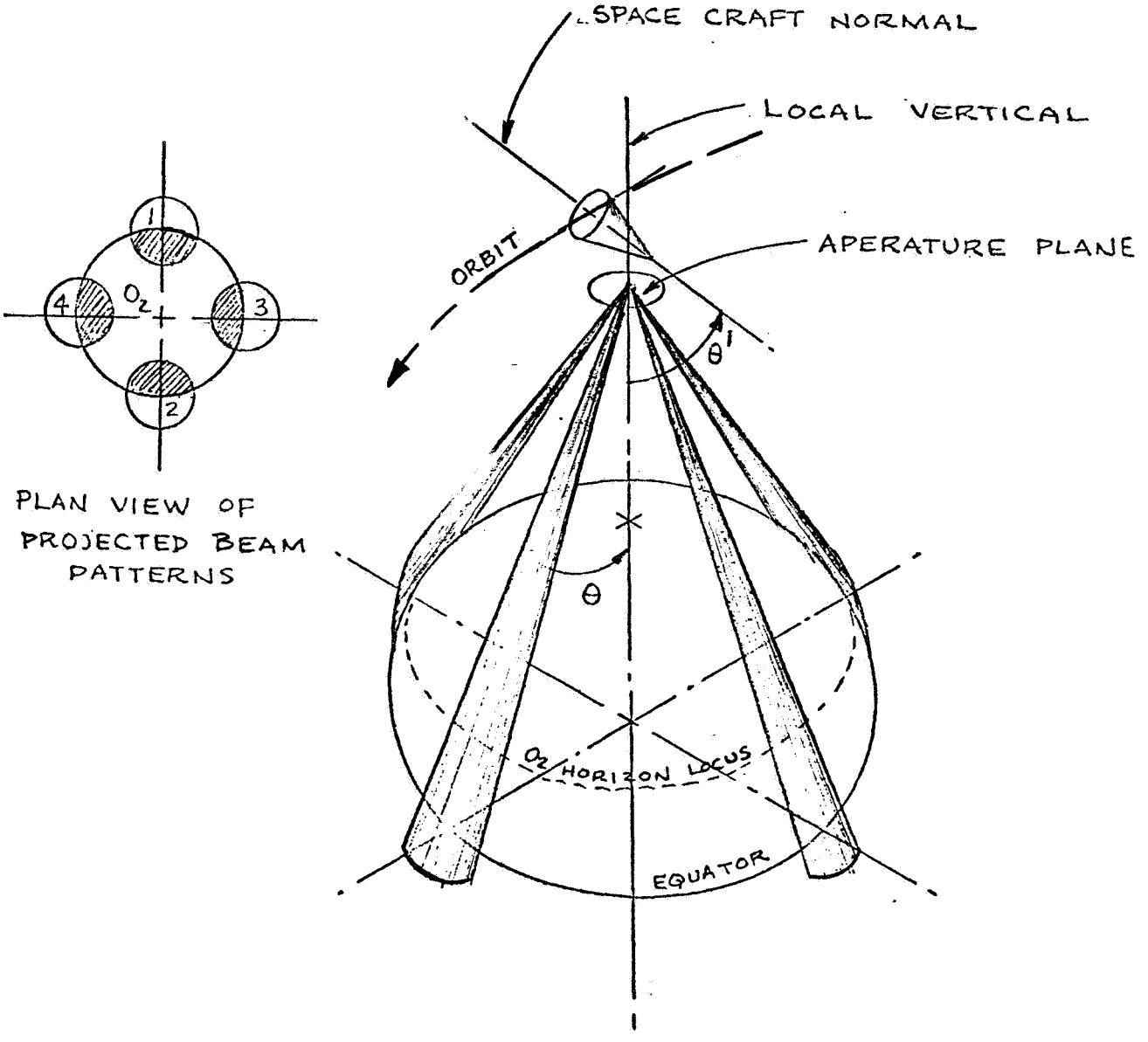

FIGURE A-4

THERMAL BALANCE TRACKING SENSOR

GEOMETRY

APPENDIX B

ERROR BUDGET AND ACCURACY TRADE-OFF

Error Budget

The fundamental postulate is that the atmospheric oxygen mantle when viewed from space provides a uniform non-fluctuating, spatially symmetrical signal suitable for radiometric sensing of the earth vertical direction.

The earth vertical accuracy goal was specified as a standard deviation of 0.33 arc minutes (3 sigma value of 1 arc minute). This goal dictated the design approach. Considerable system simplification is possible for missions which can tolerate earth vertical errors as little as three times the specified goal.

The system design is complicated by the fact that a large percentage of the system budget error is determined by non-reducible mechanical tolerances, readout errors, and following errors associated with the tracking control subsystem. This allows only a small error to be allotted to the antenna and receiver resulting in a relatively large antenna aperture requirement. This imposes additional requirements on the servo control system, causing an iterative increase in the system size and complexity.

Although this study has been addressed to the solution of this high accuracy problem, attention is called to the fact that the fundamental postulate concerning the characteristics of the atmospheric oxygen mantle is subject to question. Assuming that the first priority, and hence, the prime objective is to prove the concept, then the inescapable conclusion is that we must either precisely measure the temperature of the atmosphere in the region of operation or alternatively configure an experiment capable of measuring temperature differences between the horizons. The atmospheric region of interest is that of 10,000 feet and above were available data is sparse or non-existent.

Here no error was allocated for opposing horizon temperature differences. The initial postulate that the oxygen horizon is circularly uniform, and exhibits spherically homogenous radiation was treated as an initial condition. The validity of this would be the objective of an early experiment; since the stability of the oxygen horizon may limit the accuracy that can be achieved.

The system error budget shown in Table B-1 is predicated on the above qualification.

TABLE B-1

SYSTEM ERROR BUDGETS

Error Source	Standard Deviation (arc minutes)	Variance (arc minutes)
Platform Alignment	0.16	0.0256
Differential Squint Angle Error*	0.08	0.0064
Servo Error	0.08	0.0064
Gimbal Readout Error*	0.08	0.0064
Beam Symmetry	Balanced to zero	
Boresight Stability	0.12	0.0144
Electrical Noise	0.18	0.0324
Total		0.0812
R.S.S.	0.285	

*Depends on encoder used; i.e., the readout error for a 17 bit encoder would be 0.16 arc minutes; for a 18 bit encoder, 0.08 arc minutes; and for a 20 bit encoder, 0.02 arc minutes.

In the above error budget, the platform alignment error is composed of those errors assignable separately to the individual coordinate system axes, inter-axis errors related to leveling and orthogonality and to coordinate transformation computations. The magnitude of this error is determined by the optical alignment procedures used. The indicated errors are consistent with what has been achieved with high precision ground based tracking antenna systems.

The differential squint angle error is associated with the "linkage system" which must control paired antenna boresight angles to arc seconds. The method is based on an internal servo loop in which the individual linkage elements track a reference element. The residual error

in this case is determined primarily by the angle encoders used in the loop. An 18 bit encoder was assumed for the values given in Table B-1.

The servo error includes servo noise, dynamic lag and torques resulting from disturbance signals entering the servo at various points within the control loop. The allowed error is consistent with what has been achieved with two-axis gimbal control systems.

The display of the angle of the earth vertical line in the spacecraft coordinate system is obtained from angle encoders mounted on the gimbal platform. The encoder error in this case is included in the gimbal error shown in Table B-1.

Non-symmetry of the antenna beams is assumed to be determinant and thus no error has been budgeted for this condition. Antenna boresight stability, however, is considered to be a function of the stability of the antenna aperture distribution; or more precisely, the depth of null that can be achieved with balanced beams. A practical limit of antenna beam splitting to 1/1000 or 30 db depth of null has been assumed.

The electrical noise in the system is a function of the receiver noise figure and bandwidth. The variance in the noise distribution is a function of the integration time constant. The standard deviation in the receiver noise is related to an angular error through the difference pattern of the antenna aperture distribution. In theory, the variance in the electrical noise can be made arbitrarily small by increasing the receiver bandwidth, the integration time constant, or both. In practice, the receiver noise figure is a function of bandwidth; hence, an upper limit is imposed on the bandwidth for which a sensitivity improvement can be achieved. Further, with respect to this particular application, the altitude regime within which the oxygen mantle radiation originates is a function of frequency; consequently, for wide bandwidth systems it may become more difficult to accept the validity of the initial postulate that the atmospheric oxygen emission is spherically homogenous.

The budgeted electrical noise error is consistent with the sensitivity that has been achieved with radiometers at 60 GHz using a 10 second time constant and 20 MHz bandwidth.

Accuracy vs Equipment Complexity

It is noted that the accuracy of the radiometric angle tracking system can be represented as the square root of the sum of the squares (R.S.S.) combination of three error terms as follows:

$$\Delta\theta = \sqrt{\Delta\theta_1^2 + \Delta\theta_2^2 + \Delta\theta_3^2}$$

Where

$\Delta\theta$ = Standard deviation in the composite error distribution.

$\Delta\theta_1$ = The uncertainity in pointing due to lack of knowledge concerning the oxygen source radiation characteristics.

$\Delta\theta_2$ = The uncertainity in pointing due to mechanical tolerances, environmental changes, wear, allignment errors, servo noise, etc:

$\Delta\theta_3$ = The uncertainity in the electrical boresight due to the sensor (antenna and receiver) noise.

If we assume that $\Delta\theta_1$, is negligible, or rather that the validity of this assumption is one of the objectives of an early experiment, then we can allot the budget errors for a 0.33 arc minute standard deviation as follows:

$\Delta\theta_1 = 0$

$\Delta\theta_2 = 0.235$ arc minutes

$\Delta\theta_3 = 0.235$ arc minutes

and $\Delta\theta = \sqrt{0.109} = 0.33$

The corresponding budgeted errors shown in Table B-1 are slightly less than the above values to allow some safety factor in specifying component tolerances.

The precision to which the null point of the pattern distribution, to the point of zero crossing of the S-curve, can be determined is limited by antenna noise, receiver noise, and the magnitude of the energy available from the source (oxygen mantle). The antenna noise results from side and backlobe responses to extraneous radiation and to mechanical distortions which cause defocusing of the antenna. Experience indicates that the lower limit to which the boresight point can be determined is approximately one part in one thousand of the beam angle for large signal-to-noise ratios (output signal-deflection-to-noise standard deviation $\geq 10^3$). This then sets the minimum value of $\Delta\theta_3$ at $10^{-3}\,\theta_A$.

Hence, the 0.23 arc minute budget for this cause allows a maximum antenna beamwidth in the order of 3 degrees. The specified 2 degree beam allows some safety margin.

If however, the $\Delta\theta$ goal were increased to say 1.7 arc minutes and we allowed 1 arc minute for each of the three error terms the situation changes in a dramatic fashion. In this case a 16 degree beam would be suitable and a significant reduction in size would occur. A further increase in the accuracy goal would allow the beam size to approximately double and the requirement for a squint angle adjustment as a function of altitude is considerably simplified or possibly eliminated. An upper limit on the beam size is imposed at $\theta_A \rightarrow 120^\circ$ at which point the leading and trailing edges of the individual beam patterns will have gone full circle and start to overlap.

The conculsions here are quite obvious:

(1) It is the practical limit of antenna beam splitting to approximately one part in one-thousand that determines the required antenna beam angle size. This limitation is independent of the sensitivity of the radiometer provided that a sufficient signal-to-noise ratio is obtained.

(2) If the goal for the total system error is increased from 0.33 arc minutes to a value of 2 or 3 arc minutes, the antenna design no longer represents a problem -- particularly since a squint angle adjustment is no longer required to accommodate an elliptical orbit with an apogee of 1000 nautical miles and a perigee of 100 nautical miles. Fixed antenna beams of relatively small aperture would be fully applicable to meeting such a system requirement.

(3) A 2-3 arc minute total system error would be highly competitive with present IR horizon sensors; consequently this would appear to be a most practical and logical approach to a near-future and, perhaps even ultimate horizon sensor system.

APPENDIX C

COMPARISON OF ANGLE TRACKING METHODS

INTRODUCTION:

In automatic tracking antenna applications, the measurement of angle off boresight is generally obtained by receiving the signal from the source to be tracked on a number of antenna beams or lobes. The received signal amplitudes are then compared in a prescribed way. A number of methods of comparison have been developed. These, in general, fall into two categories described as (1) simultaneous lobing or monopulse, and (2) sequential lobing.

The number of antenna lobes, their location, and the manner of their use determine the specific category for a given antenna system. Because of the general complexity and number of possible antenna patterns and combinations, it is advantageous to approximate the main lobe patterns separately and analytically, and to combine the expressions for the patterns according to the manner in which the system operates.

In general, for small angles off the antenna axis, the field patterns for the principle lobes of the contributing feed centers can be well approximated by a cosine function of the deviation. To determine the boresight point of the aperture distribution three different lobe configurations are usually considered, as follows:

(1) Four lobes with axes making equal angles with the antenna axis and lying in planes through the antenna axis making $\pm 45^{\circ}$ angles with the vertical plane through the antenna axis.

(2) Four lobes with axes making equal angles with the antenna axis and lying two in the vertical and two in the slant plane through the antenna axis.

(3) A single scanning lobe with its axis at an angle to the axis and rotated about the antenna axis at a constant angular velocity (called conical scan).

These are instrumented by placement of the feed centers (each feed center can,

of course, be obtained by the combination of the signals from one or more feeds) with reference to the aperture axis through boresight as illustrated in Figure C-1. In Figure C-1 ϕ and θ are the orthogonal angle coordinates of the aperture which describe the angular deviation from boresight.

The coupling between feeds is assumed negligible, which means that the primary and secondary pattern of each feed exist independent of the patterns for the other feeds. The receiver processes the signal power received from the antenna lobe patterns to determine the boresight error. System noise is referred to the receiver input terminals, and the tracking sensitivity is then derived as a function of the standard deviation of the error signal. The standard deviation of the angle error distribution is, by nature, proportional to the signal-to-noise ratio at the receiver input.

The system interface between the antenna and receiver is defined in terms of the power transfer characteristic at the boundary. The mechanical interface is usually obtained through a transmission line. The configuration of the line is determined by each specfic antenna configuration and may take the form of a rotary joint, a piece of flex guide, or other means of coupling.

The feed size and its distance from the lens or reflector is chosen for the desired pattern shape. The simplified patterns of the lobes, resulting from the antenna types considered, are illustrated in Figure C-2. Here, the distances "a'", measured from the feed centers as indicated in Figure C-2 are chosen so that the secondary lobe pattern is tilted a corresponding amount in either or both coordinates θ and ϕ .

Simultaneous Lobing Systems

Additive Monopulse:

Consider first the additive monopulse case. With the additive monopulse feed and hybrid combiners the signal is assumed to originate from a point source and three outputs are obtained which can be represented mathematically as follows:

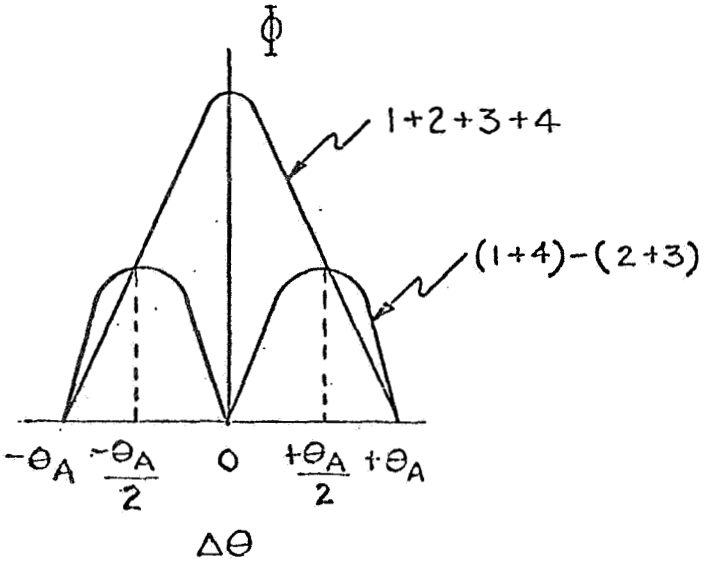

(a) Additive Monopulse

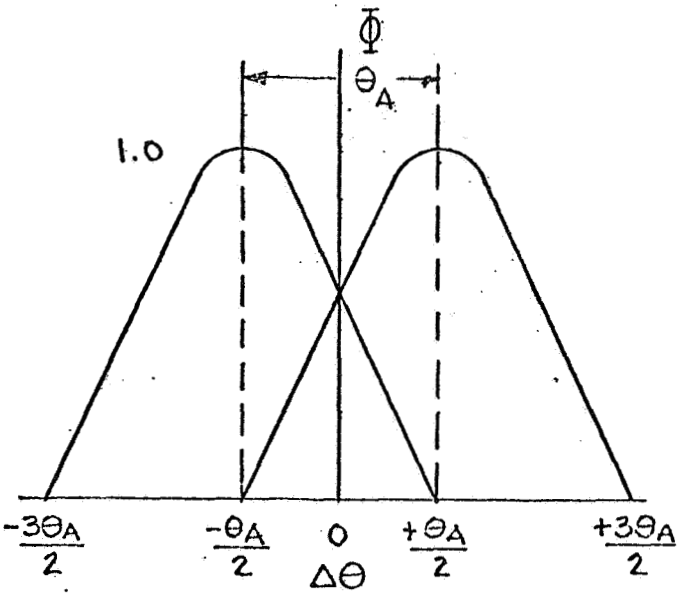

(b) Multiplicative Monopulse or Lobe Subtraction

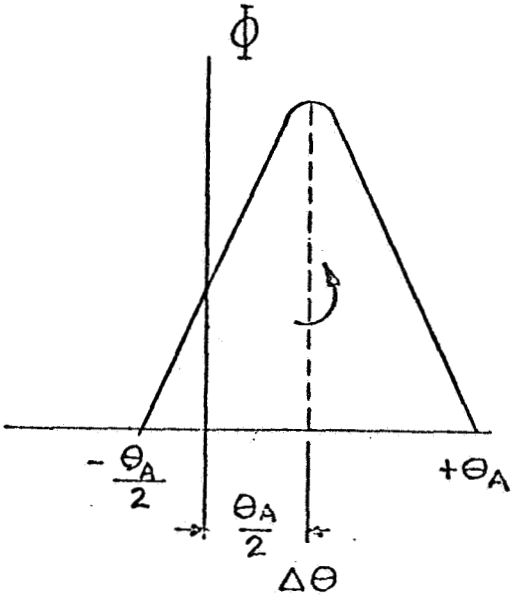

(c) Conical Scan

FIGURE C-1

TYPICAL POWER DENSITY PATTERNS
FOR GIVEN ANTENNA TYPES

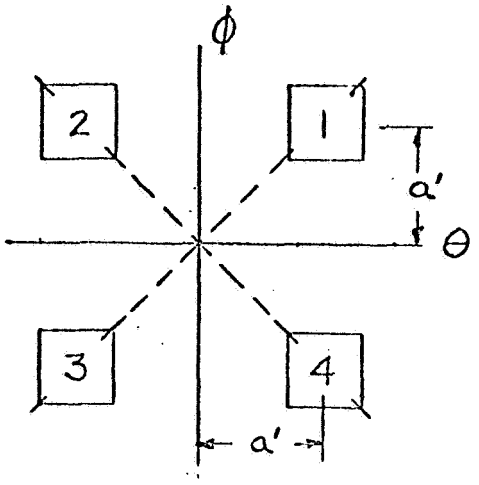

(a) Additive Monopulse

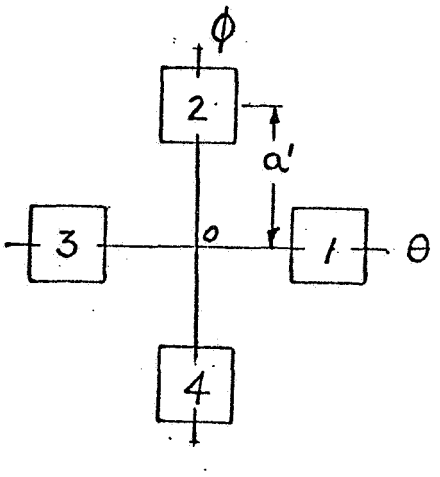

(b) Multiplicative Monopulse or Lobe Subtraction

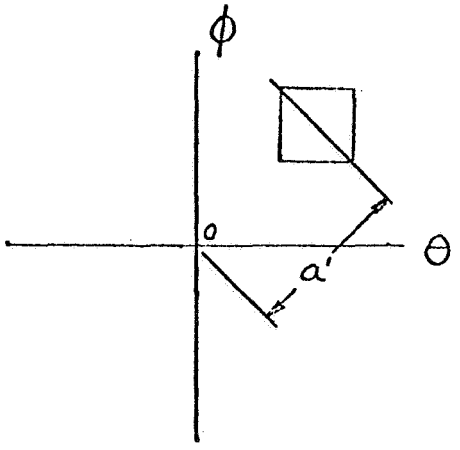

(c) Conical Scan

FIGURE C-2

COORDINATES OF APERTURE FEED CENTERS

Sum port output:

$$E_{\Sigma(t)} = V_{\Sigma(t)} \cos(\omega_o t + \phi)$$
$$= V_S \cos\left(\frac{\pi \Delta\theta}{2\theta_A}\right) \cos(\omega_o t + \phi)$$
$$\text{for } -\theta_A < \Delta\theta < +\theta_A$$

No. 1 Difference port output:

$$E_{\Delta 1(t)} = V_{\Delta 1(t)} \cos(\omega_o t + \phi)$$
$$= \frac{V_S}{\sqrt{2}} \sin\left(\frac{\pi \Delta\theta}{\theta_A}\right) \cos(\omega_o t + \phi)$$
$$\text{for } -\theta_A < \Delta\theta < +\theta_A$$

No. 2 Difference port output:

$$E_{\Delta 2(t)} = V_{\Delta 2(t)} \cos(\omega_o t + \phi)$$
$$= \frac{V_S}{\sqrt{2}} \sin\left(\frac{\pi \Delta\theta}{\theta_A}\right) \cos(\omega_o t + \phi)$$
$$\text{for } -\theta_A < \Delta\theta < +\theta_A$$

where:

$V_{\Sigma(t)}$ = amplitude coefficient of the sum port signal;

$V_{\Delta i(t)}$ = amplitude coefficient of the difference port signals;

$E_{\Sigma(t)}$ = sum port output time function;

$E_{\Delta i(t)}$ = difference port output time functions;

θ_A = the spacing between feed centers and is normally defined equal to the antenna's half power beam angle;

$\Delta\theta$ = The displacement from boresight of the phase center of the incoming radiation;

V_S = the field strength of the incoming radiation integrated over the aperture area;

ω_o = the mean frequency in radians/second of the radiation and ϕ is an arbitrary phase shift.

The sum port power is split into two equal components and used to drive the two channel detectors. The resultant S-curve (Figure C-3) is described as:

$$E_S = \left\{\left[\frac{V_{\Sigma(t)}}{\sqrt{2}} + V_{\Delta(t)}\right]^2 - \left[\frac{V_{\Sigma(t)}}{\sqrt{2}} - V_{\Delta(t)}\right]^2\right\} \cos^2(\omega_o t + \phi)$$
$$= \sqrt{2}\, V_{\Sigma(t)} V_{\Delta(t)} \left[1 + \cos 2(\omega_o t + \phi)\right]$$

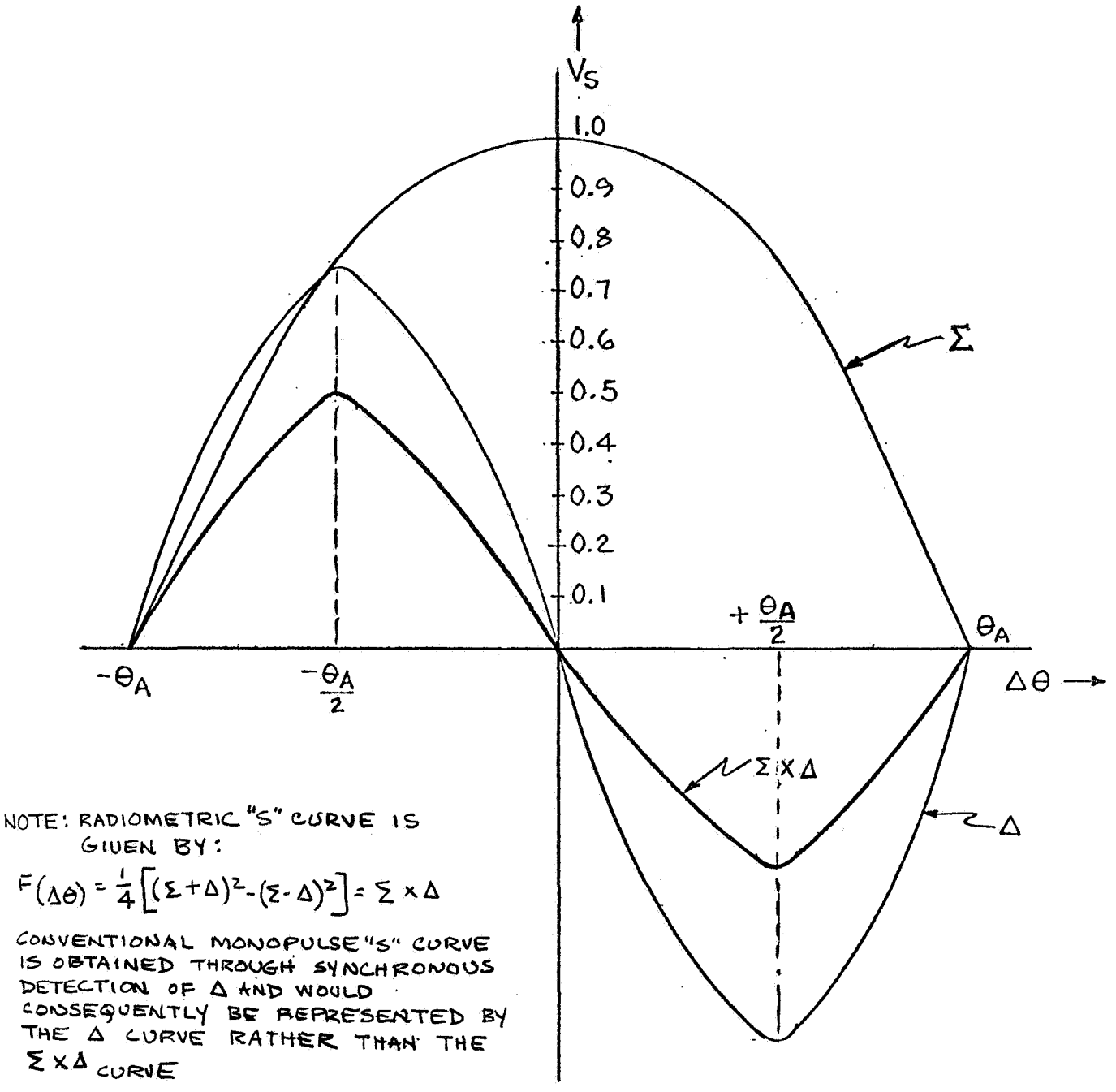

NOTE: RADIOMETRIC "S" CURVE IS GIVEN BY:

$$F(\Delta\theta) = \frac{1}{4}\left[(\Sigma+\Delta)^2-(\Sigma-\Delta)^2\right] = \Sigma \times \Delta$$

CONVENTIONAL MONOPULSE "S" CURVE IS OBTAINED THROUGH SYNCHRONOUS DETECTION OF Δ AND WOULD CONSEQUENTLY BE REPRESENTED BY THE Δ CURVE RATHER THAN THE $\Sigma \times \Delta$ CURVE

FIGURE C-3

TYPICAL "S" CURVE CONSTRUCTION

IN AN ADDITIVE MONOPULSE SYSTEM

(SECONDARY PATTERN- MAIN LOBE ONLY)

The post detection zonal filter selects the zero frequency component only giving:

$$E_S = V_S^2 \cos^2 \left(\frac{\pi \Delta\theta}{2\theta_A}\right) \sin \left(\frac{\pi \Delta\theta}{2\theta_A}\right)$$

$$\text{for } -\theta_A < \Delta\theta < +\theta_A$$

As $\Delta\theta$ approaches zero, the angle sensitivity of the antenna is calculated to be:

$$\frac{\Delta E_S}{\Delta\theta_A} = \frac{\pi V_S^2}{2\theta_A}$$

With the additive monopulse configuration, it is noted that a control signal is only obtained for that portion of the signal energy that is common to both the sum and difference ports. This will, of course, impose some restrictions on the use of this configuration.

Multiplicative Monopulse

The second type processing to be considered is multiplicative monopulse. In this case, we consider paired sets of feeds with each feed individually producing an antenna pattern which is displaced from the boresight axis; the displacement being a function of the feed centers location with respect to the focal plane of the antenna as previously indicated. These patterns, presumably identical except for the fixed displacement in the phase center position, intersect along the boresight axis of the antenna. Consequently, all signals received within the antenna aperture, except those along the boresight axis, will produce unequal amplitudes in the feeds. The designation Multiplicative Monopulse comes from the relationship:

$$A_1^2(0,+\Delta S) - A_2^2(0,-\Delta S) = \left[A_1(0,+\Delta S) + A_2(0,-\Delta S)\right]\left[A_1(0,+\Delta S) - A_2(0,-\Delta S)\right]$$

Where Δs is the displacement from the boresight, "o" represents the boresight position, and: $A_1(0,+\Delta S)$ = response of the leading lobe

$A_2(0,-\Delta S)$ = response of the trailing lobe.

Thus the product of the sum and difference terms is obtained directly by subtracting the powers in each lobe.

Consider now one paired set of feeds. Then, when the envelopes of the two signals are subtracted a null will be produced when the signals are received along the boresight axis. This subtraction of the feed signals produces a well-defined system boresight line along the antenna aperture boresight axis due to the envelope characteristic of the resultant detected signal which forms an "S" curve as indicated in Figure C-4.

The power envelope of the principle lobe patterns may be closely approximated by an expression of the form $\sin^2(x+\alpha)$ such that the patterns of the individual lobes may be described as:

$$V_{1(t)} = \frac{V_s^2}{2} \sin^2 \left[\frac{\pi \Delta\theta}{2\theta_A} + \frac{3\pi}{4}\right] \left[1+\cos 2(\omega_o t + \phi)\right]$$

$$= \frac{V_s^2}{2} \cos^2 \left[\frac{\pi \Delta\theta}{2\theta_A} + \frac{\pi}{4}\right] \left[1+\cos 2(\omega_o t + \phi)\right]$$

$$\text{for } -\frac{3\theta_A}{2} \leq \Delta\theta \leq \frac{\theta_A}{2}$$

$$V_{2(t)} = \frac{V_s^2}{2} \sin^2 \left[\frac{\pi \Delta\theta_A}{2\theta_A} + \frac{\pi}{4}\right] \left[1+\cos 2(\omega_o t + \phi)\right]$$

$$\text{for } -\frac{\theta_A}{2} \leq \Delta\theta \leq \frac{3\theta_A}{2}$$

Selecting only the d.c. component and subtracting the power pattern of Lobe #1 from that of Lobe #2 gives the resultant "S" curve as:

$$E_s = \frac{V_s^2}{2} \cos^2 \left[\left(\frac{\pi \Delta\theta}{2\theta_A} + \frac{\pi}{4}\right) - \sin^2\left(\frac{\pi \Delta\theta}{2\theta_A} + \frac{\pi}{4}\right)\right]$$

$$= \frac{V_s^2}{2} \sin \left(\frac{\pi \Delta\theta_A}{\theta_A}\right)$$

The slope of this error curve as $\Delta\theta$ approaches zero is the same as that obtained with the conventional monopulse configuration or:

$$\frac{\Delta E_s}{\Delta\theta} = \frac{\pi V_s^2}{2\theta_A}$$

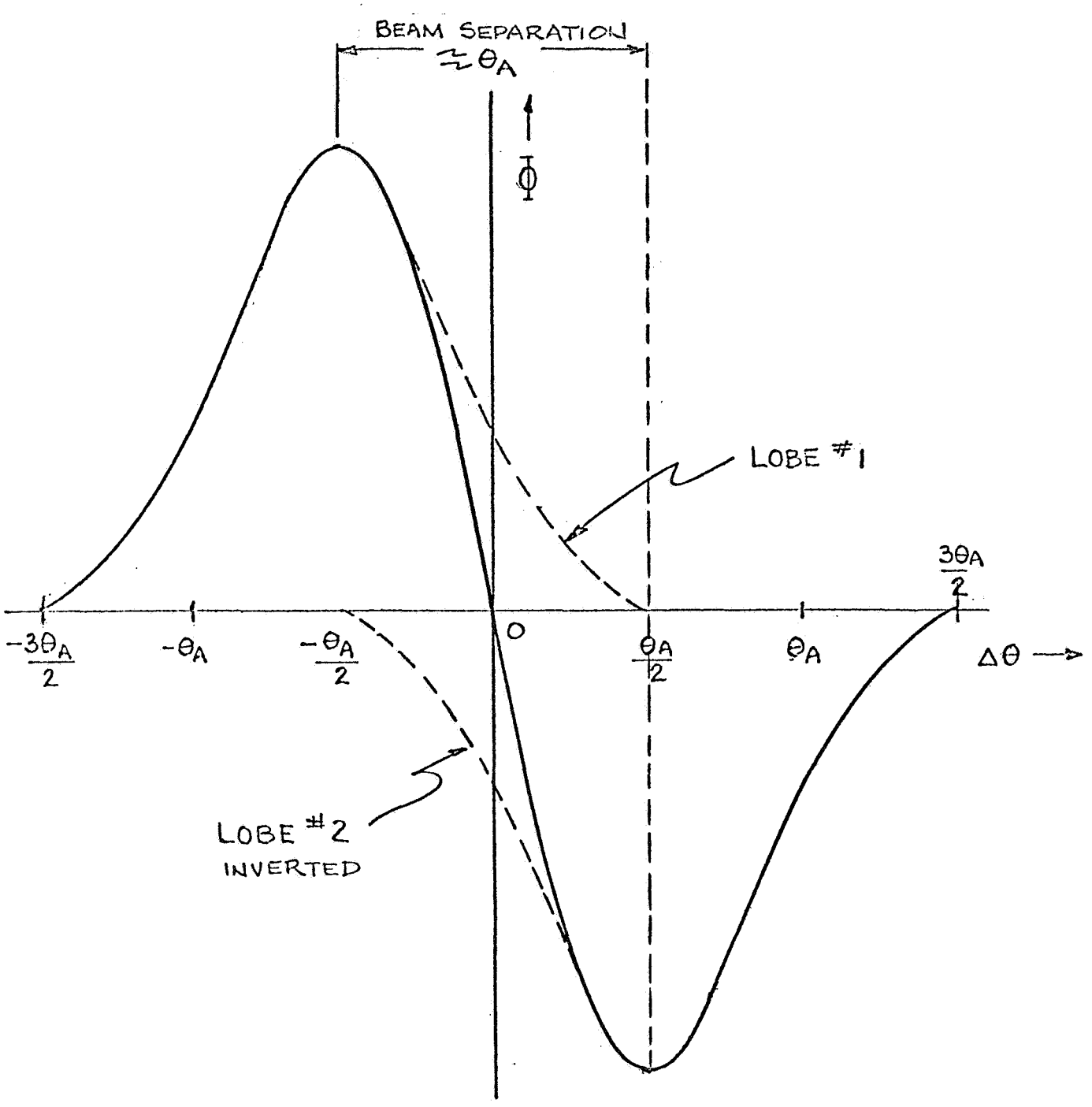

FIGURE C-4

TYPICAL "S" CURVE CONSTRUCTION
IN LOBE SUBTRACTION SYSTEM

With this configuration no requirement has been introduced with respect to the phase coherence of the signals being compared and hence the technique is applicable for use on extended sources; i.e., where the source size is much larger than the beam size.

SEQUENTIAL LOBING

Lobe Switching

In lobe switching the same configuration used in the multiplicative monopulse configuration is utilized except that the individual lobe contributions are sampled in time sequence. This results in an additional loss in signal power of one-half. The resultant slope is thus:

$$\frac{\Delta E_{SI}}{\Delta \theta_A} = \frac{\pi V_S^2}{4 \theta_A}$$

Actually, this loss is normally considered as a receiver loss rather than an antenna loss. The antenna sensitivity is in this event considered the same as for the monopulse case.

Conical Scan

A conical scanning system is a tracking technique which falls in the general category of sequential lobing. Systems of this type are characterized by a time varying aperture illumination leading to a far field pattern whose geometric axis describes the locus of the surface of a cone, the axis of which is referred to as the tracking system boresight axis.

When the target of interest is centered near the system boresight axis, the time variation of the aperture illumination leads to an amplitude modulation of the received signal which is proportional to the power received from the target as a function of the angular response of the aperture to an incoming plane wave. This modulation component, when synchronously detected in quadrature, provides two d.c. error signals which are proportional to the relative angular displacement of the target from the system boresight axis in the orthogonal coordinates dividing the antenna aperture.

The following assumptions are introduced to simplify the development of the

basic equations defining system performance in the angle tracking mode:

(1) It is assumed that the receiver and other signal processing components introduce no significant time lags with respect to the time scale associated with the arrival of the incoming radiation.

(2) The spin or synchronous detector is considered to be ideal in that its output is proportional to the power received from the target by the antenna aperture.

(3) The post-detection filter is considered to be an ideal zonal filter, passing only that portion of the spectrum from d.c. to an abrupt cut-off frequency and rejecting multiples of the scan or spin frequency.

The received signal with superimposed amplitude modulation at the spin frequency may be expressed in terms of an amplitude modulated carrier by the expression:

$$V_{(t)} = \frac{V_S}{\sqrt{2}} \left[1 + K\Delta\theta \cos\left(\omega_S t + \phi_S\right)\right] \cos\left(\omega_o t + \phi_o\right)$$

where: K = the slope of the antenna response function for a displacement equal to the half-power beam angle;

$\Delta\theta$ = the angular displacement of the incoming waveform from boresight;

ω_S = the spin rate of the antenna aperture in radians;

ω_o = the mean carrier frequency of the radiation, also in radians;

ϕ_S and ϕ_o are arbitrary phase shifts.

The antenna field pattern for the main lobe is considered to be described by cosine functions in $\Delta\theta$; i.e.:

$$\frac{V_o}{V_S} = \cos \frac{\pi\Delta\theta}{2\theta_A}$$

The derivative of V_o with respect to $\Delta\theta$ is:

$$\frac{\left(\frac{d V_o}{d \Delta\theta}\right)}{V_S} = -\left(\frac{\pi}{2\theta_A}\right)\left(\sin \frac{\pi \Delta\theta_A}{2\theta_A}\right)$$

Evaluation of this equation for $\Delta\theta = \frac{\theta_A}{2}$ gives the desired value of K as:

$$K = \frac{\pi}{2\sqrt{2}\,\theta_A}$$

The magnitude and phase of the modulation component at the spin frequency now provides a measure of the angle error (with zero modulation occurring when the source in on the boresight axis). The signal is square-law detected and filtered to select the resultant low frequency component in the form:

$$E_S = \frac{V_S^2}{4}\left[1 - \frac{\pi\Delta\theta}{\sqrt{2}\,\theta_A}\cos(\omega_S t + \phi_S) + \frac{\pi^2\Delta\theta^2}{8\theta_A^2}\cos^2(\omega_S t + \phi)\right]$$

$$= \frac{V_S^2}{4}\left[1 + \frac{\pi^2\Delta\theta^2}{8\theta_A^2}\left(1 + \cos 2(\omega_S t + \phi)\right) - \frac{\pi\Delta\theta}{\sqrt{2}\,\theta_A}\cos(\omega_S t + \phi)\right]$$

The spin frequency amplifier selects the spin frequency component only and presents to the synchronous detector the signal:

$$E_S' = \left(\frac{\pi}{4\sqrt{2}}\right)\left(\frac{\Delta\theta}{\theta_A}\right) V_S^2 \cos(\omega_S t + \phi)$$

The output from the synchronous detector represents the d.c. error signal which is proportional to the rms value of the spin frequency signal. The slope of the error function is thus:

$$\frac{\Delta E_S'}{\Delta\theta} = \frac{\pi V_S^2}{8\theta_A}$$

A loss in sensitivity of 1/4 (approximately 6 db referenced to the input power) is consequently experienced with a conical scan system when compared to either of the previously discussed monopulse configurations. With antennas of equal aperture areas,

this loss will be reduced somewhat as a consequence of a lesser receiver loss applied to this configuration.

Radiometer Interface

The expressions for receiver sensitivity have been calculated for the several types of radiometers under consideration (Appendix F). Considering only the random error due to receiver noise, the expressions for receiver sensitivity are:

Total Power Radiometer

$$\Delta T_{rms} = \frac{T\left(F + \frac{T_A}{T_o} - 1\right) T_o}{2\sqrt{2\beta T}}$$

Correlation Radiometer

$$\Delta T_{rms} = \frac{T\left(F + \frac{T_A}{T_o} - 1\right) T_o}{2\sqrt{\beta T}}$$

Switch Load Radiometer

$$\Delta T_{rms} = \frac{T\left(F + \frac{T_A}{T_o} - 1\right) T_o}{\sqrt{2\beta T}}$$

The total power equation; by definition measures the magnitude of the total power present, and is applicable to single beam configurations; i.e., with a conical scan system a total power receiver configuration is applicable since the scanning loss is taken into account by the modulation function which is introduced directly as a spatial modulation of the antenna aperture plane. The switched load configuration is used for lobe subtraction. The correlation radiometer can be used with either monopulse configurations.

The tracking accuracy is defined for the case $\Delta E_S \equiv \Delta T_{rms}$, where $V_S^2/2$ is considered equivalent to the mean signal power. The signal power is assumed to have a Johnson noise distribution and can consequently be related to a temperature through the relationship:

$$P_S = KT_S\beta$$

where: K = Boltzmann's Constant;

T_S = equivalent signal temperature;

β = receiver bandwidth.

Thus the minimum detectable signal is defined when;

$$\Delta T_{rms} \equiv \Delta T_S$$

The resulting angular noise sensitivity is:

$$SENS = \left(\frac{\Delta\theta}{\Delta P_S}\right) \Delta P_N = \left(\frac{\Delta\theta}{T_S}\right) \Delta T_{rms}$$

The resulting tracking accuracies are thus:

(1) Simultaneous Lobing

$$SENS = \frac{1}{2}\left(F + \frac{T_A}{T_O} - 1\right)\left(\frac{T_O}{T_S}\right)\left(\frac{\theta_A}{\sqrt{\beta\tau}}\right)$$

(2) Lobe Subtraction by Sequential Switching

$$SENS = \frac{1}{\sqrt{2}}\left(F + \frac{T_A}{T_O} - 1\right)\left(\frac{T_O}{T_S}\right)\left(\frac{\theta_A}{\sqrt{\beta\tau}}\right)$$

(3) Conical Scanning:

$$SENS = \sqrt{2}\left(F + \frac{T_A}{T_O} - 1\right)\left(\frac{T_O}{T_S}\right)\left(\frac{\theta_A}{\sqrt{\beta\tau}}\right)$$

It is noted that the simultaneous lobing techniques are the most sensitive followed in order by lobe switching and conical scan.

Effect of Extended Sources

The previous developments have tacitly assumed a point source. In actuality the oxygen mantle will appear as an extended source to the antenna. That is the angular extent of the source is greater than the antenna's beam angle. A good approximation to the effects associated with non-point source targets can be calculated as follows:

First assume the distribution of the source radiation can be described by a column of constant field strength; $\vec{E_i}$, over the angular extent defined by the target

size, θ_S . Further assume the main beam of the antenna will have a radiation pattern described by $\cos\ \theta$, where θ is the displacement of the center of the source disc from the boresight position of the antenna. The output from the antenna due to the source radiation is assumed to sum power wise. Thus, the output power function can be written:

$$P_i\,\theta_{A\,(\theta_S)}^{2} = \frac{\vec{E}_i^{\,2}}{4}\left[\int_{-\theta_A}^{+\theta_A}\cos\theta\,d\theta\right]^2 + \left[\vec{E}_i^{\,2}\int_{-\left(\frac{\theta_S}{2}+\theta_A\right)}^{\left(\frac{\theta_S}{2}+\theta_A\right)}\ \int_{-\frac{\theta_S}{2}}^{+\frac{\theta_S}{2}}\cos\theta\,d\theta_A\,d\theta_S\right]$$

$P_i = \frac{\vec{E}_i^{\,2}}{4}$ = power density at the antenna when normalized to take into account the directive gain of a conical section and the limits of the integral used;

θ_A = the half-power beam angle measured with a point source;

θ_S = the half-power beam angle measured with an extended source.

In the above equation the first term represents the contribution due to a single point source at the disc center as it moves through the antenna beam and the second term represents the contributions of the points (not including the disc center) along the target disc diameter. This equation evaluates to:

$$P_i\,\theta_{A\,(\theta_S)}^{2} = P_i\left[\mathrm{SIN}^2\theta_A + 2\theta_S\left(\mathrm{SIN}\,\theta_A\cos\frac{\theta_S}{2} + \cos\theta_A\,\mathrm{SIN}\,\frac{\theta_S}{2}\right)\right]$$

For values of θ_A and θ_S small with respect to a radian this reduces to:

$$\theta_{A\,(\theta_S)}^{2} = \theta_A^2 + 2\theta_S\theta_A + \theta_S^2$$

$$\text{or}\quad \theta_{A\,(\theta_S)} = \theta_A + \theta_S$$

The overall result is the elongated response obtained by the superposition of the beam and source patterns as illustrated in Figure C-5. The sensitivity of the resulting S-curve response is for the Multiplicative Monopulse lobe subtraction process not appreciably different than that developed for the point source case. This is also illustrated in Figure C-5.

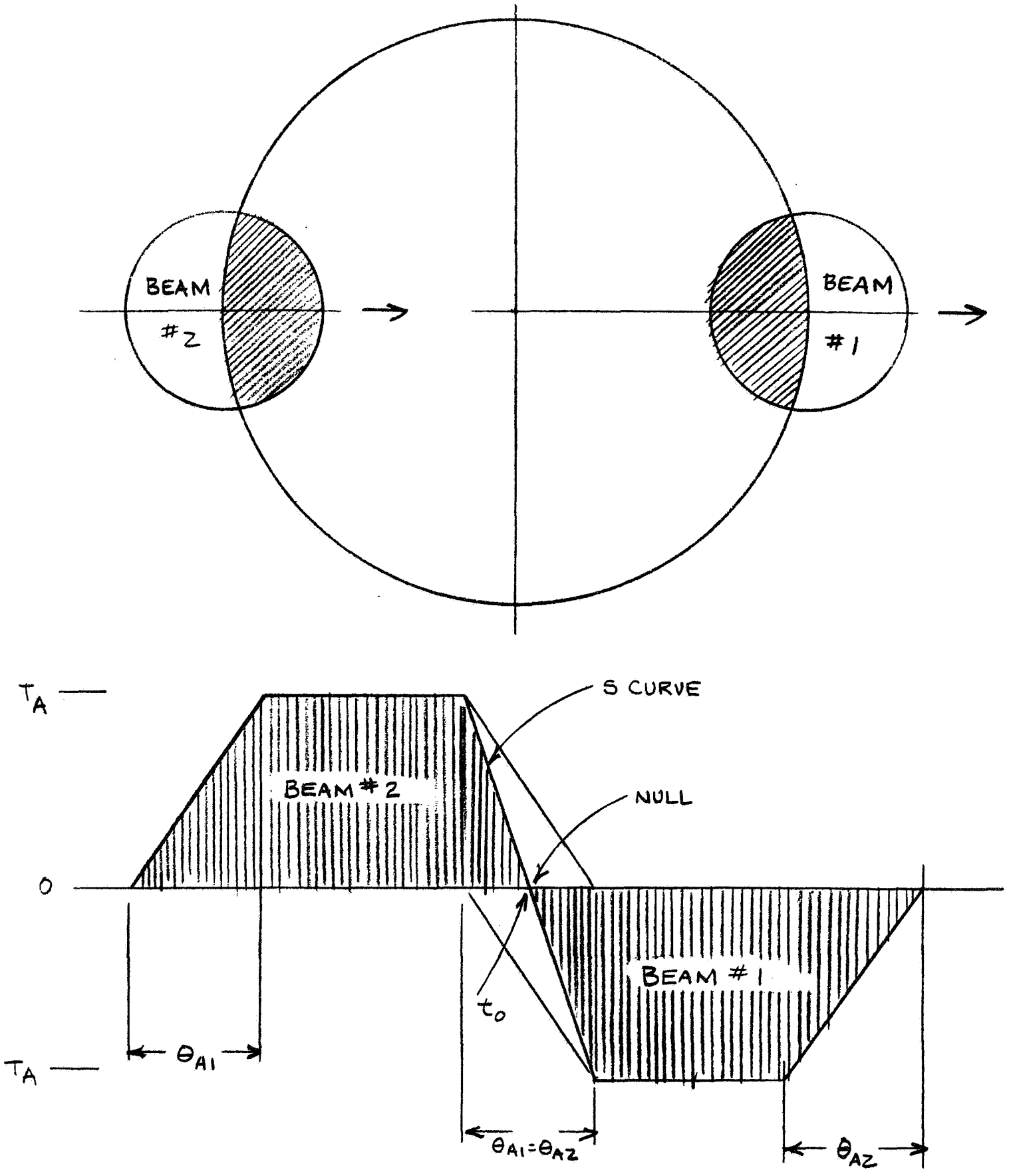

FIGURE C-5

EXTENDED TARGET RESPONSE
OF DUAL LOBE SENSOR

APPENDIX D

SOURCE CHARACTERISTICS

Introduction

The relationship between the spatial distribution of the emission spectrum and the observed antenna temperature is a result of the facts that the antenna temperature is proportional to the antenna efficiency and the function which describes the angular variation of the antenna response to external radiation as well as the temperature of that layer of the atmosphere from which the predominance of the received radiation originates. In this Appendix, we consider the nature of the source.

Altitude Weighting Functions

The computations of Meeks and Lilley (1963) assumed a plane horizontally stratified atmosphere and describe the relationship between the emission spectrum and the source regions, showing that the emission observed at a given frequency represents the average temperature in a layer of air approximately 10 km deep, with the mean altitude of the layer dependent on the frequency of observation.

More recent computations by Vilcans (1968) take into account the physically more appropriate spherically stratified atmosphere. The weighting functions derived by Vilcans for the case where the radiometer is looking directly downward can be plotted as shown in Figure D-1. The significance of these weighting functions is that by appropriately selecting the operating frequency it is possible to select the atmospheric layer whose temperature is to be observed. The desire is, of course, to select that layer which is most stable with respect to latitude.

Brightness Temperature Profile

Vilcans has also computated the brightness temperature profile at selected resonance and near resonance frequencies and for a remote single O_2 line at 118.7 GHz. The brightness temperature profiles in the valleys located between the resonance peaks, except for those

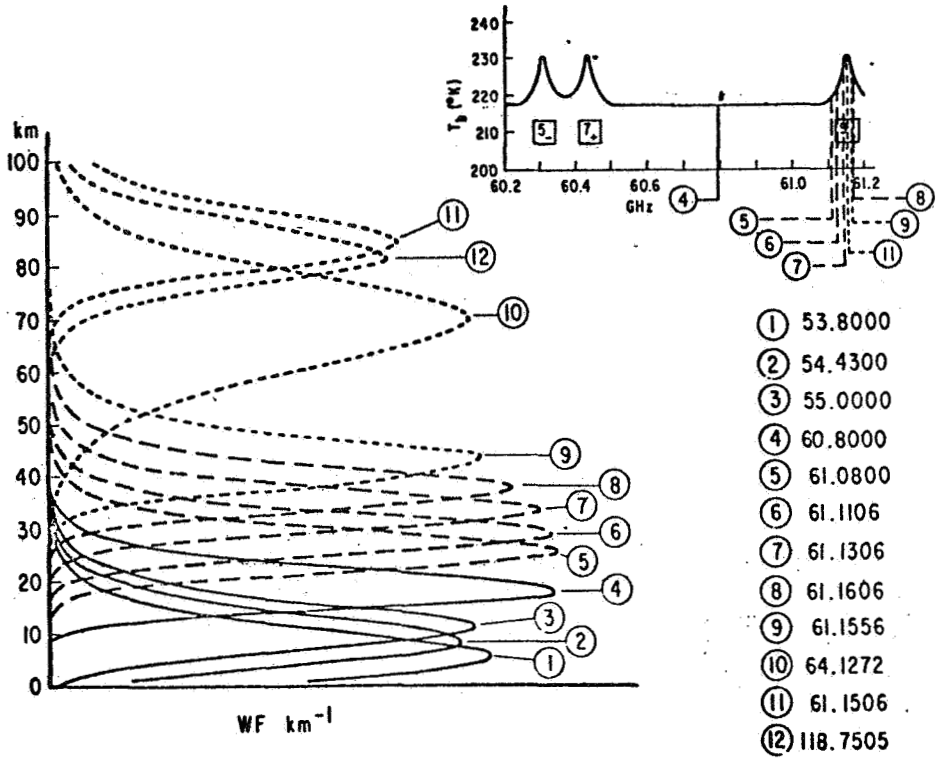

FIGURE D-1 ATMOSPHERIC WEIGHTING FUNCTIONS (VILCANS)

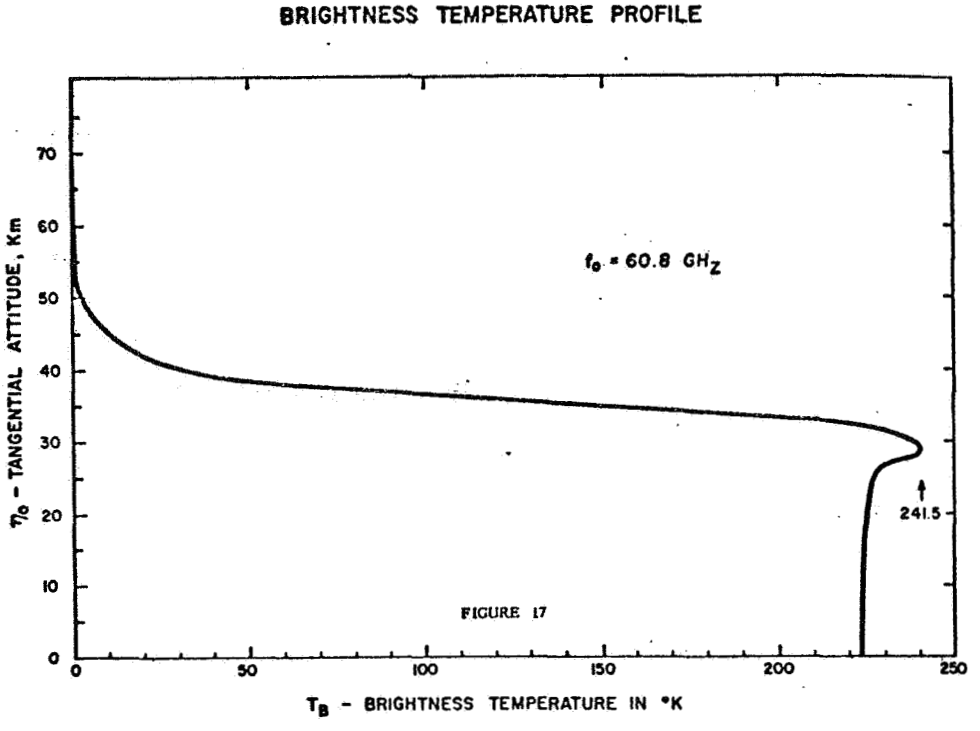

FIGURE D-2 BRIGHTNESS TEMPERATURE PROFILE (VILCANS)

far down on the skirts, are all quite similar. A typical calculated profile at 60.8 GHz is shown in Figure D-2. The depth of penetration of a ray path as a function of the distance above or below the point of tangency to the earth's surface is shown in Figure D-3. The important point to note is that the radiation peaks for layer altitudes between 18 and 29 km as the ray path is varied outward from the nadir. As the ray path direction continues to increase to higher tangential altitudes, the radiation will primarily appear from the tangenitial layer observed; however, as the atmospheric attenuation decreases with increasing tangential altitude, the measured antenna temperature will show a steady decline from its peak value at 29 km until it reaches the temperature of space. The important point to note here is that for all ray paths, the measured emission is well above the approximate 8 km height at which the effects of water vapor and surface weather becomes negligible. It is further noted from an examination of the several supplementary ARDC model atmospheres, shown in Figures D-4 and D-5, that this region is relatively thermally stable with respect to latitude, except for the ray paths close to the nadir. These paths will not, however, be separated greatly in latitude at the time of any given measurement, i.e., the nadir projects to a spot on the earth's surface.

FIGURE D-3

DEPTH OF PENETRATION VS DIRECTION OF RAY PATH

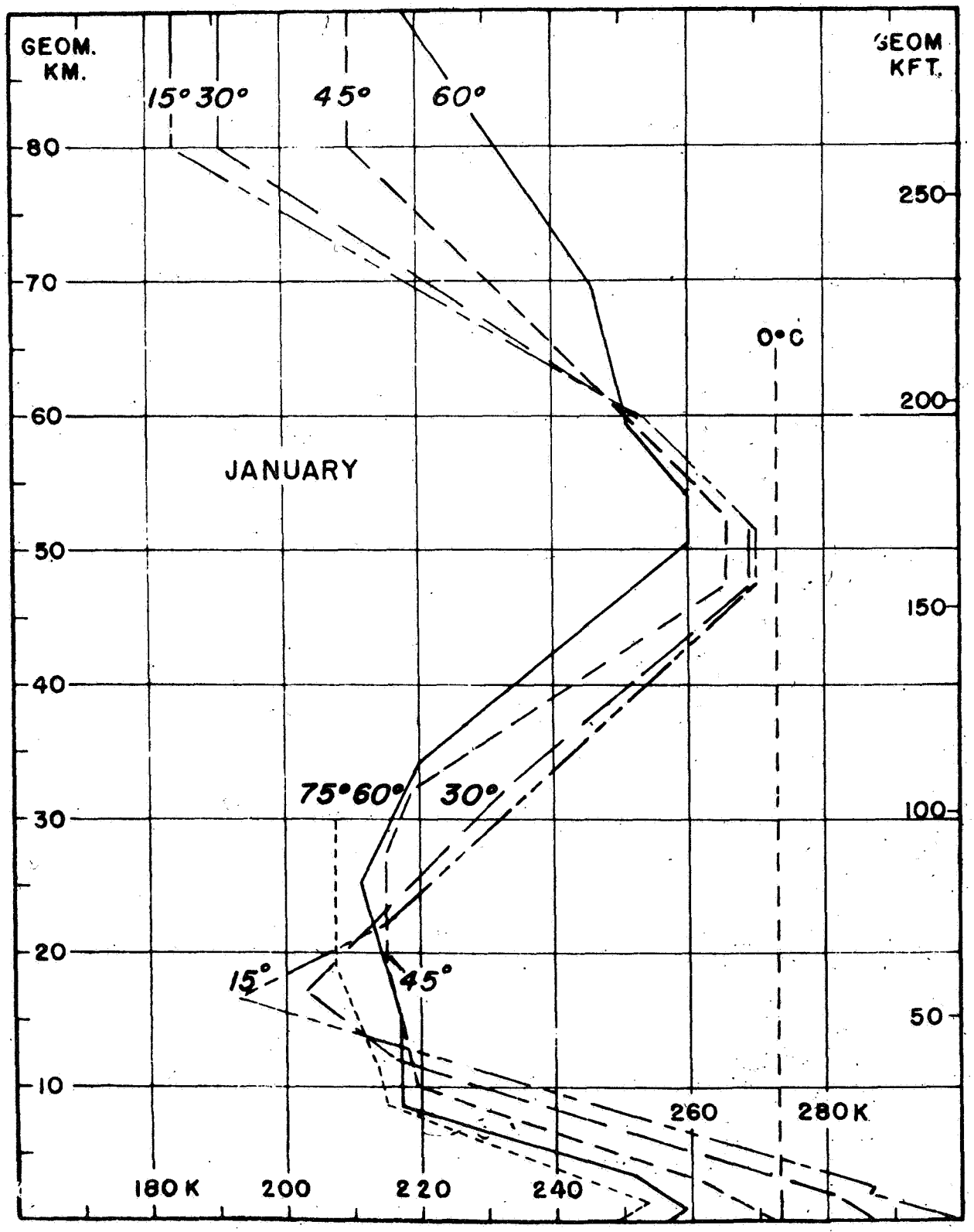

FIGURE D-4 TEMPERATURE HEIGHT PROFILES

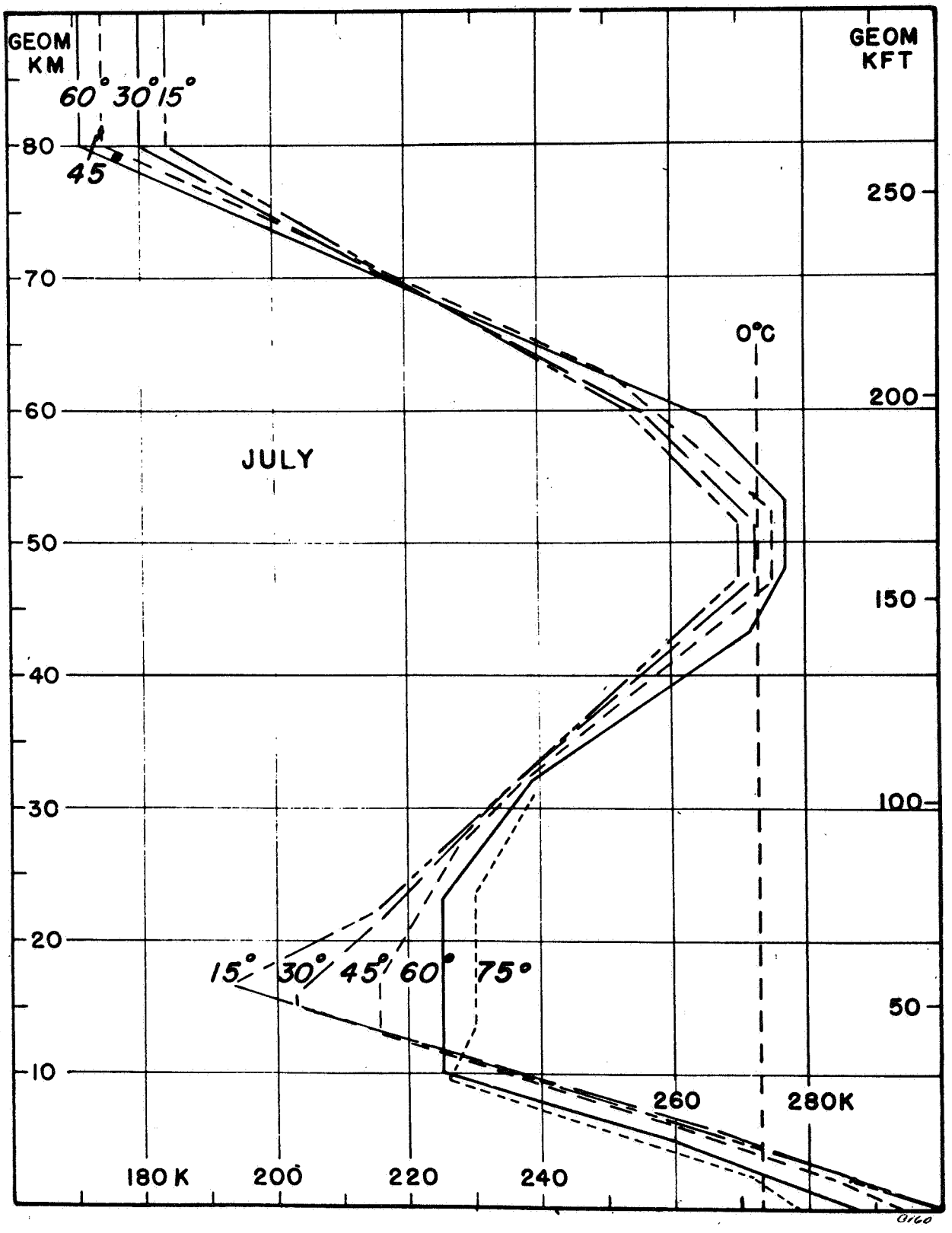

FIGURE D-5 TEMPERATURE HEIGHT PROFILES

APPENDIX E

ANTENNA SIDELOBE REQUIREMENTS AS A FUNCTION OF SOURCE CHARACTERISTICS

SUMMARY

It is necessary that some criteria be developed for the purpose of specifying the allowable antenna pattern distributions. It is further desirable that the criteria be expressed in a general way that reflects the mission requirements without forcing the antenna design to a specific beam shape.

The criteria developed here defines a conical volume in which the predominance of the received radiation must be contained. No restriction is placed upon the distribution of the pattern within the volume of the cone, except that it have a symmetrical arrangement.

The source is considered to be an isotropically radiating sphere with the resulting power distribution at the antenna determined by the depth of penetration of each individual ray path within the cone. The source distribution is perturbed by the maximum extremes as a function of latitude and season given in the ARDC model atmospheres (Appendix D).

Using these limits, it is shown that the specified accuracy can be met at the lower altitudes under these extreme conditions if approximately 99.5% of the received energy is contained in a cone having an angular dimension of $\pm 6^{\circ}$ about a line tangent to the limb of the sphere. The angular dimension along the rim of the source disc does not have a natural limitation.

GENERAL CONSIDERATIONS

The directivity of an antenna is the maximum radiation intensity divided by the average radiation intensity. The directive gain of an antenna is thus obtained by numerical integration of the formula:

$$G_o = \frac{4\pi \, \Phi_{MAX}}{\int_{\phi=0}^{2\pi} \int_{\theta=0}^{2\pi} \Phi_{(u)} \, SIN\,\theta \, d\theta \, d\phi}$$

where:

Φ_{MAX} = the radiation intensity in the direction of maximum response;

$\Phi_{(u)}$ = the radiation intensity as a function of u ;

u = a dimensionless parameter in the spherical coordinates of θ and ϕ .

Normalizing on the direction of maximum intensity and expressing the integral in terms of the unit solid angle gives:

$$G_o = \frac{1}{\oint\oint \left[\frac{\Phi_{(u)}}{\Phi_{MAX}}\right] \frac{d\Omega}{4\pi}}$$

where:

$d\Omega = SIN\,\theta \, d\theta \, d\phi$

= incremental unit solid angle.

Except for the simplest of antenna patterns, the integral can only be evaluated approximately; and thus, in general, it is practical to determine directivity accurately only on those antennas having radiation patterns which are not highly directive. For highly directional antennas, it is usually sufficient to estimate the directivity from a measurement of only the major lobe for only the normal polarization, and compare this with the directivity of an ideal conical beam or other convenient mathematical model. The ratio of the measured directivity to the directivity obtained with a true conical beam gives a measure of the total energy contained within the sidelobe structure of the pattern. The specific sidelobe distribution of any given antenna will, of course, depend upon the aperture shape and illumination function used.

THE CONICAL BEAM

The solid angle subtended by a cone is given mathematically by the expression:

$$\Omega_o = 2\pi\,(1 - \cos\,\theta_A/2)$$
$$= 4\pi\,\mathrm{SIN}^2\left(\frac{\theta_A}{4}\right)$$

where:

$\frac{\theta_A}{2}$ = the half-angle of the cone;

θ_{A_o} = the resulting half-power beam angle;

Ω_o = the solid angle subtended by the main beam between 3 db points.

For angles small compared to a radian, this reduces to:

$$\Omega_o = \frac{\pi\,\theta_{A_o}^2}{4} \text{ Steradians}$$

In terms of a spherical fraction, the beamwidth may be expressed as:

$$S_o = \frac{\Omega_o}{4\pi} = \frac{\theta_{A_o}^2}{16}$$

The directive gain of the conical section is now defined as the reciprocal of the spherical fraction, or:

$$G_{(\theta_A)} = \frac{16}{\theta_{A_o}^2}$$

PRACTICAL ANTENNAS

Assuming a rectangular aperture, the directive gain is described by a sinc function in u or:

$$G'_{(u)} = \left[\frac{\mathrm{SIN}\,u}{u}\right]^2$$

where:

$$u = \frac{\pi}{\theta_A}\,\mathrm{SIN}\Delta\theta;$$

$\Delta\theta$ = angular deviation from the boresight position.

For a circular aperture, the beam pattern is described by a Bessel Function in u. The effect of tapering the illumination down toward the aperture edge is to increase bandwidth, and reduce sidelobe levels, thus better approximating the conical beam shape. The most

commonly used aperture distribution for analysis purposes is described by $(1-\rho^2)^n$ where n is an integer. The simplest case is that for $n = 0$, the uniformly excited aperture.

For this case, the pattern reduces to:

$$G''_{o(u)} = \left[\frac{2J_1(u)}{u}\right]^2 = \left[\Lambda_{1(u)} - \frac{\Lambda_{2(u)}}{u}\right]^2$$

For $n = 1$, the illumination taper changes the pattern to:

$$G''_{1(u)} = \frac{9}{16}\,\Lambda^2_{2(u)}$$

where:

$\Lambda_{i(u)} = i!\,J_{i(u)}/(u/2)^i$ and are available in tabular form.

The main beam directivity can now be expressed most simply in terms of the ratio of the effective aperture area to the unit field area of the radiation which is $\frac{\lambda^2}{4\pi}$.

For a square aperture, the area is:

$$A' = D_e^2$$

For a circular aperture, the area is:

$$A'' = \frac{\pi D_e^2}{4}$$

where:

D_e = effective aperture diameter.

The directive gains are now:

Square Aperture:

$$G'_{(\theta_A)} = \frac{4\pi D_e^2}{\lambda^2} = \frac{4\pi}{\theta_A^2}$$

Circular Aperture:

$$G''_{(\theta_A)} = \frac{\pi^2 D_e^2}{\lambda^2} = \frac{\pi^2}{\theta_A^2}$$

where: $\theta_A \equiv \frac{\lambda}{D_e}$

The percentage of the total energy contained in the main lobe is now calculated as:

Square Aperture:

$$\left(\frac{\theta_A}{\theta_{A0}}\right)^2 \left(\frac{G'(\theta A)}{G(\theta A)}\right) = \frac{\pi}{4}$$

Circular Aperture:

$$\left(\frac{\theta_A}{\theta_{A0}}\right)^2 \left(\frac{G''(\theta A)}{G(\theta A)}\right) = \left(\frac{\pi}{4}\right)^2$$

Where $\left(\frac{\theta_A}{\theta_{A0}}\right)^2$ = Factor required to normalize the solid angles subtended by the respective beams.

Consider now the antenna temperature contributions when the respective beams sidelobe responses existing outside the allowable cone are considered to be looking at a holorum. Then:

Square Aperture:

$$T_{SL} = .215\,\alpha T_g$$

Circular Aperture:

$$T_{SL} = .37\,\alpha T_g$$

where:

T_g = temperature of the holorum;

α = a weighting function introduced to define the percentage of the sidelobe energy which lies outside the allowable cone.

Assume now two beams, one of whose sidelobes are observing a temperature T_{g1} and the other whose sidelobes are observing a temperature T_{g2}, then the differential temperature difference between antenna beams due to the sidelobe contributions is:

Square Aperture:

$$\Delta T_{SL} = 0.215\,\alpha\,(T_{g2} - T_{g1})$$

Circular Aperture:

$$\Delta T_{SL} = 0.37\,\alpha\,(T_{g2} - T_{g1})$$

Solving for α we obtain the required percentage of the sidelobe energy that can appear outside the allowed conical section as:

Square Aperture:

$$\alpha = 4.65 \left(\frac{\Delta T_{SL}}{T_{g2} - T_{g1}} \right)$$

Circular Aperture:

$$\alpha = 2.7 \left(\frac{\Delta T_{SL}}{T_{g2} - T_{g1}} \right)$$

Assume $T_{g2} - T_{g1} = 50^{\circ}K$, the maximum variation one might expect as a function of latitude for earth viewing beams, and $\Delta T_{SL} = 0.24^{\circ}K$ (10^{-3} of the $240^{\circ}K$ temperature expected at a tangential altitude of 29 km) gives the values of α as:

Square Aperture:

$$\alpha = .0223$$

This corresponds to -16.5 db of the total sidelobe energy resulting in approximately 99.5% of the energy being contained in the allowable cone.

Circular Aperture:

$$\alpha = .013$$

This corresponds to - 19 db of the total sidelobe energy also resulting in an approximately 99.5% concentration of power in the allowable response region.

These are not considered restrictive requirements, especially where the allowable response in the direction perpendicular to the source rim can be considered as the integrated responses over the angle given by:

$$\theta_A = \text{SIN}^{-1} \frac{R+h_2}{R+h_S} - \text{SIN}^{-1} \frac{R+h_1}{R+h_S} \approx \text{SIN}^{-1} \frac{R+h_2}{R+h_S} - \text{SIN}^{-1} \frac{R}{R+h_S}$$

where:

R = the earth's radius;

h_S = the spacecraft height;

h_2 = tangential altitude of peak response;

= 29 km;

h_1 = the tangential altitude to which the radiation temperature can be considered constant as a function of the depth of penetration (see Appendix D) of the ray path. For a maximum depth of penetration to 26 km at an operating frequency of 60.8 GHz, the tangential altitude can be reduced to practically zero, and for a narrow beam system will thus include all the major sidelobes as part of the allowable response region.

For the direction tangent to the source rim no natural restriction is imposed as a consequence of the source's isolation in space.

APPENDIX F

THE RADIOMETER

BACKGROUND

A radiometer is an instrument designed to measure the intensity of black body radiant energy. The analysis of the radiometric data is based on certain assumptions and laws concerning the nature of the radiometer, as well as the characteristics of the signal energy. In general, we are concerned here with millimeter wavelengths; and the applicable characteristics and actions are summarized as follows:

. . . The spectral density of the power developed across a matched antenna load as a result of the reception of radiation from a volume element of a source is proportional to the product of the efficiency of the receiving aperture and the pattern function which describes the spatial variation of the antenna aperture's response to external radiation at the operating frequency.

. . . The source is assumed to appear as a black body to the radiation resistance of the antenna; i.e.; it absorbs all incident radiation and since it is at a uniform temperature it reradiates according to Planck's Law:

$$b\,d\nu = \left(\frac{2h\nu^3}{c^2}\right)\left(\frac{d\nu}{e^{h\nu/KT}-1}\right) \qquad (1)$$

where:

b = the brightness of the source. $\frac{\text{watts}}{M^2 - \text{ster} - \text{Hz}}$

h = Planck's Constant; (6.63×10^{-34} joule-sec)

ν = frequency; Hz

K = Boltzmann's Constant; (1.38×10^{-23} joule $^{o}K^{-1}$)

T = Temperature; ^{o}K, Kinetic temperature of the media

C = velocity of propagation. $m\text{-}sec^{-1}$

. . . At microwave frequencies Planck's Law of radiation for a black body can be replaced by the Rayleigh Jeans approximation. This approximation holds in the frequency range where:

$$h\nu << KT$$

Thus:

$$b d\nu = \left(\frac{2KT}{\lambda^2} \right) d\nu \qquad (2)$$

where $\lambda = \frac{c}{\nu}$ = wavelength.

. . . The antenna response function for any antenna can be evaluated to give:

$$\oint A_{(\theta,\phi)}\, d\Omega \equiv \lambda^2 \qquad (3)$$

where:

$A(\theta,\phi)$ = effective aperture area as a function of the spherical coordinates $\theta\ \phi$;

$d\Omega$ = unit solid angle.

The received power at the antenna is thus:

$$P_A = \left(\frac{KT}{\lambda^2} \right) \int d\nu \oint A_{(\theta,\phi)} d\Omega \qquad (4)$$

$$= KT_A \beta$$

where:

P_A = the power received by the antenna in watts;

T_A = apparent temperature induced in the antenna by the source in degrees Kelvin;

$\beta = \int d\nu$ = the operating bandwidth in Hz.

. . . The noise power generated in the frequency band of interest by the radiometer is expressed in the usual manner for a Johnson noise distribution as:

$$P_R = K\beta T_R = \Phi_R \beta \qquad (5)$$

where:

T_R = effective operating noise temperature of the radiometer;

$\Phi_R = KT_R$ = the noise power density in watts/Hz.

. . . The receiver noise power and the received power are assumed to sum at the radiometer input.

. . . The radiometer averages the response over a period of time and measures the differences with respect to a previous period of time or with respect to a defined reference level.

The following sections of this Appendix describe the various types of radiometers and how they perform their function.

EQUIVALENT NOISE TEMPERATURES AS SEEN BY THE RADIOMETER

The value of T_R is conventionally expressed in terms of a receiver noise figure as:

$$T_R = (F_R - 1)\, T_o \tag{6}$$

where:

F_R = noise figure as conventionally defined;

$T_o = 290^\circ K$

The total system operating noise temperature is; of course, given by the sum:

$$T_N = T_A + T_R = \left(F_R + \frac{T_A}{T_o} - 1\right) T_o \tag{7a}$$

$$= \left(F_R + \frac{T_A}{T_o} - 1\right) \left(\frac{\Phi_o}{K}\right) \tag{7b}$$

where: $\Phi_o = K T_o = 4 \times 10^{-21}$ watts/Hz.

The minimum detectable signal for the radiometer is set by the standard deviation of the output voltage distribution where the mean voltage level is calibrated to read directly in degrees Kelvin. The standard deviation of the output distribution for a sample containing fixed temperatures is given by the general formula for statistical averaging as [32]

$$\Delta T_{rms} = \frac{T_N}{\sqrt{n}} = \frac{\left(F_R + \frac{T_A}{T_o} - 1\right) T_o}{\sqrt{n}} \tag{8}$$

where:

n = the number of degrees of freedom in the sample.

THE AVERAGING PROCESS

The number of degrees of freedom in the sample is simply determined as the ratio of the receiver bandwidth to the noise bandwidth of an ideal low pass zonal filter. The equivalent noise bandwidth for an arbitrary filter configuration is conventionally defined as either:

$$B_n' = \frac{1}{2\pi} \int_{-\infty}^{\infty} |H(\omega)|^2 \, d\omega \tag{9a}$$

(double sided filter response)

$$B_n = \frac{1}{2\pi} \int_{0}^{\infty} |H(\omega)|^2 \, d\omega \tag{9b}$$

(single-sided filter response)

Where $H_{(\omega)}$ is the transform of the impulse response of the filter. When the double-sided filter response is used it is necessary to re-define the noise power density to take into account the negative frequency contributions. Thus:

$$\Phi_o' = \frac{\Phi_o}{2} = \frac{KT_o}{2}$$

$$\equiv 2 \times 10^{-21} \text{ watts/Hz} \qquad (10)$$

The same value of noise power for a given filter response will now be obtained with both the single-sided and double-sided expressions.

Using the single-sided response for a rectangular low pass filter gives the effective noise bandwidth as:

$$B_n = \frac{1}{2\pi} \int_0^{2\pi B_e} 2\, d\omega = 2B_e \qquad (11)$$

Where $|H_{(\omega)}|^2 = 2$ within the pass band and zero elsewhere. The gain of 2 within the pass band is introduced to properly normalize the power per cycle within the low pass region to a unit bandpass configuration.

The filter time constant is defined in terms of a characteristic time interval which is associated with the impulse response. Either of two characteristic time intervals are commonly used. These time constants are defined as follows:

$$I_{(t)} = \frac{\sin 2\pi B_e t}{2\pi B_e t} \equiv \frac{\sin\left[\left(\frac{\pi}{2}\right)\left(\frac{t}{\tau}\right)\right]}{\frac{\pi}{2}\left(\frac{t}{\tau}\right)} \qquad (12)$$

where $I_{(t)}$ is the impulse response and τ is defined as the time for which the impulse response decreases to $2/\pi$ of its peak value at $t = 0$. In this case:

$$B_n = 2B_e \equiv \frac{1}{2\tau} \qquad (13)$$

CASE 2

$$I_{(t)} = \frac{\sin 2\pi B_e t}{2\pi B_e t} = \frac{\sin\left(\frac{\pi t}{\tau_2}\right)}{\frac{\pi t}{\tau_2}} \qquad (14)$$

where τ_2 is defined as the time between the zeros of the principle response centered at the origin. In this case:

$$2\pi B_e t = \pi\left(\frac{t}{\tau_2}\right)$$

$$B_e \equiv \frac{1}{2\tau_2} \qquad (15)$$

The equivalent noise bandwidth is then:

$$\mathcal{B}_n \equiv \frac{1}{T_2} \tag{16}$$

The value of n used in the general equation for statistical averaging is thus given by any of the following equally valid relationships:

$$n = \frac{\mathcal{B}}{\mathcal{B}_n} = \frac{\mathcal{B}}{2\mathcal{B}_e} = \mathcal{B}T_2 = 2\mathcal{B}T \tag{17}$$

where:

$\mathcal{B}$ = receiver bandwidth;

$\mathcal{B}_n$ = noise bandwidth of a rectangular post-detection low pass filter;

$\mathcal{B}_e$ = low pass filter bandwidth;

T_2 = time between the zeros of the principle lobe of the filter impulse response;

T = time for the impulse response to decrease to $2/\pi$ of its initial value at $t = 0$

Strictly speaking, power density can be related to Johnson noise temperature only when a rectangular frequency response is assumed. Practically such a filter is unrealizable and some modifications to the above arguments are required. The most commonly used filter configuration is that of the single stage RC low pass filter. Using the single-sided response for this filter gives the effective noise bandwidth as:

$$\mathcal{B}_{n(rc)} = \frac{1}{2\pi T_{rc}} \int_0^\infty \frac{T_{rc}\, d\omega}{1+(T_{rc}\omega)^2} = \frac{1}{4T_{rc}} \tag{18}$$

where T_{rc} is the expontenial decay time constant associated with the filters impulse response.

Now because the RC low pass filter does not cut-off sharply at its bandwidth limits, the actual noise density function will not be constant across the filter pass band; and consequently the noise power is not directly related to a noise temperature, except in approximation. Two different approximations may be defined as follows:

(1) <u>The Equivalent Half-Power Bandwidth Approximation</u>

For the RC filter the pass band is normally defined in terms of a half-power bandwidth which is related to the expontential decay time constant through the expression:

$$\mathcal{B}_{e_{rc}} = \frac{1}{2\pi T_{rc}}$$

(19)

where:

$B_{e_{rc}}$ = half power bandwidth;

The equivalent noise bandwidth is:

$$B_{n_{rc}} = \frac{1}{4T_{rc}} = \left(\frac{\pi}{2}\right) B_{e_{rc}} \tag{20}$$

Because of the step-function characteristic of the rectangular shape the half-power bandwidth of the ideal filter is equal to the full power bandwidth. The noise bandwidth of the rectangular zonal filter has been shown to be related to the filters low pass bandwidth by:

$$B_n = 2B_e \tag{21}$$

Letting $B_{e_{rc}} = B_e$ then the equivalent rectangular zonal filter bandwidth is greater than the RC filter noise bandwidth; i.e.;

$$B_n = \left(\frac{4}{\pi}\right) B_{n_{rc}} = \frac{1}{\pi T_{rc}} \tag{22}$$

Thus assuming the significant noise power is generated in the filter's half-power bandwidth regions the corresponding value of η used in calculating the standard deviation in the output distribution due to noise is:

$$\eta_1 = \pi T B T_{rc} \tag{23}$$

(2) The Equivalent Noise Bandwidth Approximation

Alternately the performance is often specified in terms of filters with equivalent noise bandwidths. In this case the equivalent zonal filter bandwidth is less than the RC filter half-power bandwidth; i.e.,

$$B_e = \left(\frac{\pi}{4}\right) B_{e_{rc}} \tag{24}$$

The proper value of η to use for this comparison is:

$$\eta_2 = 4BT_{rc} \tag{25}$$

It is, however, noted that by setting $B_n = B_{n_{(rc)}}$ one arrives at a low pass filter that will result in an equivalent output noise power to that of the ideal zonal filter of bandwidth B_e, but it does not follow that this filter will also have equivalent averaging characteristics. The general formula for statistical averaging presumes samples of constant mean value and is,

consequently, not strictly applicable to the RC filter configuration. That is, the sample interval is dependent upon the time persistence of the filter response, and is equal to the reciprocal noise bandwidth only for the rectangular filter shape.

The finite skirt response of the RC filter allows more high frequency components to be present at the output. For equivalent noise bandwidth filters, the persistence of the RC filter impulse response is consequently much less than that of the ideal zonal filter (see Figure F-1) resulting in less samples per integration time constant. The practical result is that the equivalent noise bandwidth approximation tends to err on the optimistic side. The equivalent half bandwidth approximation gives a more conservative result, and is more consistent with what is achieved in practice.

The importance of the above discussion is that in the literature the radiometer gain constant used by various authors will vary. The variations are, in general, directly traceable to the model used to describe the post detection integration process. With respect to the indicated output, the mean output is calibrated to a temperature scale; and hence, the scale factor converting output volts to degrees Kelvin is not effected by the choice of the filter model, but rather how well we know the reference temperature used for calibration.

FOR $\beta_n = \beta_{n(rc)}$

THEN $\tau_{rc} = \frac{\tau}{2}$

$$I_1(t) = \frac{\sin\left(\frac{\pi t}{2\tau}\right)}{\left(\frac{\pi t}{2\tau}\right)}$$

$$I_2(t) = e^{-\frac{2t}{\tau}}$$

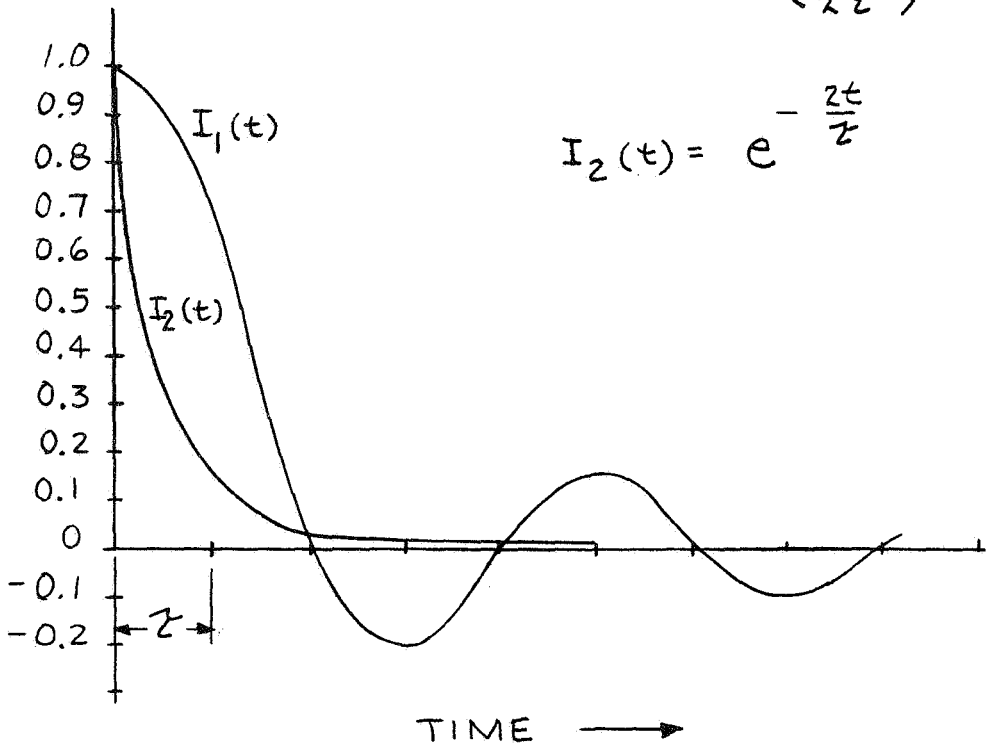

FIGURE F-1

COMPARISON OF THE TIME RESPONSES OF EQUIVALENT NOISE BANDWIDTH FILTERS CHARACTERIZED BY SIN X/X AND EXPONENTIAL IMPULSE RESPONSES.

RECEIVER SENSITIVITY

The sensitivity of a radiometer is defined in terms of a minimum detectable temperature change at the radiometer input. This minimum detectable temperature change is defined as that input temperature variation that gives rise to a change in the mean of the output distribution equal to the standard deviation (one sigma) due to system noise; i.e.,

$$\Delta T_{A_{(MIN)}} \equiv \Delta T_N \tag{26}$$

The limiting sensitivity of a radiometer is determined by two factors. The first is the internal noise of the amplifier, and the second is the fluctuations of the amplifier gain. Consider first the internal noise limitation.

The minimum detectable signal is set by fluctuations in the indicated mean temperature and this is; previously noted, given by the general formula for statistical averaging. Assuming an ideal rectangular output filter characteristic, the minimum detectable signal is calculated from any one of the following equal valid forms of the equation for the output fluctuations:

$$\Delta T_{A_{(MIN)}} = \frac{k\left(F_r + \frac{T_A}{T_o} - 1\right) T_o}{\sqrt{\beta / \beta_n}} \tag{27a}$$

$$= \frac{k\left(F_r + \frac{T_A}{T_o} - 1\right) T_o}{\sqrt{\beta / 2\beta_e}} \tag{27b}$$

$$= \frac{k\left(F_r + \frac{T_A}{T_o} - 1\right) T_o}{\sqrt{T_2 \beta}} \tag{27c}$$

$$= \frac{k\left(F_r + \frac{T_A}{T_o} - 1\right) T_o}{\sqrt{2T\beta}} \tag{27d}$$

where:

k = calibration constant dependent upon the type receiver used.

If an RC low pass filter, of equivalent half-power bandpass characteristics, is used for the averaging process the equation for the minimum detectable signal is better written:

$$\Delta T_{A_{(MIN)}} = \frac{k\left(F_r + \frac{T_A}{T_o} - 1\right) T_o}{\sqrt{\pi T_{rc} \beta}} \tag{28}$$

where:

T_{rc} = RC = time constant in terms of the exponential decay time of the filter's impulse response.

The general expression for the sensitivity of a direct coupled radiometeric receiver (Figure F-2) which describes both sources which contribute to the fluctuations at the radiometer output takes the form:

$$\Delta T_{A_{(MIN)}} = \left[\frac{R_1^2}{2\beta\tau} + \left(\frac{\Delta G}{G_o}\right)_{AV}^2\right]^{1/2} \left(F + \frac{T_A}{T_o} - 1\right) T_o \tag{29}$$

where $\left(\frac{\Delta G}{G_o}\right)_{AV}$ represents any change in the mean value or d.c. component of the output, and the output filter is assumed to be an ideal zonal configuration.

Thus, it is seen that with a direct coupled radiometer (sometimes called a total power radiometer), the gain fluctuations act as a direct variation in the noise level. This variation in noise level is considered to sum with the previous noise fluctuations in a RSS (square-root of the sum of the squares) manner. To maintain an equal error contribution due to both causes, it is necessary that a gain stability equal to the reciprocal of receiver processing gain be achieved, i.e.,

$$\left(\frac{\Delta G}{G_o}\right)_{AV} = \frac{R_1}{\sqrt{2\beta\tau}} \tag{30}$$

Dicke reduced the effects of these gain variations at a small increase in the rms sensitivity when he developed the switched radiometer (Figure F-3). The philosophy of the switched radiometer is that the input signal power can be measured by comparing its level with that of a reference signal. The effect of the switches is to produce a readily identifiable modulation on the noise power generated in the receiver itself.

The modulation component, when detected by a square-law device, will have a magnitude proportional to the difference temperature between the reference load and the input. The detected signal is then amplified by stable, narrow band amplifiers and synchronously detected. The d.c. output of the synchronous detector is then further filtered by means of a low pass filter and passed on to the output display device. Nulling by a noise injection procedure (setting $T_A = T_{ref}$ in the radiometer of Figure F-3) will, of course, completely eliminate the effect of gain variations with respect to scale accuracy, which is now determined by the accuracy of the attenuator calibration and the stability of the reference source.

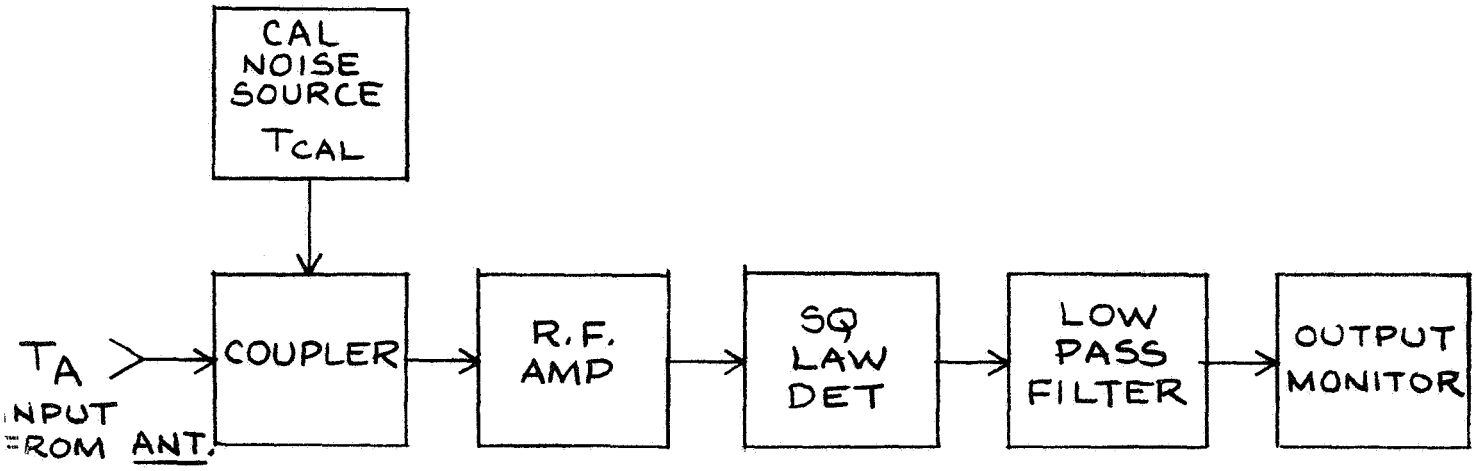

FIGURE F-2
DIRECT COUPLED RADIOMETER

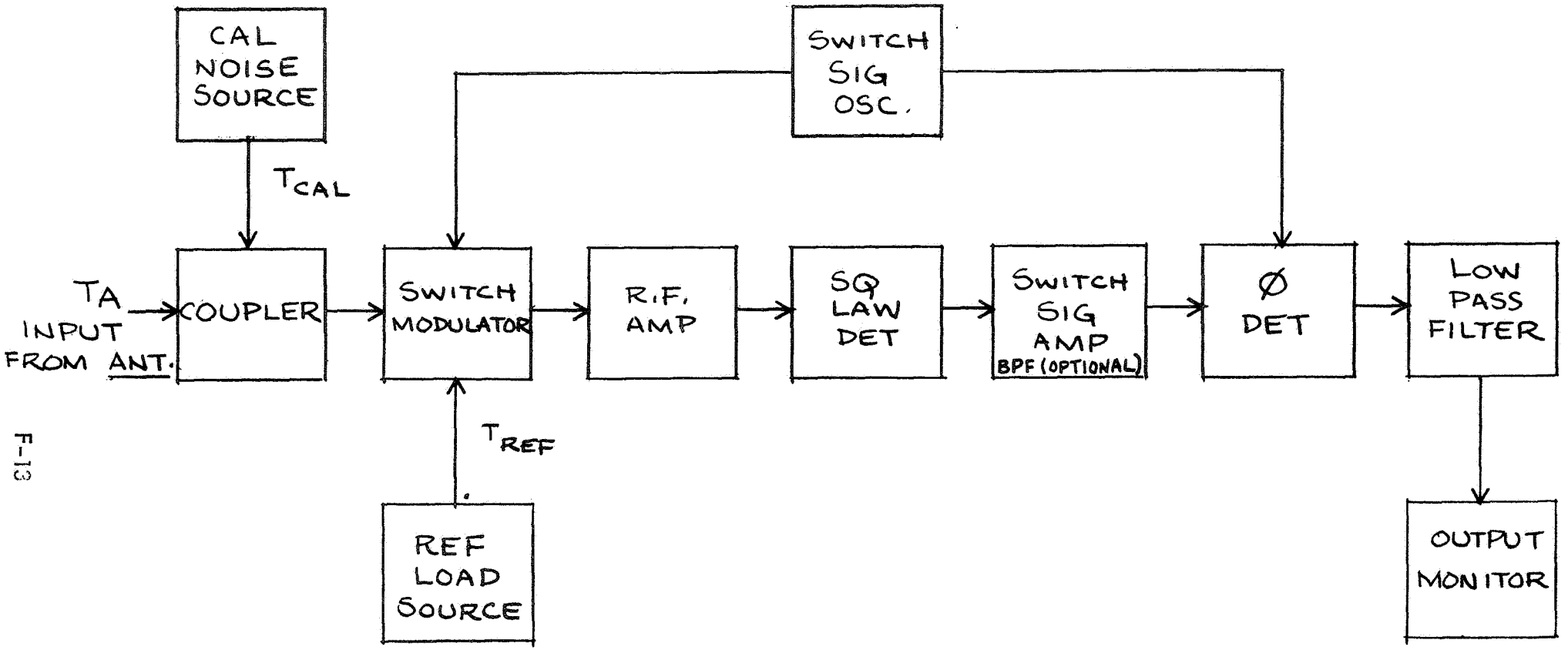

FIGURE F-3
SWITCH LOAD RADIOMETER

The complete expression for the sensitivity of a sampled load type radiometer now takes the form:

$$\Delta T_{(MIN)} = k_2 \left[\left(1 + \frac{T_A + T_R}{(F-1)T_o} + \frac{T_A + T_R^2}{2(F-1)^2 T_o^2} \right) \frac{(F-1)^2 T_o^2}{2BT} + \bar{M}^2 (T_R - T_A)^2 \right]^{1/2} \quad (31)$$

where:

$\bar{M}^2 = \left[\frac{G(t)}{G_o} - 1 \right]^2_{AV}$ = the relative mean square gain variation;

$\left[T_N^2 + T_N (T_A + T_R) + \frac{T_A^2 + T_R^2}{2} \right]^{1/2}$ = effective input noise temperature taking into account the post-detection subtraction and averaging over the sample period;

$T_N = (F-1)T_o$ = receiver noise temperature;

T_R = effective temperature of the comparison, or reference source.

To reduce the contribution of gain variations to the same level as the statistical noise fluctuation level now requires a gain stability:

$$\bar{M} = \frac{\left[1 + \frac{T_A + T_R}{(F-1)T_o} + \frac{T_A^2 + T_R^2}{2(F-1)^2 T_o^2} \right]^{1/2} (F-1)T_o}{\sqrt{2BT}\,(T_R - T_A)} \quad (32)$$

Normally, the temperature difference $T_{REF} - T_A$ is set close to zero resulting in a reasonable gain stability requirement.

With a correlation receiver* (Figure F-4), the input signal is divided between two channels, and then recombined at the output by means of a multiplier to obtain a d.c. output with a mean value ideally not biased by receiver noise. However, performance is based on the use of a balanced set of detector elements, and the sensitivity expression is now written:

$$\Delta T_{MIN} = \left[\frac{k_3^2}{2BT} + \left(1 - \frac{\Delta G}{G_o} \right)^2_{AV} \Delta G^2_{DET} \right]^{1/2} \left[1 + \frac{T_A + T_R}{(F-1)T_o} + \frac{T_A^2 + T_R^2}{2(F-1)^2 T_o^2} \right]^{1/2} (F-1)T_o \quad (33)$$

---

* The correlation function is defined as the integral of the product ot two signals; or their envelopes, as a function of delay. If the two waveforms are the same except for the delay we obtain the auto-correlation; if they are different we obtain the cross-correlation. In the receiver configuration shown, the delay is introduced by motion of the antenna, and the multiplication process by first taking the voltage sum and difference of the two inputs, and then taking the difference of the squares of the resulting waveforms; i.e., $(V_A + V_R)^2 - (V_A - V_R)^2 = 4V_A V_R$; where V_A^2 and V_R^2 are proportional to $KT_A B$ and $KT_R B$, respectively.

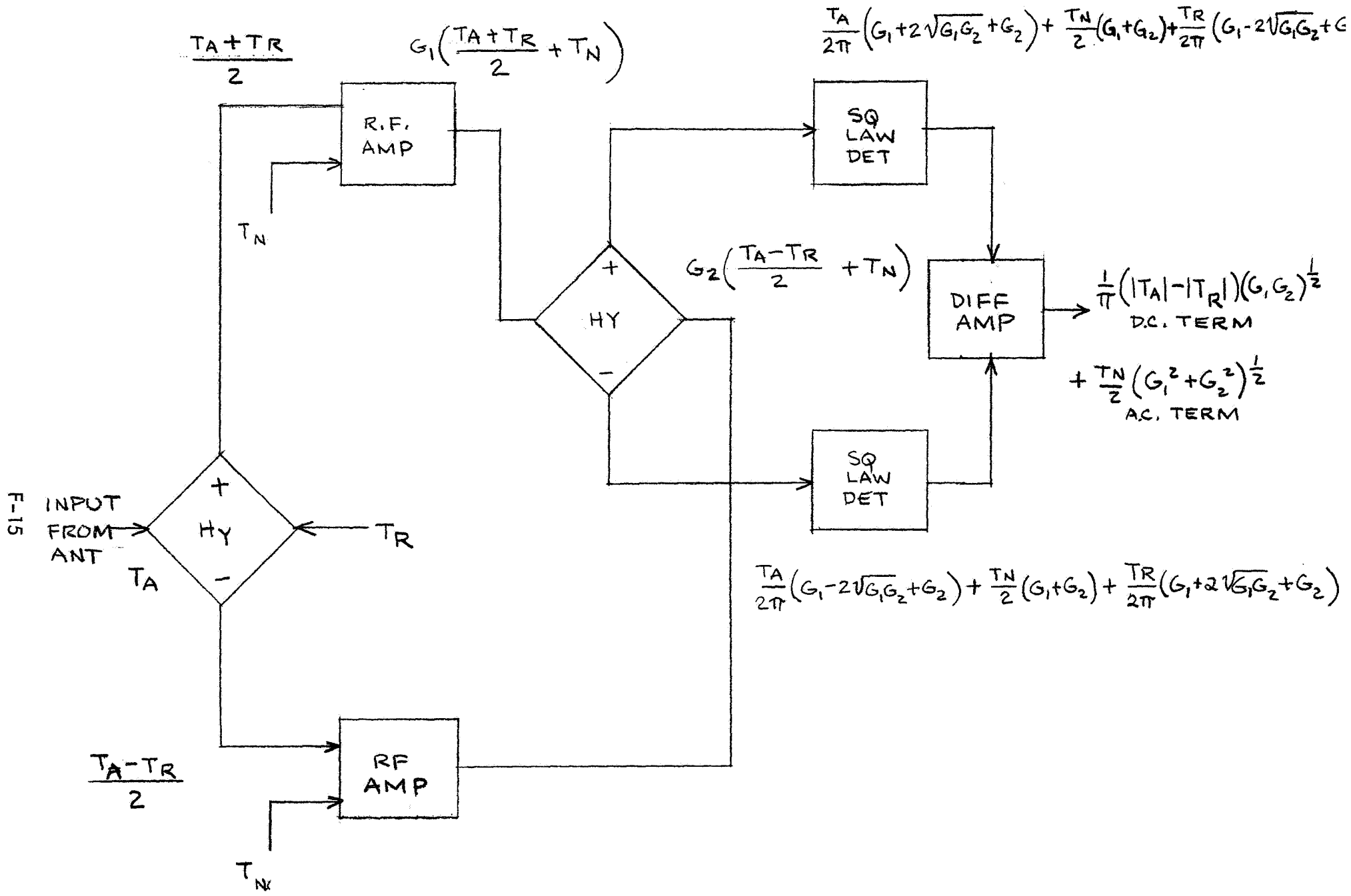

FIGURE F-4

CORRELATION RADIOMETER

where ΔG_{dET} is the change in the slopes of the balanced detector diodes as a function of drive level; i.e.,

$$\Delta G_{dET} = G_{diode_1} - G_{diode_2} \tag{34}$$

where:

G_{diode} = slope of the square-law detector transfer characteristic in volt/watt measured at the actual operating point;

$\left(\frac{\Delta G}{G_o}\right)_{AV}$ = the fractional gain variation;

$$G_o \equiv \sqrt{G_1 G_2}$$

Thus, for a $\pm \left(\frac{\Delta G}{G_o}\right)_{AV}$ fractional gain variation, the drive level to the detector diodes will be $\left(1 \pm \frac{\Delta G}{G_o}\right)_{AV} P_o$ where P_o is the nominal value of drive power for which the detector is balanced. Further, assume that for this $(\Delta G/G_o)_{AV} P_o$ change in drive level, the respective diode slopes change by ΔG_{dET}, then a d.c. bias error voltage will occur at the multiplier output equal to:

$$\Delta E_{dc} = \pm \left(1 - \frac{\Delta G}{G_o}\right)_{AV} P_o \Delta G \tag{35}$$

The fractional bias error due to gain variations is thus:

$$\frac{\Delta E_{dc}}{P_o} = \left(1 - \frac{\Delta G}{G_o}\right)_{AV} \Delta G_{dET} \tag{36}$$

The error represented by Equation 36 is in a sense a measure of the degree to which the zero base line can be established. The ability to match the slopes of the diode characteristics can become the limiting parameter with respect to the accuracy that can be achieved in the presence of a varying drive level to the multiplier. This is avoided in the switched load configuration by the use of a single detector element. This same advantage can be achieved with the correlation radiometer by driving a switched input amplifier with the outputs from the second hybrid. The switched input amplifier then drives a single detector element without introducing any additional loss in signal-to-noise ratio due to the switching. This configuration is illustrated in Figure F-5.

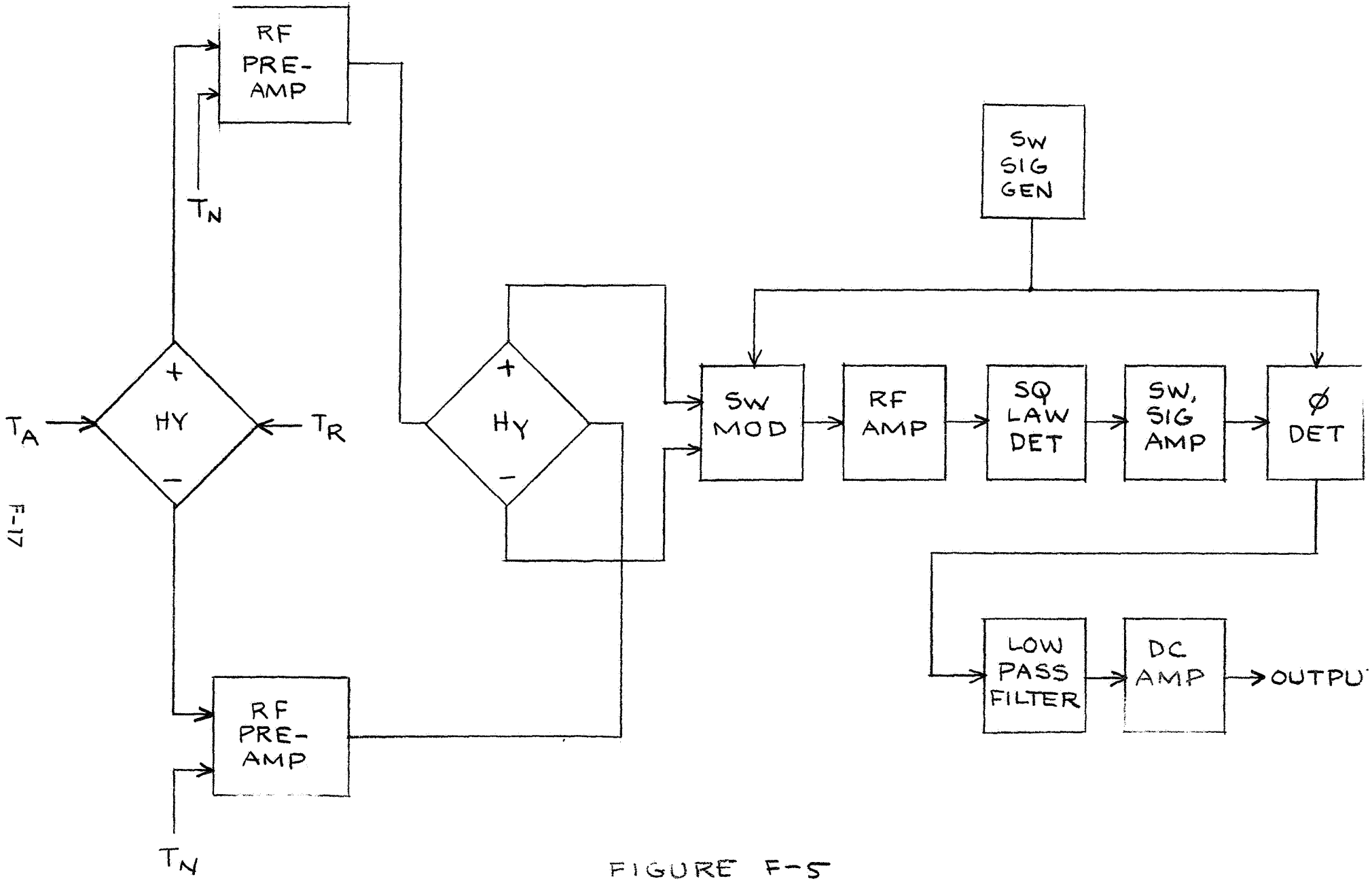

FIGURE F-5

IMPROVED VERSION OF DUAL CHANNEL CORRELATION RADIOMETER

EVALUATION OF THE RADIOMETER CALIBRATION CONSTANTS

For a total power radiometer, the output reading is obtained by directly averaging the squared mean of a Gaussian amplitude distribution. The squared mean is equal to $\frac{1}{2\pi}$ of the undetected input distributions mean square value. The noise output is taken equal to one-half the mean square value of the input noise distribution. By application of the central limit theorem of statistics, the post detection filtering causes the filtered output fluctuations to be normally distributed about the mean value. The mean value of the filter output distribution is proportional to the squared mean value of the input distribution and the noise fluctuations in the filter output distribution are proportional to one-half the filter input fluctuations or one-fourth the pre-detected input's mean square value.

As a consequence of the above facts, a loss in signal-to-noise ratio of $\pi/2$ occurs through the detector; i.e.,

$$k_1 \equiv \pi/2 \tag{37}$$

With the switched load or Dicke radiometer, the calibration constant is arrived at from the following considerations. First, note that due to sampling, only one-half of the signal energy is available, introducing a signal loss of two without a corresponding loss in noise power. Second, because of the fact that only the fundamental component of the rectangular modulation signal is effective, an additional loss in signal-to-noise of $\pi/2$ occurs. The square-law detector loss does not occur in this case because only the modulation components, and not the d.c. level are preserved by the modulation signal filter. Thus, the resultant calibration constant is twice that of the total power radiometer; or:

$$k_2 \equiv \pi \tag{38}$$

With the dual channel correlation receiver the input signal is split by a hybrid combiner into two components as illustrated in Figure 4. Each component is separately amplified and receiver noise is added through a power summation process. The amplifier outputs are recombined in a second hybrid. The operation of the hybrid combiner is such that the signal components;

which are phase coherent with respect to themselves, will combine power wise. The result will be two outputs from the combiner as follows:

$$P_1 = \frac{V_A^2}{2}\left[G_1 + 2\sqrt{G_1 G_2} + G_2\right] + \frac{V_R^2}{2}\left[G_1 - 2\sqrt{G_1 G_2} + G_2\right] + \frac{V_N^2}{2}\left(G_1^2 + G_2^2\right)^{\frac{1}{2}} \quad (39)$$

$$P_2 = \frac{V_A^2}{2}\left[G_1 - 2\sqrt{G_1 G_2} + G_2\right] + \frac{V_R^2}{2}\left[G_1 + 2\sqrt{G_1 G_2} + G_2\right] + \frac{V_N^2}{2}\left(G_1^2 + G_2\right)^{\frac{1}{2}} \quad (40)$$

These two signals which are considered to be normally distributed about their mean values, are applied to oppositely polarized square-law detectors to obtain a mean or d.c. voltage output equal to:

$$\ell_{dc} \equiv P_1 - P_2 \sim 2\left|V_A^2 - V_R^2\right|\left|G_1 G_2\right|^{1/2} \quad (41)$$

The detected noise voltages will sum in a rms manner giving:

$$\ell_{ac} \equiv \frac{V_N^2}{2}\left(G_1^2 + G_2^2\right)^{1/2}$$

Considering V_A, V_R, and V_N to be randomly distributed, then the average or d.c. value of the square of a Gaussian amplitude distribution is equal to only $1/2\,\pi$ of the input signal's mean square value; and the noise output is one-half the input signal's mean square value. The mean value of the detected noise is zero, due to the use of oppositely polarized detectors, and consequently the factor of one-half resulting from application of the Central Limit Theorem to the averaging process of a distribution with a non-zero mean is not applicable here.

The resulting signal-to-noise ratio is:

$$\frac{S}{N} = \frac{(\ell_{dc}/2\pi)}{\ell_{ac}/2} = \frac{2\left(V_A^2 - V_R^2\right)}{\pi V_N^2}\left(\frac{G_1 G_2}{G_1^2 + G_2^2}\right)^{1/2} \quad (42)$$

Letting $G_2 = G_1 + \Delta G$ gives:

$$\frac{S}{N} = \frac{2}{\pi}\left[\frac{\left(1 + \frac{\Delta G}{G_1}\right)}{2 + \frac{2\Delta G}{G_1} + \left(\frac{\Delta G}{G_1}\right)^2}\right]^{1/2}\left(\frac{V_A^2 - V_R^2}{V_N^2}\right) \quad (43)$$

For $\Delta G \equiv 0$ this reduces to:

$$S/N = \frac{\sqrt{2}}{\pi}\left(\frac{V_A^2 - V_R^2}{V_N^2}\right) \tag{44}$$

The resultant calibration constant is now $\sqrt{2}$ times greater than the value for a total power radiometer; or:

$$K_3 = \frac{\pi}{\sqrt{2}} \tag{45}$$

The sensitivity equations for the three types of radiometers; assuming an ideal square output filter are now:

Total Power:

$$\Delta T_{MIN_1} \equiv \left[\frac{\pi^2}{8\beta\tau} + \left(\frac{\Delta G}{G_o}\right)^2_{AV}\right]^{1/2}\left(F + \frac{T_A}{T_o} - 1\right)T_o \tag{46}$$

Sampled Load: *

$$\Delta T_{MIN_2} \equiv \left[\left(\frac{\pi^2}{2\beta\tau}\right)\left(1 + \frac{T_A + T_R}{(F-1)T_o} + \frac{T_A^2 + T_R^2}{2(F-1)^2 T_o^2}\right)(F-1)^2 T_o^2 + M^{-2}(T_R - T_A)^2\right]^{1/2} \tag{47}$$

Correlation:

$$\Delta T_{MIN_3} = \left[\frac{\pi^2}{4\beta\tau} + \left(1 - \frac{\Delta G}{G_o}\right)^2_{AV}\Delta G^2\right]^{1/2}\left(1 + \frac{T_A + T_R}{(F-1)T_o} + \frac{T_A^2 + T_R^2}{2(F-1)^2 T_o^2}\right)^{1/2}(F-1)T_o \tag{48}$$

When the filter is not an ideal zonal filter the appropiate modification must be introduced to take into account the change in the definition of τ.

---

* The constant term $\frac{\pi^2}{2}$ is for the case where a bandpass filter is used to select the fundamental component of the square-wave switching signal. If the filter is not used the value of the constant term would be 4; however there are some practical considerations; involving the maximum gain bandwidth product that can be achieved without overloading the synchronous detector on amplifier noise, that dictate against the use of a square-wave -- square wave comparison.

SUMMARY AND CONCLUSIONS

Ignoring gain instabilities the "total power" radiometer is the most sensitive configuration. However, for systems using a large degree of post detection averaging the gain stability rather than receiver noise limits the detection sensitivity.

Both the "sampled load", and the "correlation" radiometer configurations solve the problem of gain stability at a small loss in noise sensitivity. The "correlation" radiometer suffers the least loss in noise sensitivity, but; until recently has been considered more complex in construction. The relative merits (merit is defined as the ratio of the system sensitivity to the sensitivity achieved with a total power system) of three types discussed are summarized in tabular form below:

Type	Noise Sens.*	Gain Stability	Merit $(T_A \equiv T_{REF})$
Total Power	$\left(\frac{\pi}{2\sqrt{2\beta\tau}}\right)\left(F+\frac{T_A}{T_o}-1\right)T_o$	$\left(\frac{\Delta G}{G_o}\right)_{AV}\left(F+\frac{T_A}{T_o}-1\right)T_o$	1
Correlation	$\left(\frac{\pi}{2\sqrt{\beta\tau}}\right)\left(F+\frac{T_A}{T_o}-1\right)T_o$	$\left(1-\frac{\Delta G}{G_o}\right)_{AV}\Delta G_{DET}\left(F+\frac{T_A}{T_o}-1\right)T_o$	$\frac{\left[1+\left(\frac{8\beta\tau}{\pi^2}\right)\left(\frac{\Delta G}{G_o}\right)_{AV}^2\right]^{\frac{1}{2}}}{\sqrt{2}\left[1+\left(\frac{4\beta\tau}{\pi^2}\right)\left(1-\frac{\Delta G}{G_o}\right)_{AV}^2\Delta G_{DET}^2\right]}$
Sample Load	$\left(\frac{\pi}{\sqrt{2\beta\tau}}\right)\left(F+\frac{T_A}{T_o}-1\right)T_o$	$\pi\left(\frac{G(t)}{G_o}-1\right)_{AV}\left(T_{REF}-T_A\right)$ $= 0$ FOR $T_{REF}=T_A$	$\frac{\left[1+\left(\frac{8\beta\tau}{\pi^2}\right)\left(\frac{\Delta G}{G_o}\right)_{AV}^2\right]^{\frac{1}{2}}}{2}$

*Assuming an ideal zonal filter for the post detection processing.

APPENDIX G

RECEIVER BANDWIDTH AND INTEGRATION TRADE OFF

Receiver Bandwidth

The receiver performance can be described in terms of the figure-of-merit.

$$M_R = \frac{k_R \sqrt{B}}{F}$$

Where B = Receiver bandwidth

F = Receiver noise figure

k_R = Receiver constant dependent upon receiver class; i.e., total power, correlation, or switched load.

This criteria is complicated by the fact that the noise figure will, in general, increase with increasing bandwidth, although the exact relationship is not simply described. Further, the factors which determine the noise figure are a function of the receiver type used.

That is, radiometers may be classified according to receiver type as:

1) Crystal video
2) Tuned radio frequency
3) Superheterodyne

With a crystal video the input power is applied directly to the detector element without prior amplification. Since a crystal detector is a non-linear device, it is strictly speaking, improper to define a noise figure for it. Instead a minimum detectable signal is given as:

$$\Delta T_{i\,(MIN)} = \frac{2}{M B_i T_o} \sqrt{\frac{2 T_o B_V}{K}} = \frac{2}{M B_i T_o} \sqrt{\frac{T_o}{2 K T}}$$

Where

K = Boltzmann's constant

$T_o = 290^\circ K$

B_i = The input bandwidth

$B_V = \frac{1}{4T}$ = The bandwidth of the post-detection filter

T = The effective time constant of the output filter (ideal zonal filter assumed)

$M = \frac{\rho R}{\sqrt{R+R_A}}$ = Crystal figure-of-merit

ρ = Crystal current sensitivity in milli-amperes per milli-watt

R = Video resistance of the crystal

R_A = Equivalent noise resistance of the amplifier normally taken equal to 1200 ohms

Evaluating for equivalent time constant systems the radiometer figure-of-merit may be written as the reciprocal of $\Delta T_{i(MIN)} \sqrt{\tau}$; or:

$$M_R' = M\beta_i \sqrt{\frac{KT_o}{2}} \approx 4.5 \times 10^{-11} M\beta_i$$

In this case we note that sensitivity improves directly with increasing RF bandwidth, however, because of the small value of the constant term the sensitivity of the crystal video is several orders of magnitude poorer than that of the other types.

With the tuned radio frequency receiver the noise figure is determined by the amplifier type used; i.e., parametric, maser, tunnel diode, traveling wave tube, or transistor. Tuned radio frequency receivers tend to have the highest values of M_r for operation below approximately 35 GHz with the value of F decreasing with decreasing frequency to about 1 GHz, and the percentage bandwidth (ratio of bandwidth to operating frequency) increasing over the same frequency range. The overall effect is that M_r increases with decreasing frequency over this range. Below approximately 1 GHz the amplifier noise figure decreases with decreasing bandwidth at a rate which holds M_r fairly constant as a function of bandwidth.

For high sensitivity radiometry above approximately 35 GHz the superheterodyne approach is most often used. This results as a consequence of the lack of availability of low noise amplifiers that operate directly at these higher frequencies.

The noise figure of a receiver using a crystal mixer is:

$$F = L_c \quad (F_a + N_k - 1)$$

Where

L_c = Crystal conversion loss

F_a = Intermediate frequency amplifier noise figure

N_k = Noise ratio of crystal with a standard termination

Because of the previously noted tendancy of amplifier noise figure to increase with increasing frequency the use of a narrow band IF, $\beta \leq 100$ MHz, would allow the use of lower noise figure IF amplifiers. A further consideration in the use of narrow band systems is the use of double sideband operation. The mixer in the double sideband system has its crystal matched to both the upper and lower sideband frequencies of the input resulting in a 3 db improvement in effective noise figure.

The overall conclusion is that despite the fact that the equation for the radiometer figure-of-merit show a desirability for wide bandwidth systems, the availablility of amplifiers with lower noise figures at lower operating frequencies, and because of the basic limitations on the maximum fractional bandwidths obtainable from real amplifiers it is still possible to obtain the best sensitivities at frequencies above approximately 35 GHz with relatively narrow band systems.

Resolution in frequency also has additional advantages associated with interference rejection and introduces the possibility of using the instrument for obtaining temperature profiles of the atmosphere as well as in vertical sensing applications.

Servo Time Constant Requirements

The vehicle's orientation relative to the local coordinate frame of reference is constantly changing. The rates at which the changes are taking place defines the tracking bandwidth requirements of the servo. The tracking bandwidth of a servo is most conveniently defined in terms of an equivalent low pass filter configuration which is further characterized by a time constant associated with the impulse response. With a servo loop the equivalent time constant is defined in terms of the loop error coefficients as follows:

Type O $$\tau \equiv \frac{\tau_o}{K_p + 1}$$

Where K_p = Placement error coefficient

τ_o = Open loop amplifier time constant

τ = Closed loop servo time constant

Type I $$\tau \equiv \frac{1}{K_V}$$

Where

K_V = Velocity error coefficient

Type II $$\tau \equiv \sqrt{\frac{1}{K_A}}$$

Where

K_A = Acceleration error coefficient

A simple position following servo (Type O) requires a placement error to provide tracking inputs and has a closed loop bandwidth characteristic similar to that of a single stage R C filter.

A zero-position-error servo system (Type I) has a theoretical null for a fixed target position but requires an error to provide tracking inputs for a constant antenna velocity or for an antenna acceleration when tracking moving targets. The closed loop bandwidth characteristic is also similar to that of a single stage R.C. filter. A zero-velocity error servo (Type II) has a theoretical null for both fixed target position and constant velocity targets, but requires an error for acceleration inputs. It's closed loop bandwidth when properly damped can be made to approach the characteristics of rectangular filter.

The tracking errors, called servo-lag errors, are directly related to the position, velocity and acceleration inputs divided by the position, velocity or acceleration error coefficient for a specific design.

The error coefficients are classically defined by the final value theorem of servo-mechanisms as:

$$K_p = \lim E_{(s)}$$
$$K_V = \lim SE_{(s)}$$
$$K_a = \lim S^2 E_{(s)}$$

where:

K_p = position error coefficient

K_V = velocity error coefficient

K_a = acceleration error coefficient

S = Laplace operator

$E_{(S)}$ = the Laplace transform of the tracking loop error function.

With the classical definitions only one constant is significant for a given type system. A more general definition commonly used is obtained by defining all the error constants in terms of the low-frequency behavior of the error vs input function expanded in a Maclaurin series in s; eg, $\frac{E_{(S)}}{\theta_{i\,(S)}} = \frac{1}{1+K_p} + \frac{S}{K_V} + \frac{S^2}{K_a} \cdots$

With this definition the value of any constant is not forced to zero whenever the preceding constant is non-zero and finite. The general definitions give the same values for all steadystate error constants up to and including the one which is non-zero and finite in the classical definition.

In order to estimate the tracking system performance, an integrating amplifier is assumed at the output of the radiometer and a Type II servo model is approached. The position and velocity constants are now virtually infinite and the acceleration error is held within the bounds defined by the pull-in-range of the antenna's "S"-curve characteristic. For example, let $H_{(s)}$ be the closed loop system transfer function which, in accordance with the usual equation for feedback systems, is obtained from the open loop function $K_a G_{(s)}$ as:

$$H_{(S)} = \frac{K_a G_{(S)}}{1 + K_a G_{(S)}}$$

where; $G_{(S)}$ is the frequency varying portion of the system transfer function.

The error integrating amplifier followed by the servo motor, also a perfect integrator, will have an uncompensated transfer function of the form:

$$K_1 G_{1\,(S)} = \frac{K_1}{S^2}$$

A simple RC lead-lag network is introduced to provide the closed loop stability needed. Thus:

$$K_2 G_{2\,(S)} = \left(\frac{1}{\alpha}\right)\left(\frac{\alpha T_2 S+1}{T_2 S+1}\right)$$

where α is the high-to-low frequency gain ratio and T_2 is the network time constant.

The gain ratio is selected to provide stability over the dynamic range that the acceleration error coefficient K_a may be expected to vary. K_a is, of course, a function of the antenna "S"-curve slope and thus of the input signal-to-noise ratio.

The overall servo transfer function is now:

$$K_a G_{(S)} = K_a \left[\frac{\alpha T_2 S+1}{S^2(T_2 S+1)}\right]$$

The Laplace transform of the antenna error as a function of the input signal takes the form:

$$\frac{E(S)}{\theta_{i\,(S)}} = \frac{1}{K_a G_{(S)}+1} = \frac{S^2(T_2 S+1)}{T_2 S^3 + S^2 + K_a \alpha T_2 S + K_a}$$

For a step-input of constant acceleration $\theta_{i(S)} = \frac{a}{S^3}$ the error function transform is:

$$E_{(S)} = a\,\frac{T_S S+1}{S\left[T_S^3 + S^2 + K_a \alpha T S + K_a\right]}$$

where "a" is the applied step of input angular acceleration. It is apparent that the acceleration input and the steady-state error will approach zero for both velocity and position input changes.

The overall response, including the transients for position, velocity and acceleration inputs, is a function of the design parameters K_a, α, and T_2. The peak transient error due to any combination of inputs resulting from normal spacecraft maneuvers must of course be kept to a value less than plus or minus the half-power beam angle of the antenna to maintain lock. The maximum value of K_a is set by the bandwidth restrictions imposed by the equivalent noise bandwidth requirements of the radiometer. The tracking bandwidth has previously been defined in terms of a loop bandwidth given by:

$$\omega_l \equiv \sqrt{K_A}$$

or,

$$f_l = \sqrt{K_A}\,/\,2\pi$$

The bandpass response of a type II loop approaches that of a square filter, and the noise bandwidth is thus:

$$\omega_n \approx 2\sqrt{K_A}$$

or,

$$f_n \approx \frac{\sqrt{K_A}}{\pi}$$

The minimum time-on-target for maximum response is approximately equal to 2τ or:

$$t_o = \frac{2}{\sqrt{K_a}}$$

where t_o is the minimum time required for the target to move one beamwidth and still obtain maximum response.

The maximum input accelerations are in the order of:

$$a_{MAX} = |\theta_A| K_a \approx \left|\frac{\lambda}{D}\right| K_a$$

in the units of radians/sec^2.

The input velocities may vary over the range of 2π radians per orbit period to a maximum value given by:

$$N_{(MAX)} = \text{accuracy} \times \sqrt{K_a}$$

where the accuracy is a function of the antenna beam angle, input signal-to-noise ratio, and the servo integration time constant; i.e.

$$\text{accuracy} \sim \frac{\theta_A}{\left(\frac{S}{N}\right)(K_A)}^{1/4}$$

For a spinning antenna, the spin velocity could be the determining factor in the selection of the beam angle used.

The specified accuracy is considered to set the limit on the allowable transient error measured over the time interval 2τ. The maximum allowable input velocity can be increased if the accuracy is specified in terms of additional smoothing of the tracking data. For example, a 20 second run would allow the accuracy for a one second time constant system to be increased to one arc minute with a corresponding increase in the maximum velocity input that can be handled.

Alternately both the maximum acceleration and maximum velocity inputs can be

increased by increasing K_a; i.e., reducing the effective integration time. The minimum integration time is; of course, set by the radiometer sensitivity limitations. The radiometer requirement can be expressed in terms of the previously defined figure-of-merit.

$$M_R = \frac{k_v \sqrt{\beta}}{F}$$

The servo time constant can be reduced to the extend M^2_R can be increased. Unfortunately F is a function of B and the amplifier used. One cannot arbitrarily increase M_R to allow operation with a faster time constant system.

Further; as has been previously noted, limitations on bandwidth are also imposed by the radiation characteristics of the atmospheric oxygen.

Taking the above considerations into account it is estimated that within the forseeable future the maximum reasonable value of K_a would be in the order of 400, resulting in a minimum time constant in the order of 50 milliseconds. Using existing receivers the maximum value of K_a would be more nearly in the order of unity.

Gyro-stabilization of the tracking line or computer aid to track can also be used to take out vehicle motion with respect to the stabilization frame. This will reduce the input motion to the tracking framework to it's minimum value and thus allow the use of a long time constant tracking loop. The gimbal system would, of course, have to follow the stabilization rates of the faster time constant gyro controlled loop. The advantage of the external stabilization approach is that the components needed to instrument it to the desired accuracy are available now. The disadvantages are with respect to the increased size and power consumption associated with the stabilization sub-system.

APPENDIX H

THE SPACE ENVIRONMENT

GENERAL:

In general, problems with electronic and electro-mechanical parts are associated with the lack of gravity, vacuum (lack of atmosphere), thermal gradients, radiation and magnetic fields.

Actually, no specific altitude boundary divides the earth's atmosphere and space in terms of the decreasing atmospheric density experienced with increasing altitude. The transition region is usually considered to start at an altitude of approximately 150 to 160 km. At this level, the density is approximately 1.5×10^{-12} gms/cm^3 with a pressure of approximately 10^{-6} torr. Under these conditions, the effects of a vacuum are not noticeable. However, outgassing and sublimation are accelerated, but the oxides and other chemically adhered films which are inadvertently removed are replaced in a few seconds.

The pressure region of 10^{-10} torr is reached at an altitude of 1000 km, whereupon true vacuum characteristics exist. Outgassing and sublimation are near the maximum, and oxide layers no longer reform. All heat transfer must be conductive (convective heat transfer does not exist) and heat is lost through radiation.

In an unmanned vehicle, the environment is attenuated in most respects because:

(1) The heat shields reflect the energy of the electromagnetic spectrum or radiate excess heat energy.

(2) The solar cells absorb and convert the sun's energy.

(3) The vehicle spins about its own axis with more or less constant temperature gradients.

(4) The skin, housing, and other external materials of the vehicle attenuate and convert penetrating particle and electromagnetic radiation.

In a manned spacecraft, the situation is similar with the exception of the cabin area. The cabin area is usually pressurized to about 5psi , a condition that allows volatile materials, such as water, to evaporate easily. Consequently, the atmosphere of the cabin is relatively humid, and could conceivably contain oils and other contaminants ready to condense on any cool surface. Such an atmosphere can increase corrosion, cause condensation shorts, and cause condensation of non-conductive contaminants on contacts which result in opens.

The individual characteristics of the space environment are summarized as follows:

Gravity:

The reduction of gravity itself is not a detriment to most electronic, electromechanical, and electromagnetic parts; however, this absence could seriously affect mechanical parts such as bearings, connectors, couplings, and supports, which can no longer depend on gravity as a retaining/holding force. Pre-loaded bearings, etc., are utilized to insure application of appropriate retaining forces on the affected devices.

Vacuum:

The vacuum of space causes outgassing (evaporation of contaminants from surfaces and pores of materials) and sublimation (passing directly from the solid to the gaseous state, and again condensing to the solid form, without liquefying). The problems due to evaporation of coatings and lubricants are twofold. First, the evaporating material may condense upon other portions of the spacecraft, such as optical equipment, switching contacts, solar panels, and temperature control surfaces. Second, the surfaces may be left clean. Once the surfaces become clean or wiped clean by abrasion, no oxides or other commonly found atmosphere-dependent contaminants will form.

As bearing surfaces become clean, friction and wear increase markedly. As the friction coefficients increase, the materials weld together. Success of bearings in space thus depends upon proper design of the bearing for the load and application, and a lubricant- sealing combination which will guarantee adequate lubrication of the bearing.

Ball Brothers Research Corporation has developed standardized processes to lubricate DC torque motors, tachometers, slip rings and bearings for space and vacuum applications. Vac Kote is the generic name for the vacuum lubrication systems developed. Many Vac Kote protected devices can perform fully exposed in space for at least five years. This or a similar lubricant is used where applicable.

Thermal:

The main source of radiant heat at the satellite is the sun. The electromagnetic spectrum of the sun represents a black body at 5800°K. The dark side of a satellite (unless looking at the earth) faces a 3°K black body. Heat loss through radiation in the direction of the sun is extremely difficult; but, the satellite can lose a great deal of its energy by radiation through its dark side.

When facing the earth, the satellite sees the earth's albedo, which is approximately equal to a black body of 288°K.

If the satellite is not spinning nor able to convert energy, extreme temperature gradients would be created between the light and dark side. The thermal gradient depends upon thermal conductivity, absorption coefficient, spin, orbit, and size.

With the specific antenna design being considered here, the aperture will be facing towards the earth and its back-side will see the radiation from the earth facing side of the satellite , or the satellite will be spinning. Extreme temperature gradients are not expected.

Radiation:

From a knowledge of the time and position of an object in the solar system (velocity/acceleration and distance from the sun, proximity to the planets, etc.) and of solar activities at these times, nuclear radiation may be estimated and integrated over time to determine total doses within the spectrum of space radiation. In addition, for an earth orbit, doses from various radiation belts, thermal belts, and meteorite fluxes can also be estimated. Model environments based on collating the measurements of many experiments have been published in NASA SP 3024.

The problem of determining the total dose experienced is somewhat complicated

because the radiation is normally expressed in so many different units. However, comparisons can be made by measuring the energy absorbed in a given material when subjected to a specified radiation and then comparing the energy absorbed by the same material subjected to a different radiation. Such an experiment permits a comparison and prediction of the relative damage to various materials under the same irradiation exposure. Similarly, comparisons can be made when the same material is subjected to a combination of radiation exposures. In other words, if carbon is placed in given radiation fields, absorption can be measured and compared because a radiation field may be described by the amount of energy absorbed in a given material. An absorbed dose can be converted to ergs/gm, which is followed by a symbol for the material which absorbs that energy. The comparisons (conversions) in Table H-1 are given in ergs/gm(c), where (c) represents carbon.

TABLE H-1

Comparison of Units for Measuring Radiation Dose

Dose and Dose Rate	Equivalent
RAD	100 ERGS/gm
EV/g	1.6×10^{-12} ERGS/gm(c)
Mev/cm^2	4.5×10^{-8} ERGS/gm(c)
Roentgen (R)	87.7 ERGS/gm(c)
Photons/cm^2	4.5×10^{-8} ERGS/gm(c)
Protons/cm^2	2.5×10^{7} ERGS/gm (most materials)
Electrons/cm^2	5×10^{-6} ERGS/gm (most materials)
RAD/HR	8.3×10^{4} η/cm^2 - sec (ηV)
ηV_o	4.2×10^{-6} RAD/HR

(RADC-TR-67-108)

The possible gross radiation effects which can be expected during long exposure of certain electronic, electromechanical, and mechanical parts in space is summarized in Tables H-2 & H-3. The thresholds for nuclear radiation effects are relatively high compared to those for normal space radiation. Consequently, most parts would have a long lifetime in space. However, if parts were operated in the Van Allen, or in the Artificial Radiation Belts, radiation thresholds could be exceeded in a comparatively short time.

The low-energy electrons of the solar wind may produce the greatest damage because these electrons represent the largest part of the energy flux. However, little testing on parts or materials at these low energies has been performed. It is known that low energy electrons and protons with large fluxes will give ultra clean surfaces, without even a mono layer or oxides. However, the effects of such surfaces exposed for long periods at pressures of 10^{-12} torr, or less, and to low energy electrons with high fluxes are unknown. It is presumed that the electrons may have additional scouring effects on the surface, may anneal the surfaces and may remove some mono layers of materials exposed to them.

With respect to the particular problem at hand, it is noted that the semi-conductor diodes and transistors exhibit the lowest threshold levels, and therefore, without a proper protective shield, we would expect rather rapid damage to the receiver and control circuitry. Fortunately, most x-ray and low energy radiation sources are relatively easy to shield to prevent damage to electronic equipment. The density and absorption properties of various materials used for shielding are shown in Table H-4. The effects of the shielding are calculated as follows.

Whenever radiation traverses a thin layer of substance it is reduced in intensity by a constant fraction μ per centimeter of the substance traversed. The intensity of the radiation, after penetrating to a depth x, can be expressed by an equation of the form:

$$I = I_o \ EXP \ (-\mu x)$$

(Handbook of Chemistry and Physics)

TABLE H-2

Possible Gross Space Radiation Effects on

Specific Electronic and Electromechanical Parts

PART	EFFECT	APPROXIMATE THRESHOLD (ERGS/g) **
Antennae	Surfaces cleaned and annealed, possible crystal growth, impurities migrated.	See Materials Table
Capacitors	Capacitance changed, dissipation factor and leakage increased.	10^7 - 10^9
Coaxial connectors	Conductivity and leakage increased.	
Coaxial relays	Conductivity and leakage increased.	
Couplers, directional	V.S.W.R. and insertion loss changed.	
Diodes		
Switching	Highly susceptible to radiation, leakage current increased, minority carriers degraded.	10^2 - 10^3
Varactor	Leakage current increased, minority carriers degraded.	10^2 - 10^4
Zener	Leakage current increased, minority carriers degraded.	10^2
Filters	(See information for constituent parts.)	
Inductors	Possible insulation damaged, remanence and permeability reduced, coercive force increased.	
Junction boxes	Conductivity increased (ceramic insulator assumed).	See Materials Table
Mixers	(Same effects as for semiconductors.)	
Resistors		
Composition	Possible resistivity changed, probably negative (resistance increased).	10^6 - 10^7
Film	Similar to aging, resistivity changed, probably positive (resistance reduced).	10^8 - 10^9
Wire-wound	Possible insulation damaged.	10^5 - 10^{10} ***
Solder Joints	Possible whisker growth and crystalization.	
Transformers	Possible insulation damaged, remanence and permeability reduced, coercive forces increased.	See Materials Table
Transistors	Leakage current induced, gain decreased.	10^2 - 10^3
Traveling-wave tubes	Possible detuning and seal degradation.	10^6
Solar cells	Transmissivity of cover glass changed, available power reduced, spectual response changed, adhesive damaged.	10^2

TABLE H-2

PART	EFFECT	APPROXIMATE THRESHOLD (ERGS/g) **
Mechanical components	Film layers including oxides removed, possible cold -welding if under pressure, some diffusion of metal to metal where intimate contact exists, surface annealed, possible crystal growth, some migration of impurities in parent metals, possible hydrogen embrittlement. *	See Materials Table

* Note: Molecular hydrogen is generated as a product of radiation when protons and electrons (primary or secondary) combine on a surface after losing their radiation energy.

** Not necessarily the threshold for noticeable electrical effects.

***Depends on Bobbin Material

(RADC-TR-67-108)

TABLE H-3

RADIATION DAMAGE EFFECTS AND THRESHOLDS FOR MATERIALS

Material	Effect	Approximate Threshold*** (ergs/g)
Insulators and Dielectric Materials	Primarily mechanical properties changed; outgassing occured, causing subsequent rupture and possible chemical deterioration.	
Kraft paper		10^9
Fluorocarbon		
FEB		10^8
TFE		10^7
PTFE Glass		10^7
Epoxy Resin, Silica Filled		10^8
Polyester		
Cross-linked		10^{10}
Isocyanage Modified		10^9
Terephthalate Modified		10^{10}
Alkyd		10^{10}
Polyethylene		10^8
Polyethylene Terephthalate		10^9
Polyurethane		10^{10}
Polyvinyl Formal		10^8
Polyvinyl Chloride Composition		10^8
Resin Glass		
Silicone		10^{11}
Epoxy		10^8
Isocyanate		10^{10}
Silicone Enamel		10^9
Silicone Rubber		10^9
Silicone Resin-Mica Paper		10^{11}

TABLE H-3

RADIATION DAMAGE EFFECTS AND THRESHOLDS FOR MATERIALS (Continued)

Material	Effect	Approximate Threshold*** (ergs/g)
Epoxy Lead Filled		10^8
Force Ceramic		10^{13}
Fused Glass		10^7
Quartz		10^7
Alumina		10^{11}
Mica		10^{10}
Barium Oxide		10^{11}
Steatite		10^{10}
Boron Nitride		10^8
Spinel		10^{10}
Silicon Carbide		10^{11}
Porcelain		10^{11}
Fosterite		10^{11}
Metallic Materials	Surfaces and bulks annealed under extremely high doses.	
Permanent Magnets		
Alinco 2, 5, 12	Remanence reduced.	10^{13}
Cunico	Remanence reduced.	10^{13}
Conife	Remanence reduced.	10^{12}
Cr steel	Remanence reduced.	10^{12}
Co steel	Remanence reduced.	10^{12}
Ba ferrites	Remanence reduced.	10^{12}
Silamanel	Remanence reduced.	10^{12}
Pf Co	Remanence reduced.	10^{12}
ESD iron	Remanence reduced.	10^{12}
Soft Magnet ferrites		
Garnets	Remanence, permeability and coercive force reduced.	10^7
Spinels	Remanence, permeability and coercive force reduced.	10^7

TABLE H-3

RADIATION DAMAGE EFFECTS AND THRESHOLDS FOR MATERIALS (Continued)

Material	Effect	Approximate Threshold*** (ergs/g)
Soft Metals and Alloys		
Fe	Remanence, permeability and coercive force reduced.	10^{12}
Si-Fe	Remanence, permeability and coercive force reduced.	10^{12}
Al-Fe	Remanence, permeability and coercive force reduced.	10^{12}
Co-Fe	Remanence, permeability and coercive force reduced.	10^{12}
Numetal, 4-79 Mo	Remanence, permeability and coercive force reduced.	10^{10}
Permalloy, 5-79 Mo	Remanence, permeability and coercive force reduced.	10^{10}
Permalloy: Binary	Remanence, permeability and coercive force reduced.	10^{10}
Permalloy: Ni Fe	Remanence, permeability and coercive force reduced.	10^{12}
15 Ni Fe	Remanence, permeability and coercive force reduced.	10^{12}
Fe 5-80 Mo	Remanence and permeability reduced; coercive force unchanged.	10^{10}
Permalloy	Remanence and permeability reduced; coercive force unchanged.	10^{10}
Miscellaneous Materials		
Optical	Transmission reduced.	
Purified, Fused Silica		10^{7}
Dense Flint - Unprotected		10^{5}
Dense Flint - Protected		10^{7}
Borosilicate Crown - Protected		10^{7}
Vycor - Unprotected		10^{4}
Vycor - Protected		10^{5}
Quartz		10^{6}
Envelope Glass of Type 1723 Electron Tube		10^{5}

TABLE H-4

Density and Absorption for Various Materials

Material	Density g/cm^3	Relative Absorption
Aluminum	2.7	1
FPH with 12-4H Catalyst	0.07	0.8
Book Material, 1090S1	0.72	1.0
Lead	11.3	1.5
Copper	8.9	1.2
Indium	7.3	1.4

(information supplied by ERC)

where,

I_o = The intensity at the surface.

μ = Linear absorption coefficient in units of reciprocal distance.

The linear absorption coefficient divided by the density is called the mass absorption coefficient and represent the fraction of a beam 1 cm^2 cross section absorbed per gram of substance traversed, if the symbol ρ is used for the density of the shield material, then the equation for the dose transmission factor can be written in the form:

$$\frac{I}{I_o} = EXP\left[-\mu_M \rho X\right]$$

where,

$$\mu_M = \frac{\mu}{\rho}$$

The shield thickness

$$X_o = \left(\frac{1}{\rho \mu_M}\right) ln\left(\frac{I_o}{I_T}\right)$$

where,

$$= \frac{2.3026}{\rho \mu_M} log_{10}\left(\frac{I_o}{I_T}\right)$$

I_o = incident radiation in ergs/g

I_T = threshold level in ergs/g

ρ = density of the shield material in g/cm^3

μ_M = the mass absorption coeffiecient in cm^2/g

It is noted that the distance the radiation will penetrate a given material is a function of both the mass of the material per unit volume, and the kinetic energy of the radiation. In general the absorption coefficients will decrease with increasing energy passing through a minumum , after which they will increase with increasing energy. This characteristic complicates the statement of a general shielding requirement in that μ_m will for any given material vary over a broad range of values as a function of the radiation level.

Because of the proportionality of the absorption coefficient for a given kinetic energy to the density of a material the relative densities between materials at any energy level can be defined in terms of their relative absorption as:

$\rho_1 = \rho_o x$ relative absorption

Usually aluminum is used as the reference when defining the shielding requirements for electronic equipment; and a value of unity is assigned to its relative absorption.

The shielding requirement in g/cm^2 is now defined in terms of the product:

$$x_0 \rho_0 = \left(\frac{1}{\mu_{M_0}}\right) \ln \left(\frac{I_0}{I_T}\right)$$

$$= \frac{2.3026}{\mu_{M_0}} \log_{10} \left(\frac{I_0}{I_T}\right)$$

where:

x_0 = 1 cm

ρ_0 = density of aluminum

μ_{M_0} = mass absorption coefficient for aluminum in cm^2/g at the specific energy level for which the shielding is being provided

I_0 = incident radiation

I_T = threshold level

The expression for the thickness of an arbitrary shielding material now is conviently stated as:

$$x = \frac{\text{shielding } (g/cm^2)}{\text{density } (g/cm^3) \text{ relative absorption}} \quad (\text{dimensionless})$$

The specification of shielding in this way allows one to avoid the problem of defining the mass absorption coefficient in the specification. However, we are still faced with the necessity of defining a shielding requirement for a specific mission. This problem is beyond the scope of the present investigation, and requires a definition of the energy levels and doses to be experienced.

Magnetic Fields

Magnetic fields in space are generally of not great concern. Exceptions are:

(1) Plasma clouds which drift through space.

(2) The solar magnetic field which appears short distances from the sun, particularly during times of great solar activity. The chance of encountering plasma clouds

in interplanetary space is remote. On the other hand, the effects on solar probes (fly-bys) can be expected to be of increasing importance.

For the application under discussion here, no difficulties are expected from magnetic fields.

Shock and Vibration:

Conditions of shock and vibration are not applicable to space vehicles, except at launch as indicated in Tables 5 and 6.

TABLE H-5

ENVIRONMENTAL SERVICE CONDITIONS

Environment	Symbol	Assumptions
Satellite, Orbit	S_o	Assume laboratory zero conditions without access for maintenance.
Satellite, Launch	S_L	Assume severe conditions of noise, vibration, and other environments related to large typically inhabited systems being accelerated into orbit. These conditions may also be considered typical of satellite re-entry and landing by parachute.
Missile	M	Missile conditions may also apply to installations near main rocket engines during satellite launch.

(RADC - TR - 108)

TABLE H-6

Nominal Ranges of Environmental Stress Characteristics*

	Vibration		Noise (db)	Sand and Dust	Pressure	Relative Humidity (%)	Shock (g)	
	Frequency (cps)	Magnitude (g)					11 msec	.1/2 msec
S_0	0	0	0	0	10^{-8} mm Hg	0	0	0
S_L	10-3000	5-60	5-130	Negligible	760 - 10^{6} mm Hg	5-95	15-75	1500
M	10-3000	30-100	70-165	Minor	760 -10^{-6} mm Hg (Torr)	1-100	45-100	1500

*The percentage of time that the extremes of ranges might apply in the nominal or specific application is indeterminate.

(RADC-TR-67-108)

APPENDIX A-A

The following Tables contain the detail calculated patterns of the line source antennas discussed in Section 3.5 . Tables A-A-1 and A-A-2 are the elevation patterns for cosine and cosine squared distributions respectively. Table A-A-3 is the azimuth plane pattern for the 1-2-1 binary array and horn combination.

TABLE A-A-1

ELEVATION PATTERN -- COSINE DISTRIBUTION

ELEVATION PLANE PATTERN

ANTENNA LENGTH= 16.774 CM FREQUENCY= 60.80 GHZ

ILLUMINATION FUNCTION--COSINE

PHI IN DEGREES	E(PHI)	DB
0.00	1.0000	-.00
.20	.9869	.11
.40	.9484	.46
.60	.8865	1.05
.80	.8050	1.88
1.00	.7081	3.00
1.20	.6012	4.42
1.40	.4897	6.20
1.60	.3792	8.42
1.80	.2745	11.23
2.00	.1800	14.90
2.20	.0989	20.09
2.40	.0335	29.51
2.60	-.0155	36.19
2.80	-.0482	26.34
3.00	-.0659	23.62
3.20	-.0708	23.00
3.40	-.0654	23.68
3.60	-.0529	25.52
3.80	-.0363	28.81
4.00	-.0183	34.76
4.20	-.0014	57.38
4.40	.0127	37.92
4.60	.0227	32.87
4.80	.0282	31.01
5.00	.0291	30.72
5.20	.0262	31.64
5.40	.0203	33.85
5.60	.0126	37.98
5.80	.0044	47.21
6.00	-.0034	49.43
6.20	-.0097	40.27
6.40	-.0140	37.09
6.60	-.0159	35.95
6.80	-.0156	36.12
7.00	-.0133	37.51
7.20	-.0095	40.41
7.40	-.0049	46.15
7.60	-.0002	76.27
7.80	.0042	47.63
8.00	.0075	42.50
8.20	.0096	40.39
8.40	.0102	39.84
8.60	.0094	40.51
8.80	.0075	42.46
9.00	.0048	46.33
9.20	.0017	55.26
9.40	-.0013	57.47
9.60	-.0040	48.01
9.80	-.0059	44.60
10.00	-.0069	43.23

TABLE A-A-1 continued

ELEVATION PATTERN -- COSINE DISTRIBUTION

ELEVATION PLANE PATTERN

ANTENNA LENGTH= 16.774 CM FREQUENCY= 60.80 GHZ

ILLUMINATION FUNCTION--COSINE

PHI IN DEGREES	E(PHI)	DB
10.00	-.0069	43.23
10.50	-.0054	45.41
11.00	-.0003	71.99
11.50	.0042	47.56
12.00	.0049	46.17
12.50	.0020	53.97
13.00	-.0019	54.35
13.50	-.0039	48.17
14.00	-.0028	50.97
14.50	.0001	77.87
15.00	.0026	51.66
15.50	.0029	50.66
16.00	.0011	58.93
16.50	-.0013	57.99
17.00	-.0025	52.07
17.50	-.0018	54.73
18.00	.0000	88.74
18.50	.0017	55.45
19.00	.0020	53.98
19.50	.0009	60.97
20.00	-.0007	62.85
20.50	-.0017	55.44
21.00	-.0014	56.98
21.50	-.0002	73.74
22.00	.0010	59.67
22.50	.0015	56.60
23.00	.0009	60.97
23.50	-.0002	72.51
24.00	-.0011	59.01
24.50	-.0012	58.41
25.00	-.0005	66.16
25.50	.0005	66.34
26.00	.0011	59.38
26.50	.0009	60.55
27.00	.0002	73.24
27.50	-.0006	64.58
28.00	-.0010	60.22
28.50	-.0007	62.73
29.00	-.0001	85.32
29.50	.0006	64.27
30.00	.0009	61.25

TABLE A-A-1 continued

ELEVATION PATTERN -- COSINE DISTRIBUTION

ELEVATION PLANE PATTERN

ANTENNA LENGTH= 16.774 CM FREQUENCY= 60.80 GHZ

ILLUMINATION FUNCTION--COSINE

PHI IN DEGREES	E(PHI)	DB
30.00	.0009	61.25
30.50	.0006	64.63
31.00	-.0000	92.86
31.50	-.0006	64.70
32.00	-.0008	62.27
32.50	-.0005	65.96
33.00	.0000	89.18
33.50	.0005	65.63
34.00	.0007	63.20
34.50	.0005	66.57
35.00	.0000	112.92
35.50	-.0004	67.11
36.00	-.0006	64.08
36.50	-.0005	66.56
37.00	-.0001	82.27
37.50	.0003	69.48
38.00	.0006	65.08
38.50	.0005	66.24
39.00	.0002	74.96
39.50	-.0002	73.86
40.00	-.0005	66.59
40.50	-.0005	66.06
41.00	-.0003	70.70
41.50	.0000	87.92
42.00	.0003	69.40
42.50	.0005	66.53
43.00	.0004	68.20
43.50	.0001	77.08
44.00	-.0002	75.99
44.50	-.0004	68.46
45.00	-.0004	67.34
45.50	-.0003	70.36
46.00	-.0001	84.44
46.50	.0002	74.09
47.00	.0004	68.70
47.50	.0004	68.18
48.00	.0003	71.53
48.50	.0000	86.53
49.00	-.0002	74.92
49.50	-.0003	69.54
50.00	-.0004	68.74

TABLE A-A-1 Continued

ELEVATION PATTERN -- COSINE DISTRIBUTION

ELEVATION PLANE PATTERN

ANTENNA LENGTH= 16.774 CM FREQUENCY= 60.80 GHZ

ILLUMINATION FUNCTION--COSINE

PHI IN DEGREES	E(PHI)	DB
50.00	-.0004	68.74
50.50	-.0003	71.33
51.00	-.0001	80.93
51.50	.0001	78.83
52.00	.0003	71.23
52.50	.0003	69.31
53.00	.0003	70.39
53.50	.0002	75.25
54.00	-.0000	110.79
54.50	-.0002	75.31
55.00	-.0003	70.87
55.50	-.0003	69.95
56.00	-.0003	71.57
56.50	-.0001	76.90
57.00	.0000	99.58
57.50	.0002	76.14
58.00	.0003	71.74
58.50	.0003	70.53
59.00	.0003	71.48
59.50	.0002	75.01
60.00	.0001	85.46
60.50	-.0001	82.16
61.00	-.0002	74.47
61.50	-.0003	71.73
62.00	-.0003	71.14
62.50	-.0002	72.27
63.00	-.0002	75.54
63.50	-.0001	83.84
64.00	.0000	86.77
64.50	.0001	76.78
65.00	.0002	73.23
65.50	.0003	71.84
66.00	.0003	71.86
66.50	.0002	73.19
67.00	.0002	76.21
67.50	.0001	82.78
68.00	-.0000	96.07
68.50	-.0001	80.07
69.00	-.0002	75.47
69.50	-.0002	73.27
70.00	-.0002	72.34

TABLE A-A-1 continued

ELEVATION PATTERN -- COSINE DISTRIBUTION

ELEVATION PLANE PATTERN

ANTENNA LENGTH= 16.774 CM FREQUENCY= 60.80 GHZ

ILLUMINATION FUNCTION--COSINE

PHI IN DEGREES	E(PHI)	DB
70.00	-.0002	72.34
70.50	-.0002	72.36
71.00	-.0002	73.23
71.50	-.0002	75.08
72.00	-.0001	78.36
72.50	-.0001	84.76
73.00	.0000	102.69
73.50	.0001	83.16
74.00	.0001	78.10
74.50	.0002	75.43
75.00	.0002	73.89
75.50	.0002	73.07
76.00	.0002	72.78
76.50	.0002	72.94
77.00	.0002	73.52
77.50	.0002	74.52
78.00	.0002	75.99
78.50	.0001	78.06
79.00	.0001	81.04
79.50	.0001	85.76
80.00	.0000	96.58
80.50	-.0000	93.85
81.00	-.0001	85.52
81.50	-.0001	81.65
82.00	-.0001	79.25
82.50	-.0001	77.60
83.00	-.0002	76.40
83.50	-.0002	75.52
84.00	-.0002	74.87
84.50	-.0002	74.38
85.00	-.0002	74.02
85.50	-.0002	73.77
86.00	-.0002	73.59
86.50	-.0002	73.46
87.00	-.0002	73.39
87.50	-.0002	73.34
88.00	-.0002	73.31
88.50	-.0002	73.30
89.00	-.0002	73.30
89.50	-.0002	73.30
90.00	-.0002	73.30

TABLE A-A-2

ELEVATION PLANE -- COSINE SQUARED DISTRIBUTION

ELEVATION PLANE PATTERN

ANTENNA LENGTH= 20.335 CM FREQUENCY= 60.80 GHZ

ILLUMINATION FUNCTION--COSINE SQUARED

PHI IN DEGREES	E(PHI)	DB
0.00	1.00000	.00
.20	.98672	.12
.40	.94774	.47
.60	.88552	1.06
.80	.80391	1.90
1.00	.70784	3.00
1.20	.60289	4.40
1.40	.49482	6.11
1.60	.38913	8.20
1.80	.29065	10.73
2.00	.20321	13.84
2.20	.12945	17.76
2.40	.07074	23.01
2.60	.02720	31.31
2.80	-.00215	53.36
3.00	-.01912	34.37
3.20	-.02611	31.66
3.40	-.02578	31.77
3.60	-.02078	33.65
3.80	-.01348	37.40
4.00	-.00584	44.67
4.20	.00075	62.53
4.40	.00545	45.28
4.60	.00794	42.00
4.80	.00836	41.55
5.00	.00714	42.93
5.20	.00486	46.26
5.40	.00218	53.24
5.60	-.00035	69.02
5.80	-.00231	52.71
6.00	-.00346	49.21
6.20	-.00376	48.50
6.40	-.00330	49.64
6.60	-.00231	52.74
6.80	-.00106	59.53
7.00	.00018	74.66
7.20	.00119	58.48
7.40	.00182	54.81
7.60	.00201	53.94
7.80	.00180	54.90
8.00	.00128	57.83
8.20	.00060	64.39
8.40	-.00010	80.34
8.60	-.00068	63.31
8.80	-.00107	59.45
9.00	-.00120	58.41
9.20	-.00109	59.21
9.40	-.00080	61.96
9.60	-.00039	68.19
9.80	.00004	87.23
10.00	.00042	67.58

TABLE A-A-2 continued

ELEVATION PLANE -- COSINE SQUARED DISTRIBUTION

ELEVATION PLANE PATTERN

ANTENNA LENGTH= 20.335 CM FREQUENCY= 60.80 GHZ

ILLUMINATION FUNCTION--COSINE SQUARED

PHI IN DEGREES	E(PHI)	DB
10.00	.00042	67.58
10.50	.00076	62.33
11.00	.00028	71.17
11.50	-.00037	68.73
12.00	-.00050	66.00
12.50	-.00011	78.94
13.00	.00030	70.35
13.50	.00034	69.48
14.00	.00003	90.35
14.50	-.00025	72.17
15.00	-.00023	72.79
15.50	.00001	99.84
16.00	.00020	74.07
16.50	.00016	75.92
17.00	-.00003	90.98
17.50	-.00016	75.98
18.00	-.00011	78.82
18.50	.00003	89.31
19.00	.00013	77.85
19.50	.00008	81.41
20.00	-.00003	89.44
20.50	-.00010	79.66
21.00	-.00007	83.63
21.50	.00003	90.49
22.00	.00009	81.39
22.50	.00005	85.41
23.00	-.00002	92.28
23.50	-.00007	83.05
24.00	-.00005	86.74
24.50	.00002	94.92
25.00	.00006	84.67
25.50	.00004	87.66
26.00	-.00001	99.02
26.50	-.00005	86.33
27.00	-.00004	88.29
27.50	.00000	107.30
28.00	.00004	88.15
28.50	.00004	88.76
29.00	.00000	112.04
29.50	-.00003	90.33
30.00	-.00003	89.25

TABLE A-A-2 continued

ELEVATION PLANE -- COSINE SQUARED DISTRIBUTION

ELEVATION PLANE PATTERN

ANTENNA LENGTH= 20.335 CM FREQUENCY= 60.80 GHZ

ILLUMINATION FUNCTION--COSINE SQUARED

PHI IN DEGREES	E(PHI)	DB
30.00	-.00003	89.25
30.50	-.00001	100.91
31.00	.00002	93.26
31.50	.00003	89.96
32.00	.00001	96.58
32.50	-.00001	97.87
33.00	-.00003	91.12
33.50	-.00002	94.26
34.00	.00000	108.59
34.50	.00002	93.12
35.00	.00002	93.19
35.50	.00000	106.15
36.00	-.00001	96.77
36.50	-.00002	93.30
37.00	-.00001	98.30
37.50	.00001	105.13
38.00	.00002	94.90
38.50	.00002	95.56
39.00	.00000	108.72
39.50	-.00001	99.15
40.00	-.00002	95.32
40.50	-.00001	99.03
41.00	.00000	114.40
41.50	.00001	97.79
42.00	.00001	96.62
42.50	.00001	103.09
43.00	-.00000	106.52
43.50	-.00001	97.86
44.00	-.00001	98.07
44.50	-.00000	106.68
45.00	.00001	105.13
45.50	.00001	98.51
46.00	.00001	99.19
46.50	.00000	108.21
47.00	-.00000	106.06
47.50	-.00001	99.47
48.00	-.00001	99.81
48.50	-.00000	107.09
49.00	.00000	109.43
49.50	.00001	100.87
50.00	.00001	100.11

TABLE A-A-2 continued

ELEVATION PLANE -- COSINE SQUARED DISTRIBUTION

ELEVATION PLANE PATTERN

ANTENNA LENGTH= 20.335 CM FREQUENCY= 60.80 GHZ

ILLUMINATION FUNCTION--COSINE SQUARED

PHI IN DEGREES	E(PHI)	DB
50.00	.00001	100.11
50.50	.00001	104.71
51.00	-.00000	121.41
51.50	-.00001	103.38
52.00	-.00001	100.65
52.50	-.00001	102.56
53.00	-.00000	112.41
53.50	.00000	109.25
54.00	.00001	102.44
54.50	.00001	101.59
55.00	.00001	104.91
55.50	.00000	120.77
56.00	-.00000	107.98
56.50	-.00001	102.89
57.00	-.00001	102.43
57.50	-.00001	105.64
58.00	-.00000	118.65
58.50	.00000	110.14
59.00	.00001	104.19
59.50	.00001	102.96
60.00	.00001	104.75
60.50	.00000	111.20
61.00	-.00000	120.36
61.50	-.00000	107.45
62.00	-.00001	104.14
62.50	-.00001	103.85
63.00	-.00000	106.10
63.50	-.00000	112.78
64.00	.00000	121.81
64.50	.00000	108.87
65.00	.00001	105.26
65.50	.00001	104.38
66.00	.00001	105.47
66.50	.00000	108.98
67.00	.00000	118.68
67.50	-.00000	117.39
68.00	-.00000	109.07
68.50	-.00000	106.04
69.00	-.00001	105.07
69.50	-.00001	105.59
70.00	-.00000	107.64

TABLE A-A-2 continued

ELEVATION PLANE -- COSINE SQUARED DISTRIBUTION

ELEVATION PLANE PATTERN

ANTENNA LENGTH= 20.335 CM FREQUENCY= 60.80 GHZ
ILLUMINATION FUNCTION--COSINE SQUARED

PHI IN DEGREES	E(PHI)	DB
70.00	-.00000	107.64
70.50	-.00000	112.07
71.00	-.00000	125.07
71.50	.00000	117.27
72.00	.00000	110.33
72.50	.00000	107.35
73.00	.00001	106.02
73.50	.00001	105.75
74.00	.00000	106.40
74.50	.00000	107.99
75.00	.00000	110.86
75.50	.00000	116.16
76.00	.00000	134.59
76.50	-.00000	118.91
77.00	-.00000	112.71
77.50	-.00000	109.64
78.00	-.00000	107.88
78.50	-.00000	106.89
79.00	-.00000	106.44
79.50	-.00000	106.42
80.00	-.00000	106.76
80.50	-.00000	107.44
81.00	-.00000	108.46
81.50	-.00000	109.83
82.00	-.00000	111.64
82.50	-.00000	114.01
83.00	-.00000	117.28
83.50	-.00000	122.34
84.00	-.00000	134.15
84.50	.00000	129.73
85.00	.00000	121.96
85.50	.00000	118.31
86.00	.00000	116.04
86.50	.00000	114.48
87.00	.00000	113.36
87.50	.00000	112.54
88.00	.00000	111.94
88.50	.00000	111.52
89.00	.00000	111.23
89.50	.00000	111.07
90.00	.00000	111.01

TABLE A-A-3

AZIMUTH PLANE -- 1-2-1 BINARY DISTRIBUTION

AZIMUTH PLANE PATTERN FOR A FLARED HORN ANTENNA
FED BY THREE PARALLEL LINE SOURCES

POWER RATIO= 1:2:1 FREQ= 60.80 GHZ WIDTH= 4.437 CM

THETA IN DEGREES	E(THETA)	DB
0	1.0000	.00
5	.3324	9.57
10	-.1017	19.85
15	.1352	17.38
20	-.0244	32.27
25	-.0659	23.63
30	.0364	28.77
35	-.0431	27.30
40	-.0354	29.02
45	.0464	26.67
50	.0274	31.24
55	-.0191	34.39
60	-.0080	41.92
65	.0266	31.50
70	.0402	27.92
75	.0312	30.12
80	.0158	36.03
85	.0047	46.62
90	.0009	61.37

TABLE A-A-3 continued

AZIMUTH PLANE -- 1-2-1 BINARY DISTRIBUTION

AZIMUTH PLANE PATTERN FOR A FLARED HORN ANTENNA
FED BY THREE PARALLEL LINE SOURCES

POWER RATIO= 1:2:1 FREQ= 60.80 GHZ WIDTH= 4.437 CM

THETA IN DEGREES	E(THETA)	DB
0	1.0000	.00
1	.9643	.32
2	.8622	1.29
3	.7082	3.00
4	.5235	5.62
5	.3324	9.57
6	.1585	16.00
7	.0207	33.70
8	-.0693	23.18
9	-.1084	19.30
10	-.1017	19.85
11	-.0612	24.27
12	-.0022	53.15
13	.0588	24.61
14	.1078	19.35
15	.1352	17.38
16	.1369	17.27
17	.1144	18.83
18	.0740	22.61
19	.0245	32.20
20	-.0244	32.27
21	-.0642	23.85
22	-.0890	21.01
23	-.0964	20.32
24	-.0874	21.17
25	-.0659	23.63
26	-.0374	28.55
27	-.0082	41.76
28	.0162	35.81
29	.0317	29.97
30	.0364	28.77

TABLE A-A-3 continued

AZIMUTH PLANE -- 1-2-1 BINARY DISTRIBUTION

AZIMUTH PLANE PATTERN FOR A FLARED HORN ANTENNA
FED BY THREE PARALLEL LINE SOURCES

POWER RATIO= 1:2:1 FREQ= 60.80 GHZ WIDTH= 4.437 CM

THETA IN DEGREES	E(THETA)	DB
30	.0364	28.77
31	.0305	30.30
32	.0161	35.87
33	-.0036	48.94
34	-.0246	32.19
35	-.0431	27.30
36	-.0563	025.00
37	-.0621	24.14
38	-.0600	24.44
39	-.0505	25.93
40	-.0354	29.02
41	-.0168	35.50
42	.0028	50.96
43	.0211	33.52
44	.0361	28.86
45	.0464	26.67
46	.0515	25.77
47	.0513	25.80
48	.0465	26.65
49	.0381	28.37
50	.0274	31.24
51	.0157	36.07
52	.0043	47.34
53	-.0058	44.75
54	-.0137	37.24
55	-.0191	34.39
56	-.0216	33.30
57	-.0214	33.38
58	-.0188	34.52
59	-.0141	36.99
60	-.0080	41.92

TABLE A - A - 3 continued

AZIMUTH PLANE -- 1-2-1 BINARY DISTRIBUTION

AZIMUTH PLANE PATTERN FOR A FLARED HORN ANTENNA
FED BY THREE PARALLEL LINE SOURCES

POWER RATIO= 1:2:1 FREQ= 60.80 GHZ WIDTH= 4.437 CM

THETA IN DEGREES	E(THETA)	DB
60	-.0080	41.92
61	-.0010	60.17
62	.0064	43.82
63	.0138	37.22
64	.0206	33.73
65	.0266	31.50
66	.0316	30.00
67	.0355	29.00
68	.0382	28.37
69	.0397	28.03
70	.0402	27.92
71	.0397	28.03
72	.0384	28.32
73	.0364	28.77
74	.0340	29.37
75	.0312	30.12
76	.0281	31.02
77	.0250	32.05
78	.0218	33.22
79	.0187	34.54
80	.0158	36.03
81	.0131	37.68
82	.0105	39.54
83	.0083	41.62
84	.0063	43.96
85	.0047	46.62
86	.0033	49.65
87	.0022	53.05
88	.0015	56.69
89	.0010	59.94
90	.0009	61.37

TABLE A-A-4

OFF - AXIS PATTERNS OF A RECTANGULAR APERTURE ANTENNA

CLS-4 RECTANGULAR APERTURE ANTENNA PATTERN REV.8-30-68

APERTURE: LENGTH 6.25 INCHES WIDTH 1.97 INCHES

FREQ= 60.80 GHZ THETA = 0.0 DEGREES PAGE 1

PHI (DEG)	E(THETA, PHI)	DB
0.0	10.00-01	.00
.2	98.83-02	.10
.4	95.36-02	.41
.6	89.79-02	.94
.8	82.39-02	1.68
1.0	73.53-02	2.67
1.2	63.64-02	3.93
1.4	53.17-02	5.49
1.6	42.61-02	7.41
1.8	32.40-02	9.79
2.0	22.92-02	12.80
2.2	14.50-02	16.78
2.4	73.73-03	22.65
2.6	16.88-03	35.45
2.8	-25.14-03	31.99
3.0	-52.79-03	25.55
3.2	-67.34-03	23.43
3.4	-70.68-03	23.01
3.6	-65.12-03	23.73
3.8	-53.24-03	25.48
4.0	-37.58-03	28.50
4.2	-20.57-03	33.74
4.4	-42.53-04	47.43
4.6	97.34-04	40.23
4.8	20.28-03	33.86
5.0	26.81-03	31.43
5.2	29.24-03	30.68
5.4	27.93-03	31.08
5.6	23.56-03	32.56
5.8	17.06-03	35.36
6.0	94.29-04	40.51
6.2	16.79-04	55.50
6.4	-53.10-04	45.50
6.6	-10.85-03	39.29
6.8	-14.48-03	36.78
7.0	-16.02-03	35.91
7.2	-15.53-03	36.17
7.4	-13.29-03	37.53
7.6	-97.39-04	40.23
7.8	-54.14-04	45.33
8.0	-88.53-05	61.06
8.2	33.10-04	49.60
8.4	67.28-04	43.44
8.6	90.51-04	40.87
8.8	10.12-03	39.90
9.0	99.14-04	40.08
9.2	85.80-04	41.33
9.4	63.64-04	43.93
9.6	35.92-04	48.89
9.8	62.78-05	64.04
10.0	-21.76-04	53.25

TABLE A-A-4 continued

OFF-AXIS PATTERNS OF A RECTANGULAR APERTURE ANTENNA

FREQ= 60.80 GHZ THETA = 1.0 DEGREES PAGE 2

PHI (DEG)	E(THETA, PHI)	DB
0.0	94.93-02	.45
.2	93.81-02	.55
.4	90.53-02	.86
.6	85.24-02	1.39
.8	78.21-02	2.13
1.0	69.80-02	3.12
1.2	60.41-02	4.38
1.4	50.48-02	5.94
1.6	40.45-02	7.86
1.8	30.75-02	10.24
2.0	21.75-02	13.25
2.2	13.76-02	17.23
2.4	69.99-03	23.10
2.6	16.03-03	35.90
2.8	-23.86-03	32.45
3.0	-50.11-03	26.00
3.2	-63.93-03	23.89
3.4	-67.09-03	23.47
3.6	-61.82-03	24.18
3.8	-50.54-03	25.93
4.0	-35.68-03	28.95
4.2	-19.52-03	34.19
4.4	-40.38-04	47.88
4.6	92.40-04	40.69
4.8	19.25-03	34.31
5.0	25.45-03	31.89
5.2	27.76-03	31.13
5.4	26.51-03	31.53
5.6	22.37-03	33.01
5.8	16.19-03	35.81
6.0	89.51-04	40.96
6.2	15.94-04	55.95
6.4	-50.41-04	45.95
6.6	-10.30-03	39.75
6.8	-13.75-03	37.24
7.0	-15.21-03	36.36
7.2	-14.75-03	36.63
7.4	-12.62-03	37.98
7.6	-92.45-04	40.68
7.8	-51.39-04	45.78
8.0	-84.04-05	61.51
8.2	31.42-04	50.05
8.4	63.86-04	43.89
8.6	85.92-04	41.32
8.8	96.03-04	40.35
9.0	94.11-04	40.53
9.2	81.45-04	41.78
9.4	60.41-04	44.38
9.6	34.10-04	49.35
9.8	59.59-05	64.50
10.0	-20.65-04	53.70

TABLE A-A-4 continued

OFF-AXIS PATTERNS OF A RECTANGULAR APERTURE ANTENNA

FREQ= 60.80 GHZ THETA = 2.0 DEGREES PAGE 3

PHI (DEG)	E(THETA, PHI)	DB
0.0	80.63-02	1.87
.2	79.69-02	1.97
.4	76.90-02	2.28
.6	72.40-02	2.80
.8	66.43-02	3.55
1.0	59.29-02	4.54
1.2	51.31-02	5.80
1.4	42.88-02	7.36
1.6	34.36-02	9.28
1.8	26.12-02	11.66
2.0	18.48-02	14.67
2.2	11.69-02	18.65
2.4	59.45-03	24.52
2.6	13.61-03	37.32
2.8	-20.27-03	33.86
3.0	-42.57-03	27.42
3.2	-54.30-03	25.30
3.4	-56.99-03	24.88
3.6	-52.51-03	25.59
3.8	-42.93-03	27.35
4.0	-30.31-03	30.37
4.2	-16.58-03	35.61
4.4	-34.30-04	49.30
4.6	78.49-04	42.10
4.8	16.36-03	35.73
5.0	21.62-03	33.30
5.2	23.58-03	32.55
5.4	22.52-03	32.95
5.6	19.00-03	34.43
5.8	13.75-03	37.23
6.0	76.03-04	42.38
6.2	13.54-04	57.37
6.4	-42.82-04	47.37
6.6	-87.46-04	41.16
6.8	-11.68-03	38.65
7.0	-12.92-03	37.77
7.2	-12.53-03	38.04
7.4	-10.72-03	39.40
7.6	-78.53-04	42.10
7.8	-43.65-04	47.20
8.0	-71.39-05	62.93
8.2	26.69-04	51.47
8.4	54.25-04	45.31
8.6	72.98-04	42.74
8.8	81.57-04	41.77
9.0	79.94-04	41.94
9.2	69.18-04	43.20
9.4	51.31-04	45.80
9.6	28.96-04	50.76
9.8	50.62-05	65.91
10.0	-17.54-04	55.12

TABLE A-A-4 continued

OFF-AXIS PATTERNS OF A RECTANGULAR APERTURE ANTENNA

F
REQ= 60.80 GHZ THETA = 3.0 DEGREES PAGE 4

PHI (DEG)	E(THETA, PHI)	DB
0.0	59.70-02	4.48
.2	58.99-02	4.58
.4	56.93-02	4.89
.6	53.60-02	5.42
.8	49.18-02	6.16
1.0	43.89-02	7.15
1.2	37.99-02	8.41
1.4	31.74-02	9.97
1.6	25.44-02	11.89
1.8	19.34-02	14.27
2.0	13.68-02	17.28
2.2	86.53-03	21.26
2.4	44.01-03	27.13
2.6	10.08-03	39.93
2.8	-15.01-03	36.47
3.0	-31.51-03	30.03
3.2	-40.20-03	27.92
3.4	-42.19-03	27.50
3.6	-38.88-03	28.21
3.8	-31.78-03	29.96
4.0	-22.44-03	32.98
4.2	-12.28-03	38.22
4.4	-25.39-04	51.91
4.6	58.11-04	44.72
4.8	12.11-03	38.34
5.0	16.01-03	35.91
5.2	17.46-03	35.16
5.4	16.67-03	35.56
5.6	14.07-03	37.04
5.8	10.18-03	39.84
6.0	56.29-04	44.99
6.2	10.02-04	59.98
6.4	-31.70-04	49.98
6.6	-64.75-04	43.78
6.8	-86.44-04	41.27
7.0	-95.65-04	40.39
7.2	-92.73-04	40.66
7.4	-79.35-04	42.01
7.6	-58.14-04	44.71
7.8	-32.32-04	49.81
8.0	-52.85-05	65.54
8.2	19.76-04	54.08
8.4	40.16-04	47.92
8.6	54.03-04	45.35
8.8	60.39-04	44.38
9.0	59.18-04	44.56
9.2	51.22-04	45.81
9.4	37.99-04	48.41
9.6	21.44-04	53.37
9.8	37.48-05	68.52
10.0	-12.99-04	57.73

TABLE A-A-4 continued

OFF-AXIS PATTERNS OF A RECTANGULAR APERTURE ANTENNA

FREQ= 60.80 GHZ THETA = 4.0 DEGREES PAGE 5

PHI (DEG)	E(THETA, PHI)	DB
0.0	35.78-02	8.93
.2	35.36-02	9.03
.4	34.12-02	9.34
.6	32.13-02	9.86
.8	29.48-02	10.61
1.0	26.31-02	11.60
1.2	22.77-02	12.85
1.4	19.03-02	14.41
1.6	15.25-02	16.34
1.8	11.59-02	18.72
2.0	81.99-03	21.73
2.2	51.86-03	25.70
2.4	26.38-03	31.57
2.6	60.40-04	44.38
2.8	-89.94-04	40.92
3.0	-18.89-03	34.48
3.2	-24.09-03	32.36
3.4	-25.29-03	31.94
3.6	-23.30-03	32.65
3.8	-19.05-03	34.40
4.0	-13.45-03	37.43
4.2	-73.59-04	42.66
4.4	-15.22-04	56.35
4.6	34.83-04	49.16
4.8	72.57-04	42.78
5.0	95.93-04	40.36
5.2	10.46-03	39.61
5.4	99.92-04	40.01
5.6	84.30-04	41.48
5.8	61.03-04	44.29
6.0	33.74-04	49.44
6.2	60.07-05	64.43
6.4	-19.00-04	54.43
6.6	-38.81-04	48.22
6.8	-51.81-04	45.71
7.0	-57.33-04	44.83
7.2	-55.58-04	45.10
7.4	-47.56-04	46.46
7.6	-34.85-04	49.16
7.8	-19.37-04	54.26
8.0	-31.68-05	69.99
8.2	11.84-04	58.53
8.4	24.07-04	52.37
8.6	32.38-04	49.79
8.8	36.19-04	48.83
9.0	35.47-04	49.00
9.2	30.70-04	50.26
9.4	22.77-04	52.85
9.6	12.85-04	57.82
9.8	22.46-05	72.97
10.0	-77.84-05	62.18

TABLE A-A-4 continued

OFF-AXIS PATTERNS OF A RECTANGULAR APERTURE ANTENNA

FREQ= 60.80 GHZ THETA = 5.0 DEGREES PAGE 6

PHI (DEG)	E(THETA, PHI)	DB
0.0	12.85-02	17.82
.2	12.70-02	17.92
.4	12.26-02	18.23
.6	11.54-02	18.76
.8	10.59-02	19.50
1.0	94.50-03	20.49
1.2	81.78-03	21.75
1.4	68.34-03	23.31
1.6	54.77-03	25.23
1.8	41.63-03	27.61
2.0	29.45-03	30.62
2.2	18.63-03	34.60
2.4	94.75-04	40.47
2.6	21.70-04	53.27
2.8	-32.31-04	49.81
3.0	-67.85-04	43.37
3.2	-86.55-04	41.26
3.4	-90.83-04	40.84
3.6	-83.70-04	41.55
3.8	-68.42-04	43.30
4.0	-48.30-04	46.32
4.2	-26.43-04	51.56
4.4	-54.66-05	65.25
4.6	12.51-04	58.05
4.8	26.07-04	51.68
5.0	34.46-04	49.25
5.2	37.58-04	48.50
5.4	35.89-04	48.90
5.6	30.28-04	50.38
5.8	21.92-04	53.18
6.0	12.12-04	58.33
6.2	21.58-05	73.32
6.4	-68.25-05	63.32
6.6	-13.94-04	57.11
6.8	-18.61-04	54.60
7.0	-20.59-04	53.73
7.2	-19.96-04	53.99
7.4	-17.08-04	55.35
7.6	-12.52-04	58.05
7.8	-69.57-05	63.15
8.0	-11.38-05	78.88
8.2	42.54-05	67.42
8.4	86.46-05	61.26
8.6	11.63-04	58.69
8.8	13.00-04	57.72
9.0	12.74-04	57.90
9.2	11.03-04	59.15
9.4	81.78-05	61.75
9.6	46.17-05	66.71
9.8	80.68-06	81.86
10.0	-27.96-05	71.07

TABLE A-A-4 continued

OFF-AXIS PATTERNS OF A RECTANGULAR APERTURE ANTENNA

FREQ= 60.80 GHZ THETA = 6.0 DEGREES PAGE 7

PHI (DEG)	E(THETA, PHI)	DB
0.0	-56.29-03	24.99
.2	-55.63-03	25.09
.4	-53.68-03	25.40
.6	-50.55-03	25.93
.8	-46.38-03	26.67
1.0	-41.39-03	27.66
1.2	-35.82-03	28.92
1.4	-29.93-03	30.48
1.6	-23.99-03	32.40
1.8	-18.24-03	34.78
2.0	-12.90-03	37.79
2.2	-81.60-04	41.77
2.4	-41.50-04	47.64
2.6	-95.03-05	60.44
2.8	14.15-04	56.98
3.0	29.72-04	50.54
3.2	37.91-04	48.43
3.4	39.79-04	48.01
3.6	36.66-04	48.72
3.8	29.97-04	50.47
4.0	21.16-04	53.49
4.2	11.58-04	58.73
4.4	23.94-05	72.42
4.6	-54.80-05	65.22
4.8	-11.42-04	58.85
5.0	-15.09-04	56.42
5.2	-16.46-04	55.67
5.4	-15.72-04	56.07
5.6	-13.26-04	57.55
5.8	-96.02-05	60.35
6.0	-53.08-05	65.50
6.2	-94.51-06	80.49
6.4	29.89-05	70.49
6.6	61.06-05	64.28
6.8	81.52-05	61.77
7.0	90.20-05	60.90
7.2	87.45-05	61.17
7.4	74.83-05	62.52
7.6	54.82-05	65.22
7.8	30.47-05	70.32
8.0	49.84-06	86.05
8.2	-18.63-05	74.59
8.4	-37.87-05	68.43
8.6	-50.95-05	65.86
8.8	-56.94-05	64.89
9.0	-55.81-05	65.07
9.2	-48.30-05	66.32
9.4	-35.82-05	68.92
9.6	-20.22-05	73.88
9.8	-35.34-06	89.03
10.0	12.25-05	78.24

TABLE A-A-4 continued

OFF-AXIS PATTERNS OF A RECTANGULAR APERTURE ANTENNA

FREQ= 60.80 GHZ THETA = 7.0 DEGREES PAGE 8

PHI (DEG)	E(THETA, PHI)	DB
0.0	-17.39-02	15.20
.2	-17.18-02	15.30
.4	-16.58-02	15.61
.6	-15.61-02	16.13
.8	-14.33-02	16.88
1.0	-12.78-02	17.87
1.2	-11.06-02	19.12
1.4	-92.45-03	20.68
1.6	-74.09-03	22.60
1.8	-56.32-03	24.99
2.0	-39.84-03	27.99
2.2	-25.20-03	31.97
2.4	-12.82-03	37.84
2.6	-29.35-04	50.65
2.8	43.70-04	47.19
3.0	91.79-04	40.74
3.2	11.71-03	38.63
3.4	12.29-03	38.21
3.6	11.32-03	38.92
3.8	92.56-04	40.67
4.0	65.35-04	43.70
4.2	35.76-04	48.93
4.4	73.95-05	62.62
4.6	-16.92-04	55.43
4.8	-35.27-04	49.05
5.0	-46.62-04	46.63
5.2	-50.84-04	45.88
5.4	-48.56-04	46.27
5.6	-40.97-04	47.75
5.8	-29.66-04	50.56
6.0	-16.39-04	55.71
6.2	-29.19-05	70.70
6.4	92.33-05	60.69
6.6	18.86-04	54.49
6.8	25.18-04	51.98
7.0	27.86-04	51.10
7.2	27.01-04	51.37
7.4	23.11-04	52.72
7.6	16.93-04	55.43
7.8	94.12-05	60.53
8.0	15.39-05	76.25
8.2	-57.55-05	64.80
8.4	-11.70-04	58.64
8.6	-15.74-04	56.06
8.8	-17.59-04	55.10
9.0	-17.24-04	55.27
9.2	-14.92-04	56.53
9.4	-11.06-04	59.12
9.6	-62.46-05	64.09
9.8	-10.92-05	79.24
10.0	37.83-05	68.44

TABLE A-A-4 continued

OFF-AXIS PATTERNS OF A RECTANGULAR APERTURE ANTENNA

FREQ= 60.80 GHZ THETA = 8.0 DEGREES PAGE 9

PHI (DEG)	E(THETA, PHI)	DB
0.0	-21.68-02	13.28
.2	-21.43-02	13.38
.4	-20.68-02	13.69
.6	-19.47-02	14.21
.8	-17.87-02	14.96
1.0	-15.94-02	15.95
1.2	-13.80-02	17.20
1.4	-11.53-02	18.76
1.6	-92.41-03	20.69
1.8	-70.25-03	23.07
2.0	-49.69-03	26.07
2.2	-31.43-03	30.05
2.4	-15.99-03	35.92
2.6	-36.61-04	48.73
2.8	54.51-04	45.27
3.0	11.45-03	38.83
3.2	14.60-03	36.71
3.4	15.33-03	36.29
3.6	14.12-03	37.00
3.8	11.54-03	38.75
4.0	81.50-04	41.78
4.2	44.60-04	47.01
4.4	92.23-05	60.70
4.6	-21.11-04	53.51
4.8	-43.98-04	47.13
5.0	-58.14-04	44.71
5.2	-63.41-04	43.96
5.4	-60.56-04	44.36
5.6	-51.09-04	45.83
5.8	-36.99-04	48.64
6.0	-20.45-04	53.79
6.2	-36.41-05	68.78
6.4	11.52-04	58.77
6.6	23.52-04	52.57
6.8	31.40-04	50.06
7.0	34.75-04	49.18
7.2	33.69-04	49.45
7.4	28.82-04	50.80
7.6	21.12-04	53.51
7.8	11.74-04	58.61
8.0	19.20-05	74.33
8.2	-71.78-05	62.88
8.4	-14.59-04	56.72
8.6	-19.63-04	54.14
8.8	-21.94-04	53.18
9.0	-21.50-04	53.35
9.2	-18.61-04	54.61
9.4	-13.80-04	57.20
9.6	-77.89-05	62.17
9.8	-13.61-05	77.32
10.0	47.18-05	66.53

TABLE A-A-4 continued

OFF-AXIS PATTERNS OF A RECTANGULAR APERTURE ANTENNA

FREQ= 60.80 GHZ THETA = 9.0 DEGREES PAGE 10

PHI (DEG)	E(THETA, PHI)	DB
0.0	-19.33-02	14.28
.2	-19.10-02	14.38
.4	-18.43-02	14.69
.6	-17.36-02	15.21
.8	-15.93-02	15.96
1.0	-14.21-02	16.95
1.2	-12.30-02	18.20
1.4	-10.28-02	19.76
1.6	-82.37-03	21.68
1.8	-62.62-03	24.07
2.0	-44.30-03	27.07
2.2	-28.02-03	31.05
2.4	-14.25-03	36.92
2.6	-32.63-04	49.73
2.8	48.59-04	46.27
3.0	10.20-03	39.82
3.2	13.02-03	37.71
3.4	13.66-03	37.29
3.6	12.59-03	38.00
3.8	10.29-03	39.75
4.0	72.65-04	42.78
4.2	39.76-04	48.01
4.4	82.22-05	61.70
4.6	-18.82-04	54.51
4.8	-39.21-04	48.13
5.0	-51.83-04	45.71
5.2	-56.53-04	44.95
5.4	-53.99-04	45.35
5.6	-45.54-04	46.83
5.8	-32.97-04	49.64
6.0	-18.23-04	54.79
6.2	-32.45-05	69.77
6.4	10.26-04	59.77
6.6	20.97-04	53.57
6.8	27.99-04	51.06
7.0	30.97-04	50.18
7.2	30.03-04	50.45
7.4	25.69-04	51.80
7.6	18.83-04	54.50
7.8	10.46-04	59.61
8.0	17.11-05	75.33
8.2	-63.99-05	63.88
8.4	-13.00-04	57.72
8.6	-17.50-04	55.14
8.8	-19.55-04	54.18
9.0	-19.16-04	54.35
9.2	-16.59-04	55.61
9.4	-12.30-04	58.20
9.6	-69.44-05	63.17
9.8	-12.14-05	78.32
10.0	42.05-05	67.52

TABLE A - A.- 4 continued

OFF - AXIS PATTERNS OF A RECTANGULAR APERTURE ANTENNA

FREQ= 60.80 GHZ THETA = 10.0 DEGREES PAGE 11

PHI (DEG)	E(THETA, PHI)	DB
0.0	-12.33-02	18.18
.2	-12.19-02	18.28
.4	-11.76-02	18.59
.6	-11.07-02	19.11
.8	-10.16-02	19.86
1.0	-90.69-03	20.85
1.2	-78.49-03	22.10
1.4	-65.58-03	23.66
1.6	-52.56-03	25.59
1.8	-39.95-03	27.97
2.0	-28.26-03	30.98
2.2	-17.88-03	34.95
2.4	-90.93-04	40.83
2.6	-20.82-04	53.63
2.8	31.00-04	50.17
3.0	65.11-04	43.73
3.2	83.06-04	41.61
3.4	87.17-04	41.19
3.6	80.32-04	41.90
3.8	65.66-04	43.65
4.0	46.36-04	46.68
4.2	25.37-04	51.91
4.4	52.46-05	65.60
4.6	-12.01-04	58.41
4.8	-25.02-04	52.04
5.0	-33.07-04	49.61
5.2	-36.07-04	48.86
5.4	-34.45-04	49.26
5.6	-29.06-04	50.73
5.8	-21.04-04	53.54
6.0	-11.63-04	58.69
6.2	-20.71-05	73.68
6.4	65.50-05	63.68
6.6	13.38-04	57.47
6.8	17.86-04	54.96
7.0	19.76-04	54.08
7.2	19.16-04	54.35
7.4	16.39-04	55.71
7.6	12.01-04	58.41
7.8	66.77-05	63.51
8.0	10.92-05	79.24
8.2	-40.83-05	67.78
8.4	-82.98-05	61.62
8.6	-11.16-04	59.04
8.8	-12.48-04	58.08
9.0	-12.23-04	58.25
9.2	-10.58-04	59.51
9.4	-78.49-05	62.10
9.6	-44.30-05	67.07
9.8	-77.43-06	82.22
10.0	26.83-05	71.43

Report Distribution List For
Contract No. NAS 12-2001

ADDRESS

1 NASA/ ERC (10)
575 Technology Square
Cambridge, Massachusetts 02139
Attention: J. Vilcans

2 NASA/ERC (1)
575 Technology Square
Cambridge, Massachusetts 02139
Attention: Dr. Alfred I. Grayzel

3 NASA/ERC (10 + 1 reproducible)
575 Technology Square
Cambridge, Massachusetts 02139
Attention: Thomas F. McDonough

4 Air Force Avionics Laboratory
Research and Technology Division
Air Force Systems Command
Wright-Patterson Air Force Base,
Dayton, Ohio
Attention: Egbert D. Maynard, Jr. (1)
Lt. John Norton (1)
T. Herbert (1)

5 United State Air Force (AFSC) (1)
Systems Engineering Goup (RTD)
Wright-Patterson Air Force Base,
Dayton, Ohio
Attention: R. J. Harnett, SEKRA

6 Naval Ordinance Laboratories (1)
Silver Springs, Maryland 20910
Attention: William E. Ryan

7 Massachusetts Institute of Technology (1)
Lincoln Laboratories
P. O. Box 73
Lexington, Massachusetts 02173
Attention: Steven Zolny

8 Massachusetts Institute of Technology (1)
Cambridge, Massachusetts 02139
Attention: Dr. Robert P. Rafuse

9 Northeastern University (1)
336 Dana Research Center
360 Huntington Avenue
Boston, Massachusetts 02115
Attention: Paul W. Pelligrini

ADDRESS

10 Westinghouse Corporation (1)
Defense and Space Center
Friendship International Airport
P. O. Box 746
Baltimore, Maryland 21203
Attention: Dr. H. Grauling

11 Control Data Corporation (1)
TRG Division
400 Border Street
East Boston, Massachusetts
Attention: R. C. Gerrish

12 Lockheed Electronics Company (1)
Division of Lockheed Aircraft Corporation
Plainfield, New Jersey 07061
Attention: Bernard Berkowitz

13 McDonnell Douglas Corporation (1)
Post Office Box 516
St. Louis, Missouri 63166
Attention: McDonnell Library,
Department 218

14 Sperry Microwave Electronics Company (1)
Division of Sperry Rand Corporation
Clearwater, Florida 33516
Attention: Russell E. Strother

15 Stanford Research Institute (1)
Menlo Park, California 94025
Attention: Lloyd A. Robinson

16 Sylvania Electric Products, Inc. (1)
100 Sylvan Road
Woburn, Massachusetts 01801
Attention: Bayard R. Lincoln

17 TRW (1)
One Space Park
Redondo Beach, California
Attention: Dr. Leopold B. Valdes

18 Florida Technological University
College of Engineering
P.O. Box 25000
Orlando, Florida 32816
Attention: Dr. Ernest E. Erickson

ADDRESS

19 AFSC STLO
Massachusetts Institute of Technology
68 Albany Street
Cambridge, Massachusetts 02139
Attention: Capt. Mark R. Jensen